AUDIO EMBEDDINGS FOR SEMI-SUPERVISED ANOMALOUS SOUND DETECTION

DISSERTATION

zur Erlangung des Doktorgrades (Dr. rer. nat.)
der
Mathematisch-Naturwissenschaftlichen Fakultät
der
Rheinischen Friedrich-Wilhelms-Universität Bonn

vorgelegt von

KEVIN WILKINGHOFF

aus

HAMM

Bonn, 2024

Angefertigt mit Genehmigung der Mathematisch-Naturwissenschaftlichen Fakultät der Rheinischen Friedrich-Wilhelms-Universität Bonn

1. Gutachter: apl. Prof. Dr. Frank Kurth
2. Gutachter: Prof. Dr. Reinhard Klein

Tag der Promotion: 2. September 2024
Erscheinungsjahr: 2024

ABSTRACT

Detecting anomalous sounds is a difficult task: First, audio data is very high-dimensional and anomalous signal components are relatively subtle in relation to the entire acoustic scene. Furthermore, normal and anomalous audio signals are not inherently different because defining these terms strongly depends on the application. Third, usually only normal data is available for training a system because anomalies are rare, diverse, costly to produce and in many cases unknown in advance. Such a setting is called semi-supervised anomaly detection. In domain-shifted conditions or when only very limited training data is available, all of these problems are even more severe.

The goal of this thesis is to overcome these difficulties by teaching an embedding model to learn data representations suitable for semi-supervised anomalous sound detection. More specifically, an anomalous sound detection system is designed such that the resulting representations of the data, called embeddings, fulfill the following desired properties: First, normal and anomalous data should be easy to distinguish, which is usually not the case for audio signals because the definition of anomalies is entirely application-dependent. Second, in contrast to audio signals that are very high-dimensional and may have different durations or sampling rates and thus are difficult to handle, embeddings should have a fixed and relatively low dimension. Third, audio signals may have been recorded under very different acoustic conditions leading to strong variability between signals that, from an anomalous sound detection perspective, is not desired. Ideally, embeddings used for detecting anomalies should be mostly insensitive to these acoustic changes and only sensitive to their degree of abnormality.

The main contributions of this thesis are the following: First and foremost, angular margin losses, namely sub-cluster AdaCos, AdaProj and TACos, specifically designed to train embedding models for anomalous sound detection and for few-shot open-set sound event detection are presented. In various experiments, it is shown that the embeddings obtained with these loss functions outperform embeddings obtained by using other angular margin losses, one-class losses or pre-trained embeddings. As another contribution, it is proven that angular margin losses can be seen as a regularized multi-class version of one-class losses, which helps to cope with background noise. Furthermore, design choices for learning embeddings that are robust to acoustic domain shifts by generalizing well to previously unseen domains are presented, which results in an anomalous sound detection system significantly outperforming other state-of-the-art systems. As a last contribution, it is investigated how to obtain good decision thresholds and a novel performance metric, called F_1-EV, that measures the difficulty of estimating a good threshold is presented.

ACKNOWLEDGMENTS

First and foremost, I would like to express my deepest gratitude to my supervisor Frank Kurth for his guidance and support throughout the entire time it took me to write this thesis while granting me academic freedom in choosing the research topics I wanted to pursue. Likewise, I would like to thank Reinhard Klein for being willing to serve as a second supervisor as well as Thomas Schultz and Ulrich Schade for participating in the examination and defense of this thesis.

I am equally thankful to my colleagues at Fraunhofer FKIE with whom I had the pleasure to work and collaborate: Paul M. Baggenstoss, Alessia Cornaggia-Urrigshardt, Fabian Fritz, Fahrettin Gögköz, Lukas Henneke, Hans-Christian Schmitz, Sebastian Urrigshardt and all others not mentioned here but who also had their contributions if only by making lunch breaks much more enjoyable.

Furthermore, I would like to thank all members of the DCASE community for discussing ideas and working together on similar research topics. In particular, I would like to mention Yacine Bel-Hadj and Keisuke Imoto for being interested in collaborating with me, Toni Heittola, Annamaria Mesaros and Romain Serizel for including me in organizational duties, and all organizers of the annual anomalous sound detection task for providing most of the datasets used in this thesis.

Last but not least, I am deeply grateful for the continuous support of my wife Kristin, my parents André and Sabine, my siblings Dennis and Melina as well as their other halves Pia and Fabian, my wife's side of the family Ria, Uwe, Heike, Tobias, Angi, Smilla, Lunis, Carlotta, and all of my friends whom I will not try to list here knowing that I will most likely forget to mention too many of them.

CONTENTS

1 INTRODUCTION

In general, anomaly detection is the process of distinguishing *normal* data, which are the result of measurements or sensor input, from *anomalous* data, which substantially deviates from normal data in some way. Other even less formal definitions are to see anomalous data as every data sample that strikes the eye or is deemed interesting or perhaps surprising. There are several difficulties to overcome when trying to formalize these vague definitions. First, one needs to define *in which way* and *to what extent* data needs to deviate from normal data in order to be considered anomalous. One can distinguish *weak* anomalies, which are essentially noisy normal samples, and *strong* anomalies that should always be recognized as anomalies [3]. Thus, weak anomalies can be considered normal or anomalous, depending on the application. Furthermore, the term *normal* needs to be precisely defined since it is highly application-dependent and can be influenced by several parameters such as the time and location at which data is collected. Data that is considered normal for a given application can possibly be considered anomalous in another application or even for the same application if one of the data-influencing parameters is changed. In conclusion, one needs a well-defined goal when setting up an anomaly detection system. Sufficient amounts of data need to be collected in the right conditions for training the system such that the underlying distribution of normal data is represented sufficiently well for the application in mind. Otherwise, it cannot be ensured that anomalies detected by the system are truly the ones that should be detected.

Let X denote an infinite data space such as the space containing all audio signals. Let $X_{\text{normal}} \subset X$ and $X_{\text{anomalous}} \subset X$ denote the sets of normal and anomalous samples, respectively. For the sake of simplicity, set $X_{\text{anomalous}} \coloneqq X \backslash X_{\text{normal}}$ as this only requires the choice of normal samples to define both sets. Although using this definition, i.e. using the complement of the normal samples in the set of all theoretically possible samples, $X_{\text{anomalous}}$ may include samples that never occur in practice, these samples should certainly not be considered normal. The goal of training most anomaly detection systems is to obtain a function $\text{score} : X \to \mathbb{R}, x \mapsto \text{score}(x)$ mapping a data sample x to an anomaly score denoted by $\text{score}(x)$ such that all normal samples can be separated from anomalous samples. This means that there is a decision threshold $\theta \in \mathbb{R}$ such that

$$\text{score}(x_n) \leqslant \theta < \text{score}(x_a)$$

for all normal samples $x_n \in X_{\text{normal}}$ and for all anomalous samples $x_a \in X_{\text{anomalous}}$. In other words, anomalous samples should be mapped to much higher anomaly scores than normal samples. It is important to mention that obtaining this function score is only a desired goal and in practice anomalous samples can only rarely be

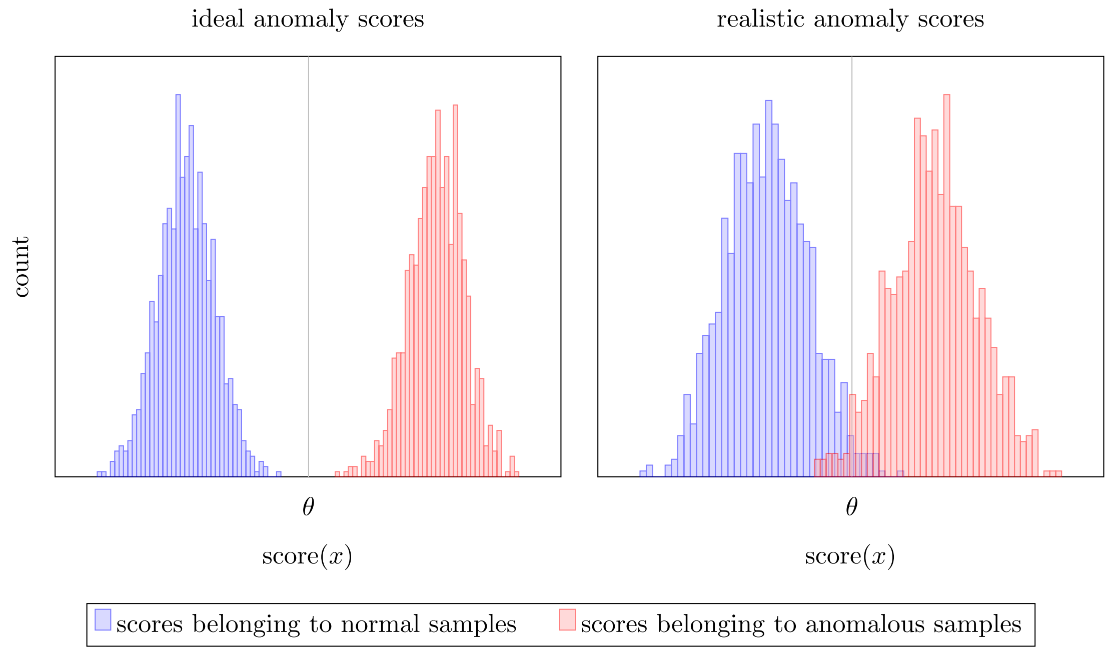

Figure 1: Histograms of anomaly scores and corresponding decision thresholds. On the left, the decision threshold θ perfectly separates the anomaly scores belonging to the normal and anomalous samples. On the right, a perfect separation is not possible because the histograms of the normal and anomalous scores overlap.

perfectly detected, i.e. there is an overlap between the anomaly scores of both sets. This is illustrated in Figure 1.

1.1 SEMI-SUPERVISED ANOMALY DETECTION

Depending on the structure of the training dataset and the given labels for this dataset, there are three different settings in which anomaly detection can take place: *Supervised*, *semi-supervised* and *unsupervised* anomaly detection [3]. These settings are presented in Table 1 and visualized with examples in Figure 2.

Table 1: Overview of different anomaly detection settings.

	training dataset	training labels	data collection
supervised	$X_{\text{train}} \subset X_{\text{normal}} \cup X_{\text{anomalous}}$	available (2 classes)	difficult
semi-supervised	$X_{\text{train}} \subset X_{\text{normal}}$	available (1 class)	moderately difficult
unsupervised	$X_{\text{train}} \subset X_{\text{normal}} \cup X_{\text{anomalous}}$	not available	simple

For *supervised* anomaly detection, the labeled training dataset consists of normal and anomalous data. In non-trivial applications it is impossible to collect all variations of data that are considered anomalous to fully capture the space

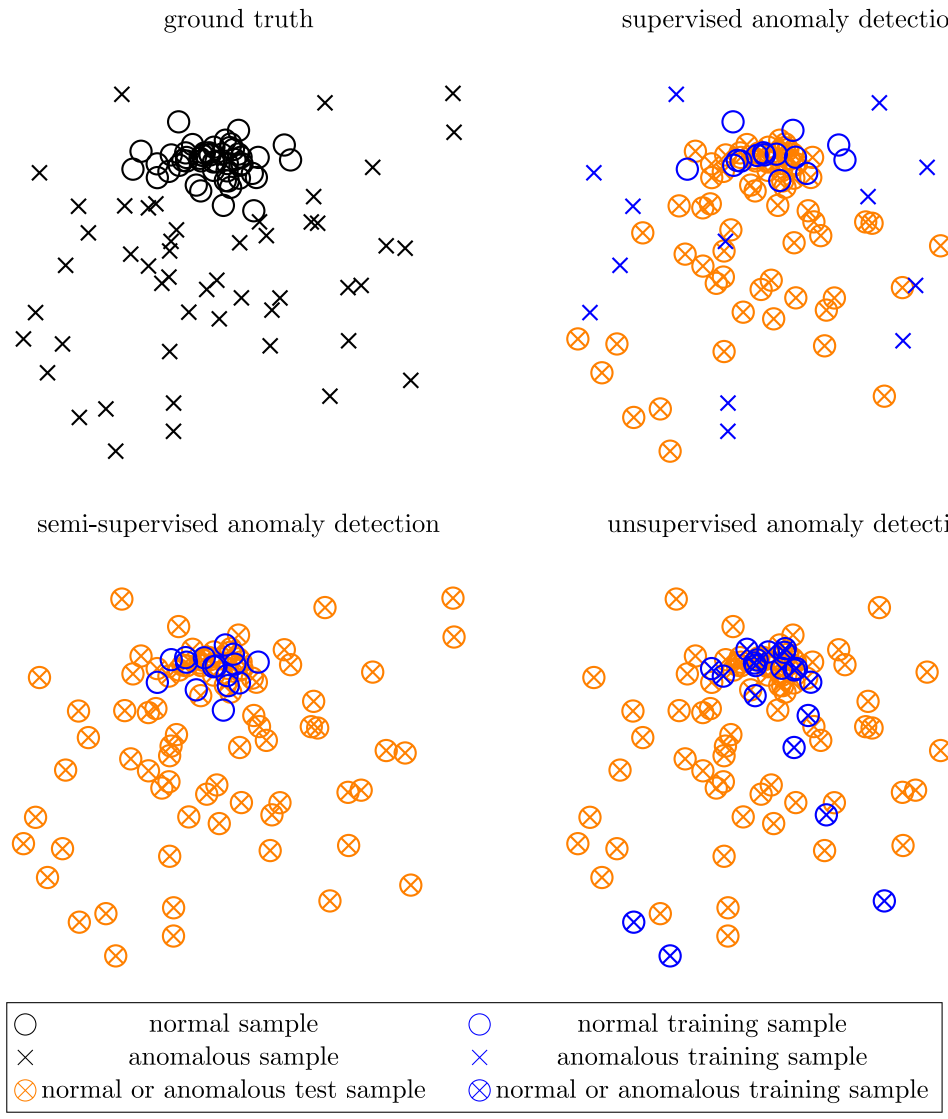

Figure 2: Illustration of different anomaly detection settings. The same dataset is shown with different samples and corresponding labels available for training an anomaly detection system.

of anomalous samples. Thus, only a limited number of boundaries between normal and anomalous samples can be learned. This is especially true in case of high-dimensional data. Still, providing examples of anomalous samples that are of particular interest and thus should always be recognized as being anomalous is useful for training the system. By definition, anomalies only rarely occur. Therefore, it is much more difficult and thus more costly to obtain realistic anomalous samples for training a system than to collect normal data. Furthermore, determining whether a sample is normal or anomalous often requires expert knowledge and can be a cumbersome task. This results in highly imbalanced classes, which poses a problem that needs to be handled appropriately.

In a *semi-supervised* setting, the training dataset contains only normal data[1]. For most applications, this is a more realistic setting because it substantially simplifies the data collection process as it only needs to be ensured that all collected samples are in fact normal. However, using only normal data for training leads to worse performance than using a dataset collected in a supervised setting because no a priori knowledge about the expected anomalous data is available.

In some cases it is even impossible to ensure that only normal data is collected and, without explicitly knowing, the training dataset may contain a mixture of normal and possibly anomalous data. This is referred to as an *unsupervised* anomaly detection setting. Compared to both other settings, it is far easier and thus less costly to collect data in this setting. Furthermore, using such a dataset for training a system usually leads to significantly worse performance as only noisy information about the underlying distribution of the normal data is available. In most cases, at least an estimate of the corruption of the training data, i.e. the ratio between normal and anomalous training samples, is needed to obtain useful results.

1.2 AUDIO EMBEDDINGS

Identifying anomalies by analyzing raw audio signals is difficult because of three reasons: First, there is no inherent property separating normal from anomalous samples since defining the normal (and the anomalous) subset is entirely application-dependent. Second, audio signals live in a high-dimensional space with a dimension equal to the duration in seconds times the sampling rate in Hertz and thus contain much redundant information for a given task. Moreover, an audio recording may also consist of several recording channels, which leads to an even higher dimension. Third, individual audio signals may have a different duration, a different sampling rate or may have been recorded in different acoustic conditions or using different sensors and thus a comparison between signals is difficult. To overcome these difficulties for a particular anomalous sound detection (ASD) application, it would be very favorable if all audio signals were mapped to the same, relatively low-dimensional vector space specifically structured such that representations of normal samples are similar to each other while substantially differing from anomalous samples and also being robust to acoustic variations. In the context of machine learning, such vector representations of the input data are called embeddings. To formalize this, an *ideal embedding function* will be defined as a

1 If only anomalous data is available for training the system, this is also called a semi-supervised setting. However, for most applications this is rarely the case since it is highly unusual that normal samples are not available and anomalous samples are usually much more difficult to collect than normal samples. Within this thesis the term is reserved for a setting with a training dataset consisting of normal samples only.

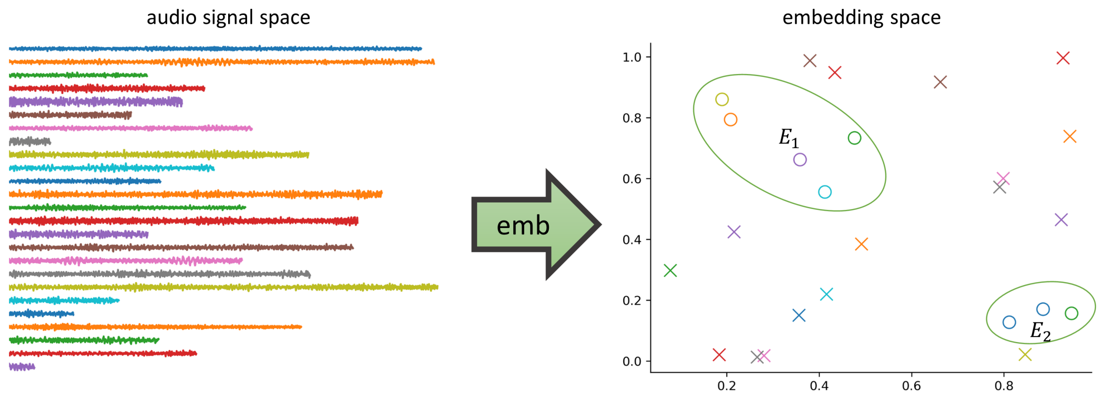

Figure 3: Illustration of an ideal embedding function for ASD.

mapping $\text{emb} : X \to \mathbb{R}^D$ with $D \in \mathbb{N}$ sufficiently small such that there are $N_e \in \mathbb{N}$ subsets $E_i \subset \mathbb{R}^D$ of the embedding space for which

$$\text{emb}(X_{\text{normal}}) = \bigcup_{i=1}^{N_e} E_i \text{ with } E_i \cap \text{emb}(X_{\text{anomalous}}) = \varnothing \text{ for all } i = 1, ..., N_e.$$

Such an ideal embedding function is depicted in Figure 3. Note that for such an ideal embedding function it holds that

$$\text{emb}(X_{\text{normal}}) \cap \text{emb}(X_{\text{anomalous}}) = \varnothing.$$

Hence, normal and anomalous samples can be perfectly separated and one can define an anomaly score function that yields perfect results. This is the reason why emb is called an *ideal* embedding function.

Learning an ideal embedding function can be accomplished by using universal function approximators such as neural networks. One of the main difficulties of semi-supervised ASD is the definition of a suitable loss function for training the network because only normal data is available for training. Obtaining an ideal embedding function, i.e. developing a neural network for extracting application-dependent audio embeddings, and designing an ASD system using these embeddings is the goal of this thesis.

1.3 EXAMPLE APPLICATIONS

In [3], the following general applications for anomaly detection are listed: Intrusion detection, credit-card fraud, interesting sensor events, medical diagnosis, law enforcement and earth science. Since the focus of this thesis lies on anomaly detection for audio data, concrete applications will only be given for systems using acoustic data. Numerous applications using other data types will be omitted for the sake of limiting the length of this section. Note that for many applications, an acoustic sensor is only one of multiple different sensors and combining all available information usually leads to much better performance. For example, one can often utilize video cameras alongside acoustic sensors. Some of the following audio-specific applications coincide with the aforementioned general applications:

- Machine condition monitoring for predictive maintenance [44, 46, 96, 108]: Here, normal sounds are recordings of fully-functioning machines in noisy factory environments and anomalies correspond to mechanical failure. Research for ASD is largely promoted through a machine condition monitoring task of the annual DCASE challenge and will serve as the main example application throughout this thesis.

- Intrusion detection in smart home environments to detect burglary [269]: Here, anomalies are sounds of persons walking through the room and looking for hidden objects in boxes and drawers. Normal sounds are emitted by furniture or electronic devices, people or objects outside or in neighboring rooms and other external sources such as traffic or thunderstorms.

- Medical diagnosis: Normal sounds correspond to a healthy state and any anomaly indicates a disease or other medical conditions. Concrete examples are detecting COVID-19 from speech [160] or detecting heart defects from heart sounds [40].

- Detecting crimes or terrorist attacks with surveillance systems in public places [75, 216]: Here, anomalous sounds consist of gunshots, shattering glass or screams whereas normal sounds are a diverse mixture of sounds such as talking people or passing cars.

- Detecting accidents with road surveillance systems [53, 127]: Normal sounds consist of regular traffic noise and anomalous sounds are mostly crashing cars.

- Detecting interesting events in bioacoustic monitoring as for example novel species or individuals that are seen as anomalies [170] or monitoring the condition of beehives [23] similarly to machine condition monitoring

- Detecting erroneous sensor measurements: This is especially important for wireless sensor networks, e.g. in underwater sensor networks [47] where there can also be issues when collecting and transmitting information.

- Acoustic *open-set classification (OSC)* problems: In addition to a fixed set of known classes that should be recognized, a test sample can also belong to none of these known classes. Therefore, OSC tasks can be decomposed into the sub-tasks anomaly detection and *closed-set classification (CSC)*: Anomaly detection is used to decide whether a given sample belongs to one of the known classes, and thus is considered normal, or to an unknown class, i.e. is an anomalous sample. CSC is used to predict to which of the known classes the sample belongs to. One can also view anomaly detection as a special case of OSC with only a single known class denoting all normal samples. Concrete examples are open-set speaker recognition [205] or open-set acoustic scene classification [149]. If not only the class but also the temporal position of a sound event contained in an audio signal of possibly long duration needs to be recognized, this is referred to as sound event detection (SED) [229, 230]. Typical examples are keyword spotting (KWS) [136] or bioacoustic event detection [153, 169]. Note that for these applications the a priori likelihood that a normal event occurs is usually much smaller than the likelihood that an uninteresting, i.e. unknown, event occurs.

It is important to emphasize that the goal of all these tasks is not to distinguish specific anomalous sounds from silence or analyze isolated sound events, which would be relatively simple. The acoustic scenes captured by most recordings contain a complex mixture of many different normal sounds, all of which can possibly result in false alarms in case the ASD system is not performing sufficiently well. Handling this mixture of sounds appropriately is one of the major challenges to overcome in ASD.

1.4 MAIN CONTRIBUTIONS

The main contributions of this thesis are the following:

- Sub-cluster AdaCos, an angular margin loss for semi-supervised ASD, is presented in Chapter 3.
- The relation between one-class losses and angular margin losses is investigated in Chapter 3.
- Multiple methods for obtaining decision thresholds are compared to each other in Chapter 4. Furthermore, F_1-EV, a novel performance measure taking the estimation of decision thresholds into account, is proposed in the same chapter.
- Several different design choices for making a system robust to (acoustic) domain shifts are proposed and compared to each other in Chapter 5. In particular, the angular margin loss AdaProj, which generalizes the sub-cluster AdaCos loss, and a self-supervised learning framework are presented.
- TACos, a loss function for obtaining embeddings that capture the temporal structure of sound events, is presented and evaluated for few-shot KWS in Chapter 6.

At the beginning of each chapter, additional contributions are stated.

1.5 THESIS OUTLINE

The remaining parts of this thesis are structured as follows:

- Chapter 2 reviews the state-of-the-art techniques for extracting audio embeddings for semi-supervised ASD as well as methods for designing ASD systems based on these embeddings.
- Chapter 3 studies the design of a semi-supervised ASD system based on audio embeddings.
- Chapter 4 examines how to estimate good decision thresholds that separate the anomaly scores of normal and anomalous samples using only anomaly scores belonging to normal samples.
- Chapter 5 investigates how to design and train an ASD system such that it is robust against acoustic domain shifts.
- Chapter 6 describes the application of ASD embeddings to acoustic OSC and SED problems.
- Chapter 7 concludes the thesis by summarizing the results and presenting possible directions for future work.

1.6 NOTATION AND PRELIMINARIES

Apart from the notation introduced in the preceding sections, the following notation will be used throughout the thesis:

- $\mathcal{P}(X)$ denotes the power set of X.
- For $N_{\text{classes}} \in \mathbb{N}$ pre-defined classes, the class index function is denoted as $\text{class} : X \to \{1, ..., N_{\text{classes}}\}$. The categorical class label function is denoted as $\text{lab} : X \to [0, 1]^{N_{\text{classes}}}$ with $\sum_{j=1}^{N_{\text{classes}}} \text{lab}(x)_j = 1$ for all $x \in X$. Note that in contrast to the class function, this definition explicitly allows that a sample (partially) belongs to more than a single class.
- Φ denotes the space of permissible neural network architectures for obtaining embeddings and W denotes the corresponding parameter space of the neural networks, i.e. $\Phi = \{\phi | \phi : X \times W \to \mathbb{R}^D\}$. Unless stated otherwise, specific building blocks of these networks may consist of fully-connected layers, convolutional layers, recurrent layers or any other layers and will only be specified if needed to ensure that all presented results are as general as possible.

All neural networks used for the experimental evaluations of this work are implemented using Tensorflow [1].

2 AUDIO EMBEDDINGS FOR ANOMALY DETECTION

The motivation for and the abstract idea of obtaining audio embeddings for semi-supervised ASD has already been presented in Section 1.2. This chapter provides an overview over different audio embeddings and the state-of-the-art methods for designing an ASD system with them. An overview of all necessary steps is shown in Figure 4. In general, an ASD system based on audio embeddings consists of a frontend for extracting input feature representations, a neural network for computing embeddings and a backend for deciding whether an embedding is normal or anomalous. The same structure is also used for machine condition monitoring, which serves as the main example application investigated in this thesis.

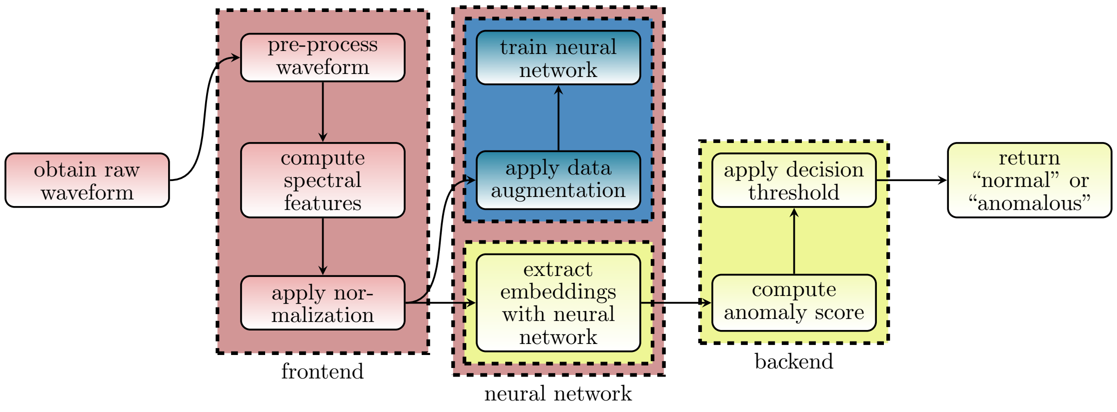

Figure 4: Essential building blocks of a general ASD system based on audio embeddings. Blocks colored in blue are only used for training the system, blocks colored in yellow are only used for inference and blocks colored in red are used for training and inference.

This chapter is structured as follows: Section 2.2 includes all steps needed for computing input feature representations of the audio signals. These steps are pre-processing the audio signal, calculating spectral features and, optionally, normalizing the features. In Section 2.3, different one-class embeddings and the loss functions for obtaining them are presented as a first type of audio embeddings for ASD. A second type of audio embeddings based on using an auxiliary classification task is reviewed in Section 2.4. Section 2.5 contains a description of a few selected audio embeddings pre-trained on large datasets. In Section 2.6, approaches for calculating an anomaly score are presented. Data augmentation techniques for training the embedding extractor are discussed in Section 2.7. Section 2.8 compares the previously presented three embedding types and Section 2.9 contains approaches for combining several ASD models. Evaluation metrics for ASD, OSC and SED are presented in Section 2.10. In Section 2.11, methods for estimating a decision threshold are reviewed. The chapter is concluded with a summary in Section 2.12.

2.1 CONTRIBUTIONS OF THE AUTHOR

Some content of this chapter is presented similarly in the following publications:

- Kevin Wilkinghoff and Alessia Cornaggia-Urrigshardt. "On choosing decision thresholds for anomalous sound detection in machine condition monitoring." In: *24th International Congress on Acoustics (ICA)*. The Acoustical Society of Korea, 2022.
- Kevin Wilkinghoff and Fabian Fritz. "On Using Pre-Trained Embeddings for Detecting Anomalous Sounds with Limited Training Data." In: *31st European Signal Processing Conference (EUSIPCO)*. IEEE, 2023, pp. 186–190.
- Kevin Wilkinghoff and Frank Kurth. "Why do Angular Margin Losses work well for Semi-Supervised Anomalous Sound Detection?" In: *IEEE/ACM Trans. Audio Speech Lang. Process.* 32 (2024), pp. 608–622.
- Kevin Wilkinghoff and Keisuke Imoto. "F1-EV Score: Measuring the Likelihood of Estimating a Good Decision Threshold for Semi-Supervised Anomaly Detection." In: *International Conference on Acoustics, Speech and Signal Processing (ICASSP)*. IEEE, 2024, pp. 256–260.

For publications that are not single-authored, individual contributions of the thesis author and all co-authors to these publications are stated in Section A.1. If not stated otherwise, the content listed in the following paragraph is the sole contribution of the thesis author.

The approaches for estimating a decision threshold as presented in Section 2.11 are also discussed in [247]. Alessia Cornaggia-Urrigshardt assisted with reviewing the literature containing these approaches. The same pre-trained embeddings as described in Section 2.5 are also listed in [250]. [252] contains a similar definition of the compactness loss (Definition 2.3) and the angular margin losses ArcFace (Definition 2.7) and AdaCos (Definition 2.8). The definition and discussion of AUC-ROC contained in Section 2.10 is based on [251].

2.2 INPUT FEATURE REPRESENTATIONS

Before using audio data as input for neural networks that are trained to extract embeddings, a few pre- and post-processing steps are or may be necessary.

2.2.1 *Pre-processing audio signals*

In many monitoring applications, all recorded audio signals have the same length. The reason is that for a continuous observation it is necessary to specify a recording protocol because anomalous sounds may appear arbitrarily in time. For example, when monitoring the condition of machines in factories, these machines are running without interruption. Unless the process of recording shall continue infinitely, one is forced to decide for a finite recording duration. This duration is application-dependent and should be long enough to ensure that normal and anomalous samples can be distinguished but as short as possible to reduce the total inference time, which also includes the recording time. Furthermore, repeatedly recording for the same fixed duration is to be preferred because this simplifies the recording process and all following steps.

In case a uniform recording length cannot be guaranteed, there are several strategies that can be used to handle recordings with varying lengths. The simplest solution is to unify the duration of all recorded audio signals. Audio signals that are too short are padded with silence or repeated and cut appropriately until the desired length is reached. Audio signals that are too long are cut into overlapping segments of the desired length and the mean of the output of the neural network obtained from these segments can be used as the result for the entire initial recording. Another strategy is to use neural network architectures that can handle varying lengths. One possibility is to use several convolutional layers followed by global pooling layers [128] applied to the temporal axis [228]. A popular example is the x-vector architecture developed for speaker recognition [210]. This architecture uses statistics such as the temporal mean and the temporal standard deviation and stacks them into a single representation as the last layer. Another approach is to use recurrent neural networks such as gated recurrent units [28] or long short-term memories [83] that are capable of handling data with varying time dimension by design. More complex approaches are more powerful but require more computational resources for training as well as more training data to avoid overfitting. Therefore, there is not a single perfect choice that can be used for all applications and ASD systems need to be carefully designed depending on the demands of a specific application.

Similarly to the recording duration, it is advisable to also fix a sampling rate that is sufficiently high for capturing normal and anomalous sounds when designing the ASD system for a specific task. This is often directly connected to the acoustic sensor, i.e. microphone to be used and may require expert knowledge. If using different sampling rates, one can decide for a fixed sampling rate and up- or downsample all recordings to this sampling rate. In case particular frequency bands completely contain all anomalous sounds, spectral filtering, e.g. with bandpass filters, can be applied to remove unimportant information and simplify the ASD task.

2.2.2 *Spectral features*

Waveforms are high-dimensional and thus many training samples are needed for training a model for ASD or any other non-trivial task [62]. This is the reason why the dimension of waveforms is often reduced before providing them as input for neural networks. Usually, this is accomplished by computing features based on classical signal processing. The most commonly used features are time-frequency representations such as magnitude spectrograms. These features consist of a frequency and time dimension and thus techniques used in image processing, as for example two-dimensional convolutional neural networks, can be utilized for computing the embeddings. Due to Heisenberg's uncertainty principle, time and frequency resolution cannot simultaneously be chosen to be arbitrarily high. Increasing the frequency resolution degrades the time resolution and vice versa. Therefore, both resolutions have to be balanced and parameter settings have to be adjusted such that the features capture all sounds of interest for a particular application sufficiently well. Apart from using standard time-frequency representations obtained by applying a short-time Fourier transform (STFT), there are many other hand-crafted features with adjustable resolutions such as Mel-frequency scaled spectrograms [211], Mel-frequency cepstral coefficients [36] or features based on perceptual linear prediction [79]. One can also use a combination of features with different resolutions or wavelets [34]. Moreover, multiple hand-crafted features capturing complementary information can be combined to utilize more information in total and improve the performance [236]. This is called ensembling and will be discussed in Section 2.9. For ASD, application-dependent a priori knowledge about the anomalies, needed to design highly sophisticated features, is only rarely available as this requires to analyze anomalous samples, which are usually not available for training. One of the major strengths of neural networks is the ability to learn meaningful data representations by themselves. To utilize this strength, input feature representations that still capture most information present in the original data should be chosen instead of highly processed features.

The vast majority of state-of-the-art ASD systems for machine condition monitoring utilize log-Mel spectrograms as input features with no adaptations to specific machine types [21, 25, 59, 60, 85, 95, 164, 184, 186, 187, 212]. There are only a few minor deviations from this: In [123, 179], a Gammatone filterbank and in [39, 134, 174] regular spectrograms are used instead of or in combination with log-Mel spectrograms. For some systems [39, 112, 135], parameters for extracting log-Mel spectrograms such as window size, hop length and number of Mel bins are manually optimized for different machine types and data domains. In [124], different non-uniform filterbanks are determined for each machine type using Fisher's F-ratio. Again, optimizing these parameters requires access to anomalous data, which is not available in a semi-supervised ASD setting and thus is infeasible. In [140], it has been shown that applying high-pass filters is beneficial to detect anomalies in machine condition monitoring showing that high-frequency information is more important than low-frequency information.

2.2.3 *Normalization*

To ensure that all dimensions of the input feature representations are scaled similarly, a normalization technique can be applied. Some ASD systems perform a standardization of the input features in cepstral domain by subtracting the mean and dividing by the standard deviation of all normal training samples [85, 95, 179]. In [184], the waveforms are rescaled to unit variance and in [135] a Teager-Kaiser energy operator is used to suppress the noise for some machine types with modest improvements in ASD performance. Another simple denoising approach is to apply a median filter along the frequency axis [21]. Other works do not explicitly state a normalization procedure [21, 59, 60, 112, 174, 187] showing that a standardization of the input representations is an optional step. However, nearly all neural network based ASD approaches perform a standardization to all intermediate representations. This is called *batch normalization* [86] and results in a more stable and faster convergence of the training algorithm. To simplify notation for the further course of this thesis, X will denote the space of appropriately pre-processed input feature representations instead of the raw waveforms unless stated otherwise.

2.3 ONE-CLASS EMBEDDINGS

The first type of embedding presented in this chapter is based on directly learning the distribution of normal data with a neural network. Using this distribution, one can compute a likelihood or distance of individual samples to distinguish between normal and anomalous samples. In general, this approach is called *inlier modeling* [96]. Since only a single class consisting of normal data is used, this is also known as *one-class classification* [156].

Among the models used for inlier modeling are deep generative models [17] such as autoregressive models [206], e.g. WaveNet [171] or a masked autoencoder for distribution estimation (MADE) [58], variational autoencoders (VAEs) [102], generative adversarial networks (GANs) [121], e.g. AnoGAN [201] or GANomaly [4], and normalizing flows [105, 172]. VAEs [102] can be seen as a generalization of autoregressive models [27] and thus a VAE with a sufficient number of hidden layers should, in theory, be able to achieve the same ASD performance as autoregressive models. Furthermore, it was shown that normalizing flows can be modified to outperform autoencoders such as VAEs [42, 43]. However, it is also known that normalizing flows have problems when detecting out-of-distribution samples, i.e. anomalies, [104, 161] and thus, by transitivity, VAEs and autogressive models are also not an ideal choice. Moreover, deep autoregressive models [59, 75], normalizing flows [42, 43, 135, 184] or GANs [39, 90] do not aim at projecting data into an embedding space and thus are out of scope for this thesis. Hence, these approaches will not be discussed in detail and the focus will be on (non-variational) autoencoders [82] in general and deep support vector data description (SVDD) for one-class classification [196, 197], which has been shown to outperform at least some generative approaches for ASD, instead.

2.3.1 *Autoencoders*

In the context of this thesis, an autoencoder [82] is a model consisting of two sub-models: An embedding model, called encoder, mapping the input to an embedding space and an additional decoder model mapping an embedding back to the input space. The formal definition of an autoencoder is as follows.

Definition 2.1 (Autoencoder)**.** Let W denote the parameter space of a neural network $\varphi : X \times W \to X$. Then, φ is called an *autoencoder* if it can be written as

$$\varphi = \varphi_d \circ \varphi_e \tag{1}$$

such that $\varphi_e : X \times W_e \to \mathbb{R}^D$, i.e. $\varphi_e \in \Phi$, and $\varphi_d : \mathbb{R}^D \times W_d \to X$ for parameter spaces W_e and W_d. φ_e and φ_d are called *encoder* and *decoder*, respectively. Embeddings $\varphi_e(x, w) \in \mathbb{R}^D$ obtained with an encoder for some $x \in X$ and $w \in W_e$ are also called *code*.

Autoencoders are trained by minimizing the reconstruction loss aiming at teaching the model to reconstruct input samples as accurately as possible. The reconstruction loss is given by the mean squared error (MSE) between the reconstructed input and the input signal and is defined as follows:

Definition 2.2 (Reconstruction loss)**.** Let $Y \subset X$ be finite and let φ denote an autoencoder. Then, the *reconstruction loss* is defined as the mean squared error between input and output of the autoencoder

$$\begin{aligned}
&\mathcal{L}_{\text{rec}} : \mathcal{P}(X) \times \{\varphi | \varphi : X \times W \to X\} \times W \to \mathbb{R}_+, \\
&\mathcal{L}_{\text{rec}}(Y, \varphi, w) := \frac{1}{|Y|} \sum_{x \in Y} \|\varphi(x, w) - x\|_2^2.
\end{aligned} \tag{2}$$

In order for an autoencoder to yield useful results, it needs to be ensured that the autoencoder learns a non-trivial mapping, i.e. not the identity mapping [64]. Otherwise, it holds that $\mathcal{L}_{\text{rec}} \equiv 0$. Hence, the embedding space does not need to have any structure and consequently embeddings of normal and anomalous samples do not need to be different. The most commonly used approaches for ensuring to learn a non-trivial mapping is to increase the difficulty of the task. A possible way to achieve this is to use a code (embedding) dimension that is much smaller than the dimension of the input space (undercomplete autoencoders) or to remove information from input samples, e.g. by randomly masking or modifying entries of the input vectors during training (denoising autoencoders) [5].

Conveniently, the reconstruction loss can also be used as an anomaly score by assuming that anomalous data substantially deviates from normal data. Then, an autoencoder trained to encode and reconstruct normal data cannot reconstruct anomalous data as accurately as normal data and thus yields a higher reconstruction error for anomalous data. However, in noisy environments an autoencoder cannot distinguish between noise and the target sounds and thus both signal components contribute to the reconstruction error with equal weight. This degrades performance, e.g. by causing false alarms, when trying to detect anomalous sounds in noisy environments such as factories.

There are several extensions and variants of basic autoencoders used for ASD. Most autoencoders encode a few consecutive frames of log-Mel spectrograms to reduce the dimension of the input to a manageable size. Usually, sub-classes of the normal data are defined and several autoencoders, one for each sub-class, are trained leading to specialized and thus more accurately modeled distributions of normal data [108]. Another idea is to use a single autoencoder for all classes that is trained to have a low reconstruction error when being conditioned on the correct sub-class and a high reconstruction error when being conditioned on another sub-class. In [95], this is accomplished by using the IDs of specific machines as class labels in the context of machine condition monitoring. In [112], the class labels of the input samples are also encoded and decoded and in [9, 179] a reconstruction loss as well as a classification loss are jointly minimized by using a (weighted) sum of both losses. [186] uses a single hierarchical VAE making use of hierarchical class labels such as machine types and model IDs, which are concatenated with the input feature representations as well as with latent representations. Furthermore, there are different asymmetric approaches regarding input and output of the autoencoder, which all improve ASD performance. In [212], an interpolation deep neural network has been proposed that reconstructs only the center frame of several consecutive frames taken from a log-Mel spectrogram with an autoencoder to remove the effect of the edge frames on the anomaly score, which are difficult to reconstruct. [59] relies on MADE [58] for density estimation, which applies binary masks to the input such that the autoencoder is an autoregressive (or a time-reversed autoregressive) model. Here, the autoencoder does not learn to reconstruct input data but learns conditional distributions, parameterized with Gaussians or a mixture of Gaussians, to predict the likelihood of the input for a specific time step while only depending on the input of previous (or subsequent) time steps. Then, the model is trained by minimizing the negative log-likelihood of the data given by the product of the learned conditional distributions. [235] generalizes the previous approach using attentive neural processes [99], which divide the input spectrogram into a context and a complementary target set. This is achieved by masking random time frames or frequency bins and also encoding the positions of the context set for computing the likelihood of the estimated target set conditioned on the context set.

2.3.2 *Compactness loss*

When using autoencoders to obtain audio embeddings for ASD, decoding the code is actually not needed. It is sufficient to only train an encoder network by computing the MSE between the code of input samples and a center $c \in \mathbb{R}^D$ of a hypersphere in the embedding space. Then, a model can be trained by minimizing the volume of the hypersphere containing all normal samples. In [197], it has been shown that such a one-class approach outperforms commonly used autoencoder architectures or GANs such as AnoGAN [201] when detecting anomalies. The compactness loss incorporating this idea is defined as follows:

Definition 2.3 (Compactness loss)**.** Let $Y \subset X$ be finite. Then, the *compactness loss* is defined as

$$\begin{aligned} &\mathcal{L}_{\text{comp}} : \mathcal{P}(X) \times \mathbb{R}^D \times \Phi \times W \to \mathbb{R}_+, \\ &\mathcal{L}_{\text{comp}}(Y, c, \phi, w) := \frac{1}{|Y|} \sum_{x \in Y} \|\phi(x, w) - c\|_2^2. \end{aligned} \tag{3}$$

The vector $c \in \mathbb{R}^D$ is called *center* and belongs to the weight parameters of the neural network.

Remark. The original definition of the compactness loss also includes an additional weight decay term for regularization [197]. Since using such a regularization term is not strictly necessary and can be used to complement any loss function, this term has been omitted here for the sake of simplicity. All presented theoretical results still hold.

After training, the (squared) Euclidean distance between the embedding of a given sample and the center can be utilized as an anomaly score: A greater distance indicates a higher likelihood for the sample to be anomalous. Similarly as for autoencoders, it needs to be ensured that deep one-class classification models do not learn a trivial solution for minimizing the compactness loss, which in this case corresponds to a parameter setting $w_c \in W$ for a center $c \in \mathbb{R}^D$ such that $\phi(x, w_c) = c$ for all $x \in X$. It is of utmost importance to prevent that the model to be trained is able to learn such a trivial solution. Otherwise, it is impossible to differentiate between normal and anomalous embeddings because all samples are mapped to the same point. Hence, preventing to learn trivial solutions is one of the major difficulties to overcome when training a one-class ASD model with normal data only.

As shown in [197], three conditions can be identified that need to be fulfilled to learn a non-trivial mapping. For simplicity, it will be assumed that all networks $\phi \in \Phi_{\text{simple}}$ have the following structure: Let $L(\phi) \in \mathbb{N}$ denote the number of layers of network $\phi \in \Phi_{\text{simple}}$. Then, $H_l(\phi)$ for $l \in \{0, ..., L(\phi)\}$ are hidden representation spaces that can either be vectors, matrices or tensors, each with a well-defined ordering of the entries allowing to index individual entries of the hidden representations. Now, set $H_0(\phi) := X$ and for $l \in \{1, ..., L(\phi)\}$ iteratively define

$$H_l(\phi) := \{\sigma_l(w(l) \cdot h_{l-1}(x) + b_l) : h_{l-1}(x) \in H_{l-1}(\phi), x \in H_0(\phi) = X\} \quad (4)$$

such that $H_{L(\phi)}(\phi) \subset \mathbb{R}^D$ where $h_l(x) \in H_l(\phi)$ denotes the hidden representation at layer l for input sample $x \in X$, "$\cdot$" denotes a linear operator, which is either a matrix multiplication or a convolution, σ_l denotes the activation function of layer l, $w(l)$ denotes the corresponding weight parameters (excluding the bias term) and b_l denotes the bias term. Using a network with such a structure, the three conditions that need to be met to avoid learning trivial solutions of the compactness loss are captured by the following propositions:

Proposition 2.4. *Using the same notation as in 2.3, let $w_0 \in W$ denote the parameter setting of $\phi \in \Phi_{simple}$ with all weights being equal to zero. Then, $c_0 := \phi(x, w_0) \in \mathbb{R}^D$ is a constant function in $x \in X$ meaning that $\mathcal{L}_{comp}(Y, c_0, \phi, w_0) \equiv 0$ for all $Y \in \mathcal{P}(X)$.*

Proof. Applying a linear operator, which for the considered neural networks can either be a matrix multiplication or a convolution, with all parameters of the operator being zero yields zero in the representation space regardless of the argument. Therefore, the output of each layer is constant, i.e. $\phi(x, w_0) = c_0$ for all $x \in X$. Hence, $\mathcal{L}_{\text{comp}}(Y, c_0, \phi, w_0) \equiv 0$. □

This proposition shows that a center $c \in \mathbb{R}^D$, which is adapted during training of the model, can be learned to be equal to c_0 yielding a trivial solution for minimizing the compactness loss with $w = w_0$. Thus, when training a network by minimizing the compactness loss it needs to be ensured that $c \neq c_0$ by using a non-trainable center. The following proposition shows that using bias terms also allow the network to learn a trivial solution.

Proposition 2.5. *Using the same notation as in 2.3, if any layer of $\phi \in \Phi_{simple}$ has a bias term, then there is a $w_c \in W$ such that $\phi(x, w_c) = c$ for all $x \in X$.*

Proof. Let l_{bias} be the index of the last layer of ϕ with a bias term $b_{l_{\text{bias}}}$. Then, for $w_c \in W$ with $w_c(l_{\text{bias}}) = 0$, it holds that $h_{l_{\text{bias}}}(x) = \sigma_{l_{\text{bias}}}(b_{l_{\text{bias}}})$ for all $x \in X$, i.e. $h_{l_{\text{bias}}}(x)$ is a constant function. Therefore, all subsequent parameters $w_c(l)$ for $l > l_{\text{bias}}$ can be chosen such that $\phi(x, w_c) = c$ for all $x \in X$ if $c \in \text{Im}(\phi)$. □

The last proposition investigates the effect of using bounded activation functions.

Proposition 2.6. *Using the same notation as in 2.3, let $H_l(\phi), H_{l+1}(\phi)$ denote hidden representation spaces belonging to two connected layers of $\phi \in \Phi_{simple}$. Let $\sigma : \mathbb{R} \to \mathbb{R}$ be a monotonic and bounded activation function with $\sup_{a \in \mathbb{R}} \sigma(a) = B \neq 0$ or $\inf_{a \in \mathbb{R}} \sigma(a) = B \neq 0$. If there is an $i \in \{1, ..., \dim(H_l(\phi))\}$ such that $h_l^{(i)} > 0$ or $h_l^{(i)} < 0$ for all $h_l \in H_l(\phi)$, i.e. one component of the hidden representation space has always the same sign. Then, there is a parameter setting $w_c \in W$ such that $\phi(x, w_c) = c$ for all $x \in X$.*

Proof. Without loss of generality assume $\sup_{a\in\mathbb{R}} \sigma(a) = B \neq 0$ and $h_l^{(i)} > 0$ for all $h_l \in H_l(\phi)$ and some $i \in \{1, ..., \dim(H_l(\phi))\}$. Then, by choosing $w_c \in W$ such that $w_c(l)^{(j,k)} = 0$ for $j \in \{1, ..., \dim(H_{l+1}(\phi))\}$ and $k \neq i$, we obtain

$$|h_{l+1}^{(j)} - B| = |\sigma(\sum_{k=1}^{\dim(H_l(\phi))} w_c(l)^{(j,k)} h_l^{(k)}) - B| = |\sigma(w_c(l)^{(j,i)} \underbrace{h_l^{(i)}}_{>0}) - B| < \epsilon$$

for all $\epsilon > 0$ and $w_c(l)^{(j,i)}$ large enough. Hence, $h_{l+1}^{(j)} = B$ is constant. Because this emulates a bias term for layer $H_{l+2}(\phi)$, using Proposition 2.5 finishes the proof. □

Remark. Note that using the commonly used rectified linear unit (ReLU) as an activation function is still possible because Proposition 2.6 only holds for activation functions with an upper or lower bound not equal to zero.

To sum up the previous propositions, a network trained by minimizing the compactness loss should use a non-trainable center that is not equal to $c_0 = \phi(x, w_0)$ as defined in Proposition 2.4, not use any bias terms and not use bounded activation functions to avoid learning a trivial mapping. These propositions also hold in case the network contains pooling or normalization layers because these layers do not utilize any weights and zero is a fixed point if the input is constant. Hence, most commonly used convolutional neural network architectures used as embedding models are captured by these statements.

Another way to prevent the model from learning a constant function is to impose an additional classification task. In [177], an additional *descriptiveness loss* is used whose goal it is to reduce inter-class similarity between classes of an arbitrary, external multi-class dataset, which is only used to regularize the one-class classification task. This is done by minimizing the categorical cross-entropy loss for classification on this additional dataset as a secondary task. For each of the two tasks, another version of the same network with identical structure and tied weights, i.e. having the same weight settings, is used. During training, both losses are jointly minimized using a weighted sum ensuring that the so-called reference network associated with the compactness loss does not learn a constant function because this would prevent the secondary network to be able to classify correctly. In [113, 114], a classification task is defined by using available meta information as classes. During training, a second term consisting of the multiplicative inverse of the compactness loss for the center of all normal samples not belonging to the target class is used to avoid learning a trivial solution.

Note that autoencoders can also be viewed as a way to regularize one-class models. In this context, the encoder is the one-class model mapping the input to an embedding space. Unless the input space X consists of a single point, learning a constant function mapping everything to the center is not an optimal solution for the reconstruction loss because all necessary information for being able to completely reconstruct an arbitrary input sample needs to be encoded, which requires obtaining different embeddings for different input samples.

2.4 AUXILIARY TASK EMBEDDINGS

Instead of directly modeling the distribution of the data to learn a mapping into an embedding space, one can also train a neural network to solve other tasks, so-called *auxiliary tasks*, not directly related to ASD. The underlying assumption is that, to solve an auxiliary task, specific information of the data needs to be captured in the embedding space and that this information is also sufficient to differentiate between normal and anomalous samples. Usually, classification tasks are used for this purpose. By essentially treating the other classes as pseudo anomalies, decision boundaries are learned for the normal data of each class. The difficulty of this approach is that one has to define suitable classes. For machine condition monitoring, possible auxiliary tasks are classifying between machine types [60, 85, 134, 266] or, additionally, between different machine states and noise settings [39, 168, 218], recognizing augmented and non-augmented versions of normal data (self-supervised learning) [60] or predicting the activity of machines [168]. Using an auxiliary task to learn embeddings is also called outlier exposure (OE) [78] because normal samples belonging to other classes than a target class can be considered proxy outliers [184].

To compute the output for many classification tasks solved by neural networks, the softmax function is used while minimizing the categorical crossentropy as a loss function for training. But when training a neural network for the purpose of extracting embeddings, the softmax function only reduces inter-class similarity without explicitly increasing intra-class similarity [223]. To address this issue, losses based on the Euclidean distance as for example triplet loss [233] and center loss [234] have been proposed. The triplet loss uses an anchor input whose distance to a positive sample belonging to the same class is minimized and whose distance to a negative sample belonging to another class maximized. Center loss avoids constructing these triplets as input for training by minimizing the distance to learned center vectors for each class. Recently, loss functions ensuring a margin between different classes such as additive margin softmax layer [223], SphereFace [133], CosFace [224], ArcFace [38] or AdaCos [264] were shown to have better generalization capabilities than losses based on the Euclidean distance because these losses enforce a low intra-class variability. For machine condition monitoring, [85] uses center loss, [134, 135] the additive margin softmax loss and [10, 39, 60, 112, 154, 266] use ArcFace. All of these losses lead to embeddings with a significantly better ASD performance than loss functions without a margin. Therefore, only angular margin losses will be discussed in detail.

2.4.1 *Angular margin losses*

The underlying idea of angular margin losses is to learn an embedding space on the unit sphere and compare two embeddings by calculating the angle between them while ensuring a margin between classes instead of only ensuring linear separability.

One of the most commonly used representative of angular margin losses is ArcFace [38], which will now be reviewed.

Definition 2.7 (ArcFace)**.** Let $Y \subset X$ be finite and $\mathrm{lab}(x)_j \in [0,1]$ denote the j-th component of the categorical class label function $\mathrm{lab} \in \Lambda(N_{\mathrm{classes}})$ where Λ denotes the space of all functions $\mathrm{lab} : X \to [0,1]^{N_{\mathrm{classes}}}$ with $\sum_{j=1}^{N_{\mathrm{classes}}} \mathrm{lab}(x)_j = 1$ for all $x \in X$. Let softmax : $\mathbb{R}^{N_{\mathrm{classes}}} \to [0,1]^{N_{\mathrm{classes}}}$ denote the softmax function, i.e.

$$\mathrm{softmax}(x)_i = \frac{\exp(x_i)}{\sum_{j=1}^{N_{\mathrm{classes}}} \exp(x_j)}. \tag{5}$$

Then, the *ArcFace* loss is defined as

$$\begin{aligned} &\mathcal{L}_{\mathrm{ang}} : \mathcal{P}(X) \times \mathbb{R}^{N_{\mathrm{classes}} \times D} \times \Phi \times W \times \Lambda(N_{\mathrm{classes}}) \times \mathbb{R}_+ \times [0, \frac{\pi}{2}] \to \mathbb{R}_+ \\ &\mathcal{L}_{\mathrm{ang}}(Y, C, \phi, w, \mathrm{lab}, s, m) \\ :=& -\frac{1}{|Y|} \sum_{x \in Y} \sum_{j=1}^{N_{\mathrm{classes}}} \mathrm{lab}(x)_j \log(\mathrm{softmax}(s \cdot \mathrm{sim}_{\mathrm{mar}}(\phi(x,w), c_j, m))) \end{aligned} \tag{6}$$

where $C = (c_1, ..., c_{N_{\mathrm{classes}}})$ and, in this case,

$$\begin{aligned} &\mathrm{softmax}(s \cdot \mathrm{sim}_{\mathrm{mar}}(\phi(x,w), c_i, m)) \\ :=& \frac{\exp(s \cdot \mathrm{sim}_{\mathrm{mar}}(\phi(x,w), c_i, m))}{\sum_{j=1}^{N_{\mathrm{classes}}} \exp(s \cdot \mathrm{sim}_{\mathrm{mar}}(\phi(x,w), c_j, m \cdot \mathrm{lab}(x)_j))} \end{aligned} \tag{7}$$

with

$$\mathrm{sim}_{\mathrm{mar}}(x, y, m) := \cos(\arccos(\mathrm{sim}(x,y)) + m) \tag{8}$$

and

$$\mathrm{sim}(x, y) := \frac{\langle x, y \rangle}{\|x\|_2 \|y\|_2} \in [-1, 1]. \tag{9}$$

The vectors $c_j \in \mathbb{R}^D$ are trainable parameters called *class centers*. The *margin* $m \in [0, \frac{\pi}{2}]$ and *scale parameter* $s \in \mathbb{R}_+$ are both hyperparameters that need to be chosen in advance.

The following intuitive explanation of why the parameter m ensures a margin between classes is similar to the one given in [223]. Define the angle α between an embedding $\phi(x,w) \in \mathbb{R}^D$ and a class center $c \in \mathbb{R}^D$ as

$$\alpha(\phi(x,w), c) := \arccos(\mathrm{sim}(\phi(x,w), c)) \in [0, \pi].$$

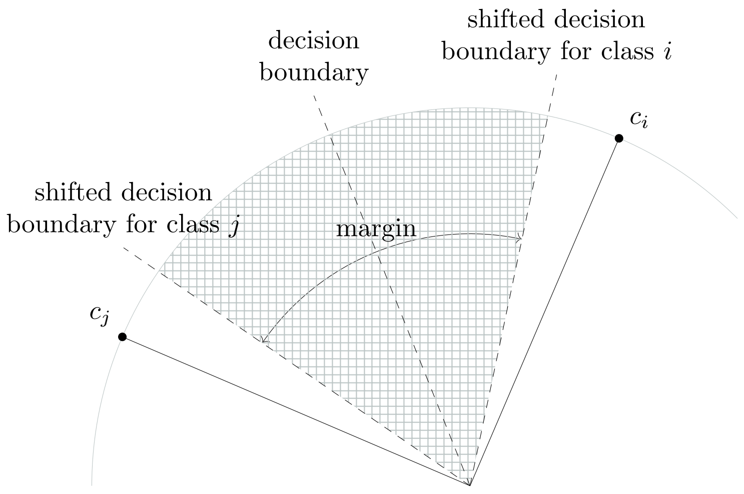
decision boundary
shifted decision boundary for class i
c_i
shifted decision boundary for class j
margin
c_j

Figure 5: Ensuring an angular margin between classes i and j by shifting the decision boundaries. This illustration is inspired by Figure 1 from [223].

Since the softmax function is componentwise strictly monotonically increasing, the following inequality needs to be fulfilled to predict class $i \in \{1, ..., N_{\text{classes}}\}$ for a given sample $x \in X$

$$\alpha(\phi(x, w), c_i) + m < \alpha(\phi(x, w), c_j) \text{ for all } j \neq i.$$

Hence, for $m = 0$ the decision boundary between two classes is the bisector of the angle between both corresponding class centers. Thus, only linear separability between the classes is ensured. For $m > 0$, the decision boundary is effectively shifted closer to c_i, which consequently reduces intra-class variability. Since *all* decision boundaries between two classes are shifted towards their corresponding class centers and thus the inequality does not depend on the choice of i, a margin depending on the chosen hyperparameter m is ensured. An illustration of this explanation can be found in Figure 5.

In [264], it has been shown that the choice of both hyperparameters, the scale parameter s and the margin m, have a significant impact on the posterior probabilities and thus also on the resulting performance. This is illustrated in Figure 6. On the one hand, a scale parameter that is too small limits the maximum posterior probability that can be achieved. This hinders the convergence of training because the model parameters will also be updated in case the angles between embeddings and class centers are already very small. Similarly, a margin that is too large impedes convergence of the training procedure because the posterior probabilities are almost equal to zero even when the angles are very small. On the other hand, a scale parameter that is too large or a margin that is too small lead to the posterior probabilities being equal to one, even for large angles, and thus the model is not sensitive to changes of the angle below a certain point. Therefore, the effect on the sensitivity of the output with respect to the angle is similar when strongly varying the magnitude for both of these parameters and a single appropriately chosen parameter is sufficient for controlling the posterior probabilities. Moreover, it has been shown experimentally that an adaptive scale parameter outperforms using two tuned, but fixed, parameters [264].

Following the main line of argumentation as presented in [264], it will now be briefly explained how the definition of this so-called *dynamically adaptive scale parameter* is motivated. For fixed $x \in X$, the scale parameter should be chosen such that it maximizes the sensitivity of the softmax probability with respect to the corresponding angle. Formally, this means to find the scale parameter $s_0 \in \mathbb{R}_+$ that fulfills

$$\frac{\partial^2}{\partial \alpha_0^2} \frac{\exp(s_0 \cdot \cos(\alpha_0))}{\exp(s_0 \cdot \cos(\alpha_0)) + \sum_{\substack{j=1 \\ \text{lab}(x)_j \neq 1}}^{N_{\text{classes}}} \exp(s_0 \cdot \text{sim}(\phi(x,w), c_j))} = 0,$$

which is a transcendental equation approximately equivalent to

$$s_0 = \frac{\log\left(\sum_{\substack{j=1 \\ \text{lab}(x)_j \neq 1}}^{N_{\text{classes}}} \exp(s_0 \cdot \text{sim}(\phi(x,w), c_j))\right)}{\cos(\alpha_0)}.$$

By conducting experimental evaluations, it can be seen that $\alpha(\phi(x,w), c_j) \approx \frac{\pi}{2}$, i.e. $\phi(x,w)$ and c_j are approximately orthogonal, and thus $\text{sim}(\phi(x,w), c_j) \approx \cos\left(\frac{\pi}{2}\right) = 0$ for all j with $\text{lab}(x)_j = 0$. Therefore, choosing a fixed scale parameter $\tilde{s}^{(0)} \in \mathbb{R}_+$ is the same as choosing a fixed value $\alpha_0^{(0)} \in [0, \frac{\pi}{2}]$ in the equation above. A natural choice for ensuring that the scale parameter is neither too high nor too low is setting $\alpha_0^{(0)}$ to the center of this interval, i.e. $\alpha_0^{(0)} = \frac{\pi}{4}$, resulting in

$$\tilde{s}^{(0)} = (\cos\left(\frac{\pi}{4}\right))^{-1} \cdot \log\left(\sum_{\substack{j=1 \\ \text{lab}(x)_j \neq 1}}^{N_{\text{classes}}} \exp(s_0 \cdot \cos\left(\frac{\pi}{2}\right))\right) = \sqrt{2} \cdot \log(N_{\text{classes}} - 1).$$

During training, the angle $\alpha(\phi(x,w), c_i)$ is decreasing, which also decreases the sensitivity of the softmax probability to further changes of this angle (see Figure 6). To avoid this and preserve the same sensitivity, the scale parameter should also be decreased. By monitoring the median of all angles between the training samples and their corresponding class centers at training step $t \in \mathbb{N}_0$, denoted by $\alpha_{\text{med}}^{(t)} \in [0, \frac{\pi}{2}]$, the training progress can be monitored, too. However, initially these angles may be relatively large. To increase sensitivity in these early iterations, the median angle is forced to be smaller than $\frac{\pi}{4}$ by setting $\alpha_0^{(t)} = \min\{\frac{\pi}{4}, \alpha_{\text{med}}^{(t)}\}$. Furthermore, the term

$$\sum_{\substack{j=1 \\ \text{lab}(x)_j \neq 1}}^{N_{\text{classes}}} \exp(\tilde{s}^{(t-1)} \cdot \text{sim}(\phi(x,w), c_j))$$

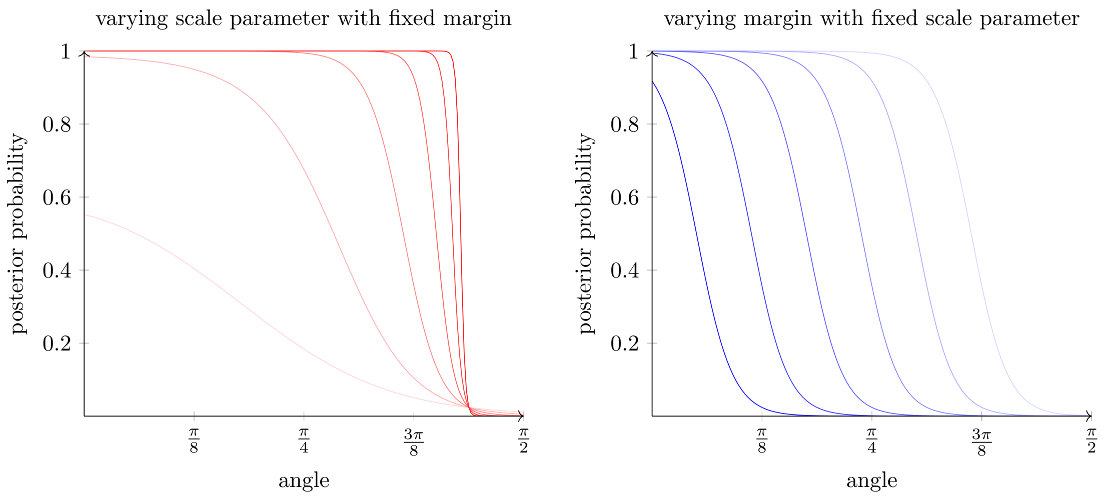

Figure 6: Effects of varying the margin and the scale parameter of an angular margin loss on the relationship between angle and posterior probability. Brighter colors indicate smaller parameters and darker colors indicate higher parameters. This illustration is based on Figure 2 from [264].

is computed for each sample of a mini-batch and the mean, denoted by $B_{\text{avg}}^{(t)}$, is taken to more accurately reflect the current training progress. In conclusion, the dynamically adaptive scale parameter for $t > 0$ is set to

$$\tilde{s}^{(t)} = \frac{\log B_{\text{avg}}^{(t)}}{\cos(\alpha_0^{(t)})} = \frac{\log B_{\text{avg}}^{(t)}}{\cos\left(\min(\frac{\pi}{4}, \alpha_{\text{med}}^{(t)})\right)}.$$

Using this dynamically adaptive scale parameter, the AdaCos loss [264] is defined as follows.

Definition 2.8 (AdaCos)**.** Using the same notation as in Definition 2.7, let $Y^{(t)} \subset Y$ denote all samples belonging to a batch of size $N_{\text{batch}} \in \mathbb{N}$, i.e. $|Y^{(t)}| = N_{\text{batch}}$. Let $\alpha(\phi(x, w), c) := \arccos(\text{sim}(\phi(x, w), c)) \in [0, \pi]$ denote the angle between $\phi(x, w) \in \mathbb{R}^D$ and $c \in \mathbb{R}^D$. Further, let the *dynamically adaptive scale parameter* $\tilde{s}^{(t)} \in \mathbb{R}_+$ at training step $t \in \mathbb{N}_0$ be defined as

$$\tilde{s}^{(t)} := \begin{cases} \sqrt{2} \cdot \log(N_{\text{classes}} - 1) & \text{if } t = 0 \\ \frac{\log B_{\text{avg}}^{(t)}}{\cos\left(\min(\frac{\pi}{4}, \alpha_{\text{med}}^{(t)})\right)} & \text{else} \end{cases} \tag{10}$$

where $\alpha_{\text{med}}^{(t)} \in [0, \frac{\pi}{2}]$ denotes the median of all angles $\alpha(\phi(x, w), c_{\text{class}(x)})$ with $x \in Y^{(t)}$ and $\text{class}(x) \in \{1, ..., N_{\text{classes}}\}$. For $w^{(t)} \in W$,

$$B_{\text{avg}}^{(t)} := \frac{1}{N_{\text{batch}}} \sum_{x \in Y^{(t)}} \sum_{\substack{j=1 \\ \text{lab}(x)_j \neq 1}}^{N_{\text{classes}}} \exp\left(\tilde{s}^{(t-1)} \cdot \text{sim}(\phi(x, w^{(t)}), c_j)\right) \tag{11}$$

is the sample-wise average over all summed logits belonging to the non-corresponding classes. Then, the *AdaCos* loss is defined as

$$\begin{aligned}&\mathcal{L}_{\text{ada}} : \mathcal{P}(X) \times \mathbb{R}^{N_{\text{classes}} \times D} \times \Phi \times W \times \Lambda(N_{\text{classes}}) \to \mathbb{R}_+\\&\mathcal{L}_{\text{ada}}(Y, C, \phi, w, \text{lab}) \coloneqq \mathcal{L}_{\text{ang}}(Y, C, \phi, w, \text{lab}, \tilde{s}, 0).\end{aligned} \tag{12}$$

2.4.2 *Handling imbalanced data*

When using an auxiliary classification task, it may be the case that the numbers of training samples for each of the considered classes are highly imbalanced. This leads to a learned bias towards specific classes when training a model, which is usually not favourable for computing embeddings and thus should be avoided. There are several techniques to counteract this effect [92, 214] as for example implemented in the imbalanced-learn package [119]. In general, one can distinguish between two major paradigms: Data-level methods and algorithm-level methods. Data-level approaches assign different likelihoods to individual samples for being used as training samples and can be divided into oversampling and undersampling methods. For oversampling, random training samples belonging to classes with fewer training samples are used multiple times until there are as many samples for each class as for the class with the highest number of training samples. For undersampling, only as many random training samples as belonging to the class with the fewest samples are used for each class. There are also more sophisticated sampling methods such as the synthetic minority over-sampling technique (SMOTE) [24]. Here, existing training samples of the minority classes are not simply sampled uniformly at random but linear interpolations between training samples and one of their nearest neighbors are used as synthetic training samples to balance the number of samples per class. Algorithm-level approaches use weights or so-called importance factors for different classes with respect to the number of samples available and apply them during training. One example is weighting the loss associated with each sample such that samples belonging to classes with fewer training samples have a greater contribution to the gradient for updating the parameters of a neural network. Another example is the Focal loss [129], which assigns more weight to samples that are not classified correctly during training.

2.5 PRE-TRAINED EMBEDDINGS

Instead of using an auxiliary task for training the embedding model on an application-dependent dataset, one can also utilize such an auxiliary task on an external dataset [190]. Usually, large datasets are used for this purpose and the resulting embeddings are called *pre-trained* embeddings. The assumption is that the learned embeddings have encountered many diverse data samples and thus should also encode information useful for detecting anomalies on a small application-dependent dataset. Using pre-trained embeddings is especially promising when the number of training samples for the actual application is very small, making it difficult to learn useful representations. Another advantage of using pre-trained embeddings is that these embeddings can be used for multiple applications or novel sound classes without the need of specifically training an individual model for each task from scratch.

There are several systems for ASD [68, 239] and OSC [162, 237] based on pre-trained audio embeddings and studies comparing these embeddings for ASD [158] or audio classification tasks [67] in settings with sufficient training data. Another approach is to use image embeddings for ASD [159] or to apply them for zero-shot audio classification [41]. In [166], it is shown that combining multiple hidden representations of pre-trained neural networks improves the performance. A few commonly used pre-trained embeddings will now be briefly reviewed:

- *VGGish* [80] is a modified version of the VGG network [207], named after the Visual Geometry Group from the University of Oxford, with a similar architecture. The network is pre-trained in a supervised manner on a preli-mary version of YouTube-8M [2], which consists of 2.6 billion audio segments from YouTube videos belonging to a total of 3628 classes. The resulting embeddings have a feature dimension of 128 with an additional time dimension resulting from a sliding window of 960 ms with no overlap applied to the waveforms.

- *Kumar* embeddings [111] are extracted using a convolutional neural network (CNN) with a VGG-style architecture [207]. The network is pre-trained in a supervised manner on the so-called balanced subset of AudioSet [57] that consists of around $22,000$ audio clips from YouTube videos belonging to 527 sound classes. The resulting embeddings have a feature dimension of 1024 and no time dimension because of a global temporal pooling operation inside the network.

- *OpenL3* [32] is a network trained to extract *look, listen, and learn (L3)* embeddings [6, 7]. There are multiple versions of this network: One is pre-trained on a music subset and the other one on an environmental subset of AudioSet [57] consisting of 296K and 195K YouTube videos, respectively. The network is trained in a self-supervised manner to decide whether a video frame and the log-spectrogram of an audio clip with a length of one second do or do not belong together using a convolutional audio and a convolutional video sub-network. During training, the embeddings of both sub-networks are concatenated and further processed with a binary classification module consisting of two fully-connected and a softmax layer. After training, only the audio sub-network is needed to extract embeddings from audio data. The resulting embeddings have a feature dimension of 512 with an additional time dimension resulting from a sliding window of one second with a hop size of 0.1 seconds applied to the waveforms.

- *Pre-trained audio neural network (PANN)* [110] is a combination of a one-dimensional sub-network applied to waveforms (Wavegram-CNN) and a two-dimensional sub-network applied to log-Mel spectrograms. Both output representations are concatenated and further processed with another two-dimensional sub-network. The entire network is pre-trained in a supervised manner on AudioSet [57] using a total of $1,934,187$ audio clips from YouTube videos belonging to 527 sound classes. As the difference in performance between including and not including Wavegram-CNN is relatively small, only the sub-network with a VGG-like architecture pre-trained on log-Mel spectrograms (CNN14) is used for the experiments conducted in this thesis. The resulting embeddings have a feature dimension of 2048 with no time dimension because of a global temporal pooling operation inside the network.

2.6 COMPUTING AN ANOMALY SCORE

After projecting audio data into a suitable embedding space, the next step in the ASD processing chain is to calculate an anomaly score. As stated in Chapter 1, an anomaly score of a sample $x \in X$ is a value $\text{score}(x) \in \mathbb{R}$ indicating how likely this sample is to be anomalous with higher values corresponding to higher likelihoods. To achieve this, a given sample x is first projected into the embedding space $\mathbb{R}^D$ by applying a neural network $\phi \in \Phi$ with parameters $w \in W$. Afterwards, a scoring function $\text{score}_{\text{emb}} : \mathbb{R}^D \to \mathbb{R}$ is applied to the embedding. Hence, the anomaly score is actually a composition of two functions, i.e. $\text{score} = \text{score}_{\text{emb}} \circ \phi$ with $\text{score}(x, w) = \text{score}_{\text{emb}}(\phi(x, w))$. This section is dedicated to presenting several possible choices for setting $\text{score}_{\text{emb}}$.

Depending on the type of model used for extracting the embeddings, there are often canonical choices for computing an anomaly score: For models trained with one-class losses, the negative sample-wise loss, e.g. the reconstruction error [33, 95, 123, 174, 186, 212, 235] or the negative log-likelihood [42, 43, 59, 235] of a single sample, can be utilized as an anomaly score. For models trained with an auxiliary classification task, the negative posterior probabilities [9, 11, 21, 60, 85, 134, 183, 232], or the cosine distance (CD) between an extracted embedding and the learned class centers can be used [10, 25, 26, 39, 134, 217, 218, 259, 266]. Other works utilize the Mahalanobis distance [39, 259] or the Euclidean distance [113, 114, 164].

It is also possible to train an additional model on the set of normal embeddings to estimate their distribution and being able to calculate an anomaly score by using this model. In [96], this is called a *sequential approach* because first an outlier-exposed model is used to extract embeddings and then inlier modeling is applied to obtain an anomaly score. Examples of such models are a Gaussian mixture model (GMM) [68, 76, 114, 115, 155, 158, 159, 187], local outlier factor (LOF) [10, 39, 114, 115, 154, 155], k-nearest neighbors (k-NN) [39, 115, 154, 155, 164, 219, 266] or probabilistic linear discriminant analysis (PLDA) [185] as done in [239]. Using such a sequential approach is especially important for pre-trained embeddings, since there is not always a canonical choice for computing an anomaly score as the training process of the embedding model is usually not related to the ASD task. In [159], the ASD performances obtained when using a GMM, a one-class support vector machine (OCSVM), an isolation forest, a Bayesian GMM, a kernel density estimator or an autoencoder for pre-trained embeddings have been compared and concluded that using a GMM or OCSVM yield the best results. Often, the dimension of pre-trained embeddings is reduced by applying techniques such as principal component analysis (PCA) [68, 158, 239] or linear discriminant analysis (LDA) [239] before inserting them into one of the previously mentioned models for calculating an anomaly score.

Note that many ASD systems utilize multiple ways for computing an anomaly score by choosing a different method for each class to optimize the ASD performance or by ensembling multiple metrics or models (see Section 2.9). Examples are to use the sum of the MSE and posterior classification probabilities [9] or using the frame-level reconstruction errors of a one-class model as input features for a GMM [76]. In [68], the dimension of the temporal mean of openL3 embeddings is reduced with PCA and the result is concatenated with reconstruction errors from autoencoders to use them as input features for a GMM.

2.7 DATA AUGMENTATION

To increase the generalization capabilities of a data-driven model, one should use as much proper training data as possible. However, available training data is usually limited and recording additional training data requires at least some effort or may not be feasible. A more efficient approach is to modify available training samples to simulate additional training data, which is called *data augmentation* [64]. In this section, the three data augmentation approaches most frequently used for ASD, namely mixup [262], SpecAugment [173] and different methods for simulating anomalous data, will be presented.

2.7.1 *Mixup*

Due to its simplicity and effectiveness, one of the most popular data augmentation techniques for audio data is *mixup* [262]. It is also used for several ASD systems [9–11, 21, 25, 60, 112, 164, 182]. The idea of mixup is to linearly interpolate between random training samples and their corresponding categorical class labels to generate new samples during training. Formally, mixup is defined as follows:

Definition 2.9 (Mixup). Let $x_1, x_2 \in X$ be random training samples. Then, for $\lambda \in [0,1]$ with $\lambda \sim \text{Beta}(\beta_{\text{mix}}, \beta_{\text{mix}})$ the sample mixing function $\text{mix}_x : X \times X \times [0,1] \to X$ and the label mixing function $\text{mix}_{\text{lab}} : [0,1]^{N_{\text{classes}}} \times [0,1]^{N_{\text{classes}}} \times [0,1] \to [0,1]^{N_{\text{classes}}}$ are defined as

$$\begin{aligned} \text{mix}_x(x_1, x_2, \lambda) &= \lambda x_1 &&+ (1-\lambda)x_2, \\ \text{mix}_{\text{lab}}(x_1, x_2, \lambda) &= \lambda \,\text{lab}(x_1) &&+ (1-\lambda)\,\text{lab}(x_2). \end{aligned}$$

Usually, $\beta_{\text{mix}} = 1$ is used without any significant difference in the resulting performance and thus $\lambda \sim \mathcal{U}(0,1)$. Also, note that

$$\begin{aligned} \sum_{j=1}^{N_{\text{classes}}} \text{mix}_{\text{lab}}(x_1, x_2, \lambda)_j &= \lambda \sum_{j=1}^{N_{\text{classes}}} \text{lab}(x_1)_j + (1-\lambda) \sum_{j=1}^{N_{\text{classes}}} \text{lab}(x_2)_j \\ &= \lambda + (1-\lambda) = 1. \end{aligned}$$

and therefore $\text{mix}_{\text{lab}}(x_1, x_2, \lambda) \in [0,1]^{N_{\text{classes}}}$ is a valid categorical class label.

There are several variants of mixup. For machine condition monitoring, it has been proposed to only mix samples of individual machines or parameter settings belonging to the same machine type [25]. Mixup can also be applied to intermediate representations of a network instead of the input representations. This modification is called manifold mixup [220]. One can also combine two samples in multiple other ways than using linear interpolations as for example by concatenating different parts of two audio signals or spectral features. A collection of ways to mix samples can be found in [213].

2.7.2 *SpecAugment*

SpecAugment is the combined application of three different data augmentation techniques, namely *frequency masking*, *time masking* and *time warping*. Originally, SpecAugment [173] has been developed to modify time-frequency representations for automatic speech recognition (ASR) but is also used for ASD [9, 11, 112, 164, 219]. For frequency and time masking, random frequency bands or time frames of random size are masked with zeros. Usually, multiple time and frequency masks of relatively small size are used. For time warping, the time dimension is randomly split into two regions of which one is squeezed and the other is stretched with a random degree. An illustration of SpecAugment can be found in Figure 7. To adjust the effects of SpecAugment, manually tuned hyperparameters for controlling the number of time and frequency masks as well as their maximum size and a time warp parameter are used. In [9], masking randomly sized squares of time-frequency representations while training an autoencoder led to a better ASD performance than when applying SpecAugment, when only masking frequencies or when only masking time frames during training. Furthermore, some works used similar methods as SpecAugment such as shifting time frames in time [21] or spectral warping [60].

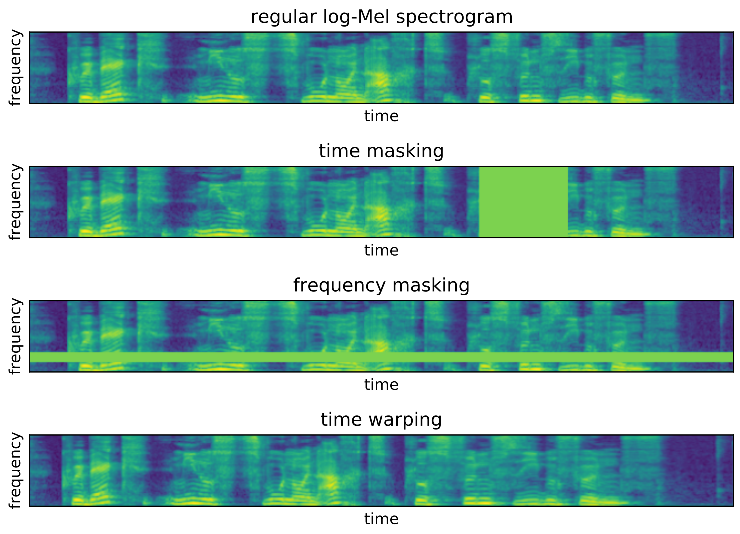

Figure 7: Illustration of the three different data augmentation techniques used when applying SpecAugment. This Figure strongly resembles Figure 1 contained in [173].

2.7.3 *Simulating anomalies*

A data augmentation approach with a completely different goal than creating additional normal samples is to *simulate anomalies* by modifying normal samples. However, to have a significant impact on the ASD performance simulated anomalies need to be realistic, i.e. very similar to real anomalies. Since acquiring specific knowledge about anomalies still requires access to anomalous training samples, this is in many cases out of scope for a specific semi-supervised ASD task. Still, there are some non-specific methods that can be applied to simulate anomalies for various tasks.

In the context of machine condition monitoring, normal data belonging to other machine IDs and machine types from the same dataset are used as proxy outliers and a binary classifier is trained for each machine ID [183, 184]. In [112], only normal data belonging to the same machine type but to other machine IDs is used to train a binary classifier. Similarly, [43] uses normal data belonging to other machine types as outliers for training a normalizing flow. Note that this is very similar to using an auxiliary classification task. The only difference is that another model is trained for each class instead of training a single model for all classes. Hence, all models trained to extract auxiliary task embeddings can also be viewed as utilizing data belonging to other classes as proxy-outliers without explicitly stating this and thus other normal sounds are implictly used as pseudo-anomalies by many state-of-the-art ASD systems.

Another idea to simulate anomalies is to modify normal samples and treat these modified samples as if they belong to an additional anomalous class, which is a

Table 2: Advantages and disadvantages of different types of audio embeddings. The rating scale consists of ++ (very advantageous), + (advantageous), − (disadvantageous) and −− (very disadvantageous).

	one-class embeddings	auxiliary task embeddings	pre-trained embeddings
ASD performance	+	++	−
OSC and SED performance	−	++	−
data requirements	+	−	++
training effort	−−	+	++
expandability	+	−−	++
data augmentation possibilities	+	++	−
affected by imbalanced data	++	−−	++
anomaly score computation	++	++	−
anomaly localization	+	−	−−

self-supervised learning (SSL) approach. In [85], pitch shifting, time stretching and image transformations of the spectrograms are used to simulate anomalies. In [134] mixup with a fixed small mixing coefficient is used to create pseudo-anomalies. [26] proposes a method called *statistics exchange* and shows that this approach outperforms applying mixup when simulating anomalies. This method consists of swapping first- and second-order statistics of two normal samples for randomly chosen consecutive frequency bands or time frames. Utilizing SSL for training an embedding model will be discussed in more detail in Section 5.7. A more complex procedure to simulate anomalous samples is described in [107]. Here, the authors propose a rejection sampling algorithm that uses latent representations of an autoencoder and a GMM to generate anomalous sounds.

2.8 COMPARISON OF DIFFERENT EMBEDDING TYPES

To recapitulate the different types of embeddings presented in the previous sections, their advantages and disadvantages as summarized in Table 2 will now be discussed. When comparing the embeddings with respect to the resulting ASD performance, auxiliary task embeddings usually perform best [50, 72], followed by one-class embeddings. Pre-trained embeddings perform worst but still yield better results than random guessing. For OSC and SED tasks, the performances obtained with different embedding types are ranked similarly because the auxiliary task can be chosen as the classification task between the known classes of interest and thus the auxiliary task embeddings are well-suited for discriminating between the known classes. For one-class embeddings, the performance is slightly worse due to differently scaled anomaly scores obtained for each class making it difficult to determine the correct known class via maximum likelihood. When comparing the data requirements for training the different types of embeddings, pre-trained embeddings do not need any training data by definition but only a few normal samples, down to a single one, to be able to compare given test samples to them.

One-class embeddings need more normal samples for training the model. Training auxiliary task embeddings not only requires access to a sufficient number of training samples but also additional meta information to be used as class labels and thus have the strongest data requirements. One can also choose to use a self-supervised auxiliary task to artificially generate class labels, but the performance is usually worse when using manually created class labels. The effort of training a model is lowest for pre-trained embeddings because the model is already trained. For auxiliary task embeddings, a single model is trained for all normal classes whereas for one-class embeddings usually several models are trained, one for each normal sound event class, unless an extended approach consisting of training a single model for multiple classes is used. This also means that when expanding the ASD system with an additional normal sound event class, for single-class embeddings one can train an additional model for this class and, for the other classes, keep the remaining models as they were. For auxiliary task embeddings, the whole system needs to be re-trained. For pre-trained embeddings, no additional training is required. There are several possibilities to apply data augmentation techniques when training an ASD system based on auxiliary task embeddings as presented in Section 2.7. Some of these techniques can also be applied when training models based on one-class embeddings. However, for pre-trained embeddings the use of data-augmentation techniques is very limited unless one applies some form of transfer learning [255] because otherwise no training is taking place. Because of the same reason, pre-trained embeddings are not affected by imbalanced classes. Furthermore, imbalanced classes do not affect one-class embeddings because the class-specific models are trained independently of each other. Although there are techniques to counter the effects of imbalanced classes for auxiliary task embeddings, severely imbalanced classes are still a problem. To compute an anomaly score, for one-class and auxiliary task embeddings there are canonical as well as several other choices (see Section 2.6) whereas for pre-trained embeddings there are in general no canonical ways to calculate anomaly scores. Last but not least, at least some one-class models can be used for localizing anomalies in time, e.g. by utilizing a time-wise reconstruction error. When using auxiliary task embeddings, in general the only direct way to localize anomalies is to use a windowing approach, which often degrades the ASD performance. For many pre-trained embeddings, it is not even possible to choose a window size because the model has been trained with a fixed, relatively large, window size.

2.9 ENSEMBLING

Different models or the embeddings obtained with them correspond to different views on the input data. Since these different views may result in complementary information about the data, multiple models can be utilized in a single system. Such a system is called an *ensemble* [54]. Usually, an ensemble outperforms all individual sub-systems but inherently requires much more computational resources.

For ASD with audio embeddings, there are two main ensembling approaches: The first approach is to utilize multiple backends for a single embedding model [168, 198, 218] and the second approach is to train multiple sub-systems with different embedding models and combine their output [59, 60, 76, 85, 95, 112, 135, 219]. Often both approaches are applied at once, resulting in even larger ensembles [33, 39, 115, 232]. Another more complex ensembling approach is presented in [21]. Here, an autoencoder and a supervised classification model are combined with an additional contrastive loss between both resulting embeddings and the system is jointly trained by minimizing all three loss functions. Note that, in general, the higher the number of models used for an ensemble the smaller the obtained performance improvements while the computational overhead in terms of memory and time is constant and thus the return on investment is diminishing. Hence, while for academic purposes one may choose to use a huge ensemble to outperform other published ASD systems, for practical applications the size of an ensemble should be considered economically.

Usually, an ensemble is created by taking the mean of anomaly scores of several models or systems [59, 60, 85, 112, 115, 168, 198, 232]. To take differently scaled anomaly scores resulting from using different backends into account, the anomaly scores are often normalized before combining them by using the anomaly scores of normal training samples as reference values. Some systems use a weighted mean of (normalized) anomaly scores [33, 39, 76, 95, 135, 218, 219] with weights that are optimized to improve the ASD performance on a development dataset. Hence, these systems also use anomalous samples as training data, which, strictly speaking, is not allowed in a semi-supervised ASD setting. However, one could also argue that every ASD system is evaluated with some anomalous samples during development and therefore uses anomalous data for training. Moreover, one can raise the questions of whether it is possible at all to define the term *normal* without having access to application-dependent anomalous samples and, in conclusion, whether unsupervised or semi-supervised anomaly detection settings truly exist. Answering these questions is out of scope for this thesis as they appear to be of purely philosophical nature. Still, the dataset of an ASD task can be designed to prevent explicitly utilizing anomalous samples for tuning hyperparameters, e.g. by using data belonging to different machine types for developing and evaluating the system (see Section 5.2).

2.10 EVALUATION METRICS

Evaluating the performance of a trained system is important to be able to compare different design choices, optimize hyperparameters during the development of a system and allows to objectively compare different systems. For this purpose, specifically designed evaluation metrics are used. In this section several commonly used metrics will be reviewed for ASD, OSC and SED.

2.10.1 *Anomaly detection*

For ASD, several evaluation metrics can be used. In general, one can distinguish between *threshold-dependent* and *threshold-independent* evaluation metrics.

Threshold-dependent evaluation metrics are based on a fixed decision threshold $\theta \in \mathbb{R}$. When viewing anomaly detection as a binary classification problem with anomalies as positive samples and normal samples as negative ones, there are two errors that can occur for a test sample $x \in X_{\text{test}} \subset X = X_{\text{normal}} \cup X_{\text{anomalous}}$:

$$x \in X_{\text{normal}} \quad \text{but} \;\; \text{score}(x) > \theta \text{ (false positive)} \tag{13}$$

or

$$x \in X_{\text{anomalous}} \quad \text{but} \;\; \text{score}(x) \leqslant \theta \text{ (false negative)}. \tag{14}$$

Let $A_{\text{pred}}(X_{\text{test}}, \text{score}, \theta) := \{x \in X_{\text{test}} : \text{score}(x) > \theta\} \subset X_{\text{test}}$ denote the set of predicted anomalies. Let X_{normal} and $X_{\text{anomalous}}$ be fixed. To count both errors for the entire test set X_{test}, we define the cardinality of the set of false positives (FP) and the set of false negatives (FN) as

$$\mathsf{FP}(X_{\text{test}}, \text{score}, \theta) := |A_{\text{pred}}(X_{\text{test}}, \text{score}, \theta) \cap X_{\text{normal}}| \tag{15}$$

and

$$\mathsf{FN}(X_{\text{test}}, \text{score}, \theta) := |(X_{\text{test}} \backslash A_{\text{pred}}(X_{\text{test}}, \text{score}, \theta)) \cap X_{\text{anomalous}}|. \tag{16}$$

Similarly, one can define the cardinality of the set of true positives (TP) and the set of true negatives (TN) as

$$\mathsf{TP}(X_{\text{test}}, \text{score}, \theta) := |A_{\text{pred}}(X_{\text{test}}, \text{score}, \theta) \cap X_{\text{anomalous}}| \tag{17}$$

and

$$\mathsf{TN}(X_{\text{test}}, \text{score}, \theta) := |(X_{\text{test}} \backslash A_{\text{pred}}(X_{\text{test}}, \text{score}, \theta)) \cap X_{\text{normal}}|. \tag{18}$$

Since the final evaluation metrics are based on these cardinalities, they are also called *intermediate statistics*. By normalizing these cardinalities, we obtain the corresponding error rates

$$\begin{aligned}
\mathsf{FPR}(X_{\text{test}}, \text{score}, \theta) &:= \frac{\mathsf{FP}(X_{\text{test}}, \text{score}, \theta)}{|X_{\text{test}} \cap X_{\text{normal}}|} && \in [0,1] \\
\mathsf{FNR}(X_{\text{test}}, \text{score}, \theta) &:= \frac{\mathsf{FN}(X_{\text{test}}, \text{score}, \theta)}{|X_{\text{test}} \cap X_{\text{anomalous}}|} && \in [0,1] \\
\mathsf{TPR}(X_{\text{test}}, \text{score}, \theta) &:= \frac{\mathsf{TP}(X_{\text{test}}, \text{score}, \theta)}{|X_{\text{test}} \cap X_{\text{anomalous}}|} && \in [0,1] \\
\mathsf{TNR}(X_{\text{test}}, \text{score}, \theta) &:= \frac{\mathsf{TN}(X_{\text{test}}, \text{score}, \theta)}{|X_{\text{test}} \cap X_{\text{normal}}|} && \in [0,1].
\end{aligned} \tag{19}$$

Note that one can easily see that $\mathsf{FPR}(X_{\text{test}}, \text{score}, \theta) = 1 - \mathsf{TNR}(X_{\text{test}}, \text{score}, \theta)$ and $\mathsf{FNR}(X_{\text{test}}, \text{score}, \theta) = 1 - \mathsf{TPR}(X_{\text{test}}, \text{score}, \theta)$. Thus, *false positive rate (FPR)* and *true negative rate (TNR)* measure one error type and *false negative rate (FNR)* and *true positive rate (TPR)* measure the other error type. For directly comparing two different anomaly detection systems, a single metric incorporating both error types is much easier to handle. The most commonly used metric for this purpose is the F_1 *score* given by

$$\begin{aligned} &\mathsf{F}_1(X_{\text{test}}, \text{score}, \theta)\\ &:= \frac{\mathsf{TP}(X_{\text{test}}, \text{score}, \theta)}{\mathsf{TP}(X_{\text{test}}, \text{score}, \theta) + 0.5(\mathsf{FP}(X_{\text{test}}, \text{score}, \theta) + \mathsf{FN}(X_{\text{test}}, \text{score}, \theta))} \\ &= \frac{2 \cdot \mathsf{TP}(X_{\text{test}}, \text{score}, \theta)}{|A_{\text{pred}}(X_{\text{test}}, \text{score}, \theta)| + |X_{\text{test}} \cap X_{\text{anomalous}}|} \in [0, 1], \end{aligned} \tag{20}$$

which is the harmonic mean of *precision* and *recall* defined as

$$\text{precision}(X_{\text{test}}, \text{score}, \theta) := \frac{\mathsf{TP}(X_{\text{test}}, \text{score}, \theta)}{|A_{\text{pred}}(X_{\text{test}}, \text{score}, \theta)|} \quad \in [0, 1] \tag{21}$$

and

$$\text{recall}(X_{\text{test}}, \text{score}, \theta) := \mathsf{TPR}(X_{\text{test}}, \text{score}, \theta) \quad \in [0, 1]. \tag{22}$$

Determining an optimal decision threshold in a semi-supervised setting is highly non-trivial (see Section 2.11) and threshold-dependent evaluation metrics largely depend on the quality of the estimated decision threshold. Hence, threshold-dependent evaluation metrics may not accurately reflect the performance of an ASD system.

Threshold-independent evaluation metrics are more objective since they do not rely on a chosen threshold and thus give a more complete picture of the performance of an anomaly detection system [3, 48]. Nevertheless, for any practical application determining a decision threshold is still needed and thus the F_1 score is still an important evaluation metric despite being less suitable for comparing system performances than threshold-independent metrics. A commonly used approach is to utilize both error types, false positives and false negatives, for all possible thresholds and plot the results against each other. Examples are the receiver operating characteristic (ROC)-curve, which uses FPR and TPR, and the detection error tradeoff (DET)-curve, which uses FPR and FNR as depicted in Figure 8. Since the curves themselves are difficult to compare to each other for different anomaly detection systems, metrics expressed as a single number are derived from these curves. One possibility is to take the *area under the receiver operating characteristic curve (AUC-ROC)* [19], which is also the most commonly used metric for evaluating ASD systems.

Let $(\theta_{\text{sorted}}(k))_{k=1,\dots,|X_{\text{test}}|} \subset \mathbb{R}$ denote a monotonically increasing sequence of threshold values. Calculating the AUC-ROC with linearly spaced thresholds requires an infinitesimally fine resolution to yield exact results. Because of this,

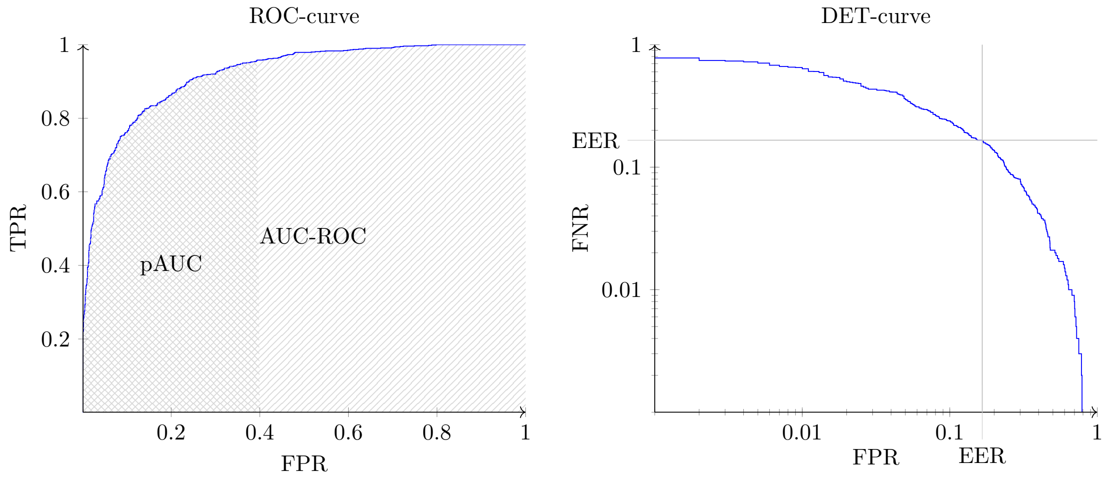

Figure 8: Examples of ROC- and DET-curves including the metrics AUC-ROC, pAUC (with $p = 0.4$) and EER. For DET-curves, usually a logarithmic scaling of the axis is used.

only the threshold values for which the intermediate statistics, i.e. FPR and TPR, change are used as this leads to improved computational efficiency and higher accuracy than linearly spaced thresholds [48]. Formally, this corresponds to setting $\theta_{\text{sorted}}(k) := \text{sort}(\text{score}(X_{\text{test}}))(k)$ where sort denotes a function sorting real values from low to high and $\text{score}(X_{\text{test}}) := \{\text{score}(x) \in \mathbb{R} : x \in X_{\text{test}}\} \subset \mathbb{R}$. Using the trapezoidal rule, the AUC-ROC score can be approximated by

$$\begin{aligned}&\text{AUC-ROC}(X_{\text{test}}, \text{score})\\ \approx &\sum_{k=1}^{|X_{\text{test}}|-1} \Delta_{\text{mean}}\mathsf{TPR}(X_{\text{test}}, \text{score}, k) \cdot \Delta_{\text{diff}}\mathsf{FPR}(X_{\text{test}}, \text{score}, k)\end{aligned} \tag{23}$$

where

$$\begin{aligned}&\Delta_{\text{diff}}\mathsf{FPR}(X_{\text{test}}, \text{score}, k)\\ :=&\mathsf{FPR}(X_{\text{test}}, \text{score}, \theta_{\text{sorted}}(k+1)) - \mathsf{FPR}(X_{\text{test}}, \text{score}, \theta_{\text{sorted}}(k))\end{aligned} \tag{24}$$

and

$$\begin{aligned}&\Delta_{\text{mean}}\mathsf{TPR}(X_{\text{test}}, \text{score}, k)\\ :=&\frac{\mathsf{TPR}(X_{\text{test}}, \text{score}, \theta_{\text{sorted}}(k+1)) + \mathsf{TPR}(X_{\text{test}}, \text{score}, \theta_{\text{sorted}}(k))}{2}.\end{aligned} \tag{25}$$

For all experiments conducted in this thesis, the implementation provided in scikit-learn [176], which is based on the trapezoidal rule, was used. A more intuitive interpretation of the AUC-ROC is given by the following theorem [3, 71]:

Theorem 2.10. *The AUC-ROC score is equal to the probability that* $\text{score}(x_n) < \text{score}(x_a)$ *holds for random samples* $x_n \in X_{normal} \cap X_{test}$ *and* $x_a \in X_{anomalous} \cap X_{test}$.

The evaluation metric *partial area under the receiver operating characteristic curve (pAUC)* is the AUC-ROC for a restricted part of the ROC-curve to any range of FPR [143], TPR [91] or both [256]. The idea is that some parts of the ROC-curve are often irrelevant in practice and by restricting the evaluation metric to a range of FPR or TPR relevant for a particular application the metric becomes more meaningful. For anomaly detection, this usually means to ensure a low FPR because for high FPR values users of an anomaly detection system will not take any occurring alarms, i.e. detected anomalies, seriously because too many of them are false alarms. Therefore, throughout this thesis pAUC will denote the AUC-ROC under low FPR ranging from 0 to a parameter $p \in (0, 1]$ to be specified.

In biometric applications such as speaker verification, often the *equal error rate (EER)* is used as an alternative threshold-independent evaluation metric. The EER is the point on the DET-curve where FPR and FNR are equal to each other. Due to the inverse relation of FNR and TPR given by $\mathsf{FNR}(X_{\text{test}}, \text{score}, \theta) = 1 - \mathsf{TPR}(X_{\text{test}}, \text{score}, \theta)$, the EER can also be easily determined using the ROC-curve.

2.10.2 *Open-set classification*

OSC can be decomposed into two subtasks: Anomaly detection and closed-set classification. Hence, there are not only false positives and false negatives as possible errors but also a so-called *confusion error* corresponding to true positive samples for which an incorrect class is predicted. One can evaluate multiple evaluation metrics for both subtasks, i.e. anomaly detection and CSC individually or combine them into a single metric. Let $\left(X_{\text{normal}}^{(i)}\right)_{i=1,\dots,N_{\text{classes}}}$ be a partition of X_{normal} where $X_{\text{normal}}^{(i)} \subset X_{\text{normal}}$ for $i = 1, \dots, N_{\text{classes}}$ denotes the i-th known class. Let $\text{pred}_{\text{class}} : X \to \{1, \dots, N_{\text{classes}}\}$ denote a classifier and

$$C_{\text{pred}}^{(i)}(X_{\text{test}}, \text{pred}_{\text{class}}) := \{x \in X_{\text{test}} : \text{pred}_{\text{class}}(x) = i\} \subset X_{\text{test}} \tag{26}$$

denote all samples classified as belonging to class $i \in \{1, \dots, N_{\text{classes}}\}$. A simple way to combine two metrics, one for each subtask, is to use a weighted sum of the accuracy obtained when classifying between the known classes and the accuracy obtained for anomaly detection viewed as a binary classification task [149]:

$$\begin{aligned}
&\mathsf{ACC}(X_{\text{test}}, \text{score}, \theta, \text{pred}_{\text{class}}, X_{\text{normal}}^{(1)}, \dots, X_{\text{normal}}^{(N_{\text{classes}})}, \beta_{\text{acc}}) \\
:=&\beta_{\text{acc}} \sum_{i=1}^{N_{\text{classes}}} \frac{|C_{\text{pred}}^{(i)}(X_{\text{test}}, \text{pred}_{\text{class}}) \cap X_{\text{normal}}^{(i)}|}{|X_{\text{normal}}^{(i)} \cap X_{\text{test}}|} \\
&+ (1 - \beta_{\text{acc}}) \frac{\mathsf{TP}(X_{\text{test}}, \text{score}, \theta) + \mathsf{TN}(X_{\text{test}}, \text{score}, \theta)}{|X_{\text{test}}|} \in [0, 1]
\end{aligned} \tag{27}$$

with $\beta_{\text{acc}} \in [0, 1]$. A common choice is to set $\beta_{\text{acc}} = 0.5$ since, without prior knowledge, both subtasks are equally important.

Threshold-independent evaluation metrics for OSC can be defined similarly to the ones defined for anomaly detection. In fact, the metric top-N_{classes} EER [205] is the same as EER for anomaly detection. The idea of using this metric is that the lowest anomaly score should be obtained for any of the known classes and not for one of the unknown classes. However, this evaluation metric ignores the CSC subtask of an OSC problem and thus has only limited meaning. Another more meaningful metric, also incorporating the CSC subtask, is the top-1 EER [205]. For this evaluation metric, FNR is the same as before but the FPR is different because confused classes are another error type for normal samples and are also treated as false positives. Formally, define

$$\begin{aligned}
&\mathrm{FP}_{\text{top-1}}(X_{\text{test}}, \text{score}, \theta, \text{pred}_{\text{class}}, X_{\text{normal}}^{(1)}, ..., X_{\text{normal}}^{(N_{\text{classes}})}) \\
:=&\mathrm{FP}(X_{\text{test}}, \text{score}, \theta) \\
&+\sum_{i=1}^{N_{\text{classes}}} |X_{\text{test}} \backslash (A_{\text{pred}}(X_{\text{test}}, \text{score}, \theta) \cup C_{\text{pred}}^{(i)}(X_{\text{test}}, \text{pred}_{\text{class}})) \cap X_{\text{normal}}^{(i)}|
\end{aligned} \tag{28}$$

as well as

$$\begin{aligned}
&\mathrm{FPR}_{\text{top-1}}(X_{\text{test}}, \text{score}, \theta, \text{pred}_{\text{class}}, X_{\text{normal}}^{(1)}, ..., X_{\text{normal}}^{(N_{\text{classes}})}) \\
:=&\frac{\mathrm{FP}_{\text{top-1}}(X_{\text{test}}, \text{score}, \theta, \text{pred}_{\text{class}}, X_{\text{normal}}^{(1)}, ..., X_{\text{normal}}^{(N_{\text{classes}})})}{|X_{\text{test}} \cap X_{\text{normal}}|} \in [0, 1].
\end{aligned} \tag{29}$$

Using these definitions, one can determine the top-1 EER as the point where top-1 FPR and FNR are equal. Similarly, the top-1 AUC-ROC and top-1 pAUC can be defined by replacing the regular FPR with the top-1 FPR for the ROC-curve. Hence, all threshold-independent metrics used for anomaly detection have been generalized for OSC.

2.10.3 *Sound event detection*

When detecting sound events, not only the correct sound event class but also the temporal position of a detected event has to be recognized. Therefore, specifically designed evaluation metrics have to be used that also take the temporal position of a detected sound event into account. In this section, we will mainly follow [148] and [48] to give an overview of evaluation metrics for SED, which in most cases are threshold-dependent evaluation metrics.

First, one can distinguish between *segment-based*, *event-based* (also called *collar-based*) and *intersection-based* [16, 51] evaluation metrics [48] for SED. Segment-based metrics divide the audio signal into temporal segments of fixed size and each annotated event that is contained in a given segment needs to be detected by the SED system. However, this causes long events ranging over multiple segments to have a higher contribution to the score. Furthermore, interruptions of detections belonging to single events may occur unnoticed. Event-based evaluation metrics solve these issues by comparing on- and offsets of annotated and detected events and checking whether the differences are below a pre-defined value, called *collar*. If they are below this collar, the corresponding detections are regarded as errors. But for these metrics, ambiguous definitions of sound events that can either be labeled or detected as a single long event or multiple short events have a strong impact on the performance. Intersection based metrics solve these issues by comparing the size of the intersection of a detected event and the corresponding annotation of the same event, normalized by the total length of the annotated event, to a pre-defined threshold [51].

Another distinction to be made is between *micro-averaged* or *macro-averaged* evaluation metrics, which are also being referred to as *instance-based averaging* and *class-based averaging*, respectively [148]. For micro-averaging, each individual segment or sound event has the same influence on the evaluation metric. This is achieved by evaluating each segment or sound event independently. For macro-averaging, each class has the same influence on the evaluation metric. This is achieved by computing class-wise evaluation metrics and taking their mean. Micro-averaged metrics emphasize classes for which more samples are evaluated whereas macro-averaged metrics put more weight on samples belonging to classes with fewer test samples. Hence, both strategies handle imbalanced classes differently.

One possibility to calculate an evaluation metric for SED is to determine intermediate statistics such as TPs and FPs for each segment or sound event. These statistics can be combined by applying micro- or macro-averaging and then an evaluation metric such as the F_1 score can be computed. Another commonly used evaluation metric is the *error rate* that is based on three types of errors: *Substitutions*, *deletions* and *insertions*. Substitutions are identified as sound events that are mistakenly recognized as belonging to a different class than they actually do, similar to the confusion error. Deletions are annotated sound events that have not been detected (false negatives) and insertions are detections for which no corresponding sound event has been annotated (false positives). Using these three error types, the error rate is the sum over all errors divided by the total number of annotated instances to be detected. Note that macro-averaging does not consider substitutions as each class is processed individually and thus only a micro-averaged error rate can be computed.

Although, threshold-dependent evaluation metrics are usually used for SED, threshold-independent metrics can also be defined by generalizing the threshold-independent metrics for OSC but are still subject to active research [16, 48, 51]. In [16], the main idea is to compute ROC-curves for each sound event class and summarize these class-wise curves into a single curve called polyphonic sound detection (PSD)-ROC to compute a threshold-independent metric. Due to the large number of possible thresholds, these curves are often approximated using a finite set of thresholds, which may result in underestimating the true evaluation metric. [48] solves this computational issue by jointly monitoring changes of the intermediate statistics as for example TP and FP caused by changing the decision thresholds for all sound event classes and computing the final evaluation metrics from the cumulative sums of these statistics.

2.11 DECISION THRESHOLD ESTIMATION

Regardless of whether threshold-dependent or threshold-independent evaluation metrics are used when developing an ASD system, for practical applications a decision threshold is needed to decide whether a given sample is normal or anomalous. For semi-supervised ASD, i.e. without access to anomalous training samples, it is impossible to directly optimize a decision threshold through evaluation and the decision threshold needs to be estimated using normal data only. Experienced users of an ASD system can also manually adjust the decision threshold based on their expertise. But even then, a well-tuned default setting of the threshold is still helpful. Moreover, their experience is based on observing real anomalies and access to these anomalous samples would also allow to automatically set the decision threshold by optimizing a threshold-dependent evaluation metric. In a semi-supervised setting, the general idea of most estimation methods boils down to finding a decision threshold that separates the most extreme values, e.g. the largest 10 percent, of the anomaly scores belonging to normal samples from the remaining anomaly scores. By doing so, one hopes that this decision threshold is also a good estimate for separating the anomaly scores of normal and anomalous data. Most of these methods are based on the assumption that the anomaly scores have a specific distribution, typically a normal distribution, and that normal and anomalous samples belonging to the training and test dataset follow the same distributions. Hence, the quality of the estimated decision threshold does not depend on the estimation method alone but also on the chosen method for computing the anomaly scores.

There are many different approaches for finding decision thresholds [189, 257]. Arbitrary anomaly scores, which are potentially biased, can be calibrated by converting them into (pseudo-)probabilities for which thresholds can be determined [55, 56]. Then, a fixed probability of 0.5 can be used as a decision threshold for these calibrated scores. However, this does not solve the problem of estimating a decision threshold but only reformulates the problem to estimating a calibration function. For multivariate data or scores, a threshold can be determined by using the empirical distribution function of the squared Mahalanobis distance and using a critical value such as a small quantile of the chi-squared distribution, which is the theoretical distribution function of this empirical distribution, as a threshold [195]. An extension of this approach uses an adaptive threshold [52]. However, anomaly scores used for ASD are usually univariate and thus multivariate approaches are not needed. When continuously monitoring audio data streams for anomalies, these data streams themselves consist of sound events of which most are normal and only a few are anomalous. Therefore, one can utilize previously encountered events and try to detect changes occurring in the stream of anomaly scores [31, 63, 263]. As most publicly available datasets for academic use consist of multiple short recordings instead of a long audio stream, only estimation techniques that process the anomaly scores of each recording individually will be discussed in this thesis. Note that the 90th percentile used by most of these methods is the standard value that can be found in the literature but is not guaranteed to be optimal.

In the following, several threshold estimation techniques will be listed. Let $\text{score}(Y)$ denote the anomaly scores belonging to a finite number of normal training samples $Y \subset X_{\text{train}} \subset X_{\text{normal}}$.

- *Gamma distribution percentile (GDP)* assumes that the anomaly scores follow a gamma distribution. The inverse of the 90th percentile of the empirical cumulative distribution function is used as the decision threshold. This is the most commonly used approach for ASD in machine condition monitoring [11, 46, 96, 126, 163, 182, 260].

- *Histogram percentile (HP)* directly uses the histogram of the anomaly scores without fitting a distribution first. Note that this silently assumes a uniform distribution. Again, the 90th percentile is used as the decision threshold.

- *Standard deviation (SD)* assumes the anomaly scores to be normally distributed. The decision threshold is set to

$$\theta_{\text{SD}}(Y, \text{score}, \beta_{\text{SD}}) := \text{mean}(\text{score}(Y)) + \beta_{\text{SD}} \cdot \text{std}(\text{score}(Y)) \tag{30}$$

  where $\text{mean}(\text{score}(Y))$ and $\text{std}(\text{score}(Y))$ denote the mean and standard deviation of the anomaly scores and $\beta_{\text{SD}} \in \mathbb{R}_+$ is a hyperparameter to be chosen. To have a consistent evaluation with the previous two approaches, one can use $\beta_{\text{SD}} = 1.28$, which approximately corresponds to the 90th percentile.

- *Interquartile range (IQR)* utilizes the first and third quartile of the anomaly scores, denoted by $Q1(\text{score}(Y)) \in \mathbb{R}$ and $Q3(\text{score}(Y)) \in \mathbb{R}$, respectively. This means that $\text{score}(y) \geqslant Q1(\text{score}(Y))$ for 75% of the samples $y \in Y$ and $\text{score}(y) \geqslant Q3(\text{score}(Y))$ for 25% of the samples $y \in Y$. Then,

$$\theta_{\text{IQR}}(Y, \text{score}, \beta_{\text{IQR}}) := Q3(\text{score}(Y)) + \beta_{\text{IQR}} \cdot (Q3(\text{score}(Y)) - Q1(\text{score}(Y))) \tag{31}$$

  is used as a decision threshold. Therefore, the approach assumes a uniform distribution, similar to HP. Typically, a value of $\beta_{\text{IQR}} = 1.5$ is used [194]. This approach is also known as *boxplot* [189].

- *Mean absolute deviation (MAD)* is based on the assumption that the median is more robust against anomalies than the mean. Here, the decision threshold is set to

$$\begin{aligned}\theta_{\text{MAD}}(Y, \text{score}, \beta_{\text{MAD}}, \delta_{\text{MAD}}) := {} & \text{median}(\text{score}(Y)) \\ & + \delta_{\text{MAD}} \cdot \beta_{\text{MAD}} \cdot \text{median}_{y \in Y}(|\text{score}(y) - \text{median}(\text{score}(Y))|),\end{aligned} \tag{32}$$

where median(score(Y)) denotes the median of the score values score(Y) and the hyperparameter δ_{MAD} is usually set to $\delta_{\text{MAD}} = 1.4826$ [194]. For the hyperparameter β_{MAD}, [257] proposes to use $\beta_{\text{MAD}} = 3$ and [189] uses $\beta_{\text{MAD}} = 2$.

- *OCSVMs* [202] can be used to estimate the support of a distribution. This is done by discriminating between regions of high and low density using a hyperplane in a high-dimensional space. When training a OCSVM with anomaly scores, the learned hyperplane can be used as a decision threshold. For the hyperparameter ν_{SVM}, a value of 0.1 can be used which corresponds to treating 10% of the anomaly scores as anomalous, i.e. using the 90th percentile as done for the previously presented approaches.

- *Generalized extreme studentized deviate (GESD)* [193] is an iterative approach based on the Grubbs's test [69]. This statistical test assumes a normal distribution and is calculated on the so-called Grubbs statistic defined as

$$\text{Grubbs}(\text{score}(Y)) = \frac{|\max_{y \in Y} \text{score}(y) - \text{mean}(\text{score}(Y))|}{\text{std}(\text{score}(Y))} \tag{33}$$

  where mean(score(Y)) and std(score(Y)) denote the mean and standard deviation of the anomaly scores, respectively. The Grubbs statistic, denoted by Grubbs(score(Y)), is evaluated against the upper critical value of the student's t-distribution with a significance level $\delta_{\text{Grubbs}} = 0.05$ and data size $|Y|$:

$$\text{Grubbs}(\text{score}(Y)) > \frac{|Y| - 1}{\sqrt{|Y|}} \sqrt{\frac{t^2_{\delta_{\text{Grubbs}}/(2|Y|),|Y|-2}}{|Y| - 2 + t^2_{\delta_{\text{Grubbs}}/(2|Y|),|Y|-2}}}. \tag{34}$$

  Note that the Grubbs test only determines whether the highest anomaly score corresponds to an anomalous sample. For GESD, Grubbs is repeated by iteratively removing the highest anomaly score until the Grubbs condition is not met. The last anomaly score, which is removed by this procedure, is the resulting decision threshold.

- *CleverSD* [20] is another iterative approach. The idea is to iteratively apply SD to determine a decision threshold and remove the highest anomaly score from the training scores in case it is above this decision threshold. This procedure is repeated until the highest anomaly score is below the decision threshold estimated by SD. Again, the last anomaly score removed by this approach is the resulting decision threshold.

- *Multi-stage thresholding (MST)* [257] is yet another iterative approach that generalizes cleverSD. The idea is to simply apply a non-iterative method multiple times. In contrast to cleverSD, not only the highest score but all scores above the decision threshold are removed. In [257] it has been experimentally shown that two iterations are usually sufficient.

Note that the estimation methods listed above can also be applied for unsupervised ASD where the extreme values of the anomaly scores are likely to be truly anomalous and thus the estimated decision thresholds are also more likely to be a good estimate of the optimal threshold. In a semi-supervised setting there is no guarantee that the extreme values of the anomaly scores belonging to normal samples have a similar magnitude as anomaly scores belonging to anomalous samples. Both can can be very different, which is the reason why these estimated thresholds usually do not lead to optimal results. In conclusion, to some extend it is even more difficult to estimate a decision threshold in a semi-supervised setting than it is in an unsupervised setting. However, training the embedding model is more difficult in an unsupervised setting.

2.12 SUMMARY

In this chapter, state-of-the-art audio embeddings for semi-supervised ASD and the building blocks for designing an ASD system that utilizes these embeddings have been reviewed. Such a system consists of a frontend for pre-processing the audio data, an embedding model and a backend for deciding between normal and anomalous samples. Each of these three components will now be briefly summarized.

The frontend consists of computing feature representations from the raw audio signals to be used as input for the embedding models. The main goal is to reduce the high dimension of the audio signals while not losing or even highlighting information relevant for the ASD task. This consists of three steps: 1) Pre-processing the audio signals such that they have the same sampling rate and possibly the same duration, 2) computing spectral features to reduce their dimension and 3) normalizing them to ensure that all dimensions of the input representations are scaled similarly.

Next, three different types of embeddings that are computed by further processing the input feature representations with neural networks were presented: One-class embeddings, auxiliary task embeddings and pre-trained embbedings. One-class embeddings aim at learning embedding spaces that are suitable for autoencoding the input data or learn a hypersphere of minimal volume. The major difficulty is to prevent learning trivial solutions that do not require the embeddings to contain useful information for identifying anomalous data. Auxiliary task embeddings are learned by classifying between classes provided by available meta information or by applying SSL and thus may require additional knowledge about the data. Pre-trained embeddings are obtained by training an embedding model on a large dataset that does not need to be related to the target application assuming that the learned embeddings also contain useful information for the target application, which may not always be a valid assumption.

Using one of the embeddings, different ways of computing an anomaly score were presented. These mainly consist of estimating the distribution of embeddings belonging to normal samples and can be as simple as calculating the Euclidean distance to the mean of the embeddings. To train an embedding model, multiple data augmentation techniques that can be used to improve the ASD performance were examined, namely mixup, SpecAugment and simulating anomalous samples for training by modifying normal training samples. Furthermore, the three different embedding types were compared to each other with respect to multiple criteria such as performance, computational requirements and usability showing that each embedding type has advantages and disadvantages over the other two types and none is superior for every possible application. In addition, ensembling methods used to combine multiple models for boosting the ASD performance such as using a weighted sum of anomaly scores were listed, which may be used to combine the strengths of several approaches.

To measure the performance of a system and be able to compare multiple systems, evaluation metrics for ASD, OSC and SED were presented in Section 2.10. Mainly, one can differentiate between threshold-dependent performance measures that depend on a specifically chosen decision threshold applied to the anomaly scores, and threshold-independent performance measures. Estimating a decision threshold for semi-supervised ASD is a difficult task and requires sophisticated techniques. The reason is that only anomaly scores belonging to normal samples are available. Thus, one needs to assume that the extreme values of these anomaly scores, e.g. all scores above the 90th percentile have a similar magnitude as the anomaly scores belonging to anomalous samples. Then, the value separating the extreme values from the rest can be used as a decision threshold.

As seen above, semi-supervised ASD is an active research area providing many different choices when designing a system for a particular application. The goal of the next chapter is to identify approaches that perform particularly well by comparing several of the methods presented above as well as novel methods and design an ASD system based on these findings.

3 ANOMALOUS SOUND DETECTION SYSTEM DESIGN

In the previous chapter, several possibilities to design an ASD system were presented. The goal of this chapter is to design an ASD system based on audio embeddings that yields state-of-the-art performance. To this end, several design choices will be compared. As the main difficulty for semi-supervised anomaly detection is to be able to train a model without access to anomalous data, the focus will be on choosing a suitable loss function for training the embedding model and how to calculate anomaly scores.

This chapter is structured as follows: First, the experimental setup consisting of an ASD dataset and a baseline model, whose performance will be optimized, is presented. Then, different loss functions, namely one-class losses and angular margin losses will be compared to each other, both theoretically and experimentally. Third, the sub-cluster AdaCos loss, which is a generalization of the AdaCos loss, will be defined and investigated.

3.1 CONTRIBUTIONS OF THE AUTHOR

The sections of this chapter are largely based on the following key publications:

- Kevin Wilkinghoff. “Sub-Cluster AdaCos: Learning Representations for Anomalous Sound Detection.” In: *International Joint Conference on Neural Networks (IJCNN)*. IEEE, 2021.
- Kevin Wilkinghoff and Frank Kurth. “Why do Angular Margin Losses work well for Semi-Supervised Anomalous Sound Detection?” In: *IEEE/ACM Trans. Audio Speech Lang. Process.* 32 (2024), pp. 608–622.

For publications that are not single-authored, individual contributions of the thesis author and all co-authors to these publications are stated in Section A.1. If not stated otherwise, the content listed in the following paragraph is the sole contribution of the thesis author.

Section 3.2.2 and Sections 3.4.3 to 3.4.7 are based on [241]. Sections 3.3, 3.4.1 and 3.4.2. The experimental results shown in Figure 9 and Table 5 are adapted from [252] by changing the dataset used for the experiments.

3.2 EXAMPLE APPLICATION: MACHINE CONDITION MONITORING

As already announced in Section 1.3, acoustic machine condition monitoring will serve as the main example application for semi-supervised ASD in this thesis.

The main reason for this choice is that most recently published works on semi-supervised ASD utilize publicly available datasets for acoustic machine condition monitoring that belong to the annual DCASE Challenge. Also utilizing these datasets ensures that the results are reproducible and there is a commonly used experimental setup in the community to compare findings experimentally. Another advantage is that the task is well-defined because normal recordings belong to fully functioning machines and all anomalies indicate mechanical failure caused on purpose in a controlled environment. Last but not least, the dataset provides a difficult task because real factory background noise was added to all recordings, which fosters research for semi-supervised ASD.

3.2.1 *Experimental setup*

For the experiments conducted in this chapter, the dataset belonging to the task "Unsupervised Detection of Anomalous Sounds for Machine Condition Monitoring" of the DCASE2020 Challenge [108] is used[1]. The dataset contains recordings of the machine types "fan", "pump", "slider" and "valve" from MIMII [188] as well as "ToyCar" and "ToyConveyor" from ToyADMOS [106], which also contain real factory background noise. Each recording has a length of $10\,\mathrm{s}$ and a sampling rate of $16\,\mathrm{kHz}$. The dataset is divided into two subsets, a development set and an evaluation set. Each of these sets consists of a training split, which only contains normal data, and a test split, which contains normal and anomalous data. There are multiple individual machines of each type. The set of all recordings belonging to a specific machine ID is called section. During testing, the section a given recording belongs to is known and can also be used as input to the ASD system. The sections contained in the development set and evaluation set are mutually exclusive but are the same for the training and test splits. In total, there are 41 different sections. Further details about the dataset structure can be found in Table 3.

To evaluate the performance of an ASD system, the AUC-ROC and pAUC with $p = 0.1$ are determined for each section of the dataset. To obtain a single value that can be used as a performance measure to rank the systems, the arithmetic mean of all AUC-ROCs and pAUCs over all sections is calculated.

3.2.2 *Baseline model for extracting embeddings*

As stated in Section 2.4, training a model that uses an auxiliary classification task is a commonly used approach for ASD that attains state-of-the-art performance. Because of this, such an embedding model is used as a baseline model, whose performance serves as a basis for measuring improvement. The structure of the baseline model is shown in Table 4. It is based on a modified ResNet architecture

1 Although the name of the task implies an unsupervised ASD setting, it is actually semi-supervised.

Table 3: Structure of the DCASE2020 ASD dataset containing recordings of 6 machine types. The set containing all recordings belonging to one individual machine is called a section.

subset	number of sections (per machine type)	split	number of recordings (per section)	
			normal	anomalous
development set	$3-4$	training	~ 1000	0
		test	$100-200$	$100-200$
evaluation set	$3-4$	training	~ 1000	0
		test	~ 200	~ 200

Table 4: Modified ResNet architecture used as the baseline model. © 2021 IEEE

layer name	structure	output size
input	-	313×128
2D convolution	7×7, stride$= 2$	$157 \times 64 \times 16$
residual block	$\begin{pmatrix} 3 \times 3 \\ 3 \times 3 \end{pmatrix} \times 2$, stride$= 1$	$78 \times 31 \times 16$
residual block	$\begin{pmatrix} 3 \times 3 \\ 3 \times 3 \end{pmatrix} \times 2$, stride$= 1$	$39 \times 16 \times 32$
residual block	$\begin{pmatrix} 3 \times 3 \\ 3 \times 3 \end{pmatrix} \times 2$, stride$= 1$	$20 \times 8 \times 64$
residual block	$\begin{pmatrix} 3 \times 3 \\ 3 \times 3 \end{pmatrix} \times 2$, stride$= 1$	$10 \times 4 \times 128$
max pooling	10×1, stride$= 1$	$1 \times 4 \times 128$
flatten	-	512
dense (embedding)	no activation	128

[77] mainly consisting of four residual blocks. In each convolutional layer, batch normalization [86] is applied and leaky ReLU [139] with a slope coefficient of 0.1 is used as an activation function. As input feature representations, log-Mel spectrograms with 128 Mel bins, a window size of 1024 and a hop size of 512 are computed using a high-pass filter with a cutoff frequency of $200\,\mathrm{Hz}$. These features are standardized by subtracting the temporal mean and dividing with the temporal standard deviation computed by using all normal training samples. To train this embedding model, the angular margin loss AdaCos [264] is minimized by using the sections of the DCASE2020 ASD dataset corresponding to different machine IDs as classes and applying mixup [262]. More concretely, the model is trained for 400 epochs using Adam [101] with a batch size of 64. Individual design choices for improving the performance of this model will be investigated in the following sections. The minimum cosine distance of a test sample to all centers of the AdaCos loss is used to compute an anomaly score. Since only threshold-independent evaluation metrics are used to compute the performance, a decision threshold does not need to be estimated. Before evaluating the performance of this baseline model, it will be shown that using the angular margin loss AdaCos to train the model is a reasonable choice.

3.3 RELATION BETWEEN ONE-CLASS AND ANGULAR MARGIN LOSSES

When designing an ASD system based on audio embeddings, one of the major choices to make is to decide on how to train the embedding model. Compared to directly trained models, pre-trained models are known to have inferior performance in case enough training data is available because pre-trained models are less specialized. Therefore, one needs to decide between a one-class loss or an angular margin loss, which are the other two commonly used loss functions for training an embedding model, to obtain state-of-the-art performance. In this section, the relation between the compactness loss and AdaCos as representatives of one-class losses and angular margin losses, respectively, will be investigated. Before doing this, it will be shown that projecting the embeddings onto the unit sphere when using a compactness loss has several advantages.

3.3.1 *Compactness loss on the unit sphere*

The following lemma shows that the squared Euclidean distance and the cosine similarity are closely related on the unit sphere.

Lemma 3.1. *For* $e_1, e_2 \in \mathbb{R}^D$ *with* $\|e_1\|_2 = \|e_2\|_2 = 1$*, it holds that*

$$\mathrm{sim}(e_1, e_2) = 1 - \frac{\|e_1 - e_2\|_2^2}{2}. \tag{35}$$

Proof. Using only basic identities, we obtain

$$\begin{aligned}\|e_1 - e_2\|_2^2 &= \langle e_1 - e_2, e_1 - e_2 \rangle = \|e_1\|_2^2 + \|e_2\|_2^2 - 2\langle e_1, e_2 \rangle \\ &= 2\left(1 - \frac{\langle e_1, e_2 \rangle}{\|e_1\|_2 \|e_2\|_2}\right) = 2(1 - \mathrm{sim}(e_1, e_2)),\end{aligned}$$

which finishes the proof. □

Hence, the Euclidean distance and the cosine distance, which in this case is equal to the standard scalar product, are equivalent for computing an anomaly score for embeddings on the unit sphere. Projecting embeddings onto the unit sphere can be easily accomplished by dividing an embedding with its Euclidean norm because for all $0 \neq e \in \mathbb{R}^D$ it holds that

$$\left\| \frac{e}{\|e\|_2} \right\|_2 = \frac{\|e\|_2}{\|e\|_2} = 1.$$

The following definition captures this simple fact by introducing additional notation.

Definition 3.2 (Projection onto unit sphere)**.** Let $\mathcal{S}^{D-1} := \{e \in \mathbb{R}^D : \|e\|_2 = 1\} \subset \mathbb{R}^D$ denote the D-*sphere*, in the following also referred to as *unit sphere*. Then

$$\begin{aligned} &P_{\mathcal{S}^{D-1}} : \mathbb{R}^D \to \mathcal{S}^{D-1} \\ &P_{\mathcal{S}^{D-1}}(e) := \frac{e}{\|e\|_2} \end{aligned} \tag{36}$$

is the *projection onto the* D*-sphere.*

Restricting the embedding space to the unit sphere essentially reduces the embedding dimension by 1 as evident by using stereographic projection. Since the dimension of the embedding space is just a hyperparameter to be chosen and, in most cases, is higher than it needs to be, the resulting performance does not degrade. On the contrary, projecting the embeddings onto the unit sphere when using the compactness loss has several advantages. First of all, doing so prevents that the network may learn $\mathbf{0} \in \mathbb{R}^D$ as a trivial solution in case only linear operators, such as matrix multiplications or convolutions, and activation functions with 0 as a fixed point are used. Furthermore, normalizing the embedding stabilizes the training by preventing numerical issues similar to batch normalization [86]. Another advantage is that the initialization of the (non-trainable) center is simplified since two random elements of the unit sphere have equal distance with very high probability if the dimension is sufficiently high. Therefore, the center can be initialized randomly.

3.3.2 *Relation between the compactness loss and AdaCos*

The relation between the compactness loss and AdaCos is characterized by the following corollary.

Corollary 3.3. *For* $\mathrm{Im}(\phi) \subseteq \mathbb{S}^{D-1}$, *minimizing* $\mathcal{L}_{ada}(Y, C, \phi, w, \mathrm{lab})$ *with gradient descent is equivalent to minimizing*

$$\begin{aligned} &-\frac{\tilde{s}}{2}\frac{1}{|Y|}\sum_{x\in Y}\sum_{i=1}^{N_{classes}} \mathrm{lab}(x)_i \sum_{k=1}^{N_{classes}} \mathrm{softmax}(\hat{s}\cdot \mathrm{sim}(\phi(x,w), c_k)) \\ &\cdot\left(\frac{\partial}{\partial w}\|\phi(x,w)-c_i\|_2^2 - \frac{\partial}{\partial w}\|\phi(x,w)-c_k\|_2^2\right). \end{aligned} \tag{37}$$

Proof. The proof of this corollary will be postponed to Section 3.4 because the statement directly follows from a more general theorem. □

This corollary shows that minimizing the AdaCos loss increases intra-class similarity, i.e. reduces the compactness loss for each class, while at the same time decreasing inter-class similarity. Hence, AdaCos can be seen as a multi-class version of the compactness loss that explicitly ensures a margin between classes. Note that a constant function can only be a solution for a single class as a classifier requires different solutions for different classes. Therefore, using multiple normal classes prevents that the model learns a constant function as a trivial solution. In the case of a classification task, a trivial solution corresponds to learning a perfect classifier that maps each point exactly to the center of the corresponding class and is practically impossible to obtain for non-trivial classification tasks.

As already mentioned in Section 2.3, a similar strategy is employed in [85, 177] where an auxiliary classification task on a second dataset is used as a so-called *descriptiveness loss*. Compared to an angular margin loss, there are several differences even when the same dataset is used for both tasks. First and foremost, for angular margin losses the inter-class compactness loss is increased instead of only using a discriminative objective with a categorical crossentropy (CXE). Furthermore, a margin between different classes is explicitly ensured, which is not the case for the descriptiveness loss. Third, an angular margin loss uses a different weight for individual classes by utilizing softmax probabilities as shown in Corollary 3.3.

To experimentally verify the relation between the different loss functions, the development of different loss functions over time is depicted in Figure 9. It can be seen that training a model by minimizing the AdaCos loss indeed minimizes the intra-class compactness losses while maximizing the inter-class compactness losses. Note that, according to Lemma 3.1, a mean squared Euclidean distance equal to 2, as attained by the inter-class loss, corresponds to an angle equal to $\frac{\pi}{2}$, i.e. orthogonality. This is an expected behavior in the embedding space because two random elements of a relatively high-dimensional vector space are orthogonal with very high probability [65]. Furthermore, a smaller loss does not mean that

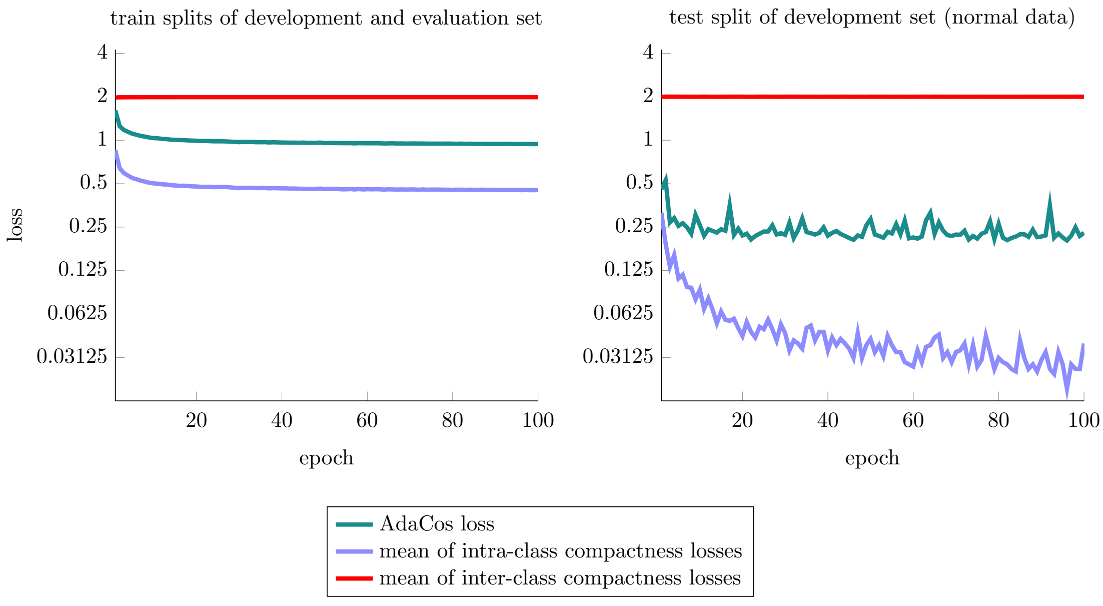

Figure 9: Temporal development of different losses obtained on the DCASE2020 dataset when training by minimizing the AdaCos loss.

the resulting ASD performance is better because minimizing any of these losses is only an auxiliary task not directly related to the ASD task.

3.3.3 *Performance evaluation*

In this section, the ASD performances obtained with different loss functions and using a different number of classes for an auxiliary classification task are compared. The results can be found in Table 5. It can be seen that the performance improves when increasing the number of classes used for training (see second column). Using more classes increases the difficulty of the classification task and thus more information needs to be captured by the embedding model to still be able to predict the correct class. When using only a single class for the entire dataset, the performance is the same as random guessing. The most likely reason is the strong and highly diverse background noise that consists of several other sound sources and thus drowns out the anomalous signal components, which are very subtle in comparison. In contrast, using an auxiliary classification task teaches the model to closely monitor frequency bands or temporal patterns that are characteristic for the target machine sounds. This enables the embedding model to ignore the background noise whereas a one-class model does not know the difference between noise and target machine sounds and thus considers all signal components as equally important. Using the pre-defined sections of the dataset as sub-classes improves the overall performance, even when training another model for each subclass. This indicates that individual machines, represented by the sections of the dataset, have a very distinct acoustic pattern and thus the only variability between

Table 5: Arithmetic means of all AUC-ROCs and pAUCs obtained with different losses using different auxiliary tasks over all sections of the DCASE2020 dataset. For intra-class compactness losses, non-trainable class centers and no bias terms are used to avoid learning trivial solutions. Best results in each column are highlighted with bold letters.

DCASE2020 development set			
loss	classes of auxiliary task (number of classes)	AUC	pAUC
intra-class compactness loss	none (1)	$49.78 \pm 0.66\%$	$50.36 \pm 0.28\%$
intra-class compactness loss	machine types (7)	$70.61 \pm 1.89\%$	$62.58 \pm 1.49\%$
intra-class compactness loss	machine types and sections, models trained individually (1)	$67.68 \pm 0.54\%$	$57.57 \pm 0.35\%$
intra-class compactness loss	machine types and sections (41)	$89.67 \pm 0.58\%$	$83.20 \pm 0.88\%$
intra-class compactness loss + CXE	machine types and sections (41)	**$90.12 \pm 0.35\%$**	**$83.86 \pm 0.60\%$**
AdaCos loss	machine types and sections (41)	$89.30 \pm 0.57\%$	$83.03 \pm 0.52\%$
DCASE2020 evaluation set			
loss	classes of auxiliary task (number of classes)	AUC	pAUC
intra-class compactness loss	none (1)	$50.08 \pm 1.07\%$	$50.39 \pm 0.59\%$
intra-class compactness loss	machine types (7)	$73.74 \pm 2.35\%$	$65.57 \pm 1.92\%$
intra-class compactness loss	machine types and sections, models trained individually (1)	$70.60 \pm 0.68\%$	$61.10 \pm 0.71\%$
intra-class compactness loss	machine types and sections (41)	$90.55 \pm 1.07\%$	$83.54 \pm 1.00\%$
intra-class compactness loss + CXE	machine types and sections (41)	**$90.84 \pm 0.43\%$**	$83.85 \pm 0.37\%$
AdaCos loss	machine types and sections (41)	$90.54 \pm 0.09\%$	**$84.09 \pm 0.68\%$**

different recordings of the same machine is the background noise. Still, training a joint embedding model leads to much better results than using individual models. Moreover, using an explicit classification task with a CXE slightly improves the performance over only increasing the intra-class similarity or using an angular margin loss. The most likely reason is that the classification task for this dataset is relatively simple due to the low variability between different recordings of the same machine, which leads to almost perfect classification results even when only using an intra-class compactness loss.

In the previous discussion of the results it was silently assumed that the background noise is similar for each class. However, if the background noise is specific for some or even all classes, then using a classification task will probably not help to improve the performance because the noise contains useful information for discriminating between the classes as well. Hence, assuming that the background noise is not class-specific is essential. For realistic applications, this is often a valid assumption because one would expect that at least some machines of different type or with a different ID are running in the same factory and share the same acoustic environment. Otherwise, defining additional sub-classes, e.g. by also providing parameter settings of machines as meta information as done in Chapter 5, may be beneficial. In any case, using an angular margin loss also decreases the intra-class compactness losses and thus will not perform worse than when only using an intra-class compactness loss.

3.4 SUB-CLUSTER ADACOS

Using an angular margin loss to learn distributions of normal data enforces a Gaussian distribution for each class because the mean squared error, which is strongly related to the cosine distance (cf. Lemma 3.1), is proportional to the negative log-likelihood of a Gaussian distribution. As Gaussian distributions are relatively simple, this may be a choice that is too restrictive to accurately model the true distribution and thus may not be optimal to distinguish between normal and anomalous samples. The fact that using a CXE as a descriptiveness loss led to slightly better performance in the experiments conducted in Section 3.3.3 provides additional evidence for this claim. The goal of this section is to relax these restrictions by utilizing multiple Gaussians for each class instead of a single one and investigate the impact on the resulting ASD performance. Introducing sub-classes enables the model to learn more sophisticated distributions for each class.

The idea of allowing multiple sub-classes for each class is also used for discriminant analysis [29, 268] and was shown to outperform standard approaches such as LDA. A similar approach for angular margin losses is sub-center ArcFace [37] that has been proposed to handle noisy class labels. Apart from the non-adaptive scale parameter, the main difference to sub-cluster AdaCos is that only the closest sub-center is considered by using the minimum over all cosine-similarities. For sub-cluster AdaCos, the sum of all softmax probabilities belonging to a single class is computed during training. Taking the sum still enables the model to handle noisy class labels by assigning them to other sub-classes. Furthermore, summing the probabilities has the advantage that it is continuously differentiable whereas using the minimum distance is not.

3.4.1 *Definition*

The following formal definition of the sub-cluster AdaCos loss is similar to the definition of the AdaCos loss (cf. Definition 2.8) but uses $N_{\text{centers}} \in \mathbb{N}$ centers instead of a single center for each class. Furthermore, the term $B_{\text{avg}}^{(t)}$ includes the distances to all samples and not just the samples belonging to non-target classes. The reason is that sub-cluster AdaCos is intended to be used with mixup. In this, mixed up samples should be treated as anomalous samples. This modification results in a larger value for $B_{\text{avg}}^{(t)}$ and thus also a larger scale parameter leading to sharper boundaries around the distributions of the classes (cf. Figure 6).

Definition 3.4 (Sub-cluster AdaCos)**.** Let $C_j \in \mathcal{P}(\mathbb{R}^D)$ with $|C_j| = N_{\text{centers}} \in \mathbb{N}$ denote all centers belonging to class $j \in \{1, ..., N_{\text{classes}}\}$. Let the *dynamically adaptive scale parameter* $\hat{s}^{(t)} \in \mathbb{R}_+$ at training step $t \in \mathbb{N}_0$ be set to

$$\hat{s}^{(t)} := \begin{cases} \sqrt{2} \cdot \log(N_{\text{classes}} \cdot N_{\text{centers}} - 1) & \text{if } t = 0 \\ \dfrac{\text{sim}_{\max}^{(t)} + \log \hat{B}_{\text{avg}}^{(t)}}{\cos\left(\min(\frac{\pi}{4}, \hat{\alpha}_{\text{med}}^{(t)})\right)} & \text{else} \end{cases} \tag{38}$$

with

$$\hat{B}_{\text{avg}}^{(t)} := \frac{1}{N_{\text{batch}}} \sum_{x \in Y^{(t)}} \sum_{j=1}^{N_{\text{classes}}} \sum_{c \in C_j} \exp\left(\hat{s}^{(t-1)} \operatorname{sim}(\phi(x, w^{(t)}), c) - \operatorname{sim}_{\max}^{(t)}\right) \tag{39}$$

where $\hat{\alpha}_{\text{med}}^{(t)} \in [0, \frac{\pi}{2}]$ denotes the median of all mixed-up angles

$$\begin{aligned} &\lambda \sum_{c^{(1)} \in C_{\text{class}(x_1)}} \alpha(\phi(\operatorname{mix}_x(x_1, x_2, \lambda), w), c^{(1)}) \\ +(1-\lambda) &\sum_{c^{(2)} \in C_{\text{class}(x_2)}} \alpha(\phi(\operatorname{mix}_x(x_1, x_2, \lambda), w), c^{(2)}) \end{aligned}$$

with $x_1, x_2 \in Y^{(t)}$, $\lambda \in [0, 1]$, and for $w^{(t)} \in W$ the stability term is given by

$$\operatorname{sim}_{\max}^{(t)} := \max_{x \in Y^{(t)}} \max_{j=1}^{N_{\text{classes}}} \max_{c \in C_j} \hat{s}^{(t-1)} \cdot \operatorname{sim}(\phi(x, w), c). \tag{40}$$

Then, the *sub-cluster AdaCos* loss is defined as

$$\begin{aligned} &\mathcal{L}_{\text{sc-ada}} : \mathcal{P}(X) \times \mathcal{P}(\mathcal{P}(\mathbb{R}^D)) \times \Phi \times W \times \Lambda(N_{\text{classes}}) \to \mathbb{R}_+ \\ &\mathcal{L}_{\text{sc-ada}}(Y, \mathcal{C}, \phi, w, \text{lab}) := -\frac{1}{|Y|} \sum_{x \in Y} \sum_{j=1}^{N_{\text{classes}}} \text{lab}(x)_j \log(\operatorname{softmax}(\hat{s} \cdot \operatorname{sim}(\phi(x, w), C_j))) \end{aligned} \tag{41}$$

where $|\mathcal{C}| = N_{\text{classes}}$ and, in this case,

$$\operatorname{softmax}(\hat{s} \cdot \operatorname{sim}(\phi(x, w), C_j)) := \sum_{c_j \in C_j} \frac{\exp(\hat{s} \cdot \operatorname{sim}(\phi(x, w), c_j))}{\sum_{k=1}^{N_{\text{classes}}} \sum_{c_k \in C_k} \exp(\hat{s} \cdot \operatorname{sim}(\phi(x, w), c_k))} \tag{42}$$

Remark. The only reason for including the stability term $-\operatorname{sim}_{\max}^{(t)}$ when calculating $\hat{B}_{\text{avg}}^{(t)}$ is to improve numerical stability by reducing the argument of the exponential function. After this computation and taking the logarithm in the computation of $\hat{s}^{(t)}$, the effects of the term $-\operatorname{sim}_{\max}^{(t)}$ are reversed by adding $\operatorname{sim}_{\max}^{(t)}$.

3.4.2 *Relation to the compactness loss*

Similar to Corollary 3.3, the relation between the sub-cluster AdaCos loss and the compactness loss is presented in the following theorem.

Theorem 3.5. *Let* $Y_j := \{x \in Y : \mathrm{lab}(x)_j = 1\}$ *for* $j \in \{1, ..., N_{classes}\}$*. Then, for* $\mathrm{Im}(\phi) \subseteq \mathcal{S}^{D-1}$ *minimizing* $\mathcal{L}_{sc\text{-}ada}(Y, \mathcal{C}, \phi, w, \mathrm{lab})$ *with gradient descent minimizes all intra-class compactness losses with weighted gradients given by*

$$\frac{\hat{s}}{2} \sum_{i=1}^{N_{classes}} \frac{1}{|Y_i|} \sum_{x \in Y_i} \sum_{c_i \in C_i} P(\tau(\phi(x, w), \mathcal{C}) = c_i | \tau(\phi(x, w), \mathcal{C}) \in C_i) \cdot \frac{\partial}{\partial w} \|\phi(x, w) - c_i\|_2^2 \tag{43}$$

while maximizing all inter-class compactness losses with weighted gradients given by

$$-\frac{\hat{s}}{2} \sum_{i=1}^{N_{classes}} \frac{1}{|Y_i|} \sum_{x \in Y_i} \sum_{k=1}^{N_{classes}} \sum_{c_k \in C_k} P(\tau(\phi(x, w), \mathcal{C}) = c_k) \cdot \frac{\partial}{\partial w} \|\phi(x, w) - c_k\|_2^2 \tag{44}$$

where

$$P(\tau(\phi(x, w), \mathcal{C}) = c_i | \tau(\phi(x, w), \mathcal{C}) \in C_i) := \frac{\exp(\hat{s} \cdot \mathrm{sim}(\phi(x, w), c_i))}{\sum_{c_i' \in C_i} \exp(\hat{s} \cdot \mathrm{sim}(\phi(x, w), c_i'))} \tag{45}$$

and

$$P(\tau(\phi(x, w), \mathcal{C}) = c_k) := \frac{\exp(\hat{s} \cdot \mathrm{sim}(\phi(x, w), c_k))}{\sum_{k=1}^{N_{classes}} \sum_{c_k' \in C_k} \exp(\hat{s} \cdot \mathrm{sim}(\phi(x, w), c_k'))} \tag{46}$$

with a cluster assignment function $\tau : \mathbb{R}^D \times \mathcal{P}(\mathcal{P}(\mathbb{R}^D)) \to \mathbb{R}^D$ *given by*

$$\tau(e, \mathcal{C}) = \arg\max_{C \in \mathcal{C}}(\arg\max_{c \in C}(\mathrm{sim}(e, c))). \tag{47}$$

Proof. Let $x \in Y$, $\phi \in \Phi$ and $\hat{s} \in \mathbb{R}_+$ be fixed and $i \in \{1, ..., N_{\mathrm{classes}}\}$ such that $\mathrm{lab}(x)_i = 1$ and $\mathrm{lab}(x)_j = 0$ for $j \neq i$. To simplify notation, define $z(w, c) := \exp(\hat{s} \cdot \mathrm{sim}(\phi(x, w), c))$. Note that, in each iteration $t > 0$, $\hat{s}^{(t)}$ is set to a fixed value before computing the gradient of the loss function by using the current weights $w^{(t)} \in W$ of the network. Therefore, $\frac{\partial \hat{s}^{(t)}}{\partial w} = 0$ although the dynamically adaptive scale parameter depends on the weights. Using Lemma 3.1, it holds that

$$\begin{aligned}\frac{\partial}{\partial w} \log\left(\sum_{c_i \in C_i} z(w, c_i)\right) &= \frac{\sum_{c_i \in C_i} z(w, c_i) \cdot \hat{s} \cdot \frac{\partial}{\partial w} \mathrm{sim}(\phi(x, w), c_i))}{\sum_{c_i' \in C_i} z(w, c_i')} \\ &= -\frac{\hat{s}}{2} \sum_{c_i \in C_i} \frac{z(w, c_i) \cdot \frac{\partial}{\partial w} \|\phi(x, w) - c_i\|_2^2}{\sum_{c_i' \in C_i} z(w, c_i')}\end{aligned}$$

and similarly

$$\begin{aligned}
&\frac{\partial}{\partial w}\log\left(\sum_{k=1}^{N_{\text{classes}}}\sum_{c_k\in C_k} z(w,c_k)\right)\\
=&\frac{\sum_{k=1}^{N_{\text{classes}}}\sum_{c_k\in C_k} z(w,c_k)\cdot\hat{s}\cdot\frac{\partial}{\partial w}\operatorname{sim}(\phi(x,w),c_k))}{\sum_{k=1}^{N_{\text{classes}}}\sum_{c_k'\in C_k} z(w,c_k')}\\
=&-\frac{\hat{s}}{2}\sum_{k=1}^{N_{\text{classes}}}\sum_{c_k\in C_k}\frac{z(w,c_k)\cdot\frac{\partial}{\partial w}\|\phi(x,w)-c_k\|_2^2}{\sum_{k=1}^{N_{\text{classes}}}\sum_{c_k'\in C_k} z(w,c_k')}\\
=&-\frac{\hat{s}}{2}\sum_{c_i\in C_i}\frac{z(w,c_i)\cdot\frac{\partial}{\partial w}\|\phi(x,w)-c_i\|_2^2}{\sum_{k=1}^{N_{\text{classes}}}\sum_{c_k'\in C_k} z(w,c_k')}\\
&-\frac{\hat{s}}{2}\sum_{\substack{k=1\\k\neq i}}^{N_{\text{classes}}}\sum_{c_k\in C_k}\frac{z(w,c_k)\cdot\frac{\partial}{\partial w}\|\phi(x,w)-c_k\|_2^2}{\sum_{k=1}^{N_{\text{classes}}}\sum_{c_k'\in C_k} z(w,c_k')}.
\end{aligned}$$

Combining both identities yields

$$\begin{aligned}
&\frac{\partial}{\partial w}\sum_{j=1}^{N_{\text{classes}}}\operatorname{lab}_j(x)\log(\operatorname{softmax}(\hat{s}\cdot\operatorname{sim}(\phi(x,w),C_j)))\\
=&\frac{\partial}{\partial w}\log\left(\sum_{c_i\in C_i}\frac{z(w,c_i)}{\sum_{k=1}^{N_{\text{classes}}}\sum_{c_k\in C_k} z(w,c_k)}\right)\\
=&\frac{\partial}{\partial w}\log\left(\sum_{c_i\in C_i} z(w,c_i)\right)-\frac{\partial}{\partial w}\log\left(\sum_{k=1}^{N_{\text{classes}}}\sum_{c_k\in C_k} z(w,c_k)\right)\\
=&-\frac{\hat{s}}{2}\sum_{c_i\in C_i}\frac{z(w,c_i)\cdot\frac{\partial}{\partial w}\|\phi(x,w)-c_i\|_2^2}{\sum_{c_i'\in C_i} z(w,c_i')}\\
&+\frac{\hat{s}}{2}\sum_{c_i\in C_i}\frac{z(w,c_i)\cdot\frac{\partial}{\partial w}\|\phi(x,w)-c_i\|_2^2}{\sum_{k=1}^{N_{\text{classes}}}\sum_{c_k'\in C_k} z(w,c_k')}\\
&+\frac{\hat{s}}{2}\sum_{\substack{k=1\\k\neq i}}^{N_{\text{classes}}}\sum_{c_k\in C_k}\frac{z(w,c_k)\cdot\frac{\partial}{\partial w}\|\phi(x,w)-c_k\|_2^2}{\sum_{k=1}^{N_{\text{classes}}}\sum_{c_k'\in C_k} z(w,c_k')}\\
=&-\frac{\hat{s}}{2}\left(\sum_{c_i\in C_i} z(w,c_i)\cdot\frac{\partial}{\partial w}\|\phi(x,w)-c_i\|_2^2\right.\\
&\cdot\left(\frac{1}{\sum_{c_i'\in C_i} z(w,c_i')}-\frac{1}{\sum_{k=1}^{N_{\text{classes}}}\sum_{c_k'\in C_k} z(w,c_k')}\right)\\
&\left.-\sum_{\substack{k=1\\k\neq i}}^{N_{\text{classes}}}\sum_{c_k\in C_k}\frac{z(w,c_k)\cdot\frac{\partial}{\partial w}\|\phi(x,w)-c_k\|_2^2}{\sum_{k=1}^{N_{\text{classes}}}\sum_{c_k'\in C_k} z(w,c_k')}\right)
\end{aligned}$$

$$
\begin{aligned}
&= -\frac{\hat{s}}{2}\Bigg(\sum_{c_i \in C_i} z(w,c_i) \cdot \frac{\partial}{\partial w}\|\phi(x,w) - c_i\|_2^2 \\
&\quad \cdot \Bigg(\sum_{\substack{k=1\\k\neq i}}^{N_{\text{classes}}} \sum_{c_k \in C_k} \frac{z(w,c_k)}{(\sum_{c_i' \in C_i} z(w,c_i'))(\sum_{k=1}^{N} \sum_{c_k' \in C_k} z(w,c_k'))}\Bigg) \\
&\quad - \sum_{\substack{k=1\\k\neq i}}^{N_{\text{classes}}} \sum_{c_k \in C_k} \frac{z(w,c_k) \cdot \frac{\partial}{\partial w}\|\phi(x,w) - c_k\|_2^2}{\sum_{k=1}^{N_{\text{classes}}} \sum_{c_k' \in C_k} z(w,c_k')}\Bigg) \\
&= -\frac{\hat{s}}{2} \sum_{\substack{k=1\\k\neq i}}^{N_{\text{classes}}} \sum_{c_k \in C_k} \frac{z(w,c_k)}{\sum_{k=1}^{N_{\text{classes}}} \sum_{c_k' \in C_k} z(w,c_k')} \\
&\quad \cdot \Bigg(\sum_{c_i \in C_i} \frac{z(w,c_i)}{\sum_{c_i' \in C_i} z(w,c_i')} \cdot \frac{\partial}{\partial w}\|\phi(x,w) - c_i\|_2^2 - \frac{\partial}{\partial w}\|\phi(x,w) - c_k\|_2^2\Bigg) \\
&= -\frac{\hat{s}}{2} \sum_{k=1}^{N_{\text{classes}}} \sum_{c_k \in C_k} \underbrace{\frac{z(w,c_k)}{\sum_{k=1}^{N_{\text{classes}}} \sum_{c_k' \in C_k} z(w,c_k')}}_{=P(\tau(\phi(x,w),\mathcal{C})=c_k)} \\
&\quad \cdot \sum_{c_i \in C_i} \underbrace{\frac{z(w,c_i)}{\sum_{c_i' \in C_i} z(w,c_i')}}_{=P(\tau(\phi(x,w))=c_i|\tau(\phi(x,w),\mathcal{C})\in C_i)} \\
&\quad \cdot \Bigg(\frac{\partial}{\partial w}\|\phi(x,w) - c_i\|_2^2 - \frac{\partial}{\partial w}\|\phi(x,w) - c_k\|_2^2\Bigg)
\end{aligned}
$$

where it is used that

$$
\begin{aligned}
&\frac{1}{\sum_{c_i' \in C_i} z(w,c_i')} - \frac{1}{\sum_{k=1}^{N_{\text{classes}}} \sum_{c_k' \in C_k} z(w,c_k')} \\
=&\frac{\sum_{k=1}^{N_{\text{classes}}} \sum_{c_k \in C_k} z(w,c_k) - \sum_{c_i \in C_i} z(w,c_i)}{(\sum_{c_i' \in C_i} z(w,c_i'))(\sum_{k=1}^{N_{\text{classes}}} \sum_{c_k' \in C_k} z(w,c_k'))} \\
=&\sum_{\substack{k=1\\k\neq i}}^{N_{\text{classes}}} \sum_{c_k \in C_k} \frac{z(w,c_k)}{(\sum_{c_i' \in C_i} z(w,c_i'))(\sum_{k=1}^{N_{\text{classes}}} \sum_{c_k' \in C_k} z(w,c_k'))}.
\end{aligned}
$$

Now, summing over all samples $x \in Y$, normalizing with $|Y|$ and taking the additive inverse yields the desired result.

When using mixup, the right hand side of the last equation needs to be replaced with a weighted sum of two terms, each corresponding to one of the two classes that are mixed-up, because there are $i_1, i_2 \in \{1, ..., N_{\text{classes}}\}$ such that $\text{lab}(x)_{i_1} \neq 0 \neq \text{lab}(x)_{i_2}$. Otherwise, the proof is exactly the same. In conclusion, the proven result still holds for mixed-up samples but includes two similar terms instead of one term. □

Note that this theorem explicitly shows that the intra-class compactness losses belonging to different sub-clusters of the same class are weighted with softmax probabilities that indicate to which sub-cluster an embedding belongs to. This allows that embeddings belong to a single sub-cluster by setting the probability belonging to one sub-cluster close to one and all other probabilities close to zero. Without these probabilistic weights, each embedding would be pulled towards the mean of all sub-clusters of the corresponding class to minimize the mean distance, which essentially means that only a single sub-cluster, i.e. one center, would be used for each class.

Using Theorem 3.5, a short proof for Corollary 3.3 will now be provided.

Proof of Corollary 3.3. The proof of Theorem 3.5 does not depend on the exact structure of the dynamically adaptive scale parameter and thus also holds for the standard AdaCos loss by replacing $\hat{s}$ with $\tilde{s}$ and using only a single sub-cluster for each class. □

3.4.3 *Comparison of backends*

According to Lemma 3.1, the cosine distance is equivalent to using a Gaussian with a spherical covariance matrix. Hence, using a GMM with a full covariance matrix and possibly multiple components is a generalization of using the cosine distance and may perform better in case the distribution of the normal samples is not spherical. This is illustrated in Figure 10. Note that this illustration is exaggerated because, by definition, an angular margin loss tries to ensure that the distribution for each class is roughly spherical. However, the resulting distributions may still be more complex, especially in higher-dimensional spaces.

Next, the choice of a suitable backend shall be investigated experimentally. For all experiments with Gaussians or GMMs, the implementation provided by scikit-learn [176] is used.

The performances obtained with different backends can be found in Table 6. As expected, using the softmax output of the embedding model instead of the cosine distance performs worst. The reason is that a softmax function models a posterior distribution over the normal classes and thus is not aiming at detecting out-of-distribution samples, i.e. anomalies. PLDA, as implemented in [208], performs slightly better but still worse than all the other backends. Since they are strongly related to each other or even equivalent, all backends using cosine distance or Gaussians with a spherical or diagonal covariance matrix perform very similarly. When using full covariance matrices, an improvement in performance can be observed and thus Gaussians or GMMs with full covariance matrices are used as a backend in the following experiments.

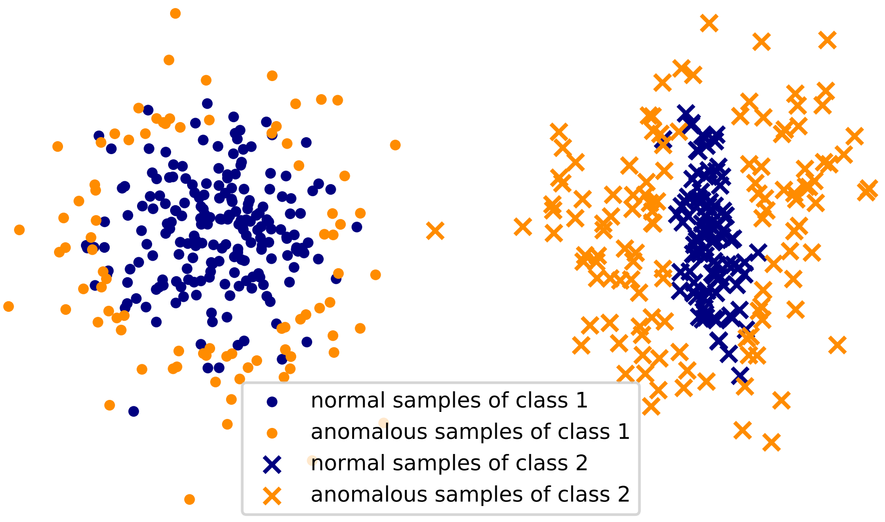

Figure 10: Scatter plot of normal and anomalous data belonging to two different classes. Both classes can be easily separated by measuring the distance to the respective class means. For class 1, anomalies can also be detected reasonably well. However, for class 2 only measuring the distance to the mean does not work well because the data is not distributed spherically. © 2021 IEEE

Table 6: Arithmetic means of AUC-ROCs and pAUCs for different machine types obtained with different backends. © 2021 IEEE

backend	development set		evaluation set	
	AUC-ROC	pAUC	AUC-ROC	pAUC
softmax output of embedding model	87.20%	81.70%	89.55%	83.79%
log-likelihood ratio of two-covariance PLDA	88.25%	82.18%	90.90%	84.32%
cosine distance to mean	88.71%	82.12%	91.13%	84.40%
mean of cosine distances to 10 closest samples	88.69%	82.12%	91.10%	84.38%
Gaussian (spherical covariance)	88.69%	82.12%	91.11%	84.38%
Gaussian (diagonal covariance)	88.71%	82.16%	91.12%	84.39%
Gaussian (full covariance)	**89.13%**	**82.59%**	**91.43%**	**84.47%**

Table 7: Arithmetic means of AUC-ROCs and pAUCs obtained with mixup and the sub-cluster AdaCos loss using only a single center per class. © 2021 IEEE

mixup	loss	development set		evaluation set	
		AUC-ROC	pAUC	AUC-ROC	pAUC
	AdaCos	86.96%	80.68%	89.63%	82.47%
	sub-cluster AdaCos	diverges	diverges	diverges	diverges
✗	AdaCos	89.13%	82.59%	91.43%	**84.47%**
✗	sub-cluster AdaCos	**91.60%**	**85.01%**	**91.64%**	83.93%

3.4.4 *Utilizing mixup*

Mixup is known to be very effective for CSC tasks. However, it is not clear whether the same benefits carry over to ASD. In addition, the definition of the dynamically adaptive scale parameter of the sub-cluster AdaCos loss, which depends on using mixup, still needs to be justified. Therefore, the effect of using mixup for ASD with angular margin losses is investigated by comparing the performances obtained with and without mixup. The results can be found in Table 7 and the following three observations can be made: First, using mixup improves the performance regardless of the angular margin loss being used. As applying mixup is simple yet effective, there appears to be no reason to not use it for ASD. Second, the dynamically adaptive scale parameter of sub-cluster AdaCos loss performs better than the original one of the AdaCos loss, which justifies the particular definition of the scale parameter. Third, when not using mixup, the sub-cluster AdaCos loss diverges. The reason is given in the following lemma.

Lemma 3.6. *When not using mixup, the dynamically adaptive scale parameter* $\hat{s}^{(t)}$ *of the sub-cluster AdaCos loss grows exponentially.*

Proof. After a few training iterations without mixup, i.e. for $t > t_0 \in \mathbb{N}$, most training samples will have a very small angle to the centers of their corresponding class and therefore $\sum_{c \in C_i} \mathrm{sim}(\phi(x, w^{(t)}), c) > 1$ for all $i \in \{1, \dots, N_{\text{classes}}\}$ and $x \in Y^{(t)} \cap Y_i$. Furthermore, as empirically shown in [264], on average $\alpha(\phi(x, w^{(t)}), c) < \frac{\pi}{2}$ and thus $\mathrm{sim}(\phi(x, w^{(t)}), c) > 0$ for most $x \in Y$ and $c \in \mathbb{R}^D$.

Hence, by using the fact that the logarithm is a concave function and applying Jensen's inequality it holds that

$$\begin{aligned}
\hat{s}^{(t)} &= \frac{\mathrm{sim}_{\max}^{(t)} + \log \hat{B}_{\mathrm{avg}}^{(t)}}{\cos\left(\min(\frac{\pi}{4}, \hat{\alpha}_{\mathrm{med}}^{(t)})\right)} \geqslant \mathrm{sim}_{\max}^{(t)} + \log \hat{B}_{\mathrm{avg}}^{(t)} \\
&= \log\left(\frac{1}{N_{\mathrm{batch}}} \sum_{x \in Y^{(t)}} \sum_{j=1}^{N_{\mathrm{classes}}} \sum_{c \in C_j} \exp\left(\hat{s}^{(t-1)} \, \mathrm{sim}(\phi(x, w^{(t)}), c)\right)\right) \\
&\geqslant \frac{1}{N_{\mathrm{batch}}} \sum_{x \in Y^{(t)}} \sum_{j=1}^{N_{\mathrm{classes}}} \sum_{c \in C_j} \hat{s}^{(t-1)} \, \mathrm{sim}(\phi(x, w^{(t)}), c) \\
&> \hat{s}^{(t-1)} \left(1 + \underbrace{\frac{1}{N_{\mathrm{batch}}} \sum_{x \in Y^{(t)}} \sum_{\substack{j=1 \\ \mathrm{lab}(x)_j \neq 1}}^{N_{\mathrm{classes}}} \sum_{c \in C_j} \mathrm{sim}(\phi(x, w^{(t)}), c)}_{>0}\right)
\end{aligned}$$

showing that $\hat{s}^{(t)}$ grows exponentially when not using mixup. Note that this inequality does not hold if only mixed-up samples are used for training. The reason is that the mixed-up samples do not have a very high cosine similarity with all of their corresponding class centers because they are positioned between classes and AdaCos increases the margin between classes. □

3.4.5 *Determining the number of sub-clusters*

In Table 8, the effect of using a different number of sub-clusters is investigated experimentally. It can be seen that using multiple sub-clusters significantly improves the performance, especially on the evaluation set. This justifies the definition of the sub-cluster AdaCos loss. Overall, the best results are obtained with 32 sub-clusters and using more sub-clusters degrades performance. Hence, the optimal number of sub-clusters is neither too high nor too low and thus is an additional hyperparameter to be tuned. Another observation is that using a GMM with components equal to the number of sub-clusters leads to slightly better performance than using a single Gaussian because the underlying distribution can be better represented. Note that using sub-clusters also allows the model to handle potential outliers or noisy samples contained in the training set by assigning them to small sub-clusters as done with the sub-center ArcFace loss [37].

3.4.6 *Replacing embeddings with input data statistics*

An alternative to training an embedding model with the goal of obtaining simple representations of the data is to compute statistics over the input features such as the temporal mean or temporal maximum. These statistics have the advantage that they do not require any training, yet, they may still contain useful information

Table 8: Arithmetic means of AUC-ROCs and pAUCs obtained with the sub-cluster AdaCos loss for different numbers of centers per class. © 2021 IEEE

number of sub-clusters	backend	development set		evaluation set	
		AUC-ROC	pAUC	AUC-ROC	pAUC
1	Gaussian	91.60%	85.01%	91.64%	83.93%
2	Gaussian	90.97%	82.54%	92.08%	85.08%
4	Gaussian	91.54%	83.53%	92.62%	84.31%
8	Gaussian	91.61%	85.24%	92.99%	85.74%
16	Gaussian	91.85%	85.61%	93.98%	88.27%
32	Gaussian	92.22%	85.69%	94.56%	87.51%
64	Gaussian	91.39%	83.58%	93.85%	85.43%
1	GMM	91.60%	85.01%	91.64%	83.93%
2	GMM	91.07%	82.70%	92.20%	85.60%
4	GMM	91.67%	83.70%	92.64%	84.35%
8	GMM	91.85%	85.46%	93.13%	86.07%
16	GMM	92.10%	85.84%	94.08%	**88.59%**
32	GMM	**92.57%**	**86.37%**	**94.69%**	87.90%
64	GMM	92.03%	84.06%	94.16%	86.19%

for detecting anomalous samples. The main difference to trained embeddings is that the information contained in these representations is not necessarily useful to discriminate between the classes of the auxiliary task. This may have a positive or negative impact on detecting anomalous samples and will now be investigated experimentally. To this end, statistics of all features belonging to individual data samples are calculated and treated as if they were trained embeddings. To compute an anomaly score, a GMM with a single Gaussian component is used as using more components did not improve the performance.

The experimental results can be found in Table 9. It can be seen that the overall performance of the statistical representations is much worse than the one obtained with trained embeddings. This is also to be expected as using an auxiliary classification task allows the embeddings to ignore the background noise whereas statistical representations are more strongly affected by noise. However, these statistical representations lead to surprisingly good performance. The temporal maximum works well for the machine type “valve” and the temporal mean works well for the two machine types “ToyCar” and “ToyConveyor”. For “ToyConveyor”, the performance is even much better than the learned embeddings. A likely reason is that the auxiliary classification task is too simple meaning that the machines of this machine type are easily recognized and thus the embeddings do not capture enough infor-

Table 9: Mean AUC-ROCs and pAUCs per machine type obtained with different representations. When using the combined representations, only the learned representations are used, except for machine type ToyConveyor where the temporal mean is used instead. © 2021 IEEE

representation	machine type	development set		evaluation set	
		AUC-ROC	pAUC	AUC-ROC	pAUC
temporal mean	fan	80.73%	66.16%	95.32%	80.62%
temporal maximum	fan	64.59%	51.48%	78.98%	57.70%
learned	fan	**87.61%**	**77.93%**	**97.60%**	**93.24%**
temporal mean	pump	82.99%	68.50%	88.24%	70.36%
temporal maximum	pump	70.13%	59.17%	68.96%	55.08%
learned	pump	**94.71%**	**88.91%**	**96.76%**	**88.30%**
temporal mean	slider	87.46%	63.95%	72.16%	53.08%
temporal maximum	slider	93.69%	76.69%	90.55%	70.65%
learned	slider	**99.55%**	**97.63%**	**97.61%**	**89.46%**
temporal mean	valve	55.59%	50.23%	54.86%	52.09%
temporal maximum	valve	98.54%	93.08%	96.35%	88.18%
learned	valve	**98.63%**	**94.62%**	**98.81%**	**95.80%**
temporal mean	ToyCar	94.10%	80.94%	91.54%	76.87%
temporal maximum	ToyCar	68.36%	53.85%	70.31%	54.90%
learned	ToyCar	**96.37%**	**91.64%**	**95.99%**	**91.93%**
temporal mean	ToyConveyor	**85.78%**	**67.76%**	**91.74%**	**78.13%**
temporal maximum	ToyConveyor	57.51%	50.39%	65.40%	53.06%
learned	ToyConveyor	73.89%	61.22%	81.37%	68.64%
temporal mean	all	80.91%	66.19%	82.31%	68.52%
temporal maximum	all	76.25%	64.71%	78.42%	63.26%
learned	all	92.57%	86.37%	94.69%	87.90%
combined	all	**94.21%**	**87.13%**	**96.42%**	**89.24%**

mation to discriminate between normal and anomalous samples. For the machine types for which one statistic works well, the other statistic performs very poorly. Hence, while these statistical representations may lead to a good performance, they need to be carefully chosen for each machine type. To obtain the best possible performance, a combined model is designed by using the learned embeddings for each machine type except "ToyConveyor" for which the temporal mean is used instead. This approach of using statistics of input features as representations was later extended in [70] by using global weighted ranking pooling [109], i.e. applying a geometric sequence of weights to time frames of a log-Mel spectrogram sorted according to their energy over all frequency bins. Global weighted ranking pooling is a generalization of both statistics used above and led to a good overall performance without training any model except for choosing the weights. However, note that determining these weights for individual machine types requires access to anomalous data for each machine type and thus is highly impractical for any given application and in fact not possible in a truly semi-supervised setting. This is the reason why no additional experiments with this approach are carried out in this thesis.

3.4.7 *Comparison to other published systems*

To show that the presented ASD system performs well, its performance is compared to the five top-performing systems of the DCASE2020 Challenge in Figure 11. It can be seen that the system outperforms all other systems and thus reaches a new state-of-the-art performance. Since all systems except the one submitted by Primus [183] are ensembles, an ensemble was also created here to allow for a fair comparison. The ensemble is obtained by training seven variations of the single model, each with a different number of sub-clusters ranging from 2^0 to 2^6, and using the sum of the anomaly scores obtained with each system as the ensembeled anomaly score. As a result, the ensembled system reaches an AUC-ROC of 97% and a pAUC of 91.24% and thus performs even better than the proposed single model system.

3.5 SUMMARY

In this chapter, different loss functions for training an embedding model were compared theoretically and empirically. More concretely, the compactness loss and the AdaCos loss as representatives of one-class and angular margin losses were compared. It was shown that both are very closely related as minimizing an angular margin loss minimizes the intra-class compactness losses for each class while also maximizing all inter-class compactness losses. Additionally, it was shown experimentally that the ASD performance is much better when using a classification task in a joint embedding space instead of not using meta information as classes or individual embedding spaces learned with one-class losses. This helps to closely monitor the target sounds to detect anomalous signal components and largely ignore the background noise.

The other main content of this chapter has been the presentation of the sub-cluster AdaCos loss, which has a similar relation to the compactness loss as the AdaCos loss. The sub-cluster AdaCos loss is an extension of AdaCos that uses multiple centers for each class to enable the embedding model to utilize sub-classes

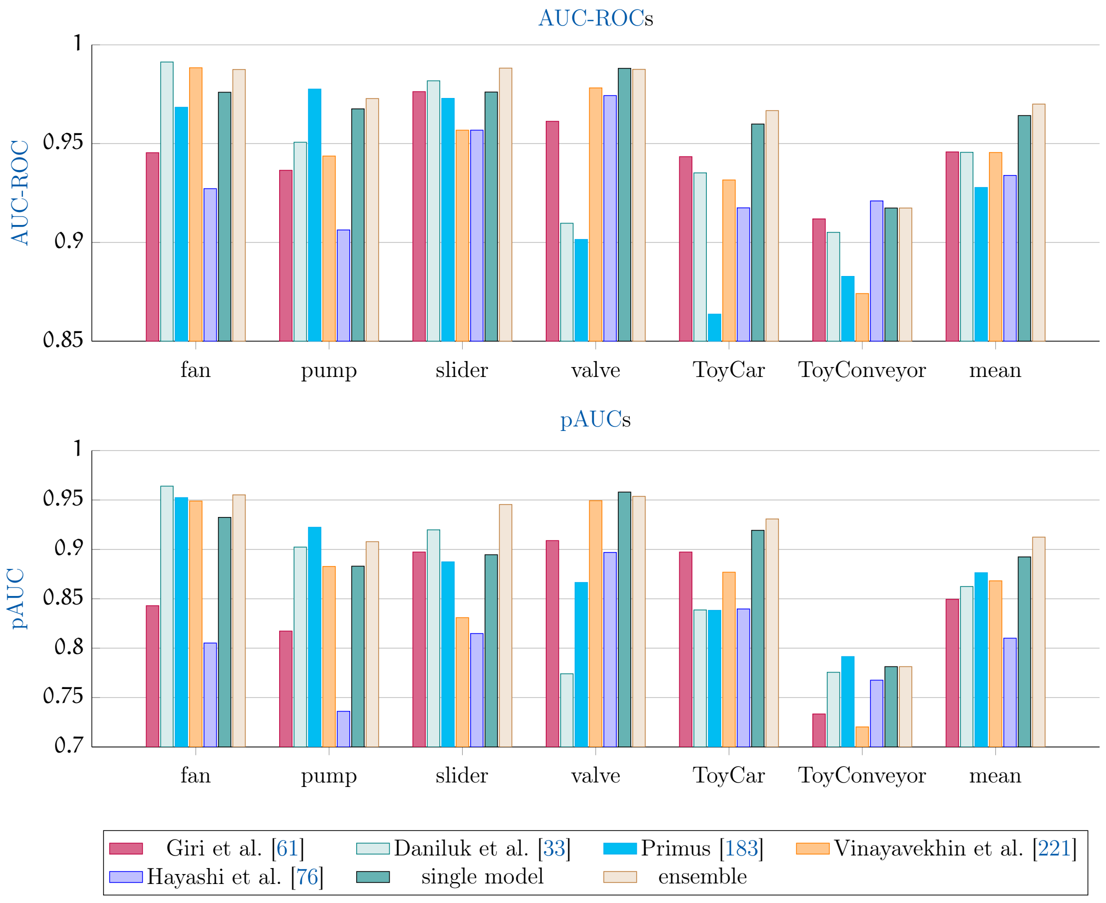

Figure 11: Comparison of the AUC-ROCs and pAUCs obtained on the evaluation set with the top five highest-ranked systems submitted to the DCASE2020 Challenge task 2, the proposed approach and an ensemble. The ensemble consists of the sum of all log-probabilities given by GMMs belonging to trained models of the proposed approach with a different number of sub-clusters, ranging from 2^0 to 2^6. © 2021 IEEE

and learn more complex distributions for the normal data than simple Gaussian distributions. Using the sub-cluster AdaCos loss, mixup and a GMM with a full covariance matrix were all shown to significantly improve the ASD performance. As a result, the proposed ASD system and an ensemble reached a new state-of-the-art performance on the DCASE2020 dataset. In a last experiment, it was shown that using statistics of the input data, as for example the temporal mean of time-frequency representations, instead of learning embeddings yields surprisingly good results. Still, the performance is worse than when using the learned embeddings.

In total, the presented ASD system reached an AUC-ROC of 97% on the DCASE2020 dataset, which is close to optimal performance. Hence, the difficulty of the ASD task needs to be increased in order to obtain additional findings. This will be done in Chapter 5 by utilizing datasets for acoustic machine condition monitoring recorded in domain-shifted conditions. But before increasing the difficulty of the task, it will be investigated how to estimate good decision thresholds.

4 DECISION THRESHOLD ESTIMATION

When using an ASD system in practice, decision thresholds need to be applied to the anomaly scores to distinguish between normal and anomalous samples. As stated in Section 2.11, several methods are available for estimating decision thresholds in a semi-supervised setting. The reader shall be reminded that only normal training data can be used for estimating the decision thresholds as already stated in Section 2.11. The reason is that anomalous training samples are not available and that test samples should be treated independently, i.e. one cannot utilize all (unlabeled) normal and anomalous test samples for estimating a threshold based on their assumed binary class distribution. Because of this, all estimation methods are based on the assumption that a threshold, which separates the extreme values of the anomaly scores belonging to normal training samples from the moderate values, is also a good choice for separating anomalous and normal samples. The goal of this chapter is to investigate how to robustly estimate good decision thresholds and how to take the difficulty of estimating a threshold into account when evaluating the performance of an ASD system.

This chapter is structured as follows: First, multiple methods for estimating a decision threshold will be compared experimentally. In a second section, the threshold-independent evaluation metric F_1-EV, which in contrast to AUC-ROC also measures the difficulty of estimating a good decision threshold, will be presented and compared to other evaluation metrics.

4.1 CONTRIBUTIONS OF THE AUTHOR

The sections of this chapter are largely based on the following key publications:

- Kevin Wilkinghoff and Alessia Cornaggia-Urrigshardt. "On choosing decision thresholds for anomalous sound detection in machine condition monitoring." In: *24th International Congress on Acoustics (ICA)*. The Acoustical Society of Korea, 2022.

- Kevin Wilkinghoff and Keisuke Imoto. "F1-EV Score: Measuring the Likelihood of Estimating a Good Decision Threshold for Semi-Supervised Anomaly Detection." In: *International Conference on Acoustics, Speech and Signal Processing (ICASSP)*. IEEE, 2024, pp. 256–260.

For publications that are not single-authored, individual contributions of the thesis author and all co-authors to these publications are stated in Section A.1. If not stated otherwise, the content listed in the following paragraph is the sole contribution of the thesis author.

Section 4.2 is based on [247]. Alessia Cornaggia-Urrigshardt helped to implement the different approaches for estimating decision thresholds. Section 4.3 is based on [251]. Keisuke Imoto proposed to include Section 4.3.4 including Figure 20. Furthermore, he provided the anomaly scores and decision thresholds of the systems submitted to the DCASE2023 ASD Challenge, which are used as a dataset as described in Section 4.3.2.

4.2 ESTIMATING A DECISION THRESHOLD

In Section 2.11, multiple methods for estimating a decision threshold were presented. However, when designing an ASD system two questions remain: "Which of these methods should be used?" and "To which anomaly scores should such a method be applied?". The goal of this section is to answer both questions. For all estimation methods evaluated in this section, 90th percentiles and the hyperparameter settings $\beta_{\text{SD}} = 1.28, \beta_{\text{MAD}} = 2, \beta_{\text{IQR}} = 0.5, \nu_{\text{SVM}} = 0.1$ as well as two iterations for MST were used as similar settings are also used in the literature and these particular settings led to reasonable results.

4.2.1 *Performance comparison of different estimation methods*

To compare the performance of the estimation methods, the F_1 score resulting from applying an estimation method to the anomaly scores obtained with the same ASD system as presented in Section 3.2.2 is used. To reduce the variance of the results, each experiment is repeated five times by retraining the ASD system and estimating a decision threshold with each method. In addition to the estimation methods, optimal decision thresholds are determined by manually varying them to optimize the performance on the test splits of the development and evaluation set. These optimal thresholds are used to analyze how close the performance obtained with an estimated decision threshold is to the best possible performance.

The F_1 scores obtained on the test split of the development set and of the evaluation set can be found in Table 10 and Table 11, respectively.

Depending on the machine type, one can observe that the absolute performances are strongly varying. This is also true for the optimum performance and therefore drawing conclusions by analyzing the absolute F_1 scores is difficult. A better approach is to measure how close the performance of an estimated decision threshold is to the performance obtained with an optimal decision threshold. This was done in a second experiment by calculating the ratio between both performances. The results are depicted in Figure 12. It can be observed that most estimation methods perform equally well except for GESD, which led to worse performance on the development and evaluation set, and GDP as well as MST-GDP, which led to slightly worse performance on the development set. Furthermore, the iterative approaches (GESD, cleverSD and MST) perform slightly better than their non-

Table 10: Comparison of F_1 scores obtained with different threshold estimation methods on the *development set* of the DCASE2020 dataset. Means of F_1 scores taken over all machine IDs belonging to single machine types obtained with five independent trials are shown. Highest F_1 score among different methods for each machine type is highlighted in bold.

method	machine type						
	fan	pump	slider	ToyCar	ToyConveyor	valve	mean
GDP	0.832	0.823	0.911	0.808	0.618	0.879	0.812
HP	0.753	0.837	0.951	0.848	0.673	0.898	0.827
SD	0.751	0.839	0.951	0.850	0.672	0.900	0.827
MAD	0.762	0.844	0.951	0.854	0.670	**0.902**	0.830
IQR	0.790	0.843	0.939	0.837	0.677	0.897	0.831
OCSVM	0.753	0.837	0.950	0.849	0.673	0.898	0.827
GESD	0.662	0.816	**0.968**	**0.864**	0.594	0.870	0.796
cleverSD	0.836	0.835	0.919	0.821	0.663	0.885	0.826
MST-GDP	**0.864**	0.810	0.888	0.773	0.611	0.865	0.802
MST-HP	0.816	0.836	0.926	0.814	0.663	0.888	0.824
MST-SD	0.827	0.833	0.919	0.806	0.659	0.882	0.821
MST-MAD	0.797	**0.849**	0.940	0.847	**0.676**	0.898	**0.835**
MST-IQR	0.833	0.834	0.916	0.806	0.659	0.883	0.822
MST-OCSVM	0.816	0.836	0.927	0.815	0.663	0.887	0.824
optimum	0.926	0.889	0.985	0.892	0.689	0.919	0.883

Table 11: Comparison of F_1 scores obtained with different threshold estimation methods on the *evaluation set* of the DCASE2020 dataset. Means of F_1 scores taken over all machine IDs belonging to single machine types obtained with five independent trials are shown. Highest F_1 score among different methods for each machine type is highlighted in bold.

method	machine type						
	fan	pump	slider	ToyCar	ToyConveyor	valve	mean
GDP	0.900	0.861	0.889	0.601	0.635	0.671	0.759
HP	0.938	0.892	**0.923**	0.584	0.597	0.656	0.765
SD	0.937	0.893	0.921	0.577	0.600	0.656	0.764
MAD	0.939	0.890	0.919	0.572	0.598	0.651	0.761
IQR	0.941	**0.894**	0.920	0.600	0.619	0.665	0.773
OCSVM	0.938	0.892	0.923	0.583	0.596	0.656	0.765
GESD	0.910	0.882	0.900	0.513	0.496	0.616	0.719
cleverSD	0.941	0.874	0.909	0.618	0.643	0.679	0.777
MST-GDP	0.907	0.852	0.885	**0.638**	**0.663**	**0.692**	0.773
MST-HP	0.943	0.885	0.915	0.618	0.636	0.676	0.779
MST-SD	0.943	0.879	0.911	0.624	0.642	0.683	**0.780**
MST-MAD	0.941	0.892	0.919	0.592	0.619	0.664	0.771
MST-IQR	**0.943**	0.875	0.910	0.626	0.643	0.684	0.780
MST-OCSVM	0.943	0.885	0.915	0.618	0.636	0.676	0.779
optimum	0.965	0.944	0.959	0.759	0.725	0.784	0.856

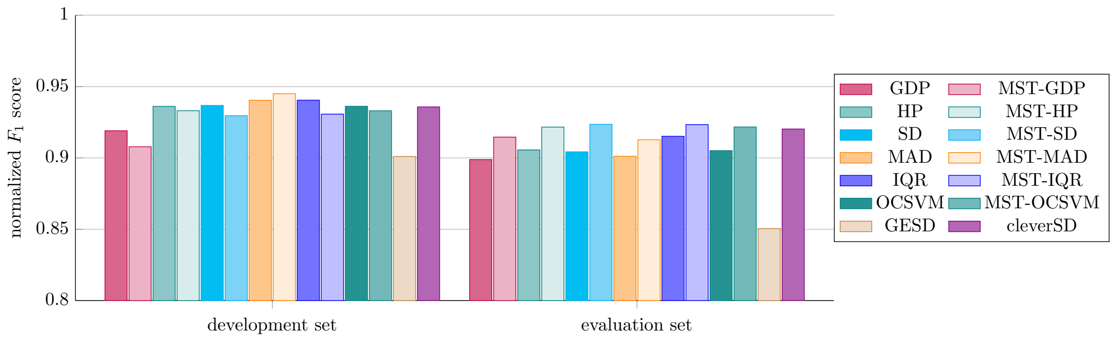

Figure 12: Normalized F_1 scores obtained with different threshold estimation methods on the DCASE2020 dataset. Means of normalized F_1 scores taken over all machine IDs belonging to single machine types obtained with five independent trials are shown.

iterative counterparts and thus should be the preferred choice when estimating decision thresholds.

4.2.2 *Choosing a set of observed anomaly scores*

Only the normal training samples are available to calculate anomaly scores and thus the same scores that have been used to train the ASD system need to be used to estimate a decision threshold. However, an alternative is to first divide the normal training samples into two disjoint sets and use one set to train the ASD system and the other set to estimate a decision threshold. The idea is to use previously unseen samples when estimating the decision thresholds as this may generate less optimistic and thus more realistic anomaly scores, which are expected to be more similar to the anomaly scores of the test samples than the ones used for training the model.

When using only a subset of the normal training samples to train the ASD system, it is expected that the performance will degrade because less information is provided. As a first experiment, it will be investigated how much normal data should at least be used to train the system and how much data can be used for estimating thresholds. This is done by computing the optimal F_1 score for models that have only been trained with a subset of the normal training samples. The results, depicted in Figure 13, show that the degradation of performance is far less severe as one would expect and is only noticeable when using less than 60% of the data for training. Moreover, even when using only 5% of training samples the degradation in performance is relatively small. A possible explanation is that the variation of fully-functioning machine sounds is not very strong when ignoring the background noise and not changing any parameter settings and thus their normal behaviour can be captured with relatively few data samples.

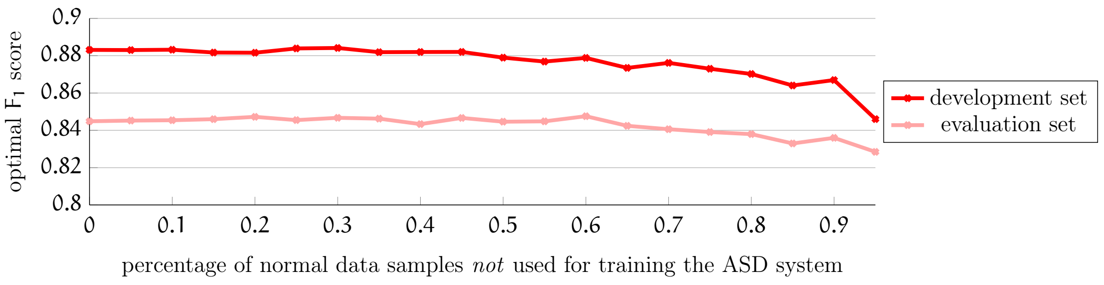

Figure 13: Optimal F_1 scores obtained on the DCASE2020 dataset when using a varying percentage of normal data samples not used for training the ASD system. Means of optimal F_1 scores taken over all machine IDs belonging to single machine types obtained with five independent trials are shown.

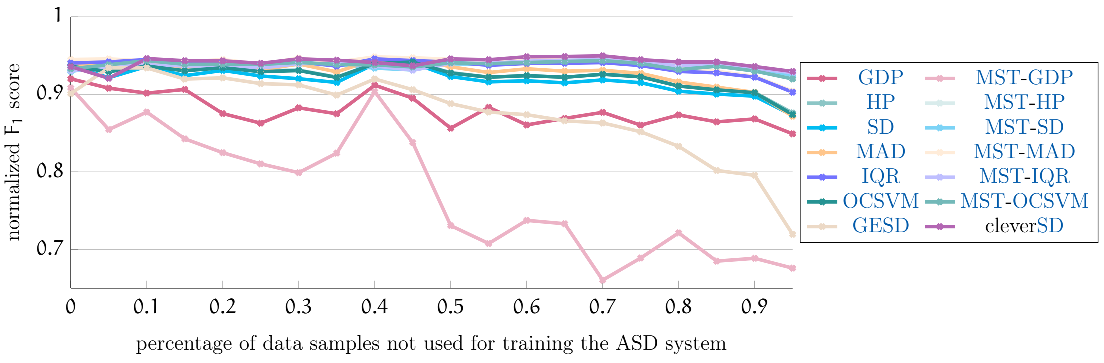

Figure 14: Normalized F_1 scores obtained with different threshold estimation methods on the development set of the DCASE2020 dataset when using a varying percentage of normal data samples not used for training the ASD system. Means of normalized F_1 scores taken over all machine IDs belonging to single machine types obtained with five independent trials are shown.

In a second experiment, the normalized F_1 scores were calculated for different partitions of the normal training samples into a set used for training the system and a set for estimating the thresholds. The results are depicted in Figure 14 and Figure 15.

The following observations can be made: First, most methods have a relatively stable performance except for GDP, MST-GDP and GESD. Second, iterative approaches perform slightly better than non-iterative estimation methods. All of these observations are consistent with the findings of the previous subsection. Thirdly and most importantly, there is no clearly visible improvement in performance when using only a subset of the normal samples for training the model. Actually, the absolute performance is decreasing because the optimal F_1 scores are also decreasing (cf. Figure 13). As a last observation, the difference in performance between the estimation methods increases the less data is used for training the system. In conclusion, only using a part of the normal samples for training and

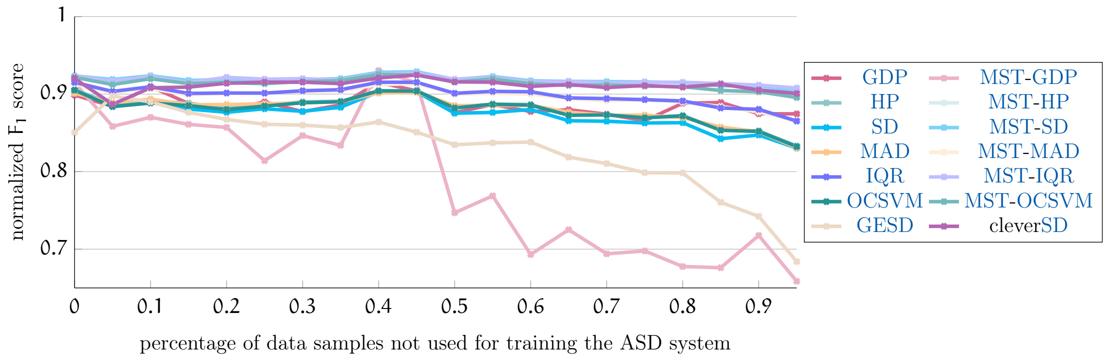

Figure 15: Normalized F_1 scores obtained with different threshold estimation methods on the evaluation set of the DCASE2020 dataset when using a varying percentage of normal data samples not used for training the ASD system. Means of normalized F_1 scores taken over all machine IDs belonging to single machine types obtained with five independent trials are shown.

the other part for estimating the decision threshold has no benefits and one can simply use all data for training the model.

4.3 F_1-EV SCORE

An AUC-ROC score equal to one means that an optimal decision threshold perfectly separating the anomaly scores of all normal samples from the ones of the anomalous samples exists (see Theorem 2.10). Despite having such a maximal AUC-ROC score, the cardinality of the set of optimal decision thresholds and thus also the difficulty of estimating this optimal threshold may strongly vary for different sets of anomaly scores. This is illustrated with toy examples in Figure 16. In practice, estimating a good decision threshold is important to be able to separate normal and anomalous samples. Therefore, the difficulty of estimating such a threshold should be included to fully measure the performance of an ASD system. A naïve solution to this problem is to use an additional threshold-dependent performance measure such as the F_1 score. However, threshold-dependent metrics depend on the specific choice of a threshold and thus are subjective. Furthermore, an objective comparison of ASD systems requires a well-defined ranking of performances, which is difficult to define when using multiple performance metrics at once. This motivates the definition of the F_1-EV score, which is a threshold-independent performance measure that incorporates the difficulty of estimating a good decision threshold.

4.3.1 *Definition*

The idea of the F_1-EV score is to calculate the expected value (EV) of a random variable that models the F_1 score of an ASD system for varying decision thresholds.

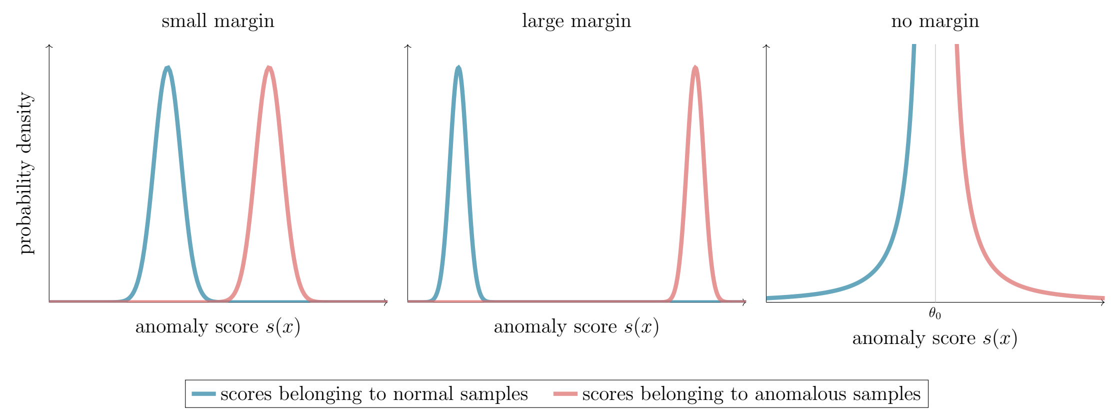

Figure 16: Toy examples of perfectly separable anomaly score distributions, each with an AUC-ROC equal to 1. On the left, the margin between normal and anomalous scores is small. In the center, the margin between the distributions is large and thus estimating a good decision threshold is much easier. On the right, the only optimal decision threshold is $\theta = \theta_0$, which is a null set with measure zero, and thus estimating this threshold also has a likelihood of zero when assuming a continuous distribution with uncountable support for estimated thresholds. Note that when estimating a decision threshold, only a finite number of anomaly scores belonging to the distribution of normal samples are available and usually both distributions are more complex and overlap. This is the reason why estimating a good decision threshold is highly non-trivial. © 2024 IEEE

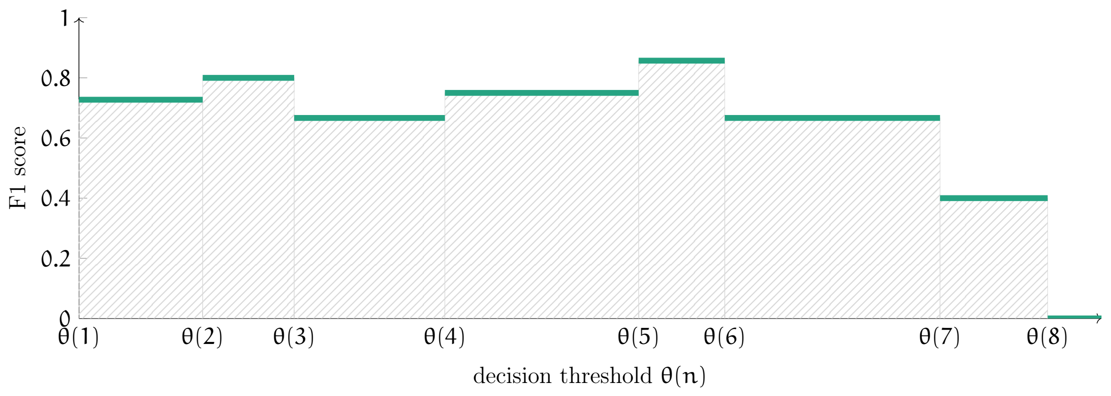

Figure 17: Example of computing F_1-EV. For illustration purposes only very few decision thresholds are shown. © 2024 IEEE

This is done by calculating the F_1 score for all possible thresholds and thus choosing a specific decision threshold is not required, i.e. the F_1-EV score is threshold-independent. A finite Riemann sum is used to calculate the EV given by the area under the F_1 score function as illustrated in Figure 17. Note that according to [35], computing the area under the precision-recall curve by using linear interpolations such as the trapezoidal rule leads to over-optimistic approximations. The F_1 score is the harmonic mean of precision and recall, which is the reason why a Riemann sum is used instead of the trapezoidal rule. Since the F_1 score function is piecewise constant with respect to the decision threshold, using more points than the anomaly scores of the provided samples when computing the area does not improve the accuracy of the approximation. The F_1-EV score will now be formally defined.

Definition 4.1 (F_1-EV score)**.** Let $(\theta_{\text{sorted}}(k))_{k=1,\dots,|X_{\text{test}}|} \subset \mathbb{R}$ denote a monotonically increasing sequence of decision thresholds, which correspond to the sorted anomaly scores obtained with the test samples. Define the normalized distance between two decision thresholds as

$$\overline{\Delta}_{\text{diff}}\theta_{\text{sorted}}(k) \coloneqq \frac{\theta_{\text{sorted}}(k+1) - \theta_{\text{sorted}}(k)}{\theta_{\text{sorted}}(|X_{\text{test}}|) - \theta_{\text{sorted}}(1)}. \tag{48}$$

Then, the F_1-EV score is defined as

$$F_1\text{-EV}(X_{\text{test}}, \text{score}, \theta_{\text{sorted}}) \coloneqq \sum_{k=1}^{|X_{\text{test}}|-1} F_1(X_{\text{test}}, \text{score}, \theta_{\text{sorted}}(k))\overline{\Delta}_{\text{diff}}\theta_{\text{sorted}}(k) \in [0,1] \tag{49}$$

with higher values indicating better performance.

Remark. When assuming a uniform distribution for randomly choosing decision thresholds in the interval $[\theta_{\text{sorted}}(1), \theta_{\text{sorted}}(|X_{\text{test}}|)]$, $\overline{\Delta}_{\text{diff}}\theta_{\text{sorted}}(k)$ corresponds to the likelihood of choosing a decision threshold yielding the same F_1 score as $\theta_{\text{sorted}}(k)$. Hence, the F_1-EV curve is indeed the expected value of a random variable modeling the F_1 score of an ASD system.

To calculate the F_1-EV score, one has to provide a range $[\theta_{\min}, \theta_{\max}] \subset \mathbb{R}$ to which all possible estimated decision thresholds belong to. Otherwise, it would always be equal to zero for a finite set of anomaly scores. In the previous definition, this range was defined by using the values $\theta_{\text{sorted}}(1)$ and $\theta_{\text{sorted}}(|X_{\text{test}}|)$ as lower and upper bounds, respectively. However, many values contained in this interval are unlikely to be chosen as decision thresholds. This is particularly true if the anomaly scores belonging to the test set contain a few outliers that strongly skew the results. Hence, robustly chosen boundaries may be beneficial to improve the F_1-EV score as a performance metric. To this end, the lower bound $\theta_{\min} \in \mathbb{R}$ is chosen to be close to the mean of the normal test samples, assuming that one would not estimate a decision threshold that is much smaller than this value. The upper bound $\theta_{\max} \in \mathbb{R}$ is more difficult to choose because some large anomaly scores may be outliers having very high values. Instead the upper bound is chosen to be close to the center $\theta_{\text{opt}} \in \mathbb{R}$ of the set of all empirically optimal decision thresholds, assuming that ideally one would not estimate a decision threshold much larger than this value. Note that these boundaries are based on the anomaly scores belonging to the normal test samples to be independent from a particular set of training samples. Although one may argue that this leads to over-optimistic results, it needs to be assumed that the normal samples of the training and test set follow the same distribution to be able to estimate a suitable decision threshold anyway. Furthermore, as shown in Section 4.2.2, holding back a few normal training samples to estimate better decision thresholds does not improve the performance indicating that this assumption is valid. Formally, the bounded F_1-EV score is defined as follows.

Definition 4.2 (Bounded F_1-EV score)**.** Let $(\theta_{\text{sorted}}(k))_{k=1,...,|X_{\text{test}}|} \subset \mathbb{R}$ denote a monotonically increasing sequence of decision thresholds, which correspond to the sorted anomaly scores obtained with the test samples. Let $\beta_{F_1\text{-EV}} \in \mathbb{R}_+$ and $\theta_{\text{opt}} \in \mathbb{R}$ denote the center of all empirically optimal decision thresholds. Define

$$\begin{aligned} \theta_{\min} &:= \text{mean}((\theta_{\text{sorted}}(k))_{k=1,...,|X_{\text{test}}|}) && -\beta_{F_1\text{-EV}} \cdot \text{std}((\theta_{\text{sorted}}(k))_{k=1,...,|X_{\text{test}}|}) \\ \theta_{\max} &:= \theta_{\text{opt}} && +\beta_{F_1\text{-EV}} \cdot \text{std}((\theta_{\text{sorted}}(k))_{k=1,...,|X_{\text{test}}|}) \end{aligned} \tag{50}$$

and set $k_{\min} := \arg\min_{k=1,...,|X_{\text{test}}|}\{\theta_{\text{sorted}}(k) : \theta_{\text{sorted}}(k) > \theta_{\min}\}$ and $k_{\max} := \arg\max_{k=1,...,|X_{\text{test}}|}\{\theta_{\text{sorted}}(k) : \theta_{\text{sorted}}(k) < \theta_{\max}\}$. Furthermore, set $K_{\text{valid}} := k_{\max} - k_{\min} + 3$ and

$$\theta_{\text{bounded}}(k) := \begin{cases} \theta_{\min} & \text{if } k = 1 \\ \theta_{\text{sorted}}(k + k_{\min} - 2) & \text{if } 2 \leqslant k \leqslant K_{\text{valid}} - 1 \\ \theta_{\max} & \text{if } k = K_{\text{valid}} \end{cases} \tag{51}$$

for $k = 1, ..., K_{\text{valid}}$. Then, the bounded F_1-EV score is defined as

$$\begin{aligned} &F_1\text{-EV}_{\text{bounded}}(X_{\text{test}}, \text{score}, \theta_{\text{bounded}}) \\ := &\sum_{k=1}^{K_{\text{valid}}-1} F_1(X_{\text{test}}, \text{score}, \theta_{\text{bounded}}(k))\overline{\Delta}_{\text{diff}}\theta_{\text{bounded}}(k) \in [0, 1] \end{aligned} \tag{52}$$

with

$$\overline{\Delta}_{\text{diff}}\theta_{\text{bounded}}(k) := \frac{\theta_{\text{bounded}}(k+1) - \theta_{\text{bounded}}(k)}{\theta_{\text{bounded}}(K_{\text{valid}}) - \theta_{\text{bounded}}(1)}. \tag{53}$$

4.3.2 *Experimental setup*

To experimentally evaluate the F_1-EV score, the anomaly scores and decision thresholds of all systems submitted to the ASD task of the DCASE2023 Challenge [44] were used. A detailed description of the DCASE2023 dataset can be found in Section 5.2. For the experiments conducted in this section, it is sufficient to know that the dataset contains recordings of 14 different machine types. Each machine type is recorded under two different acoustic conditions, called source and target domain. During testing, it is unknown to which of these two domains a given sample belongs to. Evaluations are done independently for each machine type using a single decision threshold for both domains. To compare the performances of ASD systems submitted to this challenge, the harmonic mean of the AUC-ROCs and pAUCs belonging to all 14 machine types was used. Therefore, choosing a decision threshold is not necessary and was entirely optional, which is the reason why some participants did not provide a decision threshold. For the experimental evaluations done here, only the F_1 scores of all submitted systems belonging to individual machine types that are greater than zero were used to not use invalid submissions. Furthermore, $\beta_{\mathsf{F}_1\text{-EV}} = 0.2$ is used for the bounded F_1-EV score.

4.3.3 *Experimental comparison with existing evaluation metrics*

Figure 18 and Figure 19 depict comparisons of different evaluation metrics in terms of the Pearson correlation coefficient (PCC). The following observations can be made: First of all, AUC-ROC has a low to moderate correlation with the F_1 scores resulting from the estimated (PCC $= 0.503$) and the optimal decision thresholds (PCC $= 0.497$). This affirms the motivation for introducing F_1-EV as a new performance measure. Second, the F_1-EV score has a very low correlation with AUC-ROC (PCC $= 0.199$) and a low correlation with the F_1 scores (PCC $= 0.380$ and PCC $= 0.306$). Third, the bounded F_1-EV score has a high correlation with AUC-ROC (PCC $= 0.748$) and both F_1 scores (PCC $= 0.696$ and PCC $= 0.732$). This shows that the bounded F_1-EV score works as intended and properly defined bounds for the F_1-EV score are needed to obtain useful results. Although most estimation methods lead to decision thresholds with similar performance as shown in Section 4.2, it shall be emphasized that for some submissions the estimated decision thresholds may be far from optimal. For these submissions, the correlation between the bounded F_1-EV and the F_1 score obtained with the estimated decision thresholds can be increased when using better estimates.

When inspecting Figure 18, one can see clusters looking similar to horizontal lines in all sub-figures belonging to F_1 scores of approximately two-thirds. To give an example, in sub-figure (a) this horizontal line ranges from an AUC-ROC of 0.4 to an AUC-ROC of 0.9. These lines look suspiciously wrong but can in fact be explained by the following: Since the recordings for each machine type belong to two different domains, it is possible that the provided decision thresholds yield almost perfect results for one domain while performing very poorly for the other domain. This means that either precision or recall are almost equal to 1 for both domains. Then the other value is close to 1 for only one domain while being close to 0 for the other domain and thus is approximately equal to 0.5 for both domains when assuming that both domains have approximately the same number of test samples. Since the F_1 score is the harmonic mean of precision and recall, this yields an F_1 score equal to two-thirds.

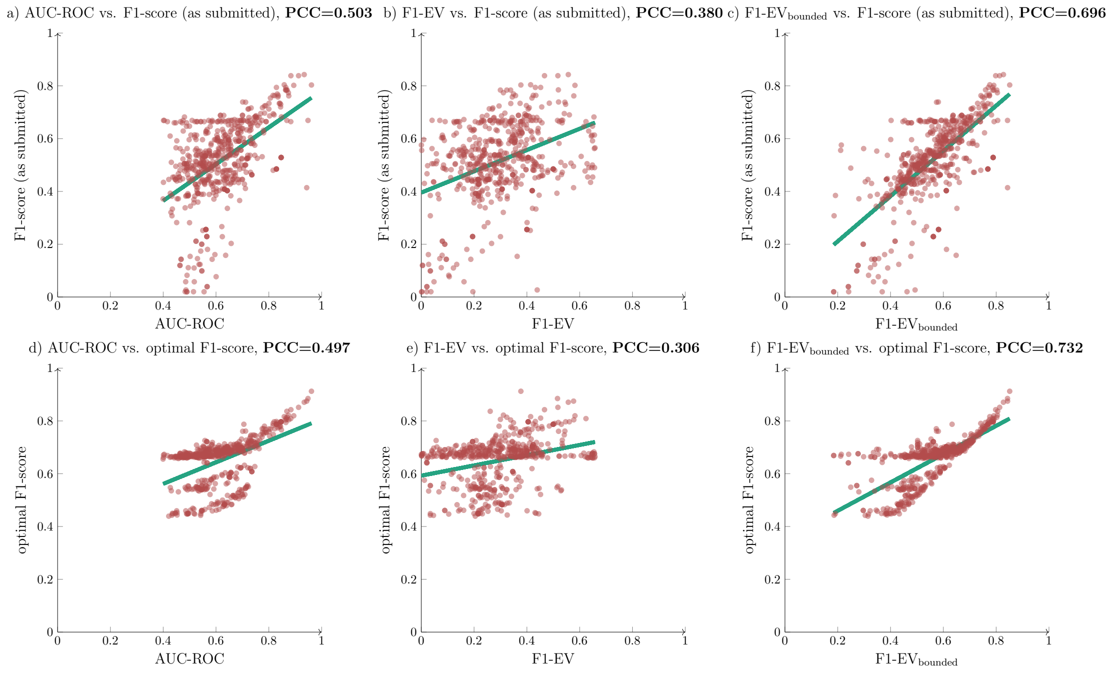

Figure 18: Comparison of several different performance measures computed on the evaluation set of task 2 of the DCASE2023 Challenge. In the top row, threshold-independent performance measures are compared to the F_1 score obtained with the submitted decision threshold. In the bottom row, threshold-independent performance measures are compared to the F_1 score obtained with an optimal decision threshold. © 2024 IEEE

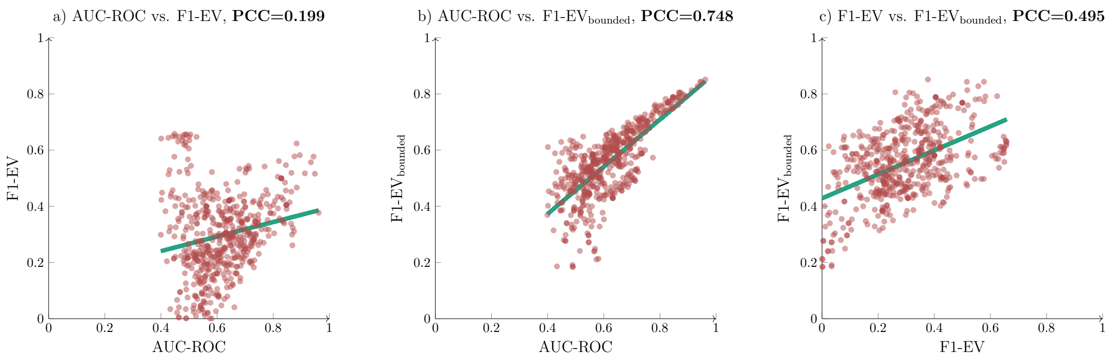

Figure 19: Comparison of threshold-independent performance measures computed on the evaluation set of task 2 of the DCASE2023 Challenge. © 2024 IEEE

4.3.4 *Choosing the hyperparameter* $\beta_{F_1\text{-EV}}$

In Figure 20, the PCCs between the bounded F_1-EV score and other performance metrics are depicted for varying values of the hyperparameter $\beta_{F_1\text{-EV}}$. This allows to investigate the sensitivity with respect to $\beta_{F_1\text{-EV}}$ and to provide recommendations for setting this hyperparameter. It can be seen that for $\beta_{F_1\text{-EV}} > 0.2$ the

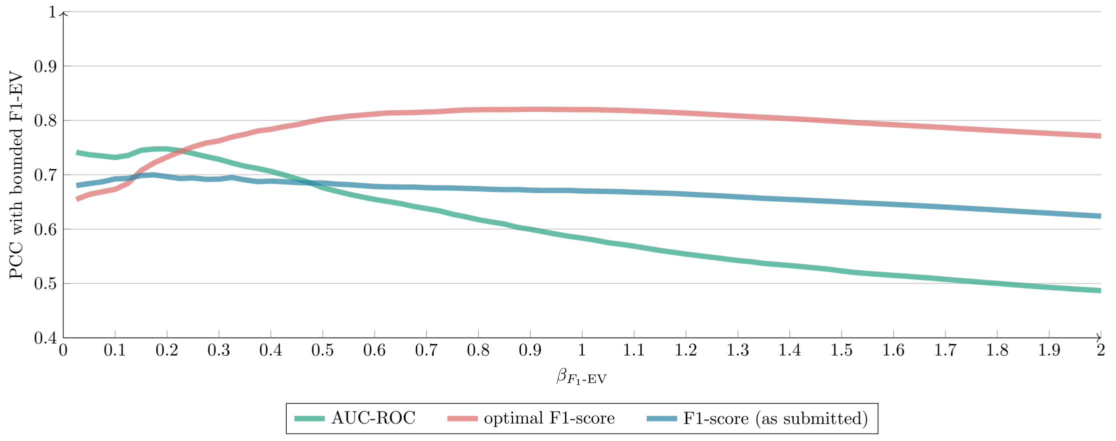

Figure 20: Sensitivity of the bounded F_1-EV score with respect to $\beta_{\mathsf{F}_1\text{-EV}}$. © 2024 IEEE

PCC between the F_1-EV score and AUC-ROC decreases. This verifies once more that both performance metrics are indeed different. Furthermore, the PCC between the F_1-EV score and optimal F_1 score increases for $\beta_{\mathsf{F}_1\text{-EV}} < 1$ and slightly decreases for $\beta_{\mathsf{F}_1\text{-EV}} > 1$ but still has a high correlation. Last and most importantly, the PCC between the F_1-EV score and submitted F_1 scores decreases for $\beta_{\mathsf{F}_1\text{-EV}} > 0.2$. However, the decrease is to less degree than it is the case for the PCC with AUC-ROC and therefore is relatively stable. Using a relatively small value for $\beta_{\mathsf{F}_1\text{-EV}}$ such as setting $\beta_{\mathsf{F}_1\text{-EV}} = 0.2$ seems to be a good choice to have a threshold-independent performance measure that is similar to AUC-ROC score but also includes the difficulty of estimating a good decision threshold.

4.4 SUMMARY

In this chapter, it was investigated how to choose a good decision threshold for semi-supervised ASD systems. For this purpose, the threshold estimation methods presented in Section 2.11 were compared experimentally. It was shown that most methods perform equally well and yield a performance between 90% to 95% of the theoretically optimal performance. More detailed comparisons revealed that MST approaches perform slightly better than non-iterative approaches, especially when less data is used for training the system. Hence, MST yields more robust decision thresholds and thus is identified as the preferred threshold estimation method. Furthermore, it was shown that not using all normal training samples for training the embedding model with the goal of obtaining more realistic anomaly scores for estimating the threshold does not improve the performance. Hence, all normal samples that are available should be used for training the embedding model.

In a second section, it was shown that AUC-ROC does not include the difficulty of estimating a good decision threshold because a maximal AUC-ROC only shows that a single optimal decision threshold exists. Moreover, the AUC-ROC score has a low correlation with the F_1 score and thus only using the AUC-ROC score for evaluating the performance of an ASD system is not sufficient. To solve this issue, the threshold-independent F_1-EV was proposed, which has a high correlation with the AUC-ROC score as well as with the estimated and optimal F_1 scores. However, it was also shown that F_1-EV requires properly defined bounds to yield meaningful results. Still, F_1-EV has a strong potential to replace the AUC-ROC as the standard evaluation metric for semi-supervised ASD.

5 DOMAIN ADAPTATION AND GENERALIZATION

A *domain shift* is a change of the underlying distribution of the data. There are several reasons for such a domain shift to occur. Examples are changing locations of acoustic sensors, changing the time at which data is collected, adding or removing other sound sources or modifying the monitored sound sources. The subset of the data space that has initially been of interest is called *source domain* $X_{\text{source}} \subset X$ and the domain shifted subset is called *target domain* $X_{\text{target}} \subset X$. Usually, there are only very few training samples available for the target domain, i.e. $|X_{\text{target}} \cap X_{\text{train}}| << |X_{\text{source}} \cap X_{\text{train}}|$. Due to this data scarcity, it is difficult to estimate the distribution of the normal data in the target domain. To still have a well-defined ASD task, one needs to make sure that shifting the domain of normal data still results in normal data and that anomalous data is mapped onto anomalous data. Thus, in the context of this thesis a domain shift is formally defined as any mapping $\text{shift}_{\text{domain}} : X_{\text{source}} \rightarrow X_{\text{target}}$ such that $\text{shift}_{\text{domain}}(x_n) \in X_{\text{normal}}$ and $\text{shift}_{\text{domain}}(x_a) \in X_{\text{anomalous}}$ for all $x_n \in X_{\text{normal}}$ and all $x_a \in X_{\text{anomalous}}$.

The main difficulty of handling domain shifts is that normal and anomalous data belonging to the target domain may both be viewed as weakly anomalous by a system trained on the source domain due to a mismatch between the underlying distributions of both domains. Note that, depending on the application, precisely defining the sets X_{source} and X_{target} may be very challenging. This is the reason why the formal definition of a domain shift as presented above is rather vague and will not be further specified. In the context of acoustic machine condition monitoring, which remains to be the application considered in this chapter, a domain shift corresponds to changing the acoustic environment, e.g. modifying the background noise or changing any parameter settings of fully-functioning machines such as the speed they are operating with.

Modifying an ASD system trained on the source domain to perform well on the target domain for which only very limited training data is available, is called *domain adaption* [96]. Ideally, this enables users to adapt the system without too much effort to react to possible changes of the acoustic environment or the monitored sound sources themselves. A possible method for domain adaption is to estimate different distributions for each domain using a jointly trained embedding space and use different backends to decide whether a sample is normal or anomalous [240]. However, adapting a system for each possible domain shift is highly impractical and costly because it requires trained personnel to collect at least some additional data belonging to the target domain, fine-tune parameters and re-train or even change entire components of an ASD system. Furthermore, normal data of the original source domain will likely not be considered normal after adapting the system to the target domain. It would be much better if the same system yields reasonable performance regardless of domain shifts without needing to adapt the system. Achieving this goal of developing a domain-independent system is called *domain generalization* [225]. Hence, the main difference to domain adaptation is that the same models and the same backend with the same decision threshold are used for the source and all possible target domains. This makes domain generalization inherently more difficult but solving this problem automatically solves all domain adaptation problems.

To learn embeddings that are robust to domain shifts, [225] distinguishes between the two main categories *domain-invariant representation learning* [15] and *feature disentanglement* [261]. The idea of domain-invariant learning is to explicitly reduce the variability between multiple different source domains in the embedding space as this will also reduce the variability to arbitrary target domains. Disentangled feature learning aims at learning embeddings as combinations of domain-invariant features, which are robust to domain shifts, and domain-dependent features, which capture the variability between different domains. In [46], these two main categories were described as a *domain-mixing-based approach*, where a domain-invariant model is used for both domains [10, 219, 242], and a *domain-classification-based approach* with different models for the source and target domain, whose domain-specific anomaly scores are combined appropriately. Evidence has been provided that using a combination of domain-dependent models or distributions [259] or using a classifier for the domains [115] leads to better performance than a domain-mixing approach. The most likely reason is that a domain-invariant training requires to remove at least some potential classes and thus simplifies the classification task, which leads to less informative embeddings. Note that classifying between different meta information, as done in [218], corresponds to a disentangled feature learning approach because each combination of provided meta information that defines a class may also define a specific domain shift.

The goal of this chapter is to present an embedding-based ASD system that reliably detects anomalous sounds regardless of the domain a given audio recording belongs to. As this task is much more difficult than an ASD task without domain shifts, re-using the system presented in Chapter 3 alone will not suffice and thus the system must be modified accordingly. To this end, several techniques for improving the performance will be presented.

This chapter is structured as follows: First, two datasets used for the experimental evaluations in domain-shifted conditions will be presented. Then, an ASD system specifically focusing on domain generalization will be designed and individual design choices will be experimentally evaluated. The decisions obtained with differently trained systems will be explained in the third section by visualizing the influence of specific regions of the input samples and the embedding space. In the fourth section, the performance obtained with this ASD system is compared to systems based on pre-trained embeddings. The loss function AdaProj, which is a generalization of the sub-cluster AdaCos loss, will be presented in the fourth section. Then, it will be investigated whether utilizing SSL improves the performance of an ASD system. The chapter is concluded by combining all techniques of the previous sections into a single system and comparing its performance to the state-of-the-art systems.

5.1 CONTRIBUTIONS OF THE AUTHOR

The sections of this chapter are largely based on the following key publications:

- Kevin Wilkinghoff. "Design Choices for Learning Embeddings from Auxiliary Tasks for Domain Generalization in Anomalous Sound Detection." In: *International Conference on Acoustics, Speech and Signal Processing (ICASSP)*. IEEE, 2023.
- Kevin Wilkinghoff and Frank Kurth. "Why do Angular Margin Losses work well for Semi-Supervised Anomalous Sound Detection?" In: *IEEE/ACM Trans. Audio Speech Lang. Process.* 32 (2024), pp. 608–622
- Kevin Wilkinghoff and Fabian Fritz. "On Using Pre-Trained Embeddings for Detecting Anomalous Sounds with Limited Training Data." In: *31st European Signal Processing Conference (EUSIPCO)*. IEEE, 2023, pp. 186–190.
- Kevin Wilkinghoff. "AdaProj: Adaptively Scaled Angular Margin Subspace Projections for Anomalous Sound Detection with Auxiliary Classification Tasks." Submitted to 9th Workshop on Detection and Classification of Acoustic Scenes and Events (DCASE), arXiv:2403.14179. 2024.
- Kevin Wilkinghoff. "Self-Supervised Learning for Anomalous Sound Detection." In: *International Conference on Acoustics, Speech and Signal Processing (ICASSP)*. IEEE, 2024, pp. 276–280.

For publications that are not single-authored, individual contributions of the thesis author and all co-authors to these publications are stated in Section A.1. If not stated otherwise, the content listed in the following paragraph is the sole contribution of the thesis author.

The contents of the following sections were published as papers by the thesis author: Section 5.3.2 is based on [243], 5.4 is based on [252], Section 5.5 is based on [250], Section 5.6 is based on [245] and Section 5.7 is based on [246]. Frank Kurth proposed to include Table 21. Fabian Fritz helped with the experimental evaluations in Section 5.5 by writing wrapper functions for the pre-trained embeddings. The experimental results presented in Section 5.8 are an extended version of Fig. 3 from [245], which also includes results using the SSL approaches presented in Section 5.6.

Table 12: Structure of the DCASE2022 ASD dataset. The dataset contains recordings of 7 machine types and is divided into sections, which contain recordings of the same machine type and are used for evaluation.

subset	number of sections (per machine type)	split	number of recordings (per section)			
			source domain		target domain	
			normal	anomalous	normal	anomalous
development set	3	training	990	0	10	0
		test	50	50	50	50
evaluation set	3	training	990	0	10	0
		test	100 normal and 100 anomalous samples			

5.2 MACHINE CONDITION MONITORING IN DOMAIN-SHIFTED CONDITIONS

All experiments in this chapter related to domain generalization for ASD use the following datasets for acoustic machine condition monitoring.

5.2.1 *DCASE2022 ASD dataset*

Table 12 contains a summary of the DCASE2022 ASD dataset [46]. Overall, the dataset has a similar structure as the DCASE2020 dataset described in Section 3.2.1 but also includes the difficulty of domain generalization. The dataset contains recordings of seven different machine types, namely “ToyCar” and “ToyTrain” from ToyAdmos2 [74] and “fan”, “gearbox”, “bearing”, “slide rail” and “valve” from MIMII-DG [45]. All recordings have a length of 10 s and a sampling rate of 16 kHz. For each machine type, there are six different sections, each corresponding to a subset of the dataset with one specific domain shift, that are used to compute the performance. Thus, there are 42 sections in total. It is important to emphasize that, in contrast to the DCASE2020 dataset, the sections do not correspond to individual machines but may contain a mixture of several machines of a known type. This makes the dataset more realistic because it should be possible to use the same ASD system for multiple machines. However, the task is also more difficult because the variability between different recordings contained in the same section is increased.

The dataset is divided into a development and an evaluation split, each containing three sections of each machine type. Both splits consist of a training subset containing only normal training samples and a test split containing normal and anomalous samples. Furthermore, each section is divided into a source domain with 990 normal training samples and a target domain that differs from the source domain by modifying machine parameter settings or the noise conditions and for

Table 13: Structure of the DCASE2023 ASD dataset. The dataset contains recordings of 14 machine types and is divided into sections, which contain recordings of the same machine type and are used for evaluation.

subset	number of sections (per machine type)	split	number of recordings (per section)			
			source domain		target domain	
			normal	anomalous	normal	anomalous
development set	1	training	990	0	10	0
		test	50	50	50	50
evaluation set	1	training	990	0	10	0
		test	200 samples			

which only ten normal training samples are available. In addition to the section and machine type, so-called *attribute information* are provided for each normal training sample as for example the speed of a toy car, different machine IDs or noise levels. For all files of both test splits, only machine types and sections are provided. Combining machine types, sections and attribute values present in the development and evaluation split of the dataset into a single label, which thus encodes the meta information for each file, results in 342 classes.

The performance obtained on this dataset is measured by calculating the AUC-ROC and pAUC with $p = 0.1$ for each section and computing the harmonic mean over all individual performance metrics. Using the harmonic mean instead of the arithmetic mean ensures that bad scores penalize the total performance result more severely to favor ASD systems that perform equally well for all sections, which is favorable for practical applications. The AUC-ROCs and pAUCs are calculated independently of the domain, i.e. using only a single ROC curve for both domains.

5.2.2 *DCASE2023 ASD dataset*

The DCASE2023 ASD dataset [44] summarized in Table 13 is similar to the DCASE2022 ASD dataset but differs in the following aspects: The major difference is that the DCASE2023 dataset is designed for so-called *first-shot ASD* meaning that there are different machine types for the development and evaluation split. This makes it impossible to fine-tune the hyperparameters of the system to individual machine types by evaluating the performance, which indirectly uses the anomalous samples of the development set as additional training samples and thus should not be allowed in a semi-supervised anomaly detection setting. For the development split, the same machine types as for the DCASE2022 dataset are used. For the evaluation split, the machine types “ToyTank”, “ToyNscale” and “ToyDrone” from ToyAdmos2+ [73] and “vacuum”, “bandsaw”, “grinder” and “shaker”

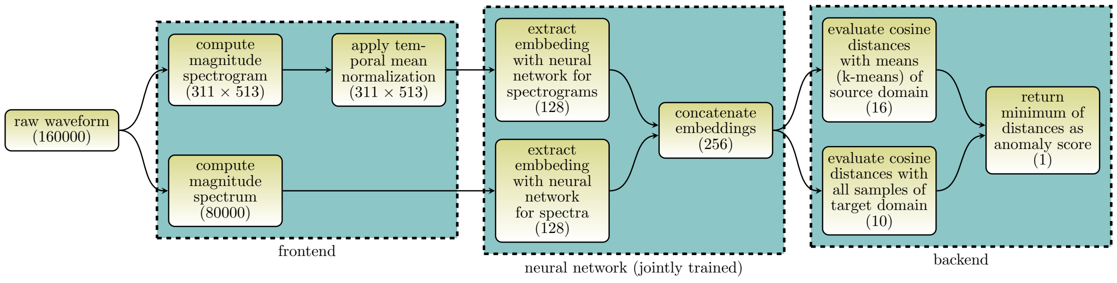
raw waveform (160000)
compute magnitude spectrogram (311 × 513)
apply temporal mean normalization (311 × 513)
compute magnitude spectrum (80000)
frontend
extract embbeding with neural network for spectrograms (128)
extract embbeding with neural network for spectra (128)
concatenate embeddings (256)
neural network (jointly trained)
evaluate cosine distances with means (k-means) of source domain (16)
evaluate cosine distances with all samples of target domain (10)
return minimum of distances as anomaly score (1)
backend

Figure 21: Structure of the proposed anomalous sound detection system for domain-shifted conditions. Representation size in each step is given in brackets. © 2023 IEEE

from MIMII-DG [45] are used. A second major change is that there is only a single section for each machine type. This increases the difficulty by making the classification task imposed by discriminating between provided meta information less challenging and thus resulting in less informative embeddings. As a third increase in difficulty, the length of the recordings belonging to different machine types varies between 6 s and 18 s.

5.3 DESIGNING AN ASD SYSTEM FOR DOMAIN GENERALIZATION

In this section, an ASD system specifically designed to work well in domain-shifted conditions will be presented and evaluated. The main idea is to use a single domain-independent embedding model that extracts embeddings of the source and target domains. Then, domain-dependent distances to normal data samples can be combined into a single domain-independent anomaly score yielding similar performance for both domains.

5.3.1 *System description*

The ASD system presented in Chapter 3 yields state-of-the-art performance for ASD without domain shifts and thus serves as a basis for developing an ASD system in domain-shifted conditions. A modified version is depicted in Figure 21. As before, the system consists of three main blocks, namely a frontend for computing feature representations, a neural network for extracting embeddings and a backend for computing anomaly scores. All three blocks will now be presented in detail. Individual design choices will be investigated experimentally in the following subsection using the DCASE2022 dataset.

The frontend uses two branches extracting different feature representations of the raw waveforms: A short-time Fourier transform (STFT) and a discrete Fourier transform (DFT) based feature. For the STFT based feature branch, magnitude spectrograms extracted with Hanning-weighted windows with a size of 1024 and a hop size of 512 are extracted. In contrast to the system presented in Section 3.2.2,

Table 14: Sub-network architecture for DFT feature branch. © 2023 IEEE

layer name	structure	output size
input	-	80000
1D convolution	256, stride= 64	1250×128
1D convolution	64, stride= 16	40×128
1D convolution	16, stride= 4	10×128
flatten	-	1280
dense	-	128
dense	-	128
dense	-	128
dense	-	128
dense (embedding)	no activation	128

no Mel filterbank is used and no logarithm is applied. The spectrograms are further pre-processed with temporal mean normalization (TMN), which essentially removes all constant frequency information while also denoising the data similar to cepstral mean normalization [192]. The main reason to apply TMN is to make both feature representations more different. For the second feature branch, DFTs are computed to capture all constant frequencies with the highest possible frequency resolution. Since machine sounds are very structured with highly repetitive patterns, utilizing as much frequency information as possible may be beneficial to detect anomalous sounds.

The neural network used to learn an embedding space utilizes another sub-network for each feature branch: A one-dimensional CNN for the DFT features (see Table 14) and a modified version of the ResNet architecture shown in Table 4 (see Table 15). The learned embeddings of both sub-networks are concatenated into a single embedding. In contrast to taking a weighted sum of both embeddings or combining them with a trainable layer, the network has no possibility to only utilize a single embedding that is most useful for solving the auxiliary task and ignore the other embedding. This ensures a higher sensitivity of the system for detecting anomalous data as anomalies may only be detectable for one of the input features. In each convolutional or dense layer of both sub-networks, batch normalization [86] and the activation function ReLU are used. The entire network is jointly trained for ten epochs with a batch size of 64 by minimizing the sub-cluster AdaCos loss with 16 sub-clusters for each class using adam [101]. Mixup [262] with a uniformly sampled mixing coefficient is used to randomly augment the data during training. The classes used for training the model consist of all possible combinations of machine types, sections and different values for provided attribute information present in the training datasets of the development and evaluation set

Table 15: Modified ResNet architecture for STFT feature branch. © 2023 IEEE

layer name	structure	output size
input	TMN	311×513
2D convolution	7×7, stride= 2	$156 \times 257 \times 16$
residual block	$\begin{pmatrix} 3 \times 3 \\ 3 \times 3 \end{pmatrix} \times 2$, stride= 1	$77 \times 128 \times 16$
residual block	$\begin{pmatrix} 3 \times 3 \\ 3 \times 3 \end{pmatrix} \times 2$, stride= 1	$39 \times 64 \times 32$
residual block	$\begin{pmatrix} 3 \times 3 \\ 3 \times 3 \end{pmatrix} \times 2$, stride= 1	$20 \times 32 \times 64$
residual block	$\begin{pmatrix} 3 \times 3 \\ 3 \times 3 \end{pmatrix} \times 2$, stride= 1	$10 \times 16 \times 128$
max pooling	10×1, stride= 1	$1 \times 16 \times 128$
flatten	-	2056
dense (embedding)	no activation	128

resulting in a total of 342 classes for the DCASE2022 dataset. Note that this training paradigm corresponds to a *feature disentanglement* approach for learning embeddings that are robust to domain-shifts. It is also possible to use multiple losses for different classification tasks instead of a single one [218, 240]. However, this did not lead to a noticeable difference in performance and thus only a single classification task is used for the sake of simplicity. Since it is possible that the network learns trivial solutions for a few classes that are very easy to identify, the strategies to prevent one-class models from learning trivial solutions are applied. More concretely, this means that no bounded activation functions, no trainable class centers, and no bias terms are used for both sub-networks. All centers are randomly initialized on the unit sphere and thus are pairwise orthogonal with very high probability.

The backend employs different strategies to compute an anomaly score in both domains. For the source domain, k-means with 16 clusters is applied to all normal training samples of the source domain. An anomaly score for the source domain is obtained by computing the minimum cosine distance to all resulting clusters. For the target domain, the minimum cosine distance to all normal training samples of the target domain is used as an anomaly score. As the final step, a domain-independent anomaly score is given by the minimum of both domain-specific anomaly scores.

Table 16: Comparison between using or not using trainable cluster centers and bias terms on the DCASE2022 dataset. © 2023 IEEE

		trainable cluster centers		non-trainable cluster centers	
dataset	domain	AUC-ROC (%)	pAUC (%)	AUC-ROC (%)	pAUC (%)
		using bias terms			
dev	source	81.65 ± 0.85	70.25 ± 1.31	82.75 ± 0.95	75.22 ± 0.78
dev	target	77.18 ± 0.88	62.05 ± 1.10	76.84 ± 1.39	61.66 ± 1.09
dev	mixed	77.73 ± 0.90	64.09 ± 1.40	79.79 ± 0.50	64.89 ± 0.41
eval	source	74.21 ± 1.14	62.84 ± 1.38	76.45 ± 0.71	65.12 ± 0.66
eval	target	71.13 ± 1.24	59.54 ± 0.86	69.19 ± 0.56	59.08 ± 1.15
eval	mixed	71.91 ± 0.98	58.84 ± 0.88	73.04 ± 0.58	59.18 ± 0.90
		not using bias terms			
dev	source	82.88 ± 0.68	71.44 ± 0.96	$\mathbf{84.19 \pm 0.75}$	$\mathbf{76.45 \pm 0.90}$
dev	target	77.68 ± 1.11	$\mathbf{62.82 \pm 1.17}$	$\mathbf{78.51 \pm 0.90}$	62.54 ± 0.87
dev	mixed	78.15 ± 0.77	64.86 ± 0.52	$\mathbf{81.36 \pm 0.66}$	$\mathbf{66.55 \pm 0.86}$
eval	source	74.34 ± 0.96	63.49 ± 0.38	$\mathbf{76.81 \pm 0.79}$	$\mathbf{65.84 \pm 0.22}$
eval	target	$\mathbf{71.30 \pm 0.33}$	$\mathbf{59.94 \pm 0.81}$	69.80 ± 0.53	59.67 ± 1.14
eval	mixed	72.15 ± 0.50	58.90 ± 0.42	$\mathbf{73.43 \pm 0.54}$	$\mathbf{59.78 \pm 0.83}$

5.3.2 *Experimental investigations of individual design choices*

To show that the design choices of the proposed ASD system actually improve the performance, multiple experiments have been conducted and will now be discussed. Each experiment was repeated five times and the mean and standard deviation of the harmonic means computed over all sections belonging to the development and evaluation split of the DCASE2022 dataset are shown.

In the first experiment it is evaluated whether applying the same strategies used to prevent the embedding model to learn trivial solutions when using one-class losses also has a positive impact on the performance when using an angular margin loss. The results presented in Table 16 show that the overall performance is significantly improved when not using bias terms and not adapting the centers during training. It is worth noting that the performance improves on the target domain but degrades on the source domain when using trainable centers. This indicates that for some classes of the source domain the embedding model indeed learns solutions that are closely resembling trivial solutions making it difficult to discriminate between normal and anomalous embeddings.

Table 17: Comparison between different input feature representations and ways of combining them on the DCASE2022 dataset. © 2023 IEEE

		individual input feature representations					
		magnitude spectrum		log-Mel magnitude spectrogram		magnitude spectrogram	
dataset	domain	AUC-ROC (%)	pAUC (%)	AUC-ROC (%)	pAUC (%)	AUC-ROC (%)	pAUC (%)
dev	source	80.75 ± 0.92	71.09 ± 1.14	70.91 ± 2.10	63.21 ± 1.10	79.18 ± 1.07	70.38 ± 0.43
dev	target	73.95 ± 1.25	61.31 ± 1.40	65.78 ± 1.48	57.05 ± 0.76	76.59 ± 1.59	60.59 ± 1.50
dev	mixed	76.81 ± 0.94	63.09 ± 1.23	68.93 ± 1.52	57.79 ± 0.55	77.60 ± 1.02	62.31 ± 1.10
eval	source	68.42 ± 1.02	59.06 ± 0.89	67.59 ± 1.01	59.96 ± 0.65	74.65 ± 0.83	64.04 ± 1.23
eval	target	63.46 ± 1.39	56.90 ± 0.95	62.09 ± 0.61	56.60 ± 0.79	69.67 ± 1.14	58.95 ± 0.74
eval	mixed	66.00 ± 1.11	57.11 ± 0.58	65.04 ± 0.68	57.00 ± 0.50	72.10 ± 0.81	58.87 ± 0.33
		combining magnitude spectrum and magnitude spectrograms					
		concatenate embeddings after training		add embeddings while training		concatenate embeddings while training	
dataset	domain	AUC-ROC (%)	pAUC (%)	AUC-ROC (%)	pAUC (%)	AUC-ROC (%)	pAUC (%)
dev	source	$\mathbf{84.68 \pm 0.86}$	74.51 ± 0.26	83.12 ± 1.18	73.25 ± 1.11	84.19 ± 0.75	$\mathbf{76.45 \pm 0.90}$
dev	target	$\mathbf{78.78 \pm 0.78}$	$\mathbf{63.00 \pm 0.36}$	77.96 ± 1.37	62.02 ± 1.11	78.51 ± 0.90	62.54 ± 0.87
dev	mixed	81.17 ± 0.66	65.23 ± 0.39	80.21 ± 0.73	64.40 ± 1.20	$\mathbf{81.36 \pm 0.66}$	$\mathbf{66.55 \pm 0.86}$
eval	source	75.27 ± 0.96	63.93 ± 0.63	75.54 ± 0.83	64.85 ± 0.73	$\mathbf{76.81 \pm 0.79}$	$\mathbf{65.84 \pm 0.22}$
eval	target	69.31 ± 0.90	59.45 ± 0.67	69.71 ± 0.39	59.08 ± 1.15	$\mathbf{69.80 \pm 0.53}$	$\mathbf{59.67 \pm 1.14}$
eval	mixed	72.18 ± 0.67	59.45 ± 0.46	72.48 ± 0.53	59.22 ± 0.66	$\mathbf{73.43 \pm 0.54}$	$\mathbf{59.78 \pm 0.83}$

In Table 17, different input feature representations and approaches for combining them are compared. The following observations can be made: First, magnitude spectrograms perform much better than log-Mel magnitude spectrograms that are used in many other ASD systems (cf. Section 2.2). The most likely reason is that high frequencies are more important than low frequencies for detecting anomalous sounds of machines [140] and using the logarithmically scaled Mel-filterbank decreases the resolution for high frequencies. Furthermore, only using the DFT-based magnitude spectra leads to surprisingly good results that are better than the ones obtained with log-Mel spectrograms but worse than when using spectrograms. Hence, a high frequency resolution is highly beneficial to detect anomalous sounds for machine condition monitoring. Not surprisingly, combining both feature branches improves the performance as providing different views on the data gives a more complete picture of the input data. Thirdly, concatenating the embeddings of the sub-networks while training leads to the best performance. Again, the reason is that the network is forced to encode as much information as possible for each individual feature branch and thus results in more informative embeddings.

In Table 18, it is experimentally verified whether applying TMN to the magnitude spectrograms improves peformance or not. It can be seen that applying TMN leads to very similar performance when only using the magnitude spectrograms. But, when utilizing both feature branches there is an improvement in performance. The reason is that both features better complement each other as the constant frequency information is removed from the spectrograms, which is exactly the in-

Table 18: Effect of temporal normalization in domain-shifted conditions. © 2023 IEEE

		without temporal normalization		with temporal normalization	
dataset	domain	AUC-ROC (%)	pAUC (%)	AUC-ROC (%)	pAUC (%)
		magnitude spectrogram			
dev	source	79.93 ± 0.71	70.98 ± 1.38	79.18 ± 1.07	70.38 ± 0.43
dev	target	76.18 ± 0.85	60.35 ± 1.23	76.59 ± 1.59	60.59 ± 1.50
dev	mixed	77.69 ± 0.47	62.52 ± 1.09	77.60 ± 1.02	62.31 ± 1.10
eval	source	75.53 ± 1.19	64.31 ± 1.08	74.65 ± 0.83	64.04 ± 1.23
eval	target	69.52 ± 0.73	**59.67 ± 0.71**	69.67 ± 1.14	58.95 ± 0.74
eval	mixed	72.19 ± 0.77	59.39 ± 0.91	72.10 ± 0.81	58.87 ± 0.33
		magnitude spectrum + magnitude spectrogram			
dev	source	83.18 ± 1.68	74.66 ± 0.71	**84.19 ± 0.75**	**76.45 ± 0.90**
dev	target	76.95 ± 0.97	62.26 ± 0.62	**78.51 ± 0.90**	**62.54 ± 0.87**
dev	mixed	80.04 ± 0.76	64.84 ± 0.51	**81.36 ± 0.66**	**66.55 ± 0.86**
eval	source	76.41 ± 0.48	65.39 ± 0.68	**76.81 ± 0.79**	**65.84 ± 0.22**
eval	target	68.89 ± 0.96	59.46 ± 0.68	**69.80 ± 0.53**	**59.67 ± 1.14**
eval	mixed	72.85 ± 0.61	**59.91 ± 0.75**	**73.43 ± 0.54**	59.78 ± 0.83

formation being captured by the DFT features, and thus both features provide a more detailed view on the data than when not applying TMN.

In Table 19, the performances obtained with different backends for computing anomaly scores are compared. More concretely, using a GMM is compared to using the cosine distance and different ways of combining the anomaly scores of both domains are evaluated. The following observations can be made. Unsurprisingly, using only domain-specific anomaly scores leads to the best performance on the domain they belong to. When comparing ways of computing anomaly scores, a domain-specific GMM leads to better performance than cosine distance on the source domain, which is consistent with the findings presented in Section 3.4.3. For the target domain, both approaches are in fact equivalent due to the small number of training samples and thus lead to the exact same performance. However, the focus of this chapter lies on generalizing to unseen domains while still performing well on the source domain without the need of adapting the model. This requires a single decision threshold for both domains. When investigating the performance on the mixed domain, a joint model performs much better than individual models or when using the sum of the individual scores. Interestingly, the joint model even outperforms the sub-model specialized on the source domain showing once more that some classes are too easily detected by this model, which leads to embeddings without sufficient information to detect anomalies. Although a joint model in combination with a GMM leads to better performance on the source domain than when using cosine distance, the cosine distance performs better on the target domain and also better in the mixed domain. As optimizing the domain-independent performance is the aim of this chapter, using cosine similarity and training a joint model is the preferred design choice.

Lastly, the optimized ASD system investigated in this section and the baseline system presented in Section 3.2.2 are compared in Table 20. One can see that all performance improvements resulting from the modifications add up and lead to a strong difference in performance, clearly favoring the modified system in domain-shifted conditions.

5.4 EXPLAINING THE DECISIONS

The goal of this section is to explain the decisions of the ASD system by visualizing the obtained results. Explaining the decisions of data-driven models is important for practical applications to increase the acceptance and trust in the results (explainable artificial intelligence (xAI) [84]). It also provides the possibility to detect potential errors and gain additional insights about possible reasons that caused these errors. For acoustic machine condition monitoring, localizing anomalous temporal regions or frequency bands is crucial to help users to find the cause of mechanical failure and thus simplifies the maintenance process. Previous work on explaining the decision of ASD systems for acoustic machine condition monitoring exists but is rather limited. In [50], uniform manifold approximation and

Table 19: Comparison between different backends on the DCASE2022 dataset. © 2023 IEEE

		GMM		cosine distance	
dataset	domain	AUC-ROC (%)	pAUC (%)	AUC-ROC (%)	pAUC (%)
		using scores from source domain model only			
dev	source	82.97 ± 0.97	77.36 ± 0.38	83.10 ± 1.02	76.87 ± 0.26
dev	target	66.52 ± 0.42	59.63 ± 0.70	71.66 ± 1.25	61.45 ± 0.83
dev	mixed	71.48 ± 0.26	58.86 ± 0.38	76.72 ± 0.78	63.37 ± 0.71
eval	source	77.46 ± 1.16	66.73 ± 0.56	76.68 ± 0.85	66.25 ± 0.51
eval	target	44.23 ± 3.67	54.87 ± 0.46	57.90 ± 1.17	55.62 ± 1.24
eval	mixed	63.83 ± 0.62	55.74 ± 0.33	67.24 ± 0.70	56.83 ± 0.92
		using scores from target domain model only			
dev	source	62.41 ± 2.80	60.54 ± 1.44	62.42 ± 2.80	60.55 ± 1.44
dev	target	**79.93 ± 0.92**	62.19 ± 1.05	**79.92 ± 0.92**	62.18 ± 1.06
dev	mixed	70.84 ± 1.13	58.36 ± 1.38	70.84 ± 1.13	58.36 ± 1.38
eval	source	52.82 ± 3.40	56.27 ± 1.17	52.80 ± 3.41	52.26 ± 1.17
eval	target	**71.15 ± 0.50**	**60.72 ± 0.95**	**71.15 ± 0.50**	**60.72 ± 0.95**
eval	mixed	62.55 ± 0.79	54.66 ± 0.92	62.55 ± 0.79	54.65 ± 0.92
		using sum of scores from both domain models			
dev	source	75.94 ± 2.70	70.34 ± 2.69	79.44 ± 1.95	73.29 ± 2.60
dev	target	78.64 ± 1.12	63.28 ± 0.94	78.84 ± 1.23	62.67 ± 0.98
dev	mixed	77.10 ± 1.59	65.12 ± 1.63	77.83 ± 1.56	66.11 ± 1.61
eval	source	64.57 ± 1.35	60.96 ± 1.21	68.96 ± 1.11	63.09 ± 0.87
eval	target	66.69 ± 0.54	58.73 ± 0.97	67.84 ± 0.48	58.80 ± 1.33
eval	mixed	65.70 ± 0.91	57.26 ± 0.77	67.98 ± 0.64	58.12 ± 0.71
		using scores from joint model for both domains			
dev	source	**84.57 ± 0.70**	**77.57 ± 0.41**	84.19 ± 0.75	76.45 ± 0.90
dev	target	77.26 ± 1.02	**63.12 ± 1.24**	78.51 ± 0.90	62.54 ± 0.87
dev	mixed	80.06 ± 0.35	64.67 ± 0.70	**81.36 ± 0.66**	**66.55 ± 0.86**
eval	source	**78.15 ± 0.95**	**67.55 ± 0.63**	76.81 ± 0.79	65.84 ± 0.22
eval	target	65.17 ± 0.48	58.59 ± 0.79	69.80 ± 0.53	59.67 ± 1.14
eval	mixed	71.35 ± 0.53	59.32 ± 0.83	**73.43 ± 0.54**	**59.78 ± 0.83**

Table 20: Effect of the presented design choices for improving the performance in domain-shifted conditions. © 2023 IEEE

		standard design choices		presented design choices	
dataset	domain	AUC-ROC (%)	pAUC (%)	AUC-ROC (%)	pAUC (%)
dev	source	71.65 ± 1.07	62.71 ± 0.74	$\mathbf{84.19 \pm 0.75}$	$\mathbf{76.45 \pm 0.90}$
dev	target	63.63 ± 1.11	55.28 ± 0.84	$\mathbf{78.51 \pm 0.90}$	$\mathbf{62.54 \pm 0.87}$
dev	mixed	67.72 ± 0.79	55.94 ± 0.54	$\mathbf{81.36 \pm 0.66}$	$\mathbf{66.55 \pm 0.86}$
eval	source	69.11 ± 1.05	58.46 ± 0.42	$\mathbf{76.81 \pm 0.79}$	$\mathbf{65.84 \pm 0.22}$
eval	target	61.33 ± 0.70	54.82 ± 0.78	$\mathbf{69.80 \pm 0.53}$	$\mathbf{59.67 \pm 1.14}$
eval	mixed	64.59 ± 0.74	55.22 ± 0.66	$\mathbf{73.43 \pm 0.54}$	$\mathbf{59.78 \pm 0.83}$

projection (UMAP) [144] was used to visualize stacked consecutive frames of log(-Mel) magnitude spectrograms or openL3 embeddings [32] as dimension-reduced representations in a vector space. In [140], it has been shown that high frequency information is much more important than low frequency information for detecting anomalous machine sounds by using local interpretable model-agnostic explanations (LIME) [191] applied to sounds (SLIME) [151]. This verifies the choice of applying a high-pass filter to the input data representations (cf. Section 3.2.2).

5.4.1 *Visualizing the input as viewed by the model*

To visualize how using an auxiliary classification task affects the decision making of the ASD system based on specific regions, *randomized input sampling for explanation (RISE)* [181] is used. RISE applies random binary masks to the input and evaluates the performance with the masked input. Then, so-called *importance maps* are generated by repeating both steps many times for the same input sample and summing all masks weighted with the corresponding performance. Finally, the importance maps are normalized with the expected value of a random binary mask. As a result, such an importance map visualizes the importance of specific regions on the resulting performance. For the experiments conducted in this section, only the sub-model based on magnitude spectrograms of the ASD system described in Section 5.3.2 is used because these time-frequency representations allow to detect and visualize temporal patterns and frequency bands of interest.

The spectrograms used by the ASD system have a very high dimension with a temporal dimension of $D_{\text{time}} = 311$ and a frequency dimension of $D_{\text{freq}} = 513$. Hence, there are $2^{T \cdot F} = 2^{159543}$ possible binary masks for these spectrograms and thus too many iterations for RISE would be required. To reduce the dimension of the search space, the following strategies were employed: First, the temporal and frequency dimension were treated individually by masking individual time frames and frequency bands with a probability of 0.25 and combining both masks

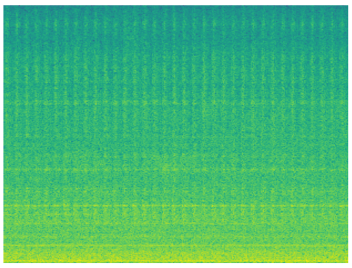
(a) Spectrogram of an anomalous gearbox sound.

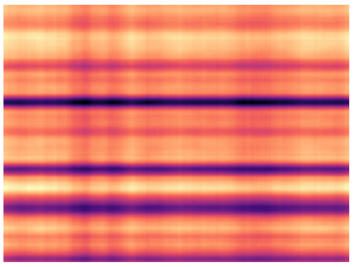
(b) Importance map of an anomalous gearbox sound when using sub-cluster AdaCos.

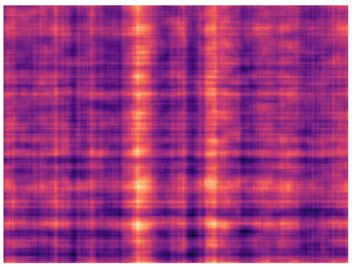
(c) Importance map of an anomalous gearbox sound when using compactness loss.

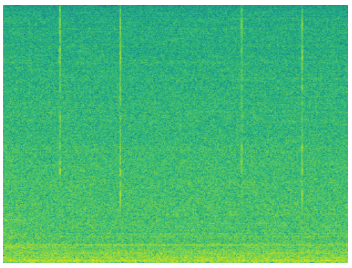
(d) Spectrogram of a normal valve sound.

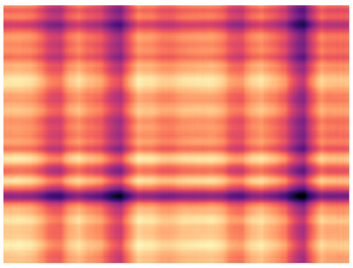
(e) Importance map of a normal valve sound when using sub-cluster AdaCos.

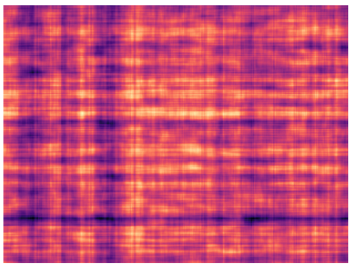
(f) Importance map of a normal valve sound when using compactness loss.

Figure 22: Log-scaled spectrograms (left column), importance maps obtained with RISE when training with the sub-cluster AdaCos loss and classifying between different machine types, sections and attribute information (middle column), and importance maps obtained with RISE when training with an intra-class compactness loss and without an auxiliary classification task (right column) for two different recordings belonging to the test split of the development set (rows). For the importance maps, blue colors indicate normal regions and yellow colors indicate regions that are found to be anomalous by the model. All subfigures use individual color scales to improve visual appearance for differently scaled importance maps and thus colors of different subfigures cannot be compared to each other. © 2024 IEEE

by multiplying them. This results in a reduction from $2^{\mathsf{T}\cdot\mathsf{F}}$ to $2^{\mathsf{T}+\mathsf{F}}$ possibilities. Note that for machine condition monitoring, such an approach is not too restrictive because machine sounds are highly structured, meaning that they are mostly constant over time (e.g. fans), are constant for some duration (e.g. slider rails) or consist of short sound events over a wide frequency range (e.g. valves). A further reduction of the search space was achieved by up-sampling and cropping small binary masks as also proposed for the original RISE algorithm [181]. For the time masks a size of 20 and for frequency masks a size of 34 were used, resulting in a search space of 2^{54}, which is still huge but much smaller than the original space. In all experiments, $640,000$ iterations were used to generate a single importance map.

Figure 22 contains log-scaled magnitude spectrograms of two samples and importance maps resulting from a model trained by minimizing the sub-cluster AdaCos loss and from a model trained by minimizing an intra-class compactness loss. Note that the results of the ASD system are not perfect and thus specific regions as visualized by the model do not need to be correct. Moreover, there are only single binary labels available for each recording, stating whether the sample is normal or anomalous. Hence, there is no ground truth about specific regions of the spectrograms available for further inspection. Manual inspection is not economical as the author of this thesis does not have the required application-dependent expertise to do this. Still, for the purpose of comparing a model trained with an auxiliary classification task and a one-class model, these visualizations are sufficiently detailed. The results obtained for both samples will now be discussed in detail.

For the first sample, which is an anomalous sound of a gearbox, the model trained with an auxiliary classification task monitors specific frequency bands that are found to be normal (blue horizontal lines in Figure 22(b)). Interestingly, these monitored regions correspond to the frequency bands that contain high energy and thus can also be found in Figure 22(a). The frequency band that is considered to be most anomalous by this model is located between the bottom two normal frequency bands and contains only low energy. Therefore, a normal sound is expected to have more or even less energy there. In contrast, the one-class model whose importance map is depicted in Figure 22(c) does not seem to monitor specific frequencies. Moreover, there are two anomalous temporal locations present (vertical lines in yellow). These do not seem to correspond to specific sound events in the recording because, when comparing it to the spectrogram, there are no visually noticeable events at these temporal locations. Thus, these seem to be errors made by the one-class model.

Similar results can be seen for the second sample containing a normal valve sound. Here, four sound events of very short durations can be seen in the spectrogram depicted in Figure 22(d). The importance map of the model trained with an auxiliary classification task considers these events to be normal since there are four vertical blue lines present in Figure 22(e). However, these events are not clearly visible in the importance map of the one-class model as shown in Figure 22(f). Here, the importance map looks almost completely random except for a frequency band that is considered to be normal but does not correspond to any region of the spectrogram with higher energy. Overall, these results support the claim that using an auxiliary classification task leads to more meaningful embeddings as the importance maps are noticeably more structured than the ones obtained for a one-class model.

5.4.2 *Visualizing the embedding space*

Another approach to explain the results of the ASD system is to visually inspect the embedding space using t-distributed stochastic neighbor embeddings (t-SNEs). Note that, according to Lemma 3.1, using Euclidean and cosine distance to measure the similarity of embeddings are equivalent approaches on the unit sphere

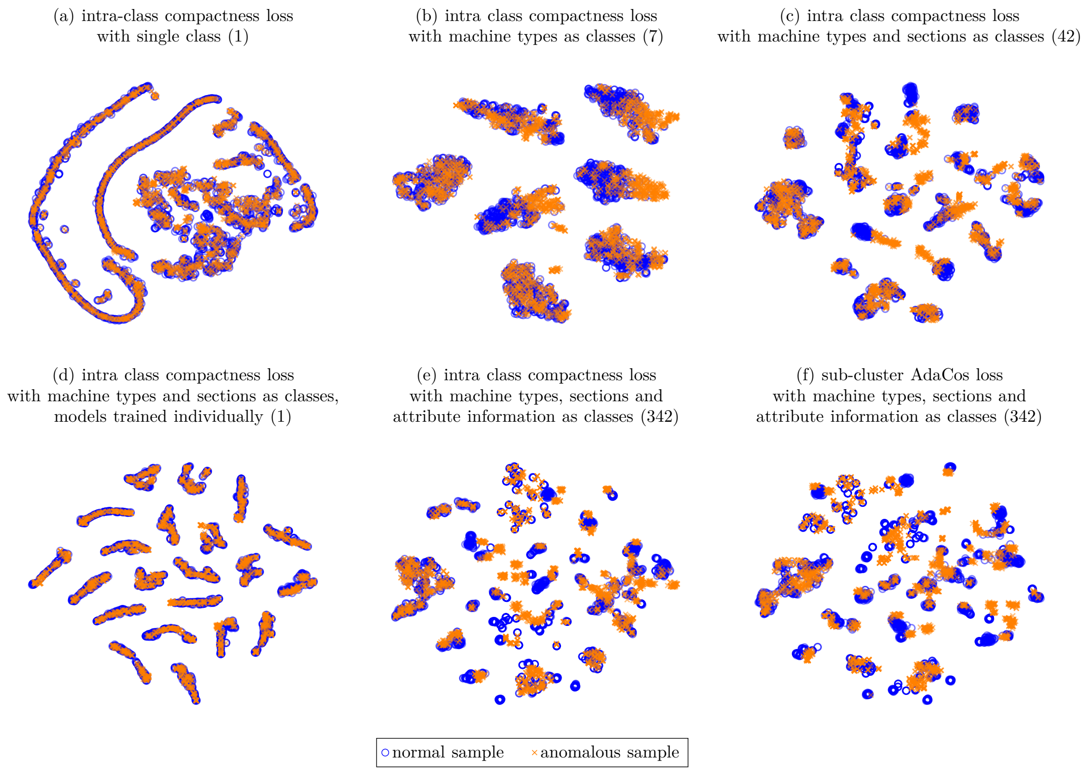

Figure 23: Visualizations of the test split of the development set in the learned embedding space for different loss functions and auxiliary tasks using t-SNE. Numbers in brackets denote the number of different classes used for the auxiliary task. © 2024 IEEE

and thus a standard implementation of t-SNE based on the Euclidean distance, as provided in scikit-learn [176], can be used. The results are depicted in Figure 23. Similar to the experimental results obtained on the DCASE2020 dataset that were presented in Section 3.3.3, it can be seen that using more classes helps to separate normal and anomalous samples (Figure 23(b), (c), (e) and (f)). In contrast, there is no visual difference between normal and anomalous samples when using a single or individual one-class losses (Figure 23(a) and (d)). It shall be noted that the model has also not learned a trivial solution as this would result in a uniformly distributed t-SNE embedding space. Therefore, the regularization techniques applied to the one-class losses prevented the embedding space from collapsing to a single point. All of these visual impressions are verified in Table 21 by measuring the distance between each anomalous sample and the closest normal sample. As stated in Chapter 3, the most likely reason for this significant difference in performance obtained with different loss functions is the same as before, namely the background noise. Teaching the model to discriminate between different classes enables it to closely monitor target machine sounds and more robustly detect deviations from normal behavior by mostly ignoring the background noise. As shown in Figure 23, this is not the case for individual one-class losses.

Table 21: Mean and standard deviation of the average Euclidean distance between the t-SNE projections of each anomalous sample and the closest normal sample over five trials for different losses and using different auxiliary tasks. © 2024 IEEE

loss	classes of auxiliary task (number of classes)	average distance
intra-class compactness loss	none (1)	0.485 ± 0.007
intra-class compactness loss	machine types (7)	1.636 ± 0.037
intra-class compactness loss	machine types and sections (42)	2.175 ± 0.075
intra-class compactness loss	machine types and sections, models trained individually (1)	0.559 ± 0.002
intra-class compactness loss	machine types, sections and attribute information (342)	2.646 ± 0.045
sub-cluster AdaCos loss	machine types, sections and attribute information (342)	2.947 ± 0.022

5.5 COMPARISON TO PRE-TRAINED EMBEDDINGS

Without a sufficient amount of training data, using pre-trained embeddings is a promising approach for many closed-set classification tasks. Since there are only a few normal training samples available for the target domain, this motivates to compare the performance of the ASD system presented in the previous section to a system based on pre-trained embeddings. To this end, the four pre-trained embeddings VGGish, OpenL3, PANN and Kumar presented in Section 2.5 will be evaluated.

5.5.1 *System design for pre-trained embeddings*

To utilize the pre-trained embeddings for ASD, a shallow classifier is trained as proposed in [32, 67, 162]. Similar to a directly trained model, this classifier predicts the correct meta information using the pre-trained embeddings as input. Before inserting the embeddings as input, they are standardized using batch normalization [86] as this has been shown to improve performance [32]. The model consists of three layers with 512, 128 and 128 neurons. For the first two layers, ReLU is used as an activation function and batch normalization is applied. Prior to the last layer, dropout [81] is applied with a probability of 50%. The last layer consists of a linear transformation and a projection onto the hypersphere by using the sub-cluster AdaCos loss with 16 sub-clusters per class. The model is trained for 100 epochs with a batch size of 64 using Adam [101]. As for the directly trained model, mixup [262] is applied, no bias terms are used and the randomly initialized centers are not adapted during training to avoid learning trivial solutions for easily recognizable classes. Anomaly scores are obtained by estimating the distribution of the normal training samples belonging to single sections of the dataset with a GMM and computing the log-likelihood of individual test samples. For the openL3 embeddings, the model pre-trained on environmental sounds is used because these are more closely related to machine sounds than music.

Table 22: Harmonic means of AUC-ROCs obtained with different ways to handle the temporal dimension of pre-trained embeddings. © 2023 IEEE

dataset	embeddings	mean of embeddings			mean of scores	native
		before training	during training	after training		
dev set	VGGish	**65.78 ± 0.37**	64.98 ± 0.25	58.47 ± 0.58	59.27 ± 0.58	not available
dev set	OpenL3	**70.94 ± 1.36**	70.83 ± 0.93	59.85 ± 0.49	62.67 ± 1.36	not available
dev set	PANN	64.80 ± 0.25	**66.30 ± 0.55**	59.66 ± 0.32	60.47 ± 0.17	64.21 ± 0.17
dev set	Kumar	**66.04 ± 0.76**	65.85 ± 0.83	58.94 ± 1.00	62.22 ± 0.98	60.97 ± 0.52
eval set	VGGish	**64.69 ± 0.34**	63.91 ± 0.73	58.30 ± 0.98	59.78 ± 0.53	not available
eval set	OpenL3	**69.06 ± 0.42**	68.70 ± 0.94	62.44 ± 0.46	65.02 ± 1.04	not available
eval set	PANN	63.55 ± 0.27	**65.29 ± 0.39**	58.57 ± 1.07	60.34 ± 0.62	63.33 ± 0.36
eval set	Kumar	63.56 ± 0.59	**64.05 ± 0.27**	56.95 ± 0.86	61.04 ± 0.44	60.13 ± 0.24

5.5.2 *Experimental results*

In the following, multiple experiments are conducted to investigate how to design an ASD system based on pre-trained embeddings. The networks for extracting OpenL3 and VGGish embeddings use a sliding window resulting in embeddings with a temporal dimension, i.e. multiple vector-sized embeddings per sample. To obtain a single anomaly score for a given file, a proper strategy for handling all embeddings belonging to this file needs to be chosen. Possible choices are to compute the mean of the embeddings before, during or after training or to compute the mean of the individual anomaly scores. An experimental comparison of the performances obtained with these strategies can be found in Table 22. For PANN and Kumar embeddings, which do not have a temporal dimension, a sliding window with a length of 960 ms is used to artificially create a temporal dimension allowing to also evaluate the same strategies for these embeddings. In contrast to the results presented in [67], the best results are obtained when combining the embeddings before or during training and not after training, which led to significantly worse results. Interestingly, artificially creating a time-dimension for PANN and Kumar embeddings increases the performance. This shows that some information important for detecting anomalous samples is lost when using the pre-trained models to full extent.

As discussed in Section 2.6 and experimentally investigated for directly trained ASD systems, there are several possible backends for computing an anomaly score. One can directly estimate the distribution with a GMM, apply PCA or LDA before estimating the distribution or train a shallow classifier using different loss functions. In Table 23, the performances obtained with different backends are compared. It can be seen that training a shallow classifier results in significantly better performance than when not doing so. As for the directly trained system, sub-cluster AdaCos in combination with using the cosine distance leads to the best results for all four pre-trained embedding types.

Table 23: Harmonic means of AUC-ROCs for different backends and considered embeddings. Only deviations from the standard system are stated in the header of the table. © 2023 IEEE

dataset	embeddings	without trained shallow classifier			with trained shallow classifier		
		-	PCA	LDA	-	CXE as loss	cosine distance as backend
dev set	VGGish	60.22 ± 0.25	60.25 ± 0.43	62.90 ± 0.13	64.45 ± 0.60	65.40 ± 0.55	$\mathbf{65.78 \pm 0.37}$
dev set	OpenL3	66.82 ± 0.19	66.33 ± 0.12	64.66 ± 0.24	67.83 ± 1.24	68.99 ± 0.61	$\mathbf{70.94 \pm 1.36}$
dev set	PANN	60.36 ± 0.09	61.48 ± 0.18	60.09 ± 0.45	64.39 ± 0.75	63.82 ± 0.56	$\mathbf{66.30 \pm 0.55}$
dev set	Kumar	61.47 ± 0.26	61.92 ± 0.29	61.82 ± 0.26	64.22 ± 0.63	64.08 ± 1.54	$\mathbf{65.85 \pm 0.83}$
eval set	VGGish	57.48 ± 0.36	57.47 ± 0.18	61.47 ± 0.20	62.00 ± 1.26	63.77 ± 0.63	$\mathbf{64.69 \pm 0.34}$
eval set	OpenL3	63.76 ± 0.23	62.62 ± 0.22	64.65 ± 0.33	67.18 ± 0.43	67.69 ± 0.89	$\mathbf{69.06 \pm 0.42}$
eval set	PANN	56.18 ± 0.13	60.08 ± 0.08	57.83 ± 1.01	63.11 ± 0.48	61.63 ± 0.48	$\mathbf{65.29 \pm 0.39}$
eval set	Kumar	60.00 ± 0.12	60.56 ± 0.13	61.56 ± 0.27	61.27 ± 0.30	63.42 ± 0.48	$\mathbf{64.05 \pm 0.27}$

Table 24: Harmonic means of AUC-ROCs for different input representations. © 2023 IEEE

dataset	VGGish	OpenL3	PANN	Kumar	no embedding
dev set	65.78 ± 0.37	70.94 ± 1.36	66.30 ± 0.55	65.85 ± 0.83	$\mathbf{81.36 \pm 0.66}$
eval set	64.69 ± 0.34	69.06 ± 0.42	65.29 ± 0.39	64.05 ± 0.27	$\mathbf{73.43 \pm 0.54}$

As a last experiment, the best performances obtained with pre-trained embeddings are compared to the previously presented ASD system that is directly trained on the input data. The experimental results can be found in Table 24 and the following observations can be made: First of all, training a model directly on the data leads to much better results than using pre-trained embeddings. The most likely reason is that pre-trained embeddings do not capture subtle differences between normal and anomalous samples similar to embeddings obtained with one-class losses. This is also supported by the findings in [67], stating that very noisy recordings are a problem for models that have not been trained on the same dataset. Second, OpenL3 embedding perform second best and VGGish, PANN and Kumar embeddings perform worse while having very similar results. A possible explanation may be that these three embeddings are trained using a supervised training objective and OpenL3 embeddings are the only embeddings resulting from SSL. This observation has also been made in [67].

Overall, the results indicate that using pre-trained models does not help to improve the performance for ASD tasks as the underlying models are too general even when only a few data samples are available. However, using a sufficient number of training samples for the source domain results in an embedding space that also yields a reasonable performance on the target domain. In Section 5.5, more experiments with pre-trained embeddings will be conducted for few-shot OSC.

5.6 ADAPROJ

In Section 3.4, it was shown that the sub-cluster AdaCos loss, which allows the embedding model to learn less restrictive distributions by utilizing multiple centers for each class, improves the resulting ASD performance. The idea of the AdaProj loss, which will be presented in this section, is to further generalize the sub-cluster AdaCos loss by enlarging the space of optimal solutions. More concretely, the distance to linear subspaces spanned by the centers, which act as basis vectors, instead of the distance to the centers themselves is measured when training the embedding model. This extends the set of of optimal solutions from a few points, namely the sub-clusters, to entire linear sub-spaces for each class and allows the network to learn more complex distributions of the normal data samples. As a result, it is expected that this helps to identify anomalies in the embedding space. Another advantage is that the embedding model has more freedom to solve multiple classification tasks at once imposed by different types of meta information, which may be related to very different characteristics of the input space and thus should also not manifest in the same geometric properties in the embedding space. For example, one would expect that recordings belonging to different machine types are more different to each other than recordings of the same machine with different parameter settings.

Other works also use orthogonal projections onto sub-spaces when learning embeddings for related applications. In [258], two different orthogonal sub-spaces for normal and anomalous data are explicitly enforced through a loss function when training an autoencoder for detecting anomalous images. For semi-supervised image classification, class-specific subspace projections are learned by using a reconstruction loss in combination with a discriminative loss to ensure that these subspaces are different [125]. Still, both approaches are very different from AdaProj as autoencoders need to also reconstruct the noise and non-target sound events, which degrades the performance of an ASD system and thus should be avoided.

5.6.1 *Definition*

Before defining the AdaProj loss, additional notation will be introduced.

Definition 5.1 (Projection onto linear span)**.** Let $e \in \mathbb{R}^D$ be an embedding and let $C \subset \mathbb{R}^D$ denote basis vectors. Then, the *projection* $P_{\text{span}(C)}$ *onto the linear span* of the embedding space, denoted by $\text{span}(C) \subset \mathbb{R}^D$, containing all finite linear combinations of the basis vectors is defined as

$$\begin{aligned} &P_{\text{span}(C)} : \mathbb{R}^D \to \text{span}(C) \\ &P_{\text{span}(C)}(e) := \sum_{c \in C} \langle e, c \rangle c. \end{aligned} \tag{54}$$

Using this notation, the formal definition of the AdaProj loss is as follows.

Definition 5.2 (AdaProj)**.** Using the same notation as introduced in Definitions 3.2 and 3.4, define the logit for class $k \in \{1, ..., N_{\text{classes}}\}$ measuring the distance between an embedding and its projection to a linear subspace as

$$\begin{aligned} &d_{\text{proj}} : \mathbb{R}^D \times \mathcal{P}(\mathbb{R}^D) \to \mathbb{R}_+ \\ &d_{\text{proj}}(\phi(x, w), C_k) := \hat{s} \cdot \|P_{\mathcal{S}^{D-1}}(\phi(x, w)) - P_{\mathcal{S}^{D-1}}(P_{\text{span}(\mathcal{C}_k)}(\phi(x, w)))\|_2^2. \end{aligned} \tag{55}$$

Then, the *AdaProj* loss is defined as

$$\begin{aligned} &\mathcal{L}_{\text{proj}} : \mathcal{P}(X) \times \mathcal{P}(\mathcal{P}(\mathbb{R}^D)) \times \Phi \times W \times \Lambda(N_{\text{classes}}) \to \mathbb{R}_+ \\ &\mathcal{L}_{\text{proj}}(Y, \mathcal{C}, \phi, w, \text{lab}) := -\frac{1}{|Y|} \sum_{x \in Y} \sum_{j=1}^{N_{\text{classes}}} \text{lab}(x)_j \log(\text{softmax}(\hat{s} \cdot d_{\text{proj}}(\phi(x, w), C_j))) \end{aligned} \tag{56}$$

where $\tilde{s} \in \mathbb{R}_+$ is the dynamically adaptive scale parameter of the AdaCos loss. For the AdaProj loss, the centers $\mathcal{C}$ are called *basis vectors*.

Remark. Since all embeddings and the linear subspaces are projected onto the unit sphere, Lemma 3.1 implies that

$$\|P_{\mathcal{S}^{D-1}}(x) - P_{\mathcal{S}^{D-1}}(P_{\text{span}(\mathcal{C}_k)}(x))\|_2^2 = 2(1 - \text{sim}(P_{\mathcal{S}^{D-1}}(x), P_{\mathcal{S}^{D-1}}(P_{\text{span}(\mathcal{C}_k)}(x)))).$$

This is the reason why the AdaProj loss is an angular margin loss.

The following Lemma formally proves the claim that the space of optimal solutions for the AdaProj loss is indeed larger than the solution space of the sub-cluster AdaCos loss.

Lemma 5.3. *Let* $e \in \mathbb{R}^D$ *and let* $C \subset \mathbb{R}^D$ *contain pairwise orthonormal elements. If* $e \in \text{span}(C) \cap \mathcal{S}^{D-1}$*, then*

$$\|P_{\mathcal{S}^{D-1}}(e) - P_{\mathcal{S}^{D-1}}(P_{\text{span}(C)}(e))\|_2^2 = 0. \tag{57}$$

Proof. Let $e \in \text{span}(C) \cap \mathcal{S}^{D-1} \subset \mathbb{R}^D$ with $|C| = N_{\text{centers}}$. Therefore, $\|e\|_2 = 1$ and there are $\lambda_j \in \mathbb{R}$ such that $e = \sum_{j=1}^{N_{\text{centers}}} \lambda_j c_j$. Hence, it holds that

$$\begin{aligned} e = \sum_{j=1}^{N_{\text{centers}}} \lambda_j c_j &= \sum_{j=1}^{N_{\text{centers}}} \sum_{i=1}^{N_{\text{centers}}} \lambda_i \langle c_i, c_j \rangle c_j = \sum_{j=1}^{N_{\text{centers}}} \langle \sum_{i=1}^{N_{\text{centers}}} \lambda_i c_i, c_j \rangle c_j \\ &= \sum_{j=1}^{N_{\text{centers}}} \langle e, c_j \rangle c_j = P_{\text{span}(C)}(e), \end{aligned} \tag{58}$$

which finishes the proof. □

For each class-specific subspace, the randomly sampled basis vectors are approximately orthogonal with very high probability [65]. Therefore, each subspace has a dimension of $|C|$ with very high probability and thus $|C| < D$ needs to be ensured to not allow the entire embedding space as a solution. Still, the size of the solution space for the AdaProj loss is much higher than for the sub-cluster AdaCos loss, for which only the sub-clusters themselves are optimal solutions.

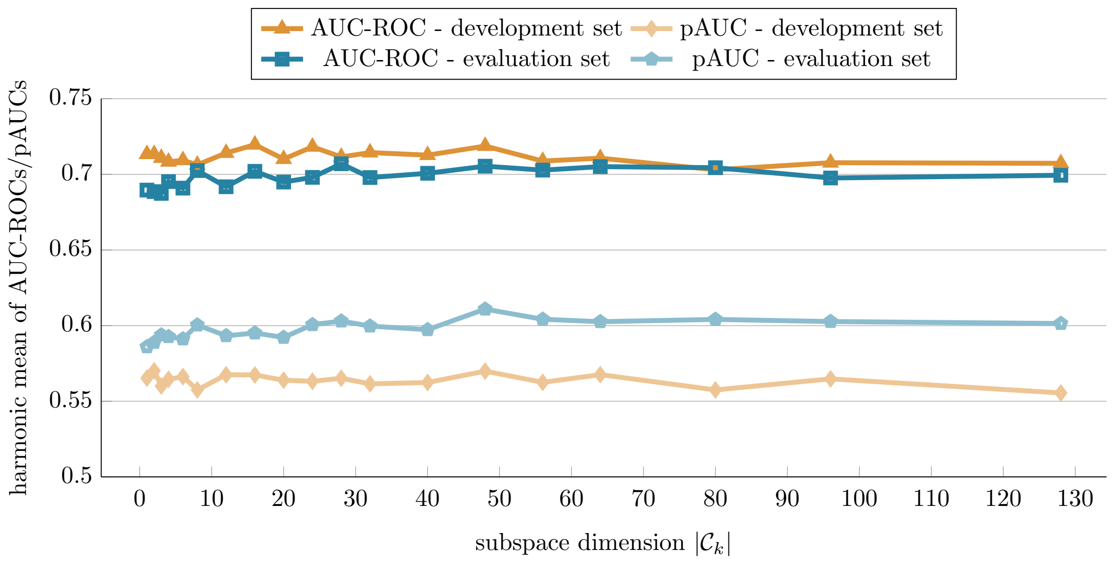

Figure 24: Domain-independent performance obtained on the DCASE2023 dataset with different subspace dimensions for the AdaProj loss. The means over ten independent trials are shown. © 2024 IEEE

5.6.2 *Choosing a sub-space dimension*

The impact of altering the subspace dimension of the AdaProj loss on the resulting performance is depicted in Figure 24. For all experimental evaluations in this and the next subsection, the ASD system presented in Section 5.3.2 with a few modifications is used. Most importantly, the sub-cluster AdaCos loss is replaced with AdaProj when training the embedding model. Additionally, the embedding dimension of the sub-networks is increased from 128 to 256 and 32 instead of 16 clusters are used when applying k-means to the embeddings belonging to the normal training samples of the source domain. The reason for increasing the dimensions of the sub-spaces is to grant the embedding model more freedom in learning class-specific distributions.

When inspecting the experimental results contained in Figure 24, it can be seen that for low to medium subspace dimensions the performance is approximately constant on the development set. On the evaluation set, medium subspace dimensions lead to slightly better performance than low subspace dimensions. For both dataset splits, the performance starts to degrade when being higher than approximately 48. In conclusion, the chosen subspace dimension should be neither too high nor too low. Therefore, a dimension of 32 was used in the following experiments.

5.6.3 *Performance evaluation*

As a next step, the AdaProj loss is compared to other loss functions on the DCASE2022 and the DCASE2023 dataset by only replacing the loss function of

Table 25: ASD performance obtained with different loss functions on the DCASE2022 and DCASE2023 datasets. Harmonic means of all AUC-ROCs and pAUCs over all sections of each dataset are depicted in percent. Arithmetic mean and standard deviation of the results over ten independent trials are shown. Best results in each column are highlighted with bold letters. © 2024 IEEE

DCASE2022 development set

loss function	source domain		target domain		domain-independent	
	AUC-ROC	pAUC	AUC-ROC	pAUC	AUC-ROC	pAUC
intra-class compactness loss	81.8 ± 1.6	74.9 ± 1.7	75.3 ± 1.0	**63.4 ± 0.6**	79.2 ± 0.9	64.7 ± 1.1
intra-class compactness loss + CXE	82.5 ± 1.8	75.5 ± 0.9	75.5 ± 0.7	61.6 ± 0.9	79.0 ± 0.8	65.0 ± 0.7
AdaCos loss	82.6 ± 1.4	76.0 ± 1.1	76.5 ± 1.2	62.3 ± 1.4	79.8 ± 0.7	**65.5 ± 0.9**
sub-cluster AdaCos loss	83.2 ± 2.1	75.9 ± 1.3	**77.6 ± 1.0**	62.1 ± 1.5	80.0 ± 1.4	65.2 ± 1.1
AdaProj loss	**84.3 ± 1.1**	**76.3 ± 1.1**	77.2 ± 1.2	62.2 ± 1.1	**80.6 ± 0.8**	**65.5 ± 1.3**

DCASE2022 evaluation set

loss function	source domain		target domain		domain-independent	
	AUC-ROC	pAUC	AUC-ROC	pAUC	AUC-ROC	pAUC
intra-class compactness loss	74.7 ± 0.9	64.2 ± 1.3	65.9 ± 0.8	57.8 ± 0.9	70.3 ± 0.8	58.9 ± 0.8
intra-class compactness loss + CXE	75.6 ± 0.7	66.9 ± 0.8	69.3 ± 0.7	59.3 ± 0.7	72.6 ± 0.4	60.3 ± 0.7
AdaCos loss	77.2 ± 0.5	65.9 ± 1.4	68.6 ± 1.1	58.6 ± 0.7	73.0 ± 0.4	59.7 ± 0.6
sub-cluster AdaCos loss	77.0 ± 0.7	66.5 ± 0.9	68.3 ± 0.8	58.8 ± 0.6	72.9 ± 0.6	59.5 ± 0.5
AdaProj loss	**77.4 ± 1.0**	**67.0 ± 0.6**	**69.7 ± 0.6**	**59.6 ± 0.6**	**73.6 ± 0.7**	**60.5 ± 0.7**

DCASE2023 development set

loss function	source domain		target domain		domain-independent	
	AUC-ROC	pAUC	AUC-ROC	pAUC	AUC-ROC	pAUC
intra-class compactness loss	67.0 ± 2.1	62.4 ± 1.0	69.1 ± 1.4	**56.4 ± 1.1**	67.7 ± 1.2	56.9 ± 0.9
intra-class compactness loss + CXE	70.6 ± 1.8	64.1 ± 1.8	71.2 ± 1.4	55.5 ± 1.6	70.4 ± 1.0	**57.4 ± 1.1**
AdaCos loss	**70.7 ± 1.3**	**64.3 ± 1.1**	71.2 ± 1.1	55.4 ± 1.3	70.9 ± 0.9	56.8 ± 0.9
sub-cluster AdaCos loss	68.3 ± 1.7	62.0 ± 1.5	71.8 ± 1.5	55.6 ± 1.5	70.4 ± 0.9	56.3 ± 0.8
AdaProj loss	70.3 ± 1.7	61.8 ± 1.6	**72.2 ± 1.4**	55.1 ± 1.1	**71.4 ± 1.0**	56.2 ± 0.7

DCASE2023 evaluation set

loss function	source domain		target domain		domain-independent	
	AUC-ROC	pAUC	AUC-ROC	pAUC	AUC-ROC	pAUC
intra-class compactness loss	73.5 ± 1.8	63.4 ± 1.8	58.8 ± 2.5	55.7 ± 1.3	64.0 ± 1.5	55.8 ± 0.9
intra-class compactness loss + CXE	74.3 ± 1.5	**64.0 ± 1.6**	61.6 ± 2.0	55.7 ± 0.9	67.5 ± 0.8	57.5 ± 1.0
AdaCos loss	**74.7 ± 1.5**	63.8 ± 1.8	61.6 ± 3.4	57.1 ± 1.4	68.0 ± 1.6	58.0 ± 1.1
sub-cluster AdaCos loss	73.2 ± 1.9	61.6 ± 1.4	62.0 ± 2.2	55.8 ± 1.3	66.5 ± 1.6	56.2 ± 1.0
AdaProj loss	74.2 ± 1.8	62.9 ± 1.0	**64.4 ± 2.0**	**57.7 ± 0.8**	**69.8 ± 1.3**	**60.0 ± 0.5**

arithmetic mean over all datasets

loss function	source domain		target domain		domain-independent	
	AUC-ROC	pAUC	AUC-ROC	pAUC	AUC-ROC	pAUC
intra-class compactness loss	74.3	66.2	67.3	58.3	70.3	59.1
intra-class compactness loss + CXE	75.8	**67.6**	69.4	58.0	72.4	60.1
AdaCos loss	76.3	67.5	69.5	58.4	72.9	60.0
sub-cluster AdaCos loss	75.4	66.5	69.9	58.1	72.5	59.3
AdaProj loss	**76.6**	66.3	**70.9**	**58.7**	**73.9**	**60.6**

the embedding model and keeping all other components of the system the same. The results can be found in Table 25. Overall, the AdaProj loss outperforms all other loss functions, especially on the evaluation split of the DCASE2023 dataset. A possible explanation is that the classification task on the DCASE2023 dataset is simpler than on the DCASE2022 dataset due to the reduced number of classes and thus the embedding model may be able to learn solutions that are almost trivial for certain classes. This means that for these classes the embeddings do not contain enough information to be able to discriminate between embeddings of normal and anomalous samples. Since the solutions spaces of the AdaProj loss are much larger, a trivial solution only needs to be contained in a sub-space but the learned distribution may have a very complex structure inside this space, which allows to still be able to detect anomalies.

As a second observation, one can see that the sub-cluster AdaCos performs worse than AdaCos, which seems to contradict the results presented in Section 3.4. However, in the experiments conducted in Section 3.4 the centers have been adapted during training, which is not the case in these experiments. Without adapting the centers, all sub-clusters have approximately the same distance to each other because they are very likely to be orthogonal regardless of whether they belong to the same target class or not. This has two consequences: First, the sub-cluster AdaCos loss is actually more restrictive than the AdaCos loss and results in learning more compact distributions for each class to ensure low inter-class similarity to all sub-clusters of the other classes. This makes it difficult to distinguish between normal and anomalous samples. Second, in most cases only a single sub-cluster for each class is utilized by the model to ensure high intra-class similarity while still ensuring low inter-class similarity. This favors learning even more compact distributions for the normal samples.

5.7 SELF-SUPERVISED LEARNING

Throughout this thesis, it has been shown that the performance of an ASD system degrades when decreasing the amount of meta information used for training the embedding model. This difficulty is one focus of the task imposed by the DCASE2023 ASD dataset, which contains only a single section for each machine type. To still be able to learn informative embeddings yielding a good performance, the difficulty of the auxiliary classification task needs to be increased. Self-supervised learning (SSL) [132] is a type of unsupervised learning that does not require any class labels but augments the data in specific ways and trains the network to recognize these augmentations. To be able to correctly recognize specific augmentations, the embedding model needs to learn the structure of the original data resulting in more information being captured that may also be useful to detect anomalous data. Other applications of SSL are to learn representations for speech-related [152] or general-purpose audio tasks [165, 167].

As already stated in Section 2.7, there are also several works applying SSL to ASD using different data augmentation techniques. Examples are detecting pitch-shifted and time-stretched recordings [85], recognizing linear combinations of similar target sounds [134] generated with mixup [262], mixing first- and second-order statistics of time-frequency representations [26] and pre-training an autoencoder using a modified version of variance-invariance-covariance regularization [12]. Some works on ASD denote auxiliary classification tasks based on meta information [43, 60] as SSL. However, since SSL tasks do not require any manually annotated labels, training paradigms completely relying on meta information should be called supervised tasks instead.

As seen in Section 5.5, openL3 embeddings, which are the only embeddings based on SSL, performed best of the investigated pre-trained embeddings. This can be seen as additional evidence that applying SSL when directly training an embedding model on the data may improve the performance. Investigating this is the goal of this section.

5.7.1 *Approaches*

In this section, different SSL approaches for ASD will be presented. The first approach, called statistics exchange (StatEx) [26], was proposed to simulate anomalous samples that are used for training a discriminative ASD system. The anomalies are simulated by exchanging first and second order statistics over the time or frequency axis of the time-frequency representations of two random training samples. The following definition formalizes this.

Definition 5.4 (Statistics exchange (original)). Let $x_1, x_2 \in \mathbb{R}^{T\times F}$ with $T, F \in \mathbb{N}$ denote the time-frequency representations of two random training samples. Let μ_1, μ_2 denote the first-order statistics over the time or frequency dimension of x_1 and x_2, respectively, and σ_1, σ_2 denote the corresponding second-order statistics. Then, the augmented sample $x_{\text{new}}(x_1, x_2)$ and its categorical label $\text{lab}(x_{\text{new}}(x_1, x_2))$ are given by

$$\begin{aligned} x_{\text{new}}(x_1, x_2) &:= \frac{x_1 - \mu_1}{\sigma_1}\sigma_2 + \mu_2 \in \mathbb{R}^{T\times F} \\ \text{lab}(x_{\text{new}}(x_1, x_2)) &:= \big(\text{lab}(x_1)_1 \cdot \text{lab}(x_2), ..., \text{lab}(x_1)_{N_{\text{classes}}} \cdot \text{lab}(x_2)\big) \in [0,1]^{N^2_{\text{classes}}}. \end{aligned} \tag{59}$$

If the statistics over the time axis are used, this approach is called *frequency StatEx*. If the statistics over the frequency axis are used, it is called *temporal StatEx*.

Remark. For the original definition of StatEx, frequency bands or temporal regions smaller than the selected maximum size imposed by the dimensions of the spectrogram are used. For the sake of simplicity, the entire signals are used in this work as the difference in performance is neglectable.

When using StatEx, another anomaly is simulated for each normal training sample contained in a batch. Both versions are used for training the embedding model, essentially doubling the batch size. For the normal training samples, the original classes are used. For the simulated anomalies, the number of classes increases quadratically. Depending on the number of original classes, training an embedding model may therefore quickly become infeasible. Because of this, the following variant of StatEx is proposed.

Definition 5.5 (Statistics exchange (variant))**.** Using the same notation as in Definition 5.4 and the same definition of the augmented sample $x_{\text{new}}(x_1, x_2) \in \mathbb{R}^{T\times F}$, the categorical label of x_{new} is set to

$$\text{lab}(x_{\text{new}}(x_1, x_2)) = (\mathbf{0}, 0.5 \cdot \text{lab}(x_1), 0.5 \cdot \text{lab}(x_2)) \in [0,1]^{3N_{\text{classes}}} \tag{60}$$

where $\mathbf{0} = (0, ..., 0) \in [0,1]^{N_{\text{classes}}}$.

This StatEx variant has the advantage that only three times as many classes are needed instead of increasing the number of classes quadratically. Another modification is that a probability of 50% is used to decide whether to apply StatEx or not during training instead of using all original samples and their augmented version. This ensures that the batch size does not increase when using StatEx. When not applying StatEx, i.e. using an original training sample $x_{\text{new}}(x_1, x_2) = x_1$ the categorical label is set to

$$\text{lab}(x_{\text{new}}(x_1, x_2)) := (\text{lab}(x_1), \mathbf{0}, \mathbf{0}) \in [0,1]^{3N_{\text{classes}}}. \tag{61}$$

Applying TMN sets the temporal mean of each sample to zero and thus impedes using frequency StatEx. Therefore, only temporal StatEx is applied when training the embedding model while using TMN to pre-process the input features.

As a second SSL approach, feature exchange (FeatEx), which is inspired by the training procedure of the OpenL3 embeddings [6, 7, 32], will be presented. The reader is reminded that these embeddings are trained by comparing video frames to audio clips with a length of 1 s and training the network to predict whether the embeddings extracted from a frame and a clip belong together or not (cf. Section 2.5). Since the ASD system only utilizes audio data, directly applying this approach is impossible. Instead, the embeddings belonging to both feature branches are used. Formally, FeatEx is defined as:

Definition 5.6 (Feature exchange)**.** For embedding model $\phi = (\phi_{\text{STFT}}, \phi_{\text{DFT}}) \in \Phi$ with parameter settings $w = (w_{\text{STFT}}, w_{\text{DFT}}) \in W$ and two random training samples $x_1, x_2 \in X_{\text{train}}$, let $\phi(x_1, w) = (\phi_{\text{STFT}}(x_1, w_{\text{STFT}}), \phi_{\text{DFT}}(x_1, w_{\text{DFT}})) \in \mathbb{R}^D$ and $\phi(x_2, w) = (\phi_{\text{STFT}}(x_2, w_{\text{STFT}}), \phi_{\text{DFT}}(x_2, w_{\text{DFT}}))) \in \mathbb{R}^D$ denote the concatenated embeddings of both sub-networks $\phi_{\text{STFT}}, \phi_{\text{DFT}}$ belonging to these samples. Then, an augmented embedding $e_{\text{new}}(x_1, x_2, \phi, w) \in \mathbb{R}^D$ and its categorical label are set to

$$\begin{aligned} e_{\text{new}}(x_1, x_2, \phi, w) &= (\phi_{\text{STFT}}(x_1, w_{\text{STFT}}), \phi_{\text{DFT}}(x_2, w_{\text{DFT}}))) \in \mathbb{R}^D \\ \text{lab}(e_{\text{new}}(x_1, x_2, \phi, w)) &= (\mathbf{0}, 0.5 \cdot \text{lab}(x_1), 0.5 \cdot \text{lab}(x_2)) \in [0,1]^{3N_{\text{classes}}} \end{aligned} \tag{62}$$

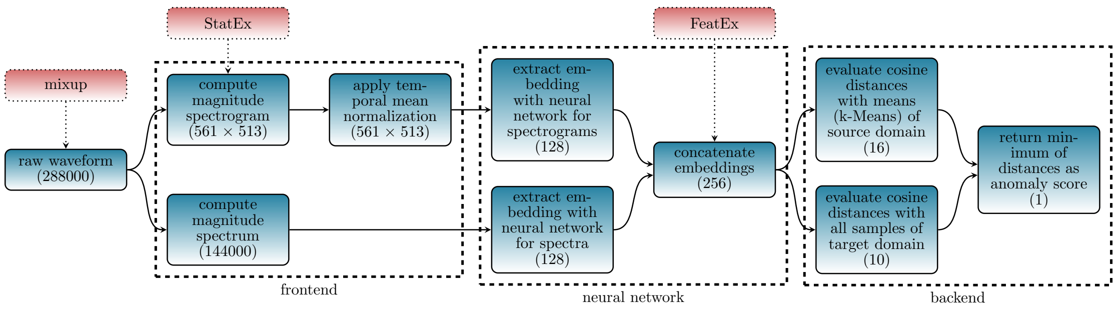
StatEx
FeatEx
mixup
raw waveform (288000)
compute magnitude spectrogram (561 × 513)
apply temporal mean normalization (561 × 513)
compute magnitude spectrum (144000)
extract embedding with neural network for spectrograms (128)
extract embedding with neural network for spectra (128)
concatenate embeddings (256)
evaluate cosine distances with means (k-Means) of source domain (16)
evaluate cosine distances with all samples of target domain (10)
return minimum of distances as anomaly score (1)
frontend
neural network
backend

Figure 25: Illustration of an ASD system utilizing multiple SSL approaches. The baseline system is colored in blue and the SSL approaches are colored in red. Representation size in each step is given in brackets. © 2024 IEEE

where $\mathbf{0} = (0, ..., 0) \in [0, 1]^{N_{\text{classes}}}$.

As for the StatEx variant, the number of classes is tripled when applying FeatEx and a probability of 50% is used to decide whether to apply FeatEx or not.

5.7.2 *Combining multiple approaches*

Each SSL approach forces the embedding model to capture more information in the embeddings by increasing the difficulty of the classification task the model needs to solve. Therefore, multiple SSL approaches can all be used for training a single system. The system presented in Section 5.3.1 using the StatEx variant, FeatEx as well as mixup [262] (see Section 2.7.3) is illustrated in Figure 25. For the experimental evaluations in the following section, mixup is only used with a probability of 50% when also using any other SSL approach. If the model is trained without StatEx or FeatEx, mixup is applied with a probability of 100% to each training sample. The model is trained with a combined loss function consisting of two classification losses. The first loss is the standard classification task based on provided meta information and uses the mixed-up labels for training. The second loss is based on the sequentially applied SSL approaches and thus uses $9 \cdot N_{\text{classes}}$ total classes. Both losses are realized with sub-cluster AdaCos losses with 16 sub-clusters for each class. As before, non-trainable class centers are used for the standard classification task. For the SSL loss, trainable class centers are used as the embedding model should learn to detect augmented samples as pseudo-anomalies close to the distributions of the normal, non-augmented samples to refine the boundary of these distributions.

Note that, although mixup utilizes class labels, it also imposes an additional self-supervised task of needing to estimate the mixing coefficient of linear interpolations between random training samples. Hence, it can be seen as a label-dependent SSL approach. In theory, mixup could also be applied without using class labels and teaching the model to only estimate the mixing coefficient. But as previously shown, utilizing meta information is important to effectively handle the noise and thus a classification task should be used.

5.7.3 *Performance evaluation*

As a first experiment, the performances obtained with individual SSL approaches and the combined approach are compared to the baseline performance obtained when not using any SSL. The results can be found in Table 26. Overall, it can be seen that the SSL approaches significantly improve the performance of the baseline system. Furthermore, one can observe that, in general, FeatEx performs better than StatEx. When only using StatEx without the standard classification task, the performance decreases as opposed to only using FeatEx, which slightly improves the performance. This indicates that the proposed FeatEx approach is superior to StatEx. When combining any SSL approach with the regular classification loss, both approaches, FeatEx and StatEx, perform better compared to only using the baseline system, which shows that applying SSL is highly beneficial. Moreover, combining both SSL approaches seems to marginally improve performance over only applying one of them. Another observation is that the performance improvements are much bigger on the DCASE2023 dataset than on the DCASE2022 dataset. This is consistent with the experimental findings for the AdaProj loss. Once more, the most likely reason is that a less difficult classification task caused by less available meta information leads to less informative embeddings. Therefore, essential information needed to discriminate between embeddings of normal and anomalous data is not captured, which degrades performance.

In a second experiment, whose results can be found in Table 27, three design choices are investigated: 1) using class labels based on the meta information for the SSL losses, 2) using non-trainable centers for the SSL losses and 3) not applying TMN but also using temporal StatEx. Comparing the performances obtained when altering any of these design choices to the performance obtained with the original system, one can see that all changes lead to worse performance, especially on the evaluation set. This justifies the proposed design of the ASD system and the SSL approaches.

5.8 PUTTING IT ALL TOGETHER

The goal of this section is to compare the performance obtained with the presented systems of this chapter to the state-of-the-art performance. Furthermore, the AdaProj loss and SSL are combined in a single system by replacing both sub-cluster AdaCos losses of the system used in Section 5.7 with AdaProj losses to see if this improves performance. For all evaluated systems, ensembles are used by taking the sum of the anomaly scores belonging to 10 individually trained versions of the same system. A comparison between the systems presented in this chapter and the ten top-performing systems of the DCASE2023 Challenge can be found

Table 26: Harmonic means of AUC-ROCs and pAUCs taken over all machine IDs obtained when using different SSL approaches. Highest AUC-ROCs and pAUCs in each column are highlighted in bold letters. Arithmetic mean and standard deviation over five independent trials are shown. © 2024 IEEE

DCASE2022 development set

SSL approach	source domain		target domain		domain-independent	
	AUC-ROC	pAUC	AUC-ROC	pAUC	AUC-ROC	pAUC
baseline	84.2 ± 0.8%	76.5 ± 0.9%	78.5 ± 0.9%	62.5 ± 0.9%	81.4 ± 0.7%	66.6 ± 0.9%
StatEx variant	80.5 ± 1.8%	69.5 ± 1.9%	75.3 ± 1.7%	60.0 ± 0.9%	76.4 ± 1.5%	62.4 ± 1.2%
FeatEx	82.1 ± 0.9%	72.8 ± 0.8%	77.2 ± 1.0%	62.8 ± 0.6%	78.5 ± 0.6%	65.2 ± 0.6%
regular and StatEx variant	85.2 ± 0.9%	77.5 ± 1.2%	**78.9 ± 0.9%**	63.2 ± 1.6%	82.2 ± 0.6%	67.0 ± 1.0%
regular and FeatEx	85.1 ± 0.9%	76.3 ± 1.8%	77.9 ± 0.9%	62.7 ± 0.8%	81.6 ± 0.7%	67.0 ± 0.9%
combined approach	**86.0 ± 0.9%**	**77.6 ± 0.8%**	78.2 ± 0.7%	**64.4 ± 1.1%**	**82.5 ± 0.8%**	**68.2 ± 1.1%**

DCASE2022 evaluation set

SSL approach	source domain		target domain		domain-independent	
	AUC-ROC	pAUC	AUC-ROC	pAUC	AUC-ROC	pAUC
baseline	76.8 ± 0.8%	65.8 ± 0.2%	69.8 ± 0.5%	59.7 ± 1.1%	73.4 ± 0.5%	59.8 ± 0.8%
StatEx variant	74.2 ± 0.6%	61.6 ± 1.4%	70.6 ± 0.5%	59.0 ± 0.7%	72.2 ± 0.3%	58.2 ± 0.7%
FeatEx	76.3 ± 0.9%	64.5 ± 1.2%	**72.3 ± 0.6%**	61.0 ± 0.7%	73.9 ± 0.5%	60.0 ± 0.9%
regular and StatEx variant	76.9 ± 0.4%	65.8 ± 0.9%	71.2 ± 0.3%	60.3 ± 0.7%	73.9 ± 0.3%	59.9 ± 0.6%
regular and FeatEx	**78.1 ± 0.4%**	**67.0 ± 1.1%**	72.2 ± 0.4%	**61.3 ± 0.5%**	**74.9 ± 0.4%**	**61.5 ± 0.6%**
combined approach	77.7 ± 0.8%	**67.0 ± 0.5%**	71.6 ± 1.0%	61.2 ± 0.9%	74.2 ± 0.3%	61.2 ± 0.3%

DCASE2023 development set

SSL approach	source domain		target domain		domain-independent	
	AUC-ROC	pAUC	AUC-ROC	pAUC	AUC-ROC	pAUC
baseline	69.8 ± 1.8%	60.9 ± 0.9%	72.3 ± 1.8%	55.6 ± 0.9%	71.3 ± 0.6%	56.1 ± 0.8%
StatEx variant	67.8 ± 1.5%	59.2 ± 0.8%	69.7 ± 1.7%	54.7 ± 1.1%	69.0 ± 1.2%	55.7 ± 1.0%
FeatEx	68.4 ± 1.0%	60.2 ± 0.5%	74.4 ± 0.7%	**57.6 ± 1.0%**	71.7 ± 0.4%	57.5 ± 0.7%
regular and StatEx variant	70.3 ± 1.8%	62.0 ± 1.6%	72.2 ± 1.4%	56.2 ± 1.2%	71.2 ± 0.7%	57.0 ± 1.4%
regular and FeatEx	**72.9 ± 2.0%**	**63.0 ± 1.3%**	**75.7 ± 0.8%**	57.0 ± 1.6%	**74.4 ± 1.0%**	**58.0 ± 1.4%**
combined approach	71.2 ± 1.6%	62.7 ± 1.3%	75.0 ± 1.5%	56.1 ± 1.4%	73.1 ± 0.9%	57.3 ± 0.6%

DCASE2023 evaluation set

SSL approach	source domain		target domain		domain-independent	
	AUC-ROC	pAUC	AUC-ROC	pAUC	AUC-ROC	pAUC
baseline	72.5 ± 0.8%	62.4 ± 1.2%	63.1 ± 2.6%	57.5 ± 0.8%	67.9 ± 1.0%	58.8 ± 0.8%
StatEx variant	70.0 ± 1.2%	59.7 ± 0.9%	66.7 ± 1.8%	58.4 ± 0.7%	65.8 ± 0.6%	57.1 ± 0.8%
FeatEx	69.3 ± 2.0%	59.3 ± 1.2%	**69.1 ± 1.3%**	59.0 ± 1.3%	68.1 ± 1.2%	58.1 ± 0.9%
regular and StatEx variant	72.4 ± 2.4%	62.4 ± 1.3%	65.9 ± 1.9%	59.0 ± 1.4%	69.5 ± 1.8%	60.7 ± 0.9%
regular and FeatEx	**75.9 ± 1.0%**	62.9 ± 1.3%	66.5 ± 1.9%	58.3 ± 1.0%	71.1 ± 1.1%	60.1 ± 1.3%
combined approach	75.5 ± 0.8%	**64.5 ± 0.6%**	68.7 ± 2.2%	**59.3 ± 0.7%**	**72.6 ± 0.7%**	**61.6 ± 0.5%**

Table 27: Harmonic means of AUC-ROCs and pAUCs taken over all machine types obtained on the DCASE2023 dataset by modifying design choices of the proposed SSL-based system. Arithmetic mean and standard deviation over five independent trials are shown. © 2024 IEEE

		SSL loss without class labels		non-trainable class centers		no TMN and full StatEx	
split	domain	AUC-ROC	pAUC	AUC-ROC	pAUC	AUC-ROC	pAUC
dev	source	70.8 ± 1.5%	63.2 ± 1.1%	71.5 ± 0.9%	64.8 ± 1.9%	70.9 ± 0.7%	61.0 ± 1.5%
dev	target	74.7 ± 1.5%	58.1 ± 1.6%	74.0 ± 2.0%	56.7 ± 1.0%	72.1 ± 1.4%	55.2 ± 1.0%
dev	mixed	72.3 ± 1.2%	57.9 ± 1.3%	71.6 ± 1.1%	57.7 ± 0.7%	71.3 ± 0.7%	55.6 ± 0.9%
eval	source	73.5 ± 2.4%	63.8 ± 0.6%	74.2 ± 0.7%	63.9 ± 1.3%	73.8 ± 1.3%	62.4 ± 1.5%
eval	target	62.1 ± 1.5%	57.7 ± 0.9%	58.2 ± 3.3%	57.3 ± 0.9%	66.9 ± 2.4%	58.5 ± 1.9%
eval	mixed	68.6 ± 1.2%	59.1 ± 0.7%	65.0 ± 0.9%	57.7 ± 0.6%	70.9 ± 0.8%	59.9 ± 0.8%

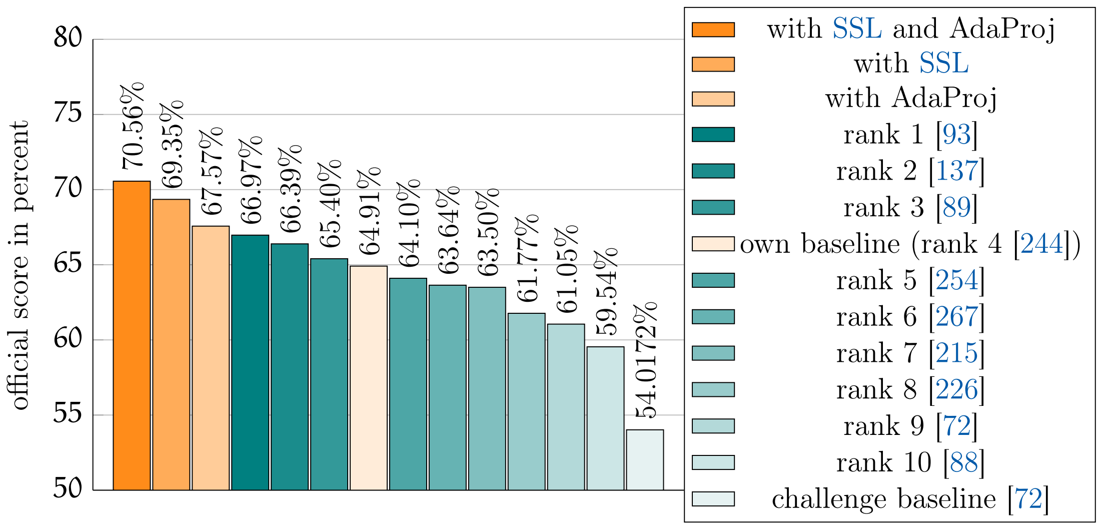

Figure 26: Comparison between the performances of the presented systems and official scores of the ten top-performing systems of the DCASE2023 Challenge. For the evaluations, ensembles consisting of ten sub-systems were used.

in Figure 26. It can be seen that the baseline system presented in Section 5.3.1 reached rank 4 and thus yields good but the best performance. When only replacing the loss functions with the AdaProj loss, the system slightly outperforms all other systems and thus yields state-of-the-art performance. However, the performance improvements obtained when applying the SSL approaches are significantly greater and the resulting system outperforms all other published systems by a large margin. Moreover, when combining AdaProj and SSL into a single system the resulting performance is even better. In conclusion, all approaches presented in this chapter are highly beneficial to improve the performance of a semi-supervised ASD system in domain-shifted conditions.

5.9 SUMMARY

In this chapter, the ASD system presented in Chapter 3 was modified to be robust to domain shifts from a source to a target domain, which are any changes of the distribution of normal data caused by altering the target sounds or the background noise. It was shown that many design choices of the system have an impact on the resulting performance. More concretely, it was shown that 1) preventing trivial solutions by not using bias terms or trainable centers, 2) utilizing STFT- and DFT-based input feature representations in combination with TMN with two sub-networks, whose embeddings are combined by concatenating them, as well as 3) using the cosine similarity as a backend all significantly improve the performance in domain-shifted conditions.

Further investigations were aimed at explaining the results obtained with the presented ASD system. To this end, the impact of specific regions of the input features on the ASD performance using RISE and visualizing the resulting embedding spaces using t-SNE were investigated. Here, it could be seen that the embeddings obtained when using an auxiliary classification task capture more meaningful structures and thus normal embeddings can be much better separated from anomalous ones. This verifies the findings presented in Chapter 3. In contrast to the source domain, there are only very few training samples provided for the target domain in domain-shifted conditions. Although pre-trained embeddings are a promising approach in settings with limited training data, the experiments conducted in this chapter showed that directly training the embedding model leads to significantly better performance than using pre-trained embeddings as input to a shallow classifier.

In case only little meta information is available for training an embedding model with an auxiliary classification task, the ASD performance decreases. Two additional modifications of the ASD system were presented to improve the performance in such a setting. First, the angular margin loss AdaProj for learning class-specific sub-spaces was proposed. This loss is a generalization of the sub-cluster AdaCos loss and enables the model to learn class-specific distributions that are more complex than a combination of Gaussians. Using AdaProj increased the ability of the system to distinguish between embeddings belonging to normal and anomalous samples. Second, multiple SSL approaches were used to increase the difficulty of the classification task and thus force the embedding model to capture more information. To this end, FeatEx, which randomly exchanges the embeddings of both sub-networks between different training samples, was presented. It was shown that combining FeatEx with StatEx, which exchanges first- and second-order statistics of two random training samples, significantly improved performance when training the embedding model with an auxiliary classification task. Utilizing AdaProj and SSL together, led to an even better performance outperforming all other published systems with a significant margin. As a result, the system presented in this chapter reached a new state-of-the-art performance on the DCASE2023 dataset.

6 FEW-SHOT OPEN-SET CLASSIFICATION

The goal of this chapter is to investigate open-set classification (OSC) as another application of ASD than acoustic machine condition monitoring, which has been extensively studied in the previous chapters. As mentioned in the introduction of this thesis, OSC can be separated into two sub-tasks: closed-set classification (CSC) and anomaly detection (AD) [238]. In the previous chapters, it has been shown that angular margin losses are an excellent choice for detecting anomalous sounds. Furthermore, angular margin losses are specifically designed for CSC and thus angular margin losses are expected to also be an excellent choice to train models for OSC. Because of this, the difficulty of the OSC tasks investigated in this chapter will be increased by only considering settings in which only very few training samples are provided. For many applications, this is a more realistic scenario than having access to many training samples for each class because it substantially simplifies the data collection and labeling process. Furthermore, keyword spotting will be used as an application for sound event detection (SED), which demands to not only recognize the correct keyword class but also to determine the precise on- and offset of each sound event.

This chapter is structured as follows. First, the ASD system presented in Section 5.3.1 will be evaluated for few-shot OSC. Similar to the experiments conducted in Section 5.5, the resulting performance will be compared to performances obtained with pre-trained embeddings. Second, the loss function TACos, which is a modification of the AdaCos loss capable of learning embeddings with a temporal structure, will be presented and evaluated for few-shot keyword spotting.

6.1 CONTRIBUTIONS OF THE AUTHOR

The sections of this chapter are largely based on the following key publications:

- Kevin Wilkinghoff and Fabian Fritz. “On Using Pre-Trained Embeddings for Detecting Anomalous Sounds with Limited Training Data.” In: *31st European Signal Processing Conference (EUSIPCO)*. IEEE, 2023, pp. 186–190.
- Kevin Wilkinghoff, Alessia Cornaggia-Urrigshardt, and Fahrettin Gökgöz. “Two-Dimensional Embeddings for Low-Resource Keyword Spotting Based on Dynamic Time Warping.” In: *14th ITG Conference on Speech Communication (ITG Speech)*. VDE-Verlag, 2021, pp. 9–13.
- Kevin Wilkinghoff and Alessia Cornaggia-Urrigshardt. “TACos: Learning Temporally Structured Embeddings for Few-Shot Keyword Spotting with

Dynamic Time Warping." In: *International Conference on Acoustics, Speech and Signal Processing (ICASSP)*. IEEE, 2024, pp. 9941–9945.

For publications that are not single-authored, individual contributions of the thesis author and all co-authors to these publications are stated in Section A.1. If not stated otherwise, the content listed in the following paragraph is the sole contribution of the thesis author.

Section 6.2 is based on [250]. Fabian Fritz helped with the experimental evaluations by writing wrapper functions for the pre-trained embeddings. Section 6.3 is mostly based on [248], which is an extension of [249]. Thus, [249] is only indirectly covered. Alessia Cornaggia-Urrigshardt helped with creating the dataset presented in Section 6.3.2 and applied DTW to the embeddings. Additionally, she evaluated the HFCC-based model presented in Section 6.3.7 and conducted the experiments related to the global and individual decision thresholds contained in Table 31.

6.2 FEW-SHOT OPEN-SET CLASSIFICATION

Before conducting any experiments, the terms *open-set classification* and *few-shot learning* will be formalized. OSC tasks can be characterized by the so-called *openness* [200], which quantifies *how open* a specific OSC task is by measuring the relation between known and unknown classes and is defined as follows:

Definition 6.1 (Openness)**.** Let $N^{\text{train}}_{\text{classes}}, N^{\text{test}}_{\text{classes}} \in \mathbb{N}$ denote the number of classes of the training subset and the test subset, respectively. Then the openness of an OSC task is defined as

$$\text{openness}(N^{\text{train}}_{\text{classes}}, N^{\text{test}}_{\text{classes}}) := 1 - \sqrt{\frac{2 \cdot N^{\text{train}}_{\text{classes}}}{N^{\text{train}}_{\text{classes}} + N^{\text{test}}_{\text{classes}}}} \in [0, 1]. \tag{63}$$

Remark. $N^{\text{train}}_{\text{classes}}$ denotes the number of known target classes and known non-target classes (known unknowns), for which training samples are provided. $N^{\text{test}}_{\text{classes}}$ not only contains the same known target and non-target classes but may also contain additional non-target classes not encountered during training (unknown unknowns). These unknown unknowns correspond to the anomalies of a semi-supervised anomaly detection task and are the essential difference between closed-set and open-set problems. In case no unknown unknowns exist, the OSC task is in fact a CSC task because all classes are known during training. Note that for realistic applications it is usually impossible to provide training samples that fully capture the space of unknown classes as it is also the case in a supervised anomaly detection setting. For the same reason, even counting $N^{\text{test}}_{\text{classes}}$ for a realistic application is impossible. Because of this, $N^{\text{test}}_{\text{classes}}$ denotes the number of classes contained in a specific set of test samples, which is always less or equal than the real number of classes of the target application.

Since the openness is such an essential characteristic of an OSC task, it can be used to describe a task or serve as a metric to compare similar tasks. A higher openness indicates more unknown classes relative to the number of known classes. An openness of 0 corresponds to a CSC task and an openness of 1 corresponds to a finite number of known classes and an infinite number of unknown non-target classes, since $N_{\text{classes}}^{\text{train}} \neq 0$.

Few-shot learning [227] describes a task for which only $K \in \mathbb{N}$ training samples are available for each class (K-*shot learning*). Hence, the size of the training dataset is very limited, making it difficult to train a model such that it generalizes well to unseen data. The most popular loss function for few-shot classification [227] is a prototypical loss [209] defined as follows:

Definition 6.2 (Prototypical loss)**.** Let $d : X \times X \to \mathbb{R}_+$ denote a metric and $Y \subset X$ be finite. For training step $t \in \mathbb{N}_0$, let $\mathcal{S}^{(t)}, \mathcal{Q}^{(t)} \subset Y$ with $\mathcal{S}^{(t)} \cap \mathcal{Q}^{(t)} = \emptyset$ denote randomly sampled subsets called *support set* and *query set*, respectively. Furthermore, define the *prototypes* $C^{(t)} = \{c_1^{(t)}, ..., c_{N_{\text{classes}}}^{(t)}\} \subset \mathbb{R}^D$ as the means of the embeddings computed from all $x \in \mathcal{S}^{(t)}$ belonging to the same class $i \in \{1, ..., N_{\text{classes}}\}$, i.e. for embedding model $\phi \in \Phi$ with parameters $w \in W$ set

$$c_i^{(t)}(\phi, w, \mathcal{S}^{(t)}) := \text{mean}(\{\phi(x, w) \in \mathbb{R}^D : x \in \mathcal{S}^{(t)}, \text{class}(x) = i\}). \tag{64}$$

Then, using the same notation as used in Definition 2.7, the *prototypical loss* at training step t is defined as

$$\begin{aligned} &\mathcal{L}_{\text{prot}}^{(t)} : \mathcal{P}(X) \times \mathcal{P}(\mathbb{R}^D) \times \Phi \times W \times \Lambda(N_{\text{classes}}) \to \mathbb{R}_+ \\ &\mathcal{L}_{\text{prot}}^{(t)}(\mathcal{Q}^{(t)}, C^{(t)}, \phi, w, \text{lab}, d) \\ := -&\frac{1}{|\mathcal{Q}^{(t)}|} \sum_{x \in \mathcal{Q}^{(t)}} \sum_{j=1}^{N_{\text{classes}}} \text{lab}(x)_j \log(\text{softmax}(d(\phi(x, w), c_j^{(t)}))) \end{aligned} \tag{65}$$

When choosing the Euclidean distance as a metric for the prototypical loss, i.e.

$$d(\phi(x, w), c_j^{(t)}) := \|\phi(x, w) - c_j^{(t)}\|_2^2, \tag{66}$$

Theorem 3.5 and Corollary 3.3 show that angular margin losses such as the AdaCos loss can also be viewed as prototypical losses or angular prototypical losses [30] with a margin between classes. The main difference between these types of loss functions is that for a prototypical loss the centers are re-calculated during training by randomly sampling a support set whereas, for an angular margin loss, they are treated as trainable parameters or not adapted at all. The similarity of the loss functions is the reason why using an angular margin loss in a *few-shot* open-set classification setting is a viable option. However, as the number of training samples is very limited, learning more complex distributions than Gaussians for each class is not feasible and thus extensions of standard angular margin losses such as the presented sub-cluster AdaCos loss (see Section 3.4) or AdaProj (see Section 5.6) should not be used. In addition, the CSC classification sub-task is challenging by

Table 28: Structure of the few-shot OSC dataset for acoustic alarm detection in domestic environments.

			number of classes		
openness	shots	validation folds	known	known unknown	unknown unknown
low (0)	1	40	24	10	0
low (0)	2	20	24	10	0
low (0)	4	10	24	10	0
middle (0.04)	1	40	24	5	5
middle (0.04)	2	20	24	5	5
middle (0.04)	4	10	24	5	5
high (0.09)	1	40	24	0	10
high (0.09)	2	20	24	0	10
high (0.09)	4	10	24	0	10

itself and thus for OSC avoiding trivial solutions is less of a problem than for ASD alone.

In theory, the very limited number of training samples available for few-shot classification should favor pre-trained embeddings over training a system directly on the dataset. This motivates the goal of this section, which is to evaluate the previously proposed ASD system for few-shot OSC and compare its performance to performances obtained with pre-trained embeddings.

6.2.1 *Dataset*

The few-shot OSC dataset used in this section aims at detecting and correctly classifying acoustic alarms in domestic environments [162]. In total, the dataset contains 34 classes with 24 known alarm sounds and 10 unknown sounds belonging to one of the classes “car horn”, “clapping”, “cough”, “door slam”, “engine”, “keyboard tapping”, “music”, “pots and pans”, “steps” and “water falling”. For each class, there are 40 recordings, each with a length of 4 s and a sampling rate of 16 kHz. There are several different versions of this dataset defined by the number of shots available for each class (1, 2 or 4) and the openness (0, 0.04 or 0.09). Each version of the dataset is divided into a training and a test subset by using cross-validation. An overview can be found in Table 28. The performance of a trained system is evaluated by using the weighted accuracy (cf. Section 2.10, Equation 27) with $\beta_{\mathrm{ACC}} = 0.5$ as a performance measure.

6.2.2 *System design*

To evaluate the performance on this few-shot OSC dataset, the ASD systems using pre-trained embeddings or the directly trained system presented in Section 5.5 were slightly modified. First of all, only a single sub-cluster per class was used for the sub-cluster AdaCos loss because only very few training samples are available for each class. Depending on the specific version of the dataset, some hyperparameters of the system were adapted to obtain more robust decision thresholds, which were needed to compute the performance of an ASD system with a threshold-dependent evaluation metric. More concretely, the number of training epochs was set to 100 times the number of shots and the batch size was set to 8 times the number of shots. Furthermore, the decision threshold was set to 0.6, 0.65 or 0.75 for low, medium or high openness settings, respectively. As a last modification, the openL3 embeddings pre-trained on the music subset instead of the environmental subset were used because acoustic alarms are more similar to music than environmental sound events.

6.2.3 *Experimental results*

A comparison of the performances obtained with different systems and different pre-trained embeddings can be found in Table 29. As expected, using more shots or having a lower openness leads to a better mean performance and a smaller variance as more training data should improve the performance and CSC is an easier problem than OSC. Furthermore, all proposed systems significantly outperform the two baseline systems proposed in [162] showing once more that the systems presented in this thesis are well designed. However, there is a strong difference in how well the systems perform. Overall, VGGish performs worst, followed by PANN, OpenL3 and Kumar embeddings and the directly trained system performs best. Moreover, all of the proposed systems have different stengths and weaknesses. The system based on OpenL3 embeddings performs best in the low openness setting, which is in fact a CSC task. In general, the directly trained model performs best for middle or high openness settings. An exception is the high openness setting when only a single shot is available for each class where Kumar embeddings perform best. The relative degradation of the performance caused by decreasing the number of shots is smaller when using pre-trained embeddings than with a directly trained model. This is expected since most parameters of the pre-trained systems belong to the embedding models, which are trained using external data, and thus, in total, only a few parameters need to be trained with the shots belonging to the application-dependent OSC dataset.

Once more, these results show that using pre-trained embeddings for detecting anomalies is not an optimal choice. Although the gap in performance is smaller for this few-shot OSC task than for the pure ASD (cf. Section 5.5) task and the dataset used here does not consist of noisy audio recordings, directly training a

Table 29: Weighted accuracies (in percent) obtained with different systems and input representations for various openness settings and number of shots per class. Mean and standard deviation of five independent trials are shown. © 2023 IEEE

		baselines [162]		proposed system using different input representations				
openness	shots	OpenL3	YAMNet	VGGish	OpenL3	PANN	Kumar	directly trained
low	1	56.8	80.1	90.0 ± 2.2	**98.1 ± 1.0**	95.6 ± 1.4	96.5 ± 1.3	97.4 ± 1.1
low	2	90.3	88.2	95.6 ± 1.6	**99.6 ± 0.3**	97.7 ± 0.8	98.5 ± 0.9	99.1 ± 0.7
low	4	97.2	94.9	98.4 ± 0.7	**99.9 ± 0.1**	98.9 ± 0.5	99.6 ± 0.4	99.7 ± 0.4
middle	1	74.1	78.3	88.7 ± 2.1	**97.0 ± 2.3**	94.9 ± 1.7	96.1 ± 1.6	96.8 ± 1.4
middle	2	86.7	85.6	93.4 ± 1.8	**99.2 ± 0.6**	95.7 ± 1.9	97.8 ± 1.3	98.7 ± 0.8
middle	4	91.3	91.9	96.2 ± 1.6	99.3 ± 0.5	97.8 ± 1.1	98.6 ± 1.3	**99.8 ± 0.2**
high	1	49.9	57.1	84.0 ± 2.6	88.8 ± 5.3	92.1 ± 2.6	**94.8 ± 2.4**	92.6 ± 4.5
high	2	58.3	61.1	87.8 ± 2.6	94.0 ± 3.2	92.9 ± 2.9	97.0 ± 1.7	**97.5 ± 1.7**
high	4	60.5	64.3	87.8 ± 2.5	96.1 ± 1.5	96.0 ± 2.1	98.4 ± 1.3	**99.1 ± 1.1**
arithmetic mean		73.9	77.9	91.3	96.9	95.7	97.5	**97.9**

system leads to better performance. For CSC tasks, the situation is different and pre-trained embeddings such as OpenL3 embeddings may slightly outperform a directly trained system. However, CSC tasks are not the focus of this thesis.

6.3 SOUND EVENT DETECTION APPLICATION: KEYWORD SPOTTING

Keyword spotting (KWS) is the task of detecting all occurrences of a small set of pre-defined words, so-called *keywords*, with precise on- and offsets in audio signals of possibly long duration [136]. Applications are activating voice assistants [150, 199], querying large databases [157] or monitoring audio streams such as radio communication transmissions [147]. All KWS tasks are inherently OSC problems since each keyword defines another class and the keywords are only a small subset of the entire search space, which may contain arbitrary speech, silence or completely different sounds not related to speech. As strongly labeled training data, i.e. samples with annotated on- and offsets of the keywords is difficult and thus costly to obtain, often only a few training samples can be provided making it a few-shot task. The main difference to the previously presented few-shot open-set classification task is the need for detecting on- and offsets during inference, which adds another layer of difficulty.

As it is the case for ASD systems, state-of-the-art KWS systems are based on learning discriminative embeddings [94, 138]. For few-shot KWS, these embeddings are also learned using a prototypical loss [98, 142, 175]. The same is true when using pre-trained embeddings [103] or for similar applications such as bio-acoustic event detection [169] or sound event detection in general [229, 230]. However, all of these networks require to choose a fixed input size resulting in the following dilemma: If the input size is too small, then insufficient information may be contained in the input data to classify correctly and the same instance may be detected multiple times. If the input size is too large, then too much irrelevant or contradicting information may be contained, which degrades the performance. Furthermore, multiple instances may be detected only once and precisely detecting on- and offsets of events is difficult. In practice, finding a balanced size is difficult and still results in severely degraded performance when dealing with keywords of different lengths.

6.3.1 *Related work*

In the following, existing approaches to tackle this problem will be discussed. For bio-acoustic event detection, it has been proposed to use multiple models with different sizes [141]. However, when increasing the number of classes this quickly becomes highly impractical. Another approach for bio-acoustic event detection is to use individual frames for classification [131]. While this may work for discriminating between animal calls belonging to different species, which may in fact be very short and often sound very differently, individual frames of short-time cepstral features do not carry enough information to correctly detect spoken keywords. The reason is that very short audio signals containing speech corresponding to individual frames all are very similar to each other if different keywords largely consist of the same phonemes. For ASR [122], a sequence-to-sequence loss such as the connectionist temporal classification (CTC) loss [66] is used, which can handle sequences of words with different lengths. However, training such a model requires enormous amounts of data with the same acoustic conditions as the expected data for the application. This problems persists when using pre-trained ASR systems [97, 145]. Furthermore, using an ASR system for KWS leads to a large computational overhead and thus is impractical when needing a very fast inference time or detecting keywords locally on sensors with very limited computational resources. For some applications where only the first instance of a keyword is of interest, computational power can be saved by using spiking neural networks and stopping the search process after finding a single keyword [87]. Still, choosing a fixed input size is required. An approach that can handle arbitrary sizes is to apply dynamic time warping (DTW) to keyword templates created by concatenating classical short-time cepstral features such as Mel-frequency cepstral coefficients (MFCCs) or human factor cepstral coefficientss (HFCCs) [116, 222]. For these, the main problem is that the performance quickly degrades in noisy conditions or for short words. In [146], the same approach was used to collect samples of individual keywords that are later used as training data for an embedding model. Although this may help to improve the performance obtained with the final KWS model, it does not solve any of the previously mentioned problems both involved approaches are suffering from. Apart from presenting an embedding-based KWS system, the goal of this section is to present a loss function that solves the problem of needing to choose a fixed input size.

6.3.2 *Dataset*

Conventional KWS datasets such as SpeechCommands [231] do not aim at detecting specific keywords in sentences but focus only on classifying isolated words or phrases. Since this eliminates one of the major difficulties of KWS, namely the need for detecting on- and offsets of keywords, the few-shot open-set dataset KWS-DailyTalk will now be introduced. This dataset is based on the ASR dataset DailyTalk [118] containing high-quality speech recordings without noise from scripted conversations. KWS-DailyTalk is divided into a training split, a validation split and a test split. The training split of KWS-DailyTalk has a length of only 39 s and consists of five isolated samples for each of the following 15 keywords: “afternoon”, “airport”, “cash”, “credit card”, “deposit”, “dollar”, “evening”, “expensive”, “house”, “information”, “money”, “morning”, “night”, “visa” and “yuan”. The validation and test split have a length of approximately 10 min each and consist of 156 and 157 sentences, respectively. Each sentence contains any number of the keywords to be detected including none of them. As a result, each keyword appears roughly 12 times. Their on- and offsets are manually annotated and the training samples stem from other conversations as the sentences contained in the validation and test splits. As an evaluation metric, the micro-averaged F_1-score (cf. Section 2.10) as implemented in [148] is used. All hyperparameters are set to optimize the performance on the validation split.

6.3.3 *System overview*

The embedding based few-shot KWS system depicted in Figure 27 has a similar structure as the previously used ASD systems. First, the waveforms are preprocessed using a frontend. Then embeddings are extracted with a neural network and a backend is applied to compute scores and output the detected keywords. One of the major differences to the previous OSC application is that individual instances of different keywords or even the same keyword may have strongly varying lengths. Moreover, a stream of arbitrary length needs to be handled during inference and may contain several acoustic events that are of interest. To be able to do this, the embeddings are designed to have a temporal dimension. All recordings are divided into small segments of a fixed size before computing embeddings with a temporal resolution. After that, the embeddings of individual segments belonging to the same recording are combined again into a single embedding. Individual keywords are detected by searching their instances provided by the training samples in test recordings using sub-sequence DTW. The details of all components will be presented in the following sections.

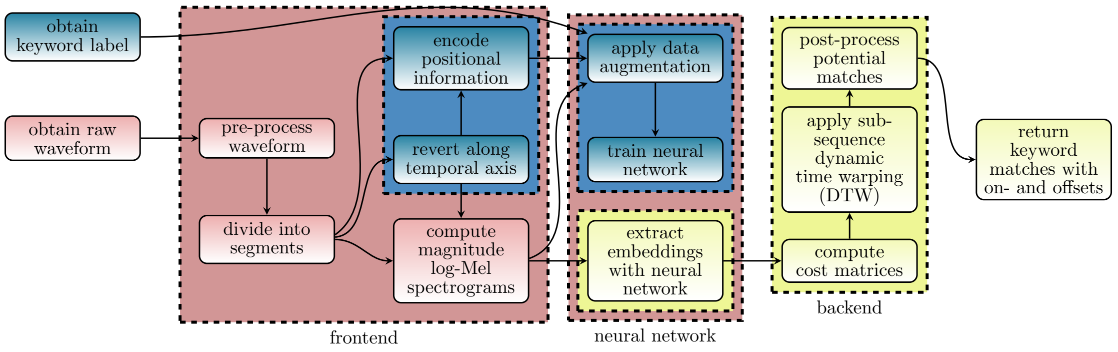
obtain keyword label
obtain raw waveform
pre-process waveform
divide into segments
encode positional information
revert along temporal axis
compute magnitude log-Mel spectrograms
apply data augmentation
train neural network
extract embeddings with neural network
post-process potential matches
apply sub-sequence dynamic time warping (DTW)
compute cost matrices
return keyword matches with on- and offsets
frontend
neural network
backend

Figure 27: Structure of the proposed KWS system. Blocks colored in blue are only used for training the system, blocks colored in yellow are only used for inference and blocks colored in red are used for training and inference. © 2024 IEEE

6.3.4 *Extracting embeddings*

The frontend applied to obtain input features representations for the embedding model is the following. First, the raw waveforms are re-sampled to 16 kHz, high-pass filtered with a cutoff frequency of 50 Hz and the amplitude is normalized by dividing with the maximum value. For training samples, a segment length $L_{\text{seg}} = 0.25\,\text{s}$ and an overlap of $\frac{L_{\text{seg}}}{5}$ are used. Any segments shorter than L_{seg} are padded with zeros. During inference, the same segment length in combination with an overlap of $\frac{256}{16\,000\,\text{Hz}}$ is used to obtain a higher temporal resolution. Furthermore, samples are padded with $\left\lfloor \frac{L_{\text{seg}} \cdot 16000}{2} \right\rfloor$ zeros such that their center aligns with the position in the original recording. After all these pre-processing steps, log-Mel magnitude spectrograms with 64 Mel bins are extracted using a STFT with Hanning-weighted windows of size 1024 and a hop size of 256. This results in a temporal dimension of $T := \left\lceil L_{\text{seg}} \cdot \frac{16000}{256} \right\rceil \in \mathbb{N}$.

The architecture of the embedding model is similar to the one used for ASD (see Table 4) and is provided in Table 30. Apart from the differently sized input representations, the differences are that no temporal max-pooling and padding is applied to retain the original temporal dimension of the input data. Furthermore, dropout with a probability of 20% is used after each residual block. The model is trained for for 1000 epochs with a batch size of 32 using adam [101] to minimize the temporal AdaCos (TACos) loss, which will be presented in Section 6.3.5. During training, random oversampling is applied to balance the number of segments belonging to different keyword classes resulting from the varying lengths of the original keyword recordings. To avoid overfitting, mixup [262] with a uniformly distributed mixing coefficient and SpecAugment [173] are applied for data augmentation purposes. In addition, the background recordings from SpeechCommands [231] are used as additional class “no speech” to reduce the number of false positives detected in segments not containing any speech.

Table 30: Modified ResNet architecture used for extracting embeddings with temporal dimension. © 2024 IEEE

layer name	structure	output size
input	-	16×64
residual block	$\begin{pmatrix} 3 \times 3 \\ 3 \times 3 \end{pmatrix} \times 2$, stride$= 1 \times 1$	$16 \times 64 \times 16$
residual block	$\begin{pmatrix} 3 \times 3 \\ 3 \times 3 \end{pmatrix} \times 2$, stride$= 1 \times 2$	$16 \times 32 \times 32$
residual block	$\begin{pmatrix} 3 \times 3 \\ 3 \times 3 \end{pmatrix} \times 2$, stride$= 1 \times 2$	$16 \times 16 \times 64$
residual block	$\begin{pmatrix} 3 \times 3 \\ 3 \times 3 \end{pmatrix} \times 2$, stride$= 1 \times 2$	$16 \times 8 \times 128$
max pooling	1×8, stride$= 1 \times 1$	16×128
dense (embedding)	linear	16×128

After training, the trained embedding model is used to extract embeddings for the segmented recordings belonging to the entire dataset. Then, embeddings of individual segments are combined by taking the mean of all frames that belong to the same time frame in the original file, resulting in a single embedding with a temporal resolution for the entire file matching the original length in time. This is illustrated in Figure 28.

6.3.5 *TACos*

The idea of the TACos loss is to have two training objectives for each segment. First, the correct keyword should be detected with a supervised loss function $\mathcal{L}_{\text{kw}}$. Second, the correct position of a segment within the keyword should be detected with a self-supervised loss $\mathcal{L}_{\text{pos}}$. Without learning the position of segments, the resulting embeddings are often constant for regions where the same keyword is contained because embeddings of segments only need to carry information about the keyword. In these cases, applying DTW is similar to directly classifying individual frames with a classifier and therefore using the embeddings as templates does not significantly improve the performance. Using $\mathcal{L}_{\text{pos}}$ as one of the training objectives, forces the embedding model to include positional information into the embeddings and thus varying the combined embeddings for entire recordings over time.

Processing keyword instances with strongly varying lengths with the same discriminative loss function requires a relative instead of an absolute encoding of the positions, which is defined as follows:

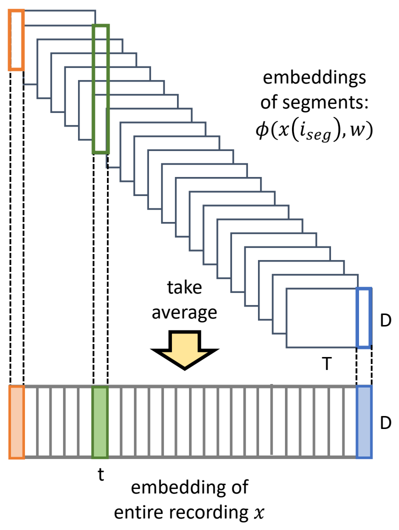
embeddings of segments: $\phi(x(i_{seg}), w)$
take average
D
T
D
t
embedding of entire recording x

Figure 28: Illustration of combining the embeddings belonging to different segments of a single recording.

Definition 6.3 (Categorical encoding of relative position)**.** Let $N_{seg}(x) \in \mathbb{N}$ denote the number of segments belonging to training sample $x \in X_{train}$ and define $N_{pos} := \max_{x \in X_{train}}\{N_{seg}(x)\}$. For $x \in X_{train}$ and segment $i_{seg} \in \{1, ..., N_{seg}(x)\}$, set the interval of active positions to

$$I_{active}(x, i_{seg}) = \left[1 + \left\lceil \frac{(i_{seg} - 1) \cdot N_{pos}}{N_{seg}(x)} \right\rceil, \left\lceil \frac{i_{seg} \cdot N_{pos}}{N_{seg}(x)} \right\rceil\right] \subset \mathbb{R}. \tag{67}$$

Then, the *categorical encoding of the relative position* $lab_{pos}(x, i_{seg}) \in [0, 1]^{N_{pos}}$ of segment $i_{seg} \in \{1, ..., N_{seg}(x)\}$ belonging to training sample $x \in X_{train}$ is defined by setting

$$lab_{pos}(x, i_{seg})_{i_{pos}} = \frac{\mathbb{1}_{I_{active}(x, i_{seg})}(i_{pos})}{\sum_{j_{pos}=1}^{N_{pos}} \mathbb{1}_{I_{active}(x, i_{seg})}(j_{pos})} \tag{68}$$

where $i_{pos} \in \{1, .., N_{pos}\}$ and $\mathbb{1}_I : \mathbb{R} \to \{0, 1\}$ denotes the characteristic function for the interval $I \subset \mathbb{R}$.

These positional encodings are used as labels for a self-supervised classification task. Note that for all instances of keywords shorter than the longest one present in the training set, multiple positions of the encoding are set to "active" with equal target probability. The position of segments not containing any speech is encoded with a uniform target distribution meaning that each position of this segment is equally (un)likely.

Now, the actual TACos loss function used for training the embedding model will be defined. A graphical illustration of the loss function can be found in Figure 29.

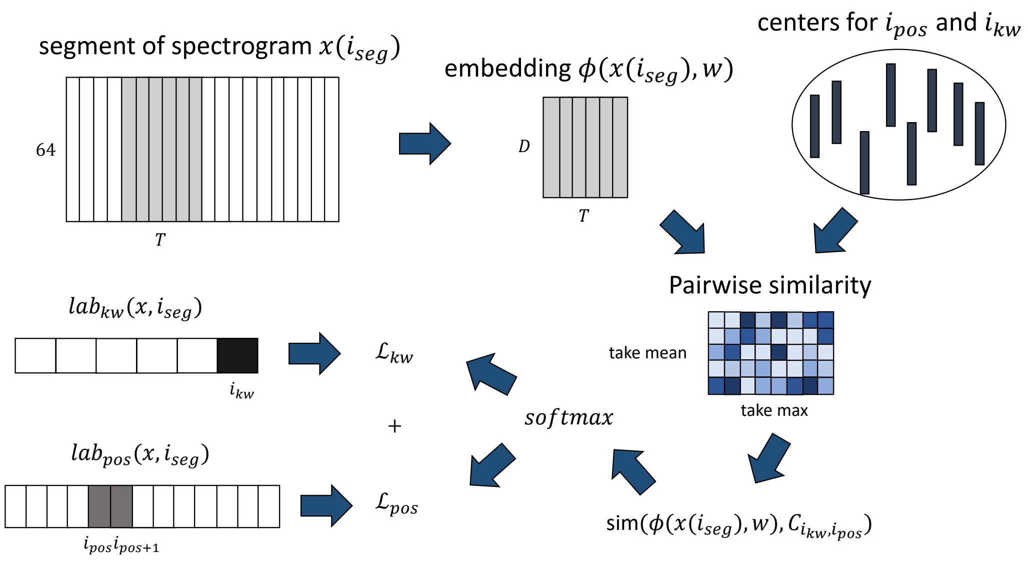

Figure 29: Illustration of the TACos loss function. © 2024 IEEE

Definition 6.4 (TACos). Using the notation introduced in Definition 6.3, let $Y \subset X$ be finite and let $x(j) \in \mathbb{R}^{T \times D}$ denote the j-th segment generated from sample $x \in X$. Furthermore, let $N_{kw} \in \mathbb{N}$ denote the number of keyword classes and let $C_{i_{kw}, i_{pos}} \in \mathcal{P}(\mathbb{R}^D)$ with $|C_{i_{kw}, i_{pos}}| = N_{centers}$ denote the trainable centers for keyword $i_{kw} \in \{1, ..., N_{kw}\}$ and position $i_{pos} \in \{1, ..., N_{pos}\}$. Define the similarity between embedding $\phi(x(i_{seg}), w) = (\phi(x(i_{seg}), w)_1, ..., \phi(x(i_{seg}), w)_T) \in \mathbb{R}^{T \times D}$ and the centers $C_{i_{kw}, i_{pos}}$ as

$$\begin{aligned} &\text{sim}(\phi(x(i_{seg}), w), C_{i_{kw}, i_{pos}}) \\ &:= \text{mean}(\{\max_{c \in C_{i_{kw}, i_{pos}}} \text{sim}(\phi(x(i_{seg}), w)_t, c) \in \mathbb{R}^D : t = 1, ..., T\}). \end{aligned} \tag{69}$$

The corresponding softmax probability of embedding $\phi(x(i_{seg}), w)$ belonging to keyword i_{kw} and position i_{pos} is defined as

$$\begin{aligned} &\text{softmax}(\hat{s} \cdot \text{sim}(\phi(x(i_{seg}), w), C_{i_{kw}, i_{pos}})) \\ &:= \frac{\exp(\hat{s} \cdot \text{sim}(\phi(x, w), C_{i_{kw}, i_{pos}}))}{\sum_{j_{kw}=1}^{N_{kw}} \sum_{j_{pos}=1}^{N_{pos}} \exp(\hat{s} \cdot \text{sim}(\phi(x(i_{seg}), w), C_{j_{kw}, j_{pos}}))} \end{aligned} \tag{70}$$

where $\hat{s} \in \mathbb{R}_+$ is the dynamically adaptive scale parameter as defined for the sub-cluster AdaCos loss in 3.4. The probability of embedding $\phi(x(i_{seg}), w)$ belonging to keyword i_{kw} is set to $\sum_{j_{pos}=1}^{N_{pos}} \text{softmax}(\hat{s} \cdot \text{sim}(\phi(x(i_{seg}), w), C_{i_{kw}, j_{pos}}))$ and the probability of embedding $\phi(x(i_{seg}), w)$ belonging to position i_{pos} is set to

$\sum_{j_{\text{kw}}=1}^{N_{\text{kw}}} \text{softmax}(\hat{s} \cdot \text{sim}(\phi(x(i_{\text{seg}}), w), C_{j_{\text{kw}}, i_{\text{pos}}}))$. Therefore, the loss functions for a single embedding $\phi(x(i_{\text{seg}}), w)$ are equal to

$$\begin{aligned}
&\mathcal{L}_{\text{kw}} : X \times \{1, ..., N_{\text{kw}}\} \times \mathcal{P}(\mathcal{P}(\mathbb{R}^D)) \times \Phi \times W \times \Lambda(N_{\text{kw}}) \to \mathbb{R}_+ \\
&\mathcal{L}_{\text{kw}}(x, i_{\text{seg}}, \mathcal{C}, \phi, w, \text{lab}_{\text{kw}}) \\
&:= \sum_{i_{\text{kw}}=1}^{N_{\text{kw}}} \text{lab}_{\text{kw}}(x, i_{\text{seg}})_{i_{\text{kw}}} \log \Big(\sum_{i_{\text{pos}}=1}^{N_{\text{pos}}} \text{softmax}(\hat{s} \cdot \text{sim}(\phi(x(i_{\text{seg}}), w), C_{i_{\text{kw}}, i_{\text{pos}}})) \Big)
\end{aligned} \tag{71}$$

and

$$\begin{aligned}
&\mathcal{L}_{\text{pos}} : X \times \{1, ..., N_{\text{pos}}\} \times \mathcal{P}(\mathcal{P}(\mathbb{R}^D)) \times \Phi \times W \times \Lambda(N_{\text{pos}}) \to \mathbb{R}_+ \\
&\mathcal{L}_{\text{pos}}(x, i_{\text{seg}}, \mathcal{C}, \phi, w, \text{lab}_{\text{pos}}) \\
&:= \sum_{i_{\text{pos}}=1}^{N_{\text{pos}}} \text{lab}_{\text{pos}}(x, i_{\text{seg}})_{i_{\text{pos}}} \log \Big(\sum_{i_{\text{kw}}=1}^{N_{\text{kw}}} \text{softmax}(\hat{s} \cdot \text{sim}(\phi(x(i_{\text{seg}}), w), C_{i_{\text{kw}}, i_{\text{pos}}})) \Big)
\end{aligned} \tag{72}$$

where $\mathcal{C} \in \mathcal{P}(\mathcal{P}(\mathbb{R}^D))$ with $|\mathcal{C}| = N_{\text{kw}} \cdot N_{\text{pos}}$. The TACos loss includes both loss functions and is defined as

$$\begin{aligned}
&\mathcal{L}_{\text{tac}} : \mathcal{P}(X) \times \mathcal{P}(\mathcal{P}(\mathbb{R}^D)) \times \Phi \times W \times \Lambda(N_{\text{kw}}) \times \Lambda(N_{\text{pos}}) \to \mathbb{R}_+ \\
&\mathcal{L}_{\text{tac}}(Y, \mathcal{C}, \phi, w, \text{lab}_{\text{kw}}, \text{lab}_{\text{pos}}) \\
&:= -\frac{1}{|Y|} \sum_{x \in Y} \frac{1}{N_{\text{seg}}(x)} \sum_{i_{\text{seg}}=1}^{N_{\text{seg}}(k)} \mathcal{L}_{\text{kw}}(x, i_{\text{seg}}, \mathcal{C}, \phi, w, \text{lab}_{\text{kw}}) + \mathcal{L}_{\text{pos}}(x, i_{\text{seg}}, \mathcal{C}, \phi, w, \text{lab}_{\text{pos}}).
\end{aligned} \tag{73}$$

For all experiments in this section, the hyperparameters $D = 128$ and $N_{\text{centers}} = 16$ were used.

To further improve the performance obtained with the KWS system, a second SSL task is used when training the embedding model. More concretely, the model is taught to recognize temporally reversed segments by creating a temporally reversed copy of each segment and creating labels in the following ways: For each keyword class, an additional class for all temporally reversed segments belonging to this keyword class is introduced, almost doubling the total number of classes. The position of temporally reversed segments is encoded with a uniform target distribution as done for the segments not containing any speech. Introducing temporally reversed segments as difficult out-of-distribution samples that still contain speech, makes the training objective much more challenging. This results in more information about the temporal structure of the speech contained in the embeddings and is expected to improve the performance by reducing the number of false alarms.

6.3.6 *DTW backend*

To actually detect appearances of keywords with their on- and offsets, sub-sequence DTW is applied in the following way: First, cost matrices are computed using the pairwise cosine distances between the embeddings belonging to test sentences and the embeddings of training samples. Using Fréchet means instead of using the individual samples, obtained by applying the dynamic time warping barycenter averaging (DBA) [180], degrades the runtime but also degrades the performance. Since DTW can be parallelized by sweeping diagonally over cost matrices, the computational overhead is still manageable and the processing times are much faster than real-time if the number of keywords and shots is not too high. Therefore, the individual samples were used for the experimental evaluations. To accumulate the costs of all cost matrices, the DTW step sizes $(1, 1)$, $(1, 2)$ and $(2, 1)$ were used. After this, a warping path is computed for each temporal position and its associated cost is normalized by the length of the corresponding path. Then, the normalized accumulated costs is used as a matching score and a decision threshold, tuned on the validation set, can be applied to find the matches. The on- and offsets of a detected keyword are given by the start and end of the warping paths, whose matching scores are below the decision threshold. For post-processing, overlapping detections are shortened such that they do not overlap and detections shorter than half the duration of the training sample are removed.

6.3.7 *Baseline systems*

To justify the design of the proposed KWS system, the following two baseline systems were used for comparison: A classical HFCC-based approach and a system using vector-sized embeddings by applying a sliding window. The HFCCs are extracted using spectrograms with a window size of 40 ms and a step size of 10 ms. In contrast to the well-known MFCCs, HFCCs use a triangular filterbank with perceptually motivated bandwidths based on the Bark-scale instead of the center frequencies resulting in filters with less overlap. This was shown to improve the performance for DTW-based KWS [222]. For the baseline system, the same sub-sequence DTW algorithm as used for the trained embeddings is applied.

For the sliding window based system, a slightly modified embedding model architecture as used for the embeddings with the temporal dimension is applied to obtain vector-sized embeddings. One modification is to also apply the max-pooling operation in the residual blocks to the temporal dimension. Another modification is to apply a flattening operation before linearly projecting the hidden representation of the network onto the embedding space. The AdaCos loss is utilized for training the embedding model. To detect keywords with on- and offsets, the following procedure is used: First, the cosine similarities between all temporally sorted embeddings of a target sentence and the keyword-specific centers of the embedding network are computed. Then, these values are compared to a decision threshold

Table 31: Event-based, micro-averaged F-score, precision and recall obtained on KWS-DailyTalk with different KWS systems. Highest F_1-scores for each feature representation are highlighted with bold letters, overall highest F_1-scores are underlined. © 2024 IEEE

feature representation	reversed segments	threshold	obtained performance					
			validation split			test split		
			F_1-score	precision	recall	F_1-score	precision	recall
HFCCs	not applicable	global	60.52%	63.25%	58.01%	56.97%	61.54%	53.04%
HFCCs	not applicable	individual	**64.71%**	69.18%	60.77%	**57.74%**	62.58%	53.59%
embeddings (sliding)	not used	global	39.76%	43.71%	36.46%	38.35%	41.14%	35.91%
embeddings (sliding)	not used	individual	46.96%	49.39%	44.75%	40.44%	40.00%	40.88%
embeddings (sliding)	used	global	44.13%	62.00%	34.25%	44.83%	59.63%	35.91%
embeddings (sliding)	used	individual	**55.43%**	54.55%	56.35%	**50.42%**	51.14%	49.72%
embeddings ($\mathcal{L}_{\text{kw}}$)	not used	global	56.04%	52.40%	60.22%	54.25%	53.80%	54.70%
embeddings ($\mathcal{L}_{\text{kw}}$)	not used	individual	58.38%	57.14%	59.67%	53.04%	53.04%	53.04%
embeddings ($\mathcal{L}_{\text{kw}}$)	used	global	64.58%	74.64%	56.91%	**61.30%**	69.72%	54.70%
embeddings ($\mathcal{L}_{\text{kw}}$)	used	individual	**66.12%**	64.89%	67.40%	60.53%	57.79%	63.54%
embeddings ($\mathcal{L}_{\text{tac}}$)	not used	global	62.78%	75.78%	53.59%	64.65%	82.76%	53.04%
embeddings ($\mathcal{L}_{\text{tac}}$)	not used	individual	63.36%	63.19%	63.54%	63.31%	68.15%	59.12%
embeddings ($\mathcal{L}_{\text{tac}}$)	used	global	65.78%	82.50%	54.70%	<u>**70.47%**</u>	89.74%	58.01%
embeddings ($\mathcal{L}_{\text{tac}}$)	used	individual	<u>**69.44%**</u>	75.00%	64.64%	69.16%	79.29%	61.33%

resulting in another binary time-series for each keyword containing possible detections. These time-series are post-processed by applying median filters with lengths equal to the nearest odd number of the mean number of frames to all shots of the corresponding keyword. As a result, boxes indicating detections of keywords are obtained, whose start- and endpoints are shifted by $-\frac{L_{\text{seg}}}{2}$ and $+\frac{L_{\text{seg}}}{2}$, respectively.

6.3.8 *Experimental comparison*

A comparison of the performance on KWS-DailyTalk obtained with different KWS systems can be found in Table 31. The following observations can be made: First and foremost, the embeddings obtained with the TACos loss perform best, which is especially apparent on the test split of the dataset. Second, the embeddings based on a sliding window perform worse while the embeddings with a temporal dimension perform better than classical HFCCs. This shows that using a sliding window is highly sub-optimal and justifies utilizing a temporal dimension. Third, using temporally reversed embeddings for training improves the performance for all embeddings. Since this simple SSL approach is applied in addition to other powerful data augmentation techniques such as mixup and SpecAugment, this shows that doing so is highly beneficial. Last but not least, individually tuned decision thresholds do not improve the performance of the embeddings with a temporal dimension on the test split. Therefore, an extensive tuning of decision thresholds is not necessary and can be omitted.

6.4 SUMMARY

In this chapter, OSC and SED were investigated as additional ASD applications in few-shot settings, meaning that only very few training samples were provided. For OSC, a dataset for acoustic alarm detection in domestic environments and, for SED, a KWS application were considered. Similar to the results presented in Section 5.5, it was shown that directly training a model for the few-shot OSC task leads to better results than using pre-trained embeddings. For a sufficiently high number of shots used for training, the results obtained with the presented system were close to optimal performance. However, the gap in performance decreased the less training samples were available and for an openness equal to zero, i.e. a CSC task, the pre-trained embeddings performed slightly better.

For the KWS task, a novel loss function, named TACos, and a few-shot KWS dataset were presented. The TACos loss aims at learning embeddings with a temporal structure and consists of a supervised task for predicting the keyword and a self-supervised task for predicting the position of a short audio segment. Additionally, a few-shot KWS system utilizing these embeddings as features for DTW was presented. Utilizing these embeddings has the advantage that the system is able to detect keywords of strongly varying lengths when monitoring audio streams because a fixed window size for processing the data is not necessary. In experimental evaluations, it was shown that also predicting the position when training the embedding model significantly improves the performance because the model is forced to learn embeddings that change over time, which makes them much better suited as features for DTW. As a result, it was shown that the performance of the proposed KWS system is better than the performance obtained with models based on hand-crafted speech features or when using an embedding model based on a sliding window. Furthermore, an SSL approach using temporally reversed segments as negative examples during training was proposed and it was shown that this approach improves the performance regardless of the model.

7 CONCLUSION

7.1 SUMMARY

Reliably detecting anomalous sounds is important for various applications ranging from monitoring machines for predictive maintenance, entire acoustic scenes for security or the health of persons to acoustic open-set classification where anomalies correspond to unknown classes. However, training an automatic ASD system is difficult because for most applications anomalous samples are not available for training. Additional challenges in a semi-supervised setting are the high dimensionality of audio data and unwanted variations resulting from changing properties of the sensors or the sound sources themselves. Furthermore, there is no inherent property that is different for normal and anomalous sounds as defining these terms entirely depends on the application. To solve all these issues, the goal of this thesis was to investigate how to obtain a mapping from the audio signal space to a relatively low-dimensional vector space, called embedding space, where normal and anomalous sounds can be distinguished easily. For the experimental evaluations, acoustic machine condition monitoring served as the main application throughout the thesis.

First, the structure of a state-of-the-art ASD system based on audio embeddings was presented by reviewing the existing literature. Such a system consists of a frontend, an embedding model and a backend. In the frontend, the audio signals are pre-processed and their dimension is reduced by converting them into time-frequency representations. Depending on the training objective, there are three different types of embedding models, each with different strengths and weaknesses. The model can be trained by using one-class losses such as the reconstruction or the compactness loss, by solving auxiliary classification tasks with angular margin losses based on provided meta information or SSL, or by using models pre-trained on large datasets. To improve the performance, data augmentation techniques and ensembling can be applied. The goal of the backend is to compute an anomaly score by measuring the distance to normal embeddings or estimating their distribution and computing the likelihood of test embeddings. In addition to discussing the structure of an ASD system, threshold-dependent and threshold-independent evaluation metrics that measure the performance of a system as well as methods for estimating a decision threshold were discussed.

In the third chapter, one-class embeddings were compared to auxiliary task embeddings. To this end, it was shown that learning a joint embedding space by utilizing a classification task, which incorporates as much meta information as possible, yields much better results than one-class models. The reason is that solving a classification task enables the embedding model to closely monitor target sounds and ignore the background noise resulting in a stronger sensitivity to anomalous deviations from normal sounds, which may be very subtle. As a theoretical result, it was proven that the AdaCos loss minimizes intra-class compactness losses while also maximizing inter-class compactness losses. This shows that both loss functions are strongly related and explains why angular margin losses lead to a good performance. Furthermore, the sub-cluster AdaCos loss was presented. It generalizes the AdaCos loss by using multiple centers for each class to learn less restrictive distributions leaving more space for anomalous samples between the normal samples. The theoretical results obtained for the AdaCos loss were also extended to the sub-cluster AdaCos loss. An ensemble using this loss function as well as mixup for training and a GMM as a backend reached a new state-of-the-art performance on the DCASE2020 dataset with an AUC-ROC of 97%, which is close to optimal.

When using an ASD system in a specific application, decision thresholds need to be specified to decide between normal and anomalous samples. Different methods for estimating a decision threshold from normal data only were compared experimentally. It was shown that most methods lead to similar results that lie between 90% and 95% of the performance obtained with an optimal decision threshold and that multi-stage approaches perform slightly better. Furthermore, holding back samples to obtain more realistic anomaly scores for estimating a threshold did not improve performance and thus is not needed. To also include the difficulty of estimating a good decision threshold, which is not captured by the AUC-ROC score, the threshold-independent evaluation metric F_1-EV was presented. In experimental evaluations, it was shown that this metric has a high correlation with the AUC-ROC score as well as with the F_1 score and thus has the potential to replace the AUC-ROC score as the standard metric for semi-supervised ASD.

The fifth chapter dealt with domain generalization for ASD, i.e. designing the system in such a way that it is robust to potential changes of the distribution of normal data. The designed system consists of two sub-networks using DFT and STFT based features as input, concatenating the resulting embeddings and calculating the cosine distance as an anomaly score. Trivial solutions for individual classes were prevented by not using any bias terms and non-trainable class centers. By visualizing the embedding space using t-SNE and utilizing RISE to explain the decisions of the proposed system, it was shown that learning a joint embedding space with multiple classes helps to capture more relevant information with the embeddings than using multiple embedding models. In comparison to systems based on pre-trained embeddings, the performance obtained with the system was significantly better despite having only very few samples for the target domains. To further improve the performance of the system, the AdaProj loss was proposed. This loss generalizes the sub-cluster AdaCos loss by learning arbitrary distributions in linear sub-spaces for each class. Additionally, it was shown that applying SSL approaches in the form of StatEx and a novel FeatEx approach, which randomly exchanges the embeddings of the two sub-networks, significantly improves the performance. An ensemble based on multiple presented systems outperformed all other published systems on the DCASE2023 dataset by a large margin and thus reached a new state-of-the-art performance.

To cover a broader range of ASD applications than acoustic machine condition monitoring, few-shot OSC and few-shot KWS applications were investigated. It was shown that the previously developed ASD system also performs well for few-shot OSC and that this system outperforms systems using pre-trained embeddings even in case only very few training samples are available for every normal class. For few-shot KWS, TACos, a novel loss function was presented. Here, embeddings with a temporal resolution are learned that can be used as templates for DTW to effectively deal with varying lengths of keywords. Besides the supervised task of predicting the correct keyword a short segment of a spectrogram belongs to, TACos utilizes two SSL approaches: Namely, also predicting the position of each segment inside a keyword sample and detecting temporally reversed segments as challenging negative samples. In experiments on a novel few-shot KWS dataset, it was shown that both SSL approaches significantly improve the performance and that a system utilizing the TACos loss outperforms systems that classify individual segments using a sliding window or use hand-crafted speech features such as HFCCs.

7.2 OUTLOOK AND FUTURE WORK

As stated in the previous section, many improvements for designing a semi-supervised ASD system based on audio embeddings were achieved. Still, the problem is far from being solved, especially in challenging conditions, and thus is expected to be an interesting research question for many years to come. In the following, possible directions for future research will be discussed.

One possible direction is to further improve the performance of ASD systems for acoustic machine condition monitoring by finding more efficient methods to handle the noise and non-target sound events other than using meta information, which may not always be available. Apart from using additional SSL approaches, applying source separation to isolate the machine sounds is a very promising approach [22, 100, 178, 203]. Although it is very difficult to achieve, one could aim for separating signals into three source: One source containing the noise and non-target sound components, another source containing the normal signal components and a third source containing the anomalous signal components. Reaching this goal would not only lead to much better performance but also greatly improve the explainability of the results, which is an important goal on its own. An additional way to improve the performance may be to investigate more sophisticated methods than randomly initializing the centers of the presented angular margin loss functions. Furthermore, the methods presented in this thesis can be applied to strongly related fields such as time series analysis [120] or structural health monitoring [13, 14] to exchange ideas developed in different research communities. Extensive knowledge of subject matter experts working in different fields may also help to introduce additional evaluation metrics such as the presented F_1-EV score that capture all practical demands placed upon an ASD systems.

Another topic for future research is to extend the presented systems for few-shot SED to zero-shot learning [117]. This means that one is interested in detecting sound events belonging to classes for which no audio samples can be provided, which enables users to search for arbitrary sound events. State-of-the-art zero-shot learning systems are taught to project pre-trained embeddings of an audio embedding space and a second embedding space utilizing another data type into a joint embedding space. This allows to compare the embedding of an arbitrary audio recording to pre-trained embeddings obtained with textual input [49, 253] or images [41]. In [130], so-called sound attribute vectors describing the sounds were introduced that enable users to define new sound classes by creating corresponding sound attribute vectors. To obtain general-purpose audio embeddings, the pre-trained models presented in Section 2.5 as well as more specialized embeddings such as wav2vec embeddings [8] or other embeddings pre-trained on a large ASR dataset [18, 103] can be used.

As a third research direction, the semi-supervised ASD setting investigated in this thesis can be extended to detecting anomalous sound events in a continuous audio stream, which can be seen as a combination of ASD and SED. The difference to ASD is that anomalous sounds need to be localized in time and not only be provided as results for isolated sounds. The difference to SED is that one does not have any training data for the anomalous sound events that are of actual interest. In conclusion, solving this task appears to be difficult. Still, in any monitoring application one usually encounters continuous audio streams and the interesting events needing immediate attention are the ones that are anomalous. Furthermore, developing such a system could also be used for active learning of unknown sound events [204, 229, 265].

A APPENDIX

A.1 KEY PUBLICATIONS

In this section, the key publications that contain substantial parts of this thesis are attached for inspection of the doctoral committee. For each publication, individual contributions of co-authors are stated explicitly. The remaining content of each publication is the sole contribution of the thesis author. Publications protected by the copyright of IEEE are subject to the following: *In reference to IEEE copyrighted material which is used with permission in this thesis, the IEEE does not endorse any of University of Bonn's products or services. Internal or personal use of this material is permitted. If interested in reprinting/republishing IEEE copyrighted material for advertising or promotional purposes or for creating new collective works for resale or redistribution, please go to http://www.ieee.org/publications_standards/publications/rights/rights_link.html to learn how to obtain a License from RightsLink. If applicable, University Microfilms and/or ProQuest Library, or the Archives of Canada may supply single copies of the dissertation.*

A.1.1 *Key publication 1*

Kevin Wilkinghoff. "Sub-Cluster AdaCos: Learning Representations for Anomalous Sound Detection." In: *International Joint Conference on Neural Networks (IJCNN)*. IEEE, 2021.
`https://ieeexplore.ieee.org/document/9534290`
© 2021 IEEE.

A.1.2 *Key publication 2*

Kevin Wilkinghoff, Alessia Cornaggia-Urrigshardt, and Fahrettin Gökgöz. "Two-Dimensional Embeddings for Low-Resource Keyword Spotting Based on Dynamic Time Warping." In: *14th ITG Conference on Speech Communication (ITG Speech)*. VDE-Verlag, 2021, pp. 9–13.
`https://ieeexplore.ieee.org/document/9657497`
© 2021 VDE, published with IEEE.
The co-authors of this publication contributed in the following ways: *Alessia Cornaggia-Urrigshardt* applied voice activity detection (VAD) as pre-processing and DTW to the resulting embeddings. She also wrote Sections 2.3, 2.4, 2.5 and

3.3, and created Figures 1 and 2. *Fahrettin Gökgöz* collected and prepared the dataset used for the experiments.

A.1.3 *Key publication 3*

Kevin Wilkinghoff and Alessia Cornaggia-Urrigshardt. "On choosing decision thresholds for anomalous sound detection in machine condition monitoring." In: *24th International Congress on Acoustics (ICA)*. The Acoustical Society of Korea, 2022.
https://wilkinghoff.com/publications/ica22_choosing.pdf
© 2022 The Acoustical Society of Korea.
The co-author of this publication contributed in the following ways: *Alessia Cornaggia-Urrigshardt* assisted with reviewing literature and implemented some of the evaluation methods. She also wrote parts of Section 3.

A.1.4 *Key publication 4*

Kevin Wilkinghoff. "Design Choices for Learning Embeddings from Auxiliary Tasks for Domain Generalization in Anomalous Sound Detection." In: *International Conference on Acoustics, Speech and Signal Processing (ICASSP)*. IEEE, 2023.
https://ieeexplore.ieee.org/document/10097176
© 2023 IEEE.

A.1.5 *Key publication 5*

Kevin Wilkinghoff and Fabian Fritz. "On Using Pre-Trained Embeddings for Detecting Anomalous Sounds with Limited Training Data." In: *31st European Signal Processing Conference (EUSIPCO)*. IEEE, 2023, pp. 186–190.
https://ieeexplore.ieee.org/document/10290003
© 2023 IEEE (CC-BY license).
The co-author of this publication contributed in the following ways: *Fabian Fritz* implemented wrapper functions for using the pre-trained embbedings.

A.1.6 *Key publication 6*

Kevin Wilkinghoff. "AdaProj: Adaptively Scaled Angular Margin Subspace Projections for Anomalous Sound Detection with Auxiliary Classification Tasks." Submitted to 9th Workshop on Detection and Classification of Acoustic Scenes and Events (DCASE), arXiv:2403.14179. 2024.
https://arxiv.org/abs/2403.14179
© 2024 Kevin Wilkinghoff.

A.1.7 *Key publication 7*

Kevin Wilkinghoff. “Self-Supervised Learning for Anomalous Sound Detection.” In: *International Conference on Acoustics, Speech and Signal Processing (ICASSP)*. IEEE, 2024, pp. 276–280.
https://arxiv.org/abs/2312.09578
© 2024 IEEE.

A.1.8 *Key publication 8*

Kevin Wilkinghoff and Alessia Cornaggia-Urrigshardt. “TACos: Learning Temporally Structured Embeddings for Few-Shot Keyword Spotting with Dynamic Time Warping.” In: *International Conference on Acoustics, Speech and Signal Processing (ICASSP)*. IEEE, 2024, pp. 9941–9945.
https://arxiv.org/abs/2305.10816
© 2024 IEEE.
The co-author of this publication contributed in the following ways: *Alessia Cornaggia-Urrigshardt* assisted with creating the dataset. She also applied DTW, tested the HFCC-based approach and evaluated global and individual decision thresholds.

A.1.9 *Key publication 9*

Kevin Wilkinghoff and Keisuke Imoto. “F1-EV Score: Measuring the Likelihood of Estimating a Good Decision Threshold for Semi-Supervised Anomaly Detection.” In: *International Conference on Acoustics, Speech and Signal Processing (ICASSP)*. IEEE, 2024, pp. 256–260.
https://arxiv.org/abs/2312.09143
© 2024 IEEE.
The co-author of this publication contributed in the following ways: *Keisuke Imoto* provided the dataset used for the experiments. He also proposed to include Section 3.3 and Figure 5.

A.1.10 *Key publication 10*

Kevin Wilkinghoff and Frank Kurth. “Why do Angular Margin Losses work well for Semi-Supervised Anomalous Sound Detection?” In: *IEEE/ACM Trans. Audio Speech Lang. Process.* 32 (2024), pp. 608–622.
https://ieeexplore.ieee.org/document/10329432
© 2024 IEEE (CC-BY license).
The co-author of this publication contributed in the following ways: *Frank Kurth* contributed through scientific supervision and improving the quality of the paper in general. He also proposed to include Table III and Figure 1.

LIST OF FIGURES

LIST OF TABLES

LIST OF ACRONYMS

AD	anomaly detection
ASD	anomalous sound detection
AUC-ROC	area under the receiver operating characteristic curve
ASR	automatic speech recognition
CD	cosine distance
CNN	convolutional neural network
CSC	closed-set classification
CTC	connectionist temporal classification
CXE	categorical crossentropy
DBA	dynamic time warping barycenter averaging
DET	detection error tradeoff
DFT	discrete Fourier transform
DTW	dynamic time warping
EER	equal error rate
EV	expected value
FeatEx	feature exchange
FN	false negatives
FNR	false negative rate
FP	false positives
FPR	false positive rate
GAN	generative adversarial network
GDP	gamma distribution percentile
GESD	generalized extreme studentized deviate

GMM	Gaussian mixture model
HFCC	human factor cepstral coefficients
HP	histogram percentile
IQR	interquartile range
k-NN	k-nearest neighbors
KWS	keyword spotting
L3	look, listen, and learn
LDA	linear discriminant analysis
LIME	local interpretable model-agnostic explanations
LOF	local outlier factor
MADE	masked autoencoder for distribution estimation
MAD	mean absolute deviation
MFCC	Mel-frequency cepstral coefficient
MSE	mean squared error
MST	multi-stage thresholding
OCSVM	one-class support vector machine
OE	outlier exposure
OSC	open-set classification
PANN	pre-trained audio neural network
pAUC	partial area under the receiver operating characteristic curve
PCA	principal component analysis
PCC	Pearson correlation coefficient
PLDA	probabilistic linear discriminant analysis
PSD	polyphonic sound detection
ReLU	rectified linear unit
RISE	randomized input sampling for explanation

ROC	receiver operating characteristic
SD	standard deviation
SED	sound event detection
SMOTE	synthetic minority over-sampling technique
SSL	self-supervised learning
StatEx	statistics exchange
STFT	short-time Fourier transform
SVDD	support vector data description
TACos	temporal AdaCos
TMN	temporal mean normalization
TN	true negatives
TNR	true negative rate
TP	true positives
TPR	true positive rate
t-SNE	t-distributed stochastic neighbor embedding
UMAP	uniform manifold approximation and projection
VAD	voice activity detection
VAE	variational autoencoder
xAI	explainable artificial intelligence

LIST OF SYMBOLS

$\mathbb{1}_I$	characteristic function for the interval I 123
$\cdot$	linear operator 17
α	angle between two embeddings on the hypersphere 20
$\hat{\alpha}^{(t)}_{\text{med}}$	median of all mixed-up angles and all class centers at training step t 54
$\alpha^{(t)}_{\text{med}}$	median of all angles belonging to the training samples and their corresponding class centers at training step t 23
β_{acc}	accuracy metric weight 36
$\beta_{F_1\text{-EV}}$	hyperparameter for F_1-EV 75
λ	mixing coefficient of mixup 27
Λ	space of all categorical class label functions 20
ϕ	neural network for obtaining embeddings 16
Φ	space of permissible neural network architectures for obtaining embeddings 8
Φ_{simple}	space of permissible neural network architectures only consisting of fully-connected or convolutional layers 16
φ	autoencoder 14
φ_d	decoder 14
φ_e	encoder 14
σ_l	activation function for layer l 17
θ	decision threshold 1
A_{pred}	predicted anomalies 33
$B^{(t)}_{\text{avg}}$	sample-wise average over all summed logits of the AdaCos loss belonging to the non-corresponding classes at training step t 23
Beta	beta distribution 27
$\hat{B}^{(t)}_{\text{avg}}$	sample-wise average over all summed logits of the sub-cluster AdaCos loss at training step t 54
b_l	bias term of layer l 17

c	center of a hypersphere, class center, prototype 16, 20, 115
C_j	all hypersphere centers belonging to class j 53
class	class index function 8
$C_{\text{pred}}^{(i)}$	all data samples classified as class i 36
d	metric 115
D	embedding dimension 5
d_{proj}	metric measuring distance between embedding and its projection onto a linear span 102
E_i	subset of the embedding space containing only normal samples 5
emb	ideal embedding function 5
F	frequency dimension 106
Grubbs	Grubbs statistic 41
H_l	hidden representation space for layer l 16
$h_l(x)$	hidden representation at layer l for input sample x 17
I_{active}	interval of active positions 123
Im	image of a function 17
i_{pos}	index of an encoded relative position 123
i_{seg}	index of a segment 123
K	number of shots for few-shot learning 115
$\mathcal{L}_{\text{ada}}$	AdaCos loss 24
$\mathcal{L}_{\text{ang}}$	angular margin loss, ArcFace 20
$\mathcal{L}_{\text{comp}}$	compactness loss 16
$\mathcal{L}_{\text{kw}}$	keyword classification loss 125
$\mathcal{L}_{\text{pos}}$	position classification loss 125
$\mathcal{L}_{\text{proj}}$	AdaProj loss 102
$\mathcal{L}_{\text{prot}}^{(t)}$	prototypical loss at training step t 115
$\mathcal{L}_{\text{rec}}$	reconstruction loss 14
$\mathcal{L}_{\text{sc-ada}}$	sub-cluster AdaCos loss 54
$\mathcal{L}_{\text{tac}}$	TACos loss 125
lab	categorical class label function 8
lab_{pos}	categorical encoding of the relative position 123
$L(\phi)$	number of layers for neural network ϕ 16
L_{seg}	segment length of input waveforms in seconds 121
m	angular margin 20

mean	arithmetic mean of a dataset 40
median	median of a dataset 41
$\mathrm{mix}_{\mathrm{lab}}$	label mixing function of mixup 28
mix_{x}	sample mixing function of mixup 28
N_{batch}	batch size 23
N_{centers}	number of centers for a single class 53
N_{classes}	number of classes 8
$N_{\mathrm{classes}}^{\mathrm{test}}$	number of test classes 114
$N_{\mathrm{classes}}^{\mathrm{train}}$	number of classes used for training 114
N_{kw}	number of keyword classes 124
N_{pos}	maximum number of segments belonging to any training sample 123
N_{seg}	number of segments belonging to a training sample 123
$\mathrm{openness}$	openness of an open-set task 114
$\mathcal{P}$	power set 8
$\mathrm{pred}_{\mathrm{class}}$	classifier function 36
$P_{\mathcal{S}^{D-1}}$	projection onto D-sphere 49
$P_{\mathrm{span}(C)}$	projection onto the linear span of C 101
$\mathcal{Q}^{(t)}$	query set at training step t 115
$\mathbb{R}_{+}$	positive real numbers including zero 14
s	scale parameter 20
$\mathcal{S}^{(t)}$	support set at training step t 115
score	anomaly score function 1
$\mathrm{score}_{\mathrm{emb}}$	anomaly score function in the embedding space 26
$\mathcal{S}^{D-1}$	D-sphere, unit sphere 49
$\hat{s}^{(t)}$	dynamically adaptive scale parameter of the sub-cluster AdaCos loss at training step t 53
$\mathrm{shift}_{\mathrm{domain}}$	domain shift 81
sim	cosine similarity 20
$\mathrm{sim}_{\mathrm{mar}}$	cosine similarity with angular margin 20
$\mathrm{sim}_{\mathrm{max}}^{(t)}$	stability term of the sub-cluster AdaCos loss at training step t 54
$\mathrm{softmax}$	softmax function 20
sort	sort function sorting real values from low to high 35

$\mathrm{span}(C)$	linear span of elements in C 101
std	standard deviation of a dataset 40
$\tilde{s}$	dynamically adaptive scale parameter 24
$\tilde{s}^{(t)}$	dynamically adaptive scale parameter of the AdaCos loss at training step t 23
t	training step 23
T	time dimension 106
$\mathcal{U}$	normal distribution 28
W	parameter space of a neural network 8
w_0	parameter setting with all weights equal to zero 17
$w(l)$	weight parameters of layer l (excluding bias term) 17
x	a data sample 1
X	data space containing raw waveforms or preprocessed feature representations 1, 13
$X_{\text{anomalous}}$	anomalous data samples 1
X_{normal}	normal data samples 1
$X_{\text{normal}}^{(i)}$	normal data samples belonging to class i 36
X_{source}	source domain 81
X_{target}	target domain 81
X_{train}	training samples 2
Y	finite subset of the data space 14
Y_j	subset of the data space containing only samples of class j 55
$Y^{(t)}$	batch at training step t 23

BIBLIOGRAPHY

[1] Martín Abadi, Paul Barham, Jianmin Chen, Zhifeng Chen, Andy Davis, Jeffrey Dean, Matthieu Devin, Sanjay Ghemawat, Geoffrey Irving, Michael Isard, et al. "Tensorflow: A system for large-scale machine learning." In: *12th USENIX Symposium on Operating Systems Design and Implementation (OSDI)*. 2016, pp. 265–283.

[2] Sami Abu-El-Haija, Nisarg Kothari, Joonseok Lee, Paul Natsev, George Toderici, Balakrishnan Varadarajan, and Sudheendra Vijayanarasimhan. "YouTube-8M: A Large-Scale Video Classification Benchmark." In: *CoRR* abs/1609.08675 (2016).

[3] Charu Aggarwal. *Outlier Analysis*. 2nd. Springer, 2017.

[4] Samet Akcay, Amir Atapour Abarghouei, and Toby P. Breckon. "GANomaly: Semi-supervised Anomaly Detection via Adversarial Training." In: *14th Asian Conference on Computer Vision (ACCV)*. Vol. 11363. Lecture Notes in Computer Science. Springer, 2018, pp. 622–637.

[5] Guillaume Alain and Yoshua Bengio. "What regularized auto-encoders learn from the data-generating distribution." In: *J. Mach. Learn. Res.* 15.1 (2014), pp. 3563–3593.

[6] Relja Arandjelovic and Andrew Zisserman. "Look, Listen and Learn." In: *International Conference on Computer Vision (ICCV)*. IEEE Computer Society, 2017, pp. 609–617.

[7] Relja Arandjelovic and Andrew Zisserman. "Objects that Sound." In: *15th European Conference on Computer Vision (ECCV)*. Vol. 11205. Lecture Notes in Computer Science. Springer, 2018, pp. 451–466.

[8] Alexei Baevski, Yuhao Zhou, Abdelrahman Mohamed, and Michael Auli. "wav2vec 2.0: A Framework for Self-Supervised Learning of Speech Representations." In: *Advances in Neural Information Processing Systems 33: Annual Conference on Neural Information Processing Systems (NeurIPS)*. 2020.

[9] Jisheng Bai, Jianfeng Chen, Mou Wang, Muhammad Saad Ayub, and Qingli Yan. "SSDPT: Self-supervised dual-path transformer for anomalous sound detection." In: *Digit. Signal Process.* 135 (2023), p. 103939.

[10] Jisheng Bai, Yafei Jia, and Siwei Huang. *JLESS Submission to DCASE2022 Task2: Batch Mixing Strategy Based Method With Aanomaly Detector for Anomalous Sound Detection*. Tech. rep. DCASE Challenge, 2022.

[11] Jisheng Bai, Mou Wang, and Jianfeng Chen. “Dual-Path Transformer For Machine Condition Monitoring.” In: *Asia-Pacific Signal and Information Processing Association Annual Summit and Conference (APSIPA)*. IEEE, 2021, pp. 1144–1148.

[12] Adrien Bardes, Jean Ponce, and Yann LeCun. “VICReg: Variance-Invariance-Covariance Regularization for Self-Supervised Learning.” In: *10th International Conference on Learning Representations ICLR*. OpenReview.net, 2022.

[13] Yacine Bel-Hadj and Wout Weijtjens. “Population-Based SHM Under Environmental Variability Using a Classifier for Unsupervised Damage Detection.” In: *14th International Workshop on Structural Health Monitoring*. 2023, pp. 1479–1488.

[14] Yacine Bel-Hadj, Wout Weijtjens, and Francisco de Nolasco Santos. “Anomaly detection and representation learning in an instrumented railway bridge.” In: *30th European Symposium on Artificial Neural Networks, Computational Intelligence and Machine Learning (ESANN)*. 2022.

[15] Shai Ben-David, John Blitzer, Koby Crammer, and Fernando Pereira. “Analysis of Representations for Domain Adaptation.” In: *Advances in Neural Information Processing Systems 19: Twentieth Annual Conference on Neural Information Processing Systems (NIPS)*. MIT Press, 2006, pp. 137–144.

[16] Çagdas Bilen, Giacomo Ferroni, Francesco Tuveri, Juan Azcarreta, and Sacha Krstulovic. “A Framework for the Robust Evaluation of Sound Event Detection.” In: *International Conference on Acoustics, Speech and Signal Processing (ICASSP)*. IEEE, 2020, pp. 61–65.

[17] Sam Bond-Taylor, Adam Leach, Yang Long, and Chris G. Willcocks. “Deep Generative Modelling: A Comparative Review of VAEs, GANs, Normalizing Flows, Energy-Based and Autoregressive Models.” In: *IEEE Trans. Pattern Anal. Mach. Intell.* 44.11 (2022), pp. 7327–7347.

[18] Holger Severin Bovbjerg and Zheng-Hua Tan. “Improving Label-Deficient Keyword Spotting Through Self-Supervised Pretraining.” In: *International Conference on Acoustics, Speech, and Signal Processing (ICASSP)*. IEEE, 2023.

[19] Andrew P. Bradley. “The use of the area under the ROC curve in the evaluation of machine learning algorithms.” In: *Pattern recognition* 30.7 (1997), pp. 1145–1159.

[20] Guido Buzzi-Ferraris and Flavio Manenti. “Outlier detection in large data sets.” In: *Computers & chemical engineering* 35.2 (2011), pp. 388–390.

[21] Xinyu Cai, Heinrich Dinkel, Zhiyong Yan, Yongqing Wang, Junbo Zhang, Zhiyong Wu, and Yujun Wang. “A Contrastive Semi-Supervised Learning Framework For Anomaly Sound Detection.” In: *6th Workshop on Detection and Classification of Acoustic Scenes and Events (DCASE)*. 2021, pp. 31–34.

[22] Estefanía Cano, Johannes Nowak, and Sascha Grollmisch. “Exploring sound source separation for acoustic condition monitoring in industrial scenarios.” In: *25th European Signal Processing Conference (EUSIPCO)*. IEEE, 2017, pp. 2264–2268.

[23] Tymoteusz Cejrowski and Julian Szymanski. “Buzz-based honeybee colony fingerprint.” In: *Comput. Electron. Agric.* 191 (2021), p. 106489.

[24] Nitesh V. Chawla, Kevin W. Bowyer, Lawrence O. Hall, and W. Philip Kegelmeyer. “SMOTE: Synthetic Minority Over-sampling Technique.” In: *J. Artif. Intell. Res.* 16 (2002), pp. 321–357.

[25] Han Chen, Yan Song, Li-Rong Dai, Ian McLoughlin, and Lin Liu. “Self-Supervised Representation Learning for Unsupervised Anomalous Sound Detection Under Domain Shift.” In: *International Conference on Acoustics, Speech and Signal Processing (ICASSP)*. IEEE, 2022, pp. 471–475.

[26] Han Chen, Yan Song, Zhu Zhuo, Yu Zhou, Yu-Hong Li, Hui Xue, and Ian McLoughlin. “An Effective Anomalous Sound Detection Method Based on Representation Learning with Simulated Anomalies.” In: *International Conference on Acoustics, Speech and Signal Processing (ICASSP)*. IEEE, 2023.

[27] Rewon Child. “Very Deep VAEs Generalize Autoregressive Models and Can Outperform Them on Images.” In: *9th International Conference on Learning Representations (ICLR)*. OpenReview.net, 2021.

[28] Kyunghyun Cho, Bart van Merriënboer, Dzmitry Bahdanau, and Yoshua Bengio. “On the properties of neural machine translation: Encoder–decoder approaches.” In: *8th Workshop on Syntax, Semantics and Structure in Statistical Translation (SSST)*. Association for Computational Linguistics (ACL). 2014, pp. 103–111.

[29] Kateryna Chumachenko, Alexandros Iosifidis, and Moncef Gabbouj. “Robust Fast Subclass Discriminant Analysis.” In: *28th European Signal Processing Conference (EUSIPCO)*. IEEE. 2020, pp. 1397–1401.

[30] Joon Son Chung, Jaesung Huh, Seongkyu Mun, Minjae Lee, Hee-Soo Heo, Soyeon Choe, Chiheon Ham, Sunghwan Jung, Bong-Jin Lee, and Icksang Han. “In Defence of Metric Learning for Speaker Recognition.” In: *21st Annual Conference of the International Speech Communication Association (Interspeech)*. ISCA, 2020, pp. 2977–2981.

[31] James Clark, Zhen Liu, and Nathalie Japkowicz. “Adaptive Threshold for Outlier Detection on Data Streams.” In: *5th International Conference on Data Science and Advanced Analytics (DSAA)*. IEEE, 2018, pp. 41–49.

[32] Aurora Cramer, Ho-Hsiang Wu, Justin Salamon, and Juan Pablo Bello. “Look, Listen, and Learn More: Design Choices for Deep Audio Embeddings.” In: *International Conference on Acoustics, Speech and Signal Processing (ICASSP)*. IEEE, 2019, pp. 3852–3856.

[33] Pawel Daniluk, Marcin Gozdziewski, Slawomir Kapka, and Michal Kosmider. *Ensemble of Auto-Encoder Based Systems for Anomaly Detection*. Tech. rep. DCASE2020 Challenge, 2020.

[34] Ingrid Daubechies. *Ten Lectures on Wavelets*. SIAM, 1992.

[35] Jesse Davis and Mark Goadrich. “The relationship between Precision-Recall and ROC curves.” In: *Twenty-Third International Conference on Machine Learning (ICML)*. Vol. 148. ACM International Conference Proceeding Series. ACM, 2006, pp. 233–240.

[36] Steven Davis and Paul Mermelstein. “Comparison of parametric representations for monosyllabic word recognition in continuously spoken sentences.” In: *IEEE Trans. Acoust. Speech Signal Process* 28.4 (1980), pp. 357–366.

[37] Jiankang Deng, Jia Guo, Tongliang Liu, Mingming Gong, and Stefanos Zafeiriou. “Sub-center ArcFace: Boosting face recognition by large-scale noisy web faces.” In: *European Conference on Computer Vision (ECCV)*. Springer. 2020, pp. 741–757.

[38] Jiankang Deng, Jia Guo, Niannan Xue, and Stefanos Zafeiriou. “ArcFace: Additive Angular Margin Loss for Deep Face Recognition.” In: *Conference on Computer Vision and Pattern Recognition (CVPR)*. IEEE, 2019, pp. 4690–4699.

[39] Yufeng Deng, Anbai Jiang, Yuchen Duan, Jitao Ma, Xuchu Chen, Jia Liu, Pingyi Fan, Cheng Lu, and Wei-Qiang Zhang. “Ensemble of Multiple Anomalous Sound Detectors.” In: *7th Workshop on Detection and Classification of Acoustic Scenes and Events (DCASE)*. Tampere University, 2022.

[40] Theekshana Dissanayake, Tharindu Fernando, Simon Denman, Sridha Sridharan, Houman Ghaemmaghami, and Clinton Fookes. “A Robust Interpretable Deep Learning Classifier for Heart Anomaly Detection Without Segmentation.” In: *IEEE J. Biomed. Health Informatics* 25.6 (2021), pp. 2162–2171.

[41] Duygu Dogan, Huang Xie, Toni Heittola, and Tuomas Virtanen. “Zero-Shot Audio Classification using Image Embeddings.” In: *30th European Signal Processing Conference (EUSIPCO)*. IEEE, 2022, pp. 1–5.

[42] Kota Dohi, Takashi Endo, and Yohei Kawaguchi. "Disentangling physical parameters for anomalous sound detection under domain shifts." In: *30th European Signal Processing Conference (EUSIPCO)*. IEEE, 2022, pp. 279–283.

[43] Kota Dohi, Takashi Endo, Harsh Purohit, Ryo Tanabe, and Yohei Kawaguchi. "Flow-Based Self-Supervised Density Estimation for Anomalous Sound Detection." In: *International Conference on Acoustics, Speech and Signal Processing (ICASSP)*. IEEE, 2021, pp. 336–340.

[44] Kota Dohi, Keisuke Imoto, Noboru Harada, Daisuke Niizumi, Yuma Koizumi, Tomoya Nishida, Harsh Purohit, Ryo Tanabe, Takashi Endo, and Yohei Kawaguchi. "Description and Discussion on DCASE 2023 Challenge Task 2: First-Shot Unsupervised Anomalous Sound Detection for Machine Condition Monitoring." In: *8th Detection and Classification of Acoustic Scenes and Events Workshop (DCASE)*. Tampere, Finland, 2023, pp. 31–35.

[45] Kota Dohi, Tomoya Nishida, Harsh Purohit, Ryo Tanabe, Takashi Endo, Masaaki Yamamoto, Yuki Nikaido, and Yohei Kawaguchi. "MIMII DG: Sound Dataset for Malfunctioning Industrial Machine Investigation and Inspection for Domain Generalization Task." In: *7th Workshop on Detection and Classification of Acoustic Scenes and Events (DCASE)*. Tampere University, 2022, pp. 1–5.

[46] Kota Dohi et al. "Description and Discussion on DCASE 2022 Challenge Task 2: Unsupervised Anomalous Sound Detection for Machine Condition Monitoring Applying Domain Generalization Techniques." In: *7th Workshop on Detection and Classification of Acoustic Scenes and Events (DCASE)*. Tampere University, 2022, pp. 26–30.

[47] Jiaxin Du, Guangjie Han, Chuan Lin, and Miguel Martínez-García. "ITrust: An Anomaly-Resilient Trust Model Based on Isolation Forest for Underwater Acoustic Sensor Networks." In: *IEEE Trans. Mob. Comput.* 21.5 (2022), pp. 1684–1696.

[48] Janek Ebbers, Reinhold Haeb-Umbach, and Romain Serizel. "Threshold Independent Evaluation of Sound Event Detection Scores." In: *International Conference on Acoustics, Speech and Signal Processing (ICASSP)*. IEEE, 2022, pp. 1021–1025.

[49] Benjamin Elizalde, Soham Deshmukh, Mahmoud Al Ismail, and Huaming Wang. "CLAP Learning Audio Concepts from Natural Language Supervision." In: *International Conference on Acoustics, Speech and Signal Processing (ICASSP)*. IEEE, 2023.

[50] Andres Fernandez and Mark D. Plumbley. "Using UMAP to Inspect Audio Data for Unsupervised Anomaly Detection Under Domain-Shift Conditions." In: *6th Workshop on Detection and Classification of Acoustic Scenes and Events (DCASE).* 2021, pp. 165–169.

[51] Giacomo Ferroni, Nicolas Turpault, Juan Azcarreta, Francesco Tuveri, Romain Serizel, Çagdas Bilen, and Sacha Krstulovic. "Improving Sound Event Detection Metrics: Insights from DCASE 2020." In: *International Conference on Acoustics, Speech and Signal Processing (ICASSP).* IEEE, 2021, pp. 631–635.

[52] Peter Filzmoser. "A multivariate outlier detection method." In: *7th International Conference on Computer Data Analysis and Modeling.* 2004, pp. 18–22.

[53] Pasquale Foggia, Nicolai Petkov, Alessia Saggese, Nicola Strisciuglio, and Mario Vento. "Audio Surveillance of Roads: A System for Detecting Anomalous Sounds." In: *IEEE Trans. Intell. Transp. Syst.* 17.1 (2016), pp. 279–288.

[54] M. A. Ganaie, Minghui Hu, Ashwani Kumar Malik, Muhammad Tanveer, and Ponnuthurai N. Suganthan. "Ensemble deep learning: A review." In: *Eng. Appl. Artif. Intell.* 115 (2022), p. 105151.

[55] Jing Gao and Pang-Ning Tan. "Converting Output Scores from Outlier Detection Algorithms into Probability Estimates." In: *6th International Conference on Data Mining (ICDM).* IEEE Computer Society, 2006, pp. 212–221.

[56] Martin Gebel. "Multivariate calibration of classifier scores into the probability space." Ph.D. thesis. University of Dortmund, 2009.

[57] Jort F. Gemmeke, Daniel P. W. Ellis, Dylan Freedman, Aren Jansen, Wade Lawrence, R. Channing Moore, Manoj Plakal, and Marvin Ritter. "Audio Set: An ontology and human-labeled dataset for audio events." In: *International Conference on Acoustics, Speech and Signal Processing (ICASSP).* IEEE, 2017, pp. 776–780.

[58] Mathieu Germain, Karol Gregor, Iain Murray, and Hugo Larochelle. "MADE: Masked Autoencoder for Distribution Estimation." In: *32nd International Conference on Machine Learning (ICML).* Vol. 37. JMLR Workshop and Conference Proceedings. JMLR.org, 2015, pp. 881–889.

[59] Ritwik Giri, Fangzhou Cheng, Karim Helwani, Srikanth V. Tenneti, Umut Isik, and Arvindh Krishnaswamy. "Group Masked Autoencoder Based Density Estimator for Audio Anomaly Detection." In: *5th the Workshop on Detection and Classification of Acoustic Scenes and Events (DCASE).* 2020, pp. 51–55.

[60] Ritwik Giri, Srikanth V. Tenneti, Fangzhou Cheng, Karim Helwani, Umut Isik, and Arvindh Krishnaswamy. "Self-Supervised Classification for Detecting Anomalous Sounds." In: *Detection and Classification of Acoustic Scenes and Events Workshop (DCASE)*. 2020, pp. 46–50.

[61] Ritwik Giri, Srikanth V. Tenneti, Karim Helwani, Fangzhou Cheng, Umut Isik, and Arvindh Krishnaswamy. *Unsupervised Anomalous Sound Detection Using Self-Supervised Classification and Group Masked Autoencoder for Density Estimation*. Tech. rep. DCASE2020 Challenge, 2020.

[62] Tobias Glasmachers. "Limits of End-to-End Learning." In: *9th Asian Conference on Machine Learning, ACML*. Vol. 77. Proceedings of Machine Learning Research. PMLR, 2017, pp. 17–32.

[63] Kaan Gökcesu, Mohammadreza Mohaghegh Neyshabouri, Hakan Gökcesu, and Suleyman Serdar Kozat. "Sequential Outlier Detection Based on Incremental Decision Trees." In: *IEEE Trans. Signal Process.* 67.4 (2019), pp. 993–1005.

[64] Ian Goodfellow, Yoshua Bengio, and Aaron Courville. *Deep Learning*. http://www.deeplearningbook.org. MIT Press, 2016.

[65] Alexander N. Gorban, Ivan Yu. Tyukin, Danil V. Prokhorov, and Konstantin I. Sofeikov. "Approximation with random bases: Pro et Contra." In: *Information Sciences* 364-365 (2016), pp. 129–145.

[66] Alex Graves, Santiago Fernández, Faustino J. Gomez, and Jürgen Schmidhuber. "Connectionist temporal classification: labelling unsegmented sequence data with recurrent neural networks." In: *23rd International Conference on Machine Learning (ICML)*. ACM, 2006, pp. 369–376.

[67] Sascha Grollmisch, Estefanía Cano, Christian Kehling, and Michael Taenzer. "Analyzing the Potential of Pre-Trained Embeddings for Audio Classification Tasks." In: *28th European Signal Processing Conference (EUSIPCO)*. IEEE, 2020, pp. 790–794.

[68] Sascha Grollmisch, David Johnson, Jakob Abeßer, and Hanna Lukashevich. "IAEO3-combining OpenL3 embeddings and interpolation autoencoder for anomalous sound detection." In: *Tech. Rep., DCASE2020 Challenge* (2020).

[69] Frank E. Grubbs. "Sample Criteria for Testing Outlying Observations." In: *The Annals of Mathematical Statistics* 21.1 (1950), pp. 27–58.

[70] Jian Guan, Youde Liu, Qiaoxi Zhu, Tieran Zheng, Jiqing Han, and Wenwu Wang. "Time-Weighted Frequency Domain Audio Representation with GMM Estimator for Anomalous Sound Detection." In: *International Conference on Acoustics, Speech and Signal Processing (ICASSP)*. IEEE, 2023.

[71] James A. Hanley and Barbara J. McNeil. "The meaning and use of the area under a receiver operating characteristic (ROC) curve." In: *Radiology* 143.1 (1982), pp. 29–36.

[72] Noboru Harada, Daisuke Niizumi, Daiki Takeuchi, Yasunori Ohishi, and Masahiro Yasuda. "First-Shot Anomaly Detection for Machine Condition Monitoring: A Domain Generalization Baseline." In: *31st European Signal Processing Conference (EUSIPCO)*. IEEE, 2023, pp. 191–195.

[73] Noboru Harada, Daisuke Niizumi, Daiki Takeuchi, Yasunori Ohishi, and Masahiro Yasuda. "ToyADMOS2+: New Toyadmos Data and Benchmark Results of the First-Shot Anomalous Sound Event Detection Baseline." In: *8th Detection and Classification of Acoustic Scenes and Events Workshop (DCASE)*. Tampere University, 2023, pp. 41–45.

[74] Noboru Harada, Daisuke Niizumi, Daiki Takeuchi, Yasunori Ohishi, Masahiro Yasuda, and Shoichiro Saito. "ToyADMOS2: Another Dataset of Miniature-Machine Operating Sounds for Anomalous Sound Detection under Domain Shift Conditions." In: *6th Workshop on Detection and Classification of Acoustic Scenes and Events (DCASE)*. 2021, pp. 1–5.

[75] Tomoki Hayashi, Tatsuya Komatsu, Reishi Kondo, Tomoki Toda, and Kazuya Takeda. "Anomalous Sound Event Detection Based on WaveNet." In: *26th European Signal Processing Conference (EUSIPCO)*. IEEE, 2018, pp. 2494–2498.

[76] Tomoki Hayashi, Takenori Yoshimura, and Yusuke Adachi. *Conformer-Based ID-Aware Autoencoder for Unsupervised Anomalous Sound Detection*. Tech. rep. DCASE2020 Challenge, 2020.

[77] Kaiming He, Xiangyu Zhang, Shaoqing Ren, and Jian Sun. "Deep Residual Learning for Image Recognition." In: *Conference on Computer Vision and Pattern Recognition (CVPR)*. IEEE, 2016, pp. 770–778.

[78] Dan Hendrycks, Mantas Mazeika, and Thomas G. Dietterich. "Deep Anomaly Detection with Outlier Exposure." In: *7th International Conference on Learning Representations (ICLR)*. OpenReview.net, 2019.

[79] Hynek Hermansky. "Perceptual linear predictive (PLP) analysis of speech." In: *The Journal of the Acoustical Society of America* 87.4 (1990), pp. 1738–1752.

[80] Shawn Hershey et al. "CNN architectures for large-scale audio classification." In: *International Conference on Acoustics, Speech and Signal Processing (ICASSP)*. IEEE, 2017, pp. 131–135.

[81] Geoffrey E. Hinton, Nitish Srivastava, Alex Krizhevsky, Ilya Sutskever, and Ruslan Salakhutdinov. "Improving neural networks by preventing co-adaptation of feature detectors." In: *CoRR* abs/1207.0580 (2012).

[82] Geoffrey Everest Hinton and Ruslan Salakhutdinov. "Reducing the Dimensionality of Data with Neural Networks." In: *Science* 313.5786 (2006), pp. 504–507.

[83] Sepp Hochreiter and Jürgen Schmidhuber. "Long short-term memory." In: *Neural computation* 9.8 (1997), pp. 1735–1780.

[84] Andreas Holzinger, Anna Saranti, Christoph Molnar, Przemyslaw Biecek, and Wojciech Samek. "Explainable AI Methods - A Brief Overview." In: *xxAI - Beyond Explainable AI - International Workshop, Held in Conjunction with ICML 2020.* Vol. 13200. Lecture Notes in Computer Science. Springer, 2020, pp. 13–38.

[85] Tadanobu Inoue, Phongtharin Vinayavekhin, Shu Morikuni, Shiqiang Wang, Tuan Hoang Trong, David Wood, Michiaki Tatsubori, and Ryuki Tachibana. "Detection of Anomalous Sounds for Machine Condition Monitoring using Classification Confidence." In: *Detection and Classification of Acoustic Scenes and Events Workshop (DCASE).* 2020, pp. 66–70.

[86] Sergey Ioffe and Christian Szegedy. "Batch normalization: accelerating deep network training by reducing internal covariate shift." In: *32nd International Conference on Machine Learning (ICML).* Vol. 37. 2015, pp. 448–456.

[87] Alan Jeffares, Qinghai Guo, Pontus Stenetorp, and Timoleon Moraitis. "Spike-inspired rank coding for fast and accurate recurrent neural networks." In: *10th International Conference on Learning Representations (ICLR).* OpenReview.net, 2022.

[88] Wang JiaJun. *Self-Supervised Representation Learning for First-Shot Unsupervised Anomalous Sound Detection.* Tech. rep. DCASE2023 Challenge, June 2023.

[89] Anbai Jiang, Qijun Hou, Jia Liu, Pingyi Fan, Jitao Ma, Cheng Lu, Yuanzhi Zhai, Yufeng Deng, and Wei-Qiang Zhang. *THUEE System for First-Shot Unsupervised Anomalous Sound Detection for Machine Condition Monitoring.* Tech. rep. DCASE2023 Challenge, 2023.

[90] Anbai Jiang, Wei-Qiang Zhang, Yufeng Deng, Pingyi Fan, and Jia Liu. "Unsupervised Anomaly Detection and Localization of Machine Audio: A GAN-Based Approach." In: *International Conference on Acoustics, Speech and Signal Processing (ICASSP).* IEEE, 2023.

[91] Yulei Jiang, Charles E. Metz, and Robert M. Nishikawa. "A receiver operating characteristic partial area index for highly sensitive diagnostic tests." In: *Radiology* 201.3 (1996), pp. 745–750.

[92] Justin M. Johnson and Taghi M. Khoshgoftaar. "Survey on deep learning with class imbalance." In: *J. Big Data* 6 (2019), p. 27.

[93] Wang Junjie, Wang Jiajun, Chen Shengbing, Sun Yong, and Liu Mengyuan. *Anomalous Sound Detection Based on Self-Supervised Learning.* Tech. rep. DCASE2023 Challenge, 2023.

[94] Herman Kamper, Weiran Wang, and Karen Livescu. "Deep convolutional acoustic word embeddings using word-pair side information." In: *International Conference on Acoustics, Speech and Signal Processing (ICASSP)*. IEEE, 2016, pp. 4950–4954.

[95] Slawomir Kapka. "ID-Conditioned Auto-Encoder for Unsupervised Anomaly Detection." In: *Detection and Classification of Acoustic Scenes and Events Workshop (DCASE)*. 2020, pp. 71–75.

[96] Yohei Kawaguchi, Keisuke Imoto, Yuma Koizumi, Noboru Harada, Daisuke Niizumi, Kota Dohi, Ryo Tanabe, Harsh Purohit, and Takashi Endo. "Description and Discussion on DCASE 2021 Challenge Task 2: Unsupervised Anomalous Detection for Machine Condition Monitoring Under Domain Shifted Conditions." In: *Detection and Classification of Acoustic Scenes and Events Workshop (DCASE)*. 2021, pp. 186–190.

[97] Byeonggeun Kim, Mingu Lee, Jinkyu Lee, Yeonseok Kim, and Kyuwoong Hwang. "Query-by-Example On-Device Keyword Spotting." In: *Automatic Speech Recognition and Understanding Workshop (ASRU)*. IEEE, 2019, pp. 532–538.

[98] Byeonggeun Kim, Seunghan Yang, Inseop Chung, and Simyung Chang. "Dummy Prototypical Networks for Few-Shot Open-Set Keyword Spotting." In: *23rd Annual Conference of the International Speech Communication Association (Interspeech)*. ISCA, 2022, pp. 4621–4625.

[99] Hyunjik Kim, Andriy Mnih, Jonathan Schwarz, Marta Garnelo, S. M. Ali Eslami, Dan Rosenbaum, Oriol Vinyals, and Yee Whye Teh. "Attentive Neural Processes." In: *7th International Conference on Learning Representations (ICLR)*. OpenReview.net, 2019.

[100] Jaechang Kim, Yunjoo Lee, Hyun Mi Cho, Dong Woo Kim, Chi Hoon Song, and Jungseul Ok. "Activity-Informed Industrial Audio Anomaly Detection Via Source Separation." In: *International Conference on Acoustics, Speech and Signal Processing (ICASSP)*. IEEE, 2023.

[101] Diederik P. Kingma and Jimmy Ba. "Adam: A Method for Stochastic Optimization." In: *3rd International Conference on Learning Representations (ICLR)*. 2015.

[102] Diederik P. Kingma and Max Welling. "An Introduction to Variational Autoencoders." In: *Found. Trends Mach. Learn.* 12.4 (2019), pp. 307–392.

[103] R. Kirandevraj, Vinod Kumar Kurmi, Vinay P. Namboodiri, and C. V. Jawahar. "Generalized Keyword Spotting using ASR embeddings." In: *23rd Annual Conference of the International Speech Communication Association (Interspeech)*. ISCA, 2022, pp. 126–130.

[104] Polina Kirichenko, Pavel Izmailov, and Andrew Gordon Wilson. "Why Normalizing Flows Fail to Detect Out-of-Distribution Data." In: *Advances in Neural Information Processing Systems 33: Annual Conference on Neural Information Processing Systems (NeurIPS)*. 2020.

[105] Ivan Kobyzev, Simon J. D. Prince, and Marcus A. Brubaker. "Normalizing Flows: An Introduction and Review of Current Methods." In: *IEEE Trans. Pattern Anal. Mach. Intell.* 43.11 (2021), pp. 3964–3979.

[106] Yuma Koizumi, Shoichiro Saito, Hisashi Uematsu, Noboru Harada, and Keisuke Imoto. "ToyADMOS: A dataset of miniature-machine operating sounds for anomalous sound detection." In: *Workshop on Applications of Signal Processing to Audio and Acoustics (WASPAA)*. IEEE. 2019, pp. 313–317.

[107] Yuma Koizumi, Shoichiro Saito, Hisashi Uematsu, Yuta Kawachi, and Noboru Harada. "Unsupervised Detection of Anomalous Sound Based on Deep Learning and the Neyman-Pearson Lemma." In: *IEEE ACM Trans. Audio Speech Lang. Process.* 27.1 (2019), pp. 212–224.

[108] Yuma Koizumi et al. "Description and Discussion on DCASE2020 Challenge Task2: Unsupervised Anomalous Sound Detection for Machine Condition Monitoring." In: *Detection and Classification of Acoustic Scenes and Events Workshop (DCASE)*. 2020, pp. 81–85.

[109] Alexander Kolesnikov and Christoph H. Lampert. "Seed, Expand and Constrain: Three Principles for Weakly-Supervised Image Segmentation." In: *14th European Conference on Computer Vision (ECCV)*. Vol. 9908. Lecture Notes in Computer Science. Springer, 2016, pp. 695–711.

[110] Qiuqiang Kong, Yin Cao, Turab Iqbal, Yuxuan Wang, Wenwu Wang, and Mark D. Plumbley. "PANNs: Large-Scale Pretrained Audio Neural Networks for Audio Pattern Recognition." In: *IEEE ACM Trans. Audio Speech Lang. Process.* 28 (2020), pp. 2880–2894.

[111] Anurag Kumar, Maksim Khadkevich, and Christian Fügen. "Knowledge Transfer from Weakly Labeled Audio Using Convolutional Neural Network for Sound Events and Scenes." In: *International Conference on Acoustics, Speech and Signal Processing (ICASSP)*. IEEE, 2018, pp. 326–330.

[112] Ibuki Kuroyanagi, Tomoki Hayashi, Yusuke Adachi, Takenori Yoshimura, Kazuya Takeda, and Tomoki Toda. "An Ensemble Approach to Anomalous Sound Detection Based on Conformer-Based Autoencoder and Binary Classifier Incorporated with Metric Learning." In: *6th Workshop on Detection and Classification of Acoustic Scenes and Events (DCASE)*. 2021, pp. 110–114.

[113] Ibuki Kuroyanagi, Tomoki Hayashi, Kazuya Takeda, and Tomoki Toda. "Anomalous Sound Detection Using a Binary Classification Model and Class Centroids." In: *29th European Signal Processing Conference (EUSIPCO)*. IEEE, 2021, pp. 1995–1999.

[114] Ibuki Kuroyanagi, Tomoki Hayashi, Kazuya Takeda, and Tomoki Toda. "Improvement of Serial Approach to Anomalous Sound Detection by Incorporating Two Binary Cross-Entropies for Outlier Exposure." In: *30th European Signal Processing Conference (EUSIPCO)*. IEEE, 2022, pp. 294–298.

[115] Ibuki Kuroyanagi, Tomoki Hayashi, Kazuya Takeda, and Tomoki Toda. *Two-stage anomalous sound detection systems using domain generalization and specialization techniques*. Tech. rep. DCASE Challenge, 2022.

[116] Frank Kurth and Dirk von Zeddelmann. "An Analysis of MFCC-like Parametric Audio Features for Keyphrase Spotting Applications." In: *ITG Symposium on Speech Communication (ITG Speech)*. VDE, 2010.

[117] Hugo Larochelle, Dumitru Erhan, and Yoshua Bengio. "Zero-data Learning of New Tasks." In: *Proceedings of the Twenty-Third AAAI Conference on Artificial Intelligence (AAAI)*. AAAI Press, 2008, pp. 646–651.

[118] Keon Lee, Kyumin Park, and Daeyoung Kim. "DailyTalk: Spoken Dialogue Dataset for Conversational Text-to-Speech." In: *International Conference on Acoustics, Speech and Signal Processing (ICASSP)*. IEEE, 2023.

[119] Guillaume Lemaitre, Fernando Nogueira, and Christos K. Aridas. "Imbalanced-learn: A Python Toolbox to Tackle the Curse of Imbalanced Datasets in Machine Learning." In: *J. Mach. Learn. Res.* 18 (2017), 17:1–17:5.

[120] Bin Li and Emmanuel Müller. "Contrastive Time Series Anomaly Detection by Temporal Transformations." In: *International Joint Conference on Neural Networks, (IJCNN)*. IEEE, 2023.

[121] Haoyuan Li and Yifan Li. "Anomaly detection methods based on GAN: a survey." In: *Appl. Intell.* 53.7 (2023), pp. 8209–8231.

[122] Jinyu Li et al. "Recent advances in end-to-end automatic speech recognition." In: *APSIPA Transactions on Signal and Information Processing* 11.1 (2022).

[123] Kai Li, Quoc-Huy Nguyen, Yasuji Ota, and Masashi Unoki. "Unsupervised Anomalous Sound Detection for Machine Condition Monitoring Using Temporal Modulation Features on Gammatone Auditory Filterbank." In: *7th Workshop on Detection and Classification of Acoustic Scenes and Events (DCASE)*. Tampere University, 2022.

[124] Kai Li, Dung Kim Tran, Xugang Lu, Masato Akagi, and Masashi Unoki. “Data-driven Non-uniform Filterbanks Based on F-ratio for Machine Anomalous Sound Detection.” In: *31st European Signal Processing Conference (EUSIPCO)*. IEEE, 2023, pp. 201–205.

[125] Lijian Li, Yunhe Zhang, and Aiping Huang. “Learnable Subspace Orthogonal Projection for Semi-supervised Image Classification.” In: *16th Asian Conference on Computer Vision (ACCV)*. Vol. 13843. Lecture Notes in Computer Science. Springer, 2022, pp. 477–490.

[126] Renjie Li, Xiaohua Gu, Fei Lu, Hongfei Song, and Jutao Pan. *Unsupervised Adversarial domain adaptive abnormal sound detection for machine condition monitoring under Domain Shift Conditions*. Tech. rep. DCASE2021 Challenge, 2021.

[127] Yanxiong Li, Xianku Li, Yuhan Zhang, Mingle Liu, and Wucheng Wang. “Anomalous Sound Detection Using Deep Audio Representation and a BLSTM Network for Audio Surveillance of Roads.” In: *IEEE Access* 6 (2018), pp. 58043–58055.

[128] Min Lin, Qiang Chen, and Shuicheng Yan. “Network In Network.” In: *2nd International Conference on Learning Representations, (ICLR)*. Ed. by Yoshua Bengio and Yann LeCun. 2014.

[129] Tsung-Yi Lin, Priya Goyal, Ross B. Girshick, Kaiming He, and Piotr Dollár. “Focal Loss for Dense Object Detection.” In: *IEEE International Conference on Computer Vision (ICCV)*. IEEE Computer Society, 2017, pp. 2999–3007.

[130] Yihan Lin, Xunquan Chen, Ryoichi Takashima, and Tetsuya Takiguchi. “Zero-Shot Sound Event Classification Using a Sound Attribute Vector with Global and Local Feature Learning.” In: *International Conference on Acoustics, Speech and Signal Processing (ICASSP)*. IEEE, 2023.

[131] Haohe Liu, Xubo Liu, Xinhao Mei, Qiuqiang Kong, Wenwu Wang, and Mark D. Plumbley. “Segment-Level Metric Learning for Few-Shot Bioacoustic Event Detection.” In: *7th Workshop on Detection and Classification of Acoustic Scenes and Events (DCASE)*. Tampere University, 2022.

[132] Shuo Liu, Adria Mallol-Ragolta, Emilia Parada-Cabaleiro, Kun Qian, Xin Jing, Alexander Kathan, Bin Hu, and Björn W. Schuller. “Audio self-supervised learning: A survey.” In: *Patterns* 3.12 (2022), p. 100616.

[133] Weiyang Liu, Yandong Wen, Zhiding Yu, Ming Li, Bhiksha Raj, and Le Song. “SphereFace: Deep Hypersphere Embedding for Face Recognition.” In: *Conference on Computer Vision and Pattern Recognition (CVPR)*. IEEE Computer Society, 2017, pp. 6738–6746.

[134] Jose A. Lopez, Hong Lu, Paulo Lopez-Meyer, Lama Nachman, Georg Stemmer, and Jonathan Huang. "A Speaker Recognition Approach to Anomaly Detection." In: *Detection and Classification of Acoustic Scenes and Events Workshop (DCASE)*. 2020, pp. 96–99.

[135] Jose A. Lopez, Georg Stemmer, Paulo Lopez-Meyer, Pradyumna Singh, Juan A. del Hoyo Ontiveros, and Héctor A. Cordourier. "Ensemble Of Complementary Anomaly Detectors Under Domain Shifted Conditions." In: *6th Workshop on Detection and Classification of Acoustic Scenes and Events (DCASE)*. 2021, pp. 11–15.

[136] Iván López-Espejo, Zheng-Hua Tan, John H. L. Hansen, and Jesper Jensen. "Deep Spoken Keyword Spotting: An Overview." In: *IEEE Access* 10 (2022), pp. 4169–4199.

[137] Zhiqiang Lv, Bing Han, Zhengyang Chen, Yanmin Qian, Jiawei Ding, and Jia Liu. *Unsupervised Anomalous Detection Based on Unsupervised Pretrained Models.* Tech. rep. DCASE2023 Challenge, 2023.

[138] Haoxin Ma, Ye Bai, Jiangyan Yi, and Jianhua Tao. "Hypersphere Embedding and Additive Margin for Query-by-example Keyword Spotting." In: *Asia-Pacific Signal and Information Processing Association Annual Summit and Conference (APSIPA ASC)*. IEEE, 2019, pp. 868–872.

[139] Andrew L. Maas, Awni Y. Hannun, and Andrew Y. Ng. "Rectifier nonlinearities improve neural network acoustic models." In: *30th International Conference on Machine Learning (ICML)*. 2013.

[140] Kimberly T. Mai, Toby Davies, Lewis D. Griffin, and Emmanouil Benetos. "Explaining the Decision of Anomalous Sound Detectors." In: *7th Workshop on Detection and Classification of Acoustic Scenes and Events (DCASE)*. Tampere University, 2022.

[141] John Martinsson, Martin Willbo, Aleksis Pirinen, Olof Mogren, and Maria Sandsten. "Few-Shot Bioacoustic Event Detection Using an Event-Length Adapted Ensemble of Prototypical Networks." In: *7th Workshop on Detection and Classification of Acoustic Scenes and Events (DCASE)*. Tampere University, 2022.

[142] Mark Mazumder, Colby R. Banbury, Josh Meyer, Pete Warden, and Vijay Janapa Reddi. "Few-Shot Keyword Spotting in Any Language." In: *22nd Annual Conference of the International Speech Communication Association (Interspeech)*. ISCA, 2021, pp. 4214–4218.

[143] Donna Katzman McClish. "Analyzing a portion of the ROC curve." In: *Medical decision making* 9.3 (1989), pp. 190–195.

[144] Leland McInnes, John Healy, Nathaniel Saul, and Lukas Großberger. "UMAP: Uniform Manifold Approximation and Projection." In: *J. Open Source Softw.* 3.29 (2018), p. 861.

[145] Li Meirong, Zhang Shaoying, Cheng Chuanxu, and Xu Wen. “Query-by-Example on-Device Keyword Spotting using Convolutional Recurrent Neural Network and Connectionist Temporal Classification.” In: *6th International Conference on Intelligent Computing and Signal Processing (ICSP)*. 2021, pp. 1291–1294.

[146] Raghav Menon, Herman Kamper, John A. Quinn, and Thomas Niesler. “Fast ASR-free and Almost Zero-resource Keyword Spotting Using DTW and CNNs for Humanitarian Monitoring.” In: *19th Annual Conference of the International Speech Communication Association (Interspeech)*. ISCA, 2018, pp. 2608–2612.

[147] Raghav Menon, Armin Saeb, Hugh Cameron, William Kibira, John A. Quinn, and Thomas Niesler. “Radio-browsing for developmental monitoring in Uganda.” In: *International Conference on Acoustics, Speech and Signal Processing (ICASSP)*. IEEE, 2017, pp. 5795–5799.

[148] Annamaria Mesaros, Toni Heittola, and Tuomas Virtanen. “Metrics for polyphonic sound event detection.” In: *Applied Sciences* 6.6 (2016), p. 162.

[149] Annamaria Mesaros, Toni Heittola, and Tuomas Virtanen. “Acoustic Scene Classification in DCASE 2019 Challenge: Closed and Open Set Classification and Data Mismatch Setups.” In: *Workshop on Detection and Classification of Acoustic Scenes and Events (DCASE)*. 2019, pp. 164–168.

[150] Assaf Hurwitz Michaely, Xuedong Zhang, Gabor Simko, Carolina Parada, and Petar S. Aleksic. “Keyword spotting for Google assistant using contextual speech recognition.” In: *Automatic Speech Recognition and Understanding Workshop (ASRU)*. IEEE, 2017, pp. 272–278.

[151] Saumitra Mishra, Bob L. Sturm, and Simon Dixon. “Local Interpretable Model-Agnostic Explanations for Music Content Analysis.” In: *18th International Society for Music Information Retrieval Conference (ISMIR)*. 2017, pp. 537–543.

[152] Abdelrahman Mohamed et al. “Self-Supervised Speech Representation Learning: A Review.” In: *IEEE J. Sel. Top. Signal Process.* 16.6 (2022), pp. 1179–1210.

[153] Veronica Morfi, Inês Nolasco, Vincent Lostanlen, Shubhr Singh, Ariana Strandburg-Peshkin, Lisa F. Gill, Hanna Pamula, David Benvent, and Dan Stowell. “Few-Shot Bioacoustic Event Detection: A New Task at the DCASE 2021 Challenge.” In: *6th Workshop on Detection and Classification of Acoustic Scenes and Events (DCASE)*. 2021, pp. 145–149.

[154] Kazuki Morita, Tomohiko Yano, and Khai Tran. *Anomalous Sound Detection Using CNN-Based Features By Self Supervised Learning*. Tech. rep. DCASE2021 Challenge, 2021.

[155] Kazuki Morita, Tomohiko Yano, and Khai Tran. *Comparitive Experiments on Spectrogram Representation for Anomalous Sound Detection.* Tech. rep. DCASE Challenge, 2022.

[156] Mary M. Moya and Don R. Hush. "Network constraints and multi-objective optimization for one-class classification." In: *Neural Networks* 9.3 (1996), pp. 463–474.

[157] Ami Moyal, Vered Aharonson, Ella Tetariy, and Michal Gishri. *Phonetic Search Methods for Large Speech Databases.* Springer Briefs in Electrical and Computer Engineering. Springer, 2013.

[158] Robert Müller, Steffen Illium, Fabian Ritz, and Kyrill Schmid. "Analysis of Feature Representations for Anomalous Sound Detection." In: *13th International Conference on Agents and Artificial Intelligence (ICAART).* SCITEPRESS, 2021, pp. 97–106.

[159] Robert Müller, Fabian Ritz, Steffen Illium, and Claudia Linnhoff-Popien. "Acoustic Anomaly Detection for Machine Sounds based on Image Transfer Learning." In: *13th International Conference on Agents and Artificial Intelligence (ICAART).* SCITEPRESS, 2021, pp. 49–56.

[160] Shreesha Narasimha Murthy and Emmanuel Agu. "Deep Learning Anomaly Detection methods to passively detect COVID-19 from Audio." In: *International Conference on Digital Health (ICDH).* IEEE, 2021, pp. 114–121.

[161] Eric T. Nalisnick, Akihiro Matsukawa, Yee Whye Teh, Dilan Görür, and Balaji Lakshminarayanan. "Do Deep Generative Models Know What They Don't Know?" In: *7th International Conference on Learning Representations (ICLR).* OpenReview.net, 2019.

[162] Javier Naranjo-Alcazar, Sergi Perez-Castanos, Pedro Zuccarello, Ana M. Torres, Jose J. Lopez, Francesc J. Ferri, and Maximo Cobos. "An open-set recognition and few-shot learning dataset for audio event classification in domestic environments." In: *Pattern Recognition Letters* (2022).

[163] Hiroki Narita and Akira Tamamori. *Unsupervised Anomalous Sound Detection Using Intermediate Representation of Trained Models and Metric Learning Based Variational Autoencoder.* Tech. rep. DCASE2021 Challenge, 2021.

[164] Ismail Nejjar, Jean Meunier-Pion, Gaëtan Frusque, and Olga Fink. "DG-Mix: Domain Generalization for Anomalous Sound Detection Based on Self-Supervised Learning." In: *7th Workshop on Detection and Classification of Acoustic Scenes and Events 2022 (DCASE).* Tampere University, 2022.

[165] Daisuke Niizumi, Daiki Takeuchi, Yasunori Ohishi, Noboru Harada, and Kunio Kashino. "BYOL for Audio: Self-Supervised Learning for General-Purpose Audio Representation." In: *International Joint Conference on Neural Networks (IJCNN).* IEEE, 2021.

[166] Daisuke Niizumi, Daiki Takeuchi, Yasunori Ohishi, Noboru Harada, and Kunio Kashino. "Composing General Audio Representation by Fusing Multilayer Features of a Pre-trained Model." In: *30th European Signal Processing Conference (EUSIPCO)*. IEEE, 2022, pp. 200–204.

[167] Daisuke Niizumi, Daiki Takeuchi, Yasunori Ohishi, Noboru Harada, and Kunio Kashino. "BYOL for Audio: Exploring Pre-Trained General-Purpose Audio Representations." In: *IEEE/ACM Trans. Audio Speech Lang. Process.* 31 (2023), pp. 137–151.

[168] Tomoya Nishida, Kota Dohi, Takashi Endo, Masaaki Yamamoto, and Yohei Kawaguchi. "Anomalous Sound Detection Based on Machine Activity Detection." In: *30th European Signal Processing Conference (EUSIPCO)*. IEEE, 2022, pp. 269–273.

[169] Inês Nolasco et al. "Few-Shot Bioacoustic Event Detection at the DCASE 2022 Challenge." In: *7th Workshop on Detection and Classification of Acoustic Scenes and Events 2022 (DCASE)*. 2022, pp. 136–140.

[170] Stavros Ntalampiras and Ilyas Potamitis. "Acoustic detection of unknown bird species and individuals." In: *CAAI Transactions on Intelligence Technology* 6.3 (2021), pp. 291–300.

[171] Aäron van den Oord, Sander Dieleman, Heiga Zen, Karen Simonyan, Oriol Vinyals, Alex Graves, Nal Kalchbrenner, Andrew W. Senior, and Koray Kavukcuoglu. "WaveNet: A Generative Model for Raw Audio." In: *The 9th ISCA Speech Synthesis Workshop (SSW)*. ISCA, 2016, p. 125.

[172] George Papamakarios, Eric T. Nalisnick, Danilo Jimenez Rezende, Shakir Mohamed, and Balaji Lakshminarayanan. "Normalizing Flows for Probabilistic Modeling and Inference." In: *J. Mach. Learn. Res.* 22 (2021), 57:1–57:64.

[173] Daniel S. Park, William Chan, Yu Zhang, Chung-Cheng Chiu, Barret Zoph, Ekin D. Cubuk, and Quoc V. Le. "SpecAugment: A Simple Data Augmentation Method for Automatic Speech Recognition." In: *20th Annual Conference of the International Speech Communication Association (Interspeech)*. ISCA, 2019, pp. 2613–2617.

[174] Jihwan Park and Sooyeon Yoo. "DCASE 2020 Task2: Anomalous Sound Detection using Relevant Spectral Feature and Focusing Techniques in the Unsupervised Learning Scenario." In: *5th Workshop on Detection and Classification of Acoustic Scenes and Events (DCASE)*. 2020, pp. 140–144.

[175] Archit Parnami and Minwoo Lee. "Few-Shot Keyword Spotting With Prototypical Networks." In: *7th International Conference on Machine Learning Technologies (ICMLT)*. ACM, 2022, pp. 277–283.

[176] Fabian Pedregosa et al. "Scikit-learn: Machine Learning in Python." In: *Journal of Machine Learning Research* 12 (2011), pp. 2825–2830.

[177] Pramuditha Perera and Vishal M. Patel. “Learning Deep Features for One-Class Classification.” In: *IEEE Transactions on Image Processing* 28.11 (2019), pp. 5450–5463.

[178] Ricardo Falcón Pérez, Gordon Wichern, François G. Germain, and Jonathan Le Roux. “Location as Supervision for Weakly Supervised Multi-Channel Source Separation of Machine Sounds.” In: *Workshop on Applications of Signal Processing to Audio and Acoustics (WASPAA)*. IEEE, 2023.

[179] Sergi Perez-Castanos, Javier Naranjo-Alcazar, Pedro Zuccarello, and Maximo Cobos. “Anomalous Sound Detection using Unsupervised and Semi-Supervised Autoencoders and Gammatone Audio Representation.” In: *5th Workshop on Detection and Classification of Acoustic Scenes and Events (DCASE)*. 2020, pp. 145–149.

[180] François Petitjean, Alain Ketterlin, and Pierre Gançarski. “A global averaging method for dynamic time warping, with applications to clustering.” In: *Pattern recognition* 44.3 (2011), pp. 678–693.

[181] Vitali Petsiuk, Abir Das, and Kate Saenko. “RISE: Randomized Input Sampling for Explanation of Black-box Models.” In: *British Machine Vision Conference (BMVC)*. BMVA Press, 2018, p. 151.

[182] Lam Pham, Anahid Jalali, Olivia Dinica, and Alexander Schindler. *DCASE Challenge 2021: Unsupervised Anomalous Sound Detection of Machinery with LeNet Architecture*. Tech. rep. DCASE2021 Challenge, 2021.

[183] Paul Primus. *Reframing Unsupervised Machine Condition Monitoring as a Supervised Classification Task with Outlier-Exposed Classifiers*. Tech. rep. DCASE2020 Challenge, 2020.

[184] Paul Primus, Verena Haunschmid, Patrick Praher, and Gerhard Widmer. “Anomalous Sound Detection as a Simple Binary Classification Problem with Careful Selection of Proxy Outlier Examples.” In: *5th Workshop on Detection and Classification of Acoustic Scenes and Events 2020 (DCASE)*. 2020, pp. 170–174.

[185] Simon J.D. Prince and James H. Elder. “Probabilistic linear discriminant analysis for inferences about identity.” In: *11th International Conference on Computer Vision (ICCV)*. IEEE. 2007.

[186] Harsh Purohit, Takashi Endo, Masaaki Yamamoto, and Yohei Kawaguchi. “Hierarchical Conditional Variational Autoencoder Based Acoustic Anomaly Detection.” In: *30th European Signal Processing Conference (EUSIPCO)*. IEEE, 2022, pp. 274–278.

[187] Harsh Purohit, Ryo Tanabe, Takashi Endo, Kaori Suefusa, Yuki Nikaido, and Yohei Kawaguchi. “Deep Autoencoding GMM-Based Unsupervised Anomaly Detection in Acoustic Signals and its Hyper-Parameter Optimization.” In: *5th Workshop on Detection and Classification of Acoustic Scenes and Events (DCASE)*. 2020, pp. 175–179.

[188] Harsh Purohit, Ryo Tanabe, Takeshi Ichige, Takashi Endo, Yuki Nikaido, Kaori Suefusa, and Yohei Kawaguchi. “MIMII Dataset: Sound Dataset for Malfunctioning Industrial Machine Investigation and Inspection.” In: *Detection and Classification of Acoustic Scenes and Events Workshop (DCASE)*. New York University, 2019, pp. 209–213.

[189] Clemens Reimann, Peter Filzmoser, and Robert G. Garrett. “Background and threshold: critical comparison of methods of determination.” In: *Science of the total environment* 346.1-3 (2005), pp. 1–16.

[190] Tal Reiss, Niv Cohen, Liron Bergman, and Yedid Hoshen. “PANDA: Adapting Pretrained Features for Anomaly Detection and Segmentation.” In: *Conference on Computer Vision and Pattern Recognition (CVPR)*. Computer Vision Foundation / IEEE, 2021, pp. 2806–2814.

[191] Marco Túlio Ribeiro, Sameer Singh, and Carlos Guestrin. “"Why Should I Trust You?": Explaining the Predictions of Any Classifier.” In: *22nd ACM SIGKDD International Conference on Knowledge Discovery and Data Mining*. ACM, 2016, pp. 1135–1144.

[192] Aaron E. Rosenberg, Chin-Hui Lee, and Frank K. Soong. “Cepstral channel normalization techniques for HMM-based speaker verification.” In: *The 3rd International Conference on Spoken Language Processing (ICSLP)*. ISCA, 1994.

[193] Bernard Rosner. “Percentage Points for a Generalized ESD Many-Outlier Procedure.” In: *Technometrics* 25.2 (1983), pp. 165–172.

[194] Peter J. Rousseeuw and Christophe Croux. “Alternatives to the median absolute deviation.” In: *Journal of the American Statistical association* 88.424 (1993), pp. 1273–1283.

[195] Peter J. Rousseeuw and Bert C. Van Zomeren. “Unmasking multivariate outliers and leverage points.” In: *Journal of the American Statistical association* 85.411 (1990), pp. 633–639.

[196] Lukas Ruff. “Deep one-class learning: a deep learning approach to anomaly detection.” PhD thesis. Technical University of Berlin, Germany, 2021.

[197] Lukas Ruff, Nico Görnitz, Lucas Deecke, Shoaib Ahmed Siddiqui, Robert A. Vandermeulen, Alexander Binder, Emmanuel Müller, and Marius Kloft. “Deep One-Class Classification.” In: *35th International Conference on Machine Learning (ICML)*. Vol. 80. Proceedings of Machine Learning Research. PMLR, 2018, pp. 4390–4399.

[198] Yuya Sakamoto and Naoya Miyamoto. *Combine Mahalanobis Distance, Interpolation Auto Encoder and Classification Approach for Anomaly Detection*. Tech. rep. DCASE2021 Challenge, 2021.

[199] Johan Schalkwyk, Doug Beeferman, Françoise Beaufays, Bill Byrne, Ciprian Chelba, Mike Cohen, Maryam Kamvar, and Brian Strope. "“Your word is my command”: Google search by voice: A case study." In: *Advances in Speech Recognition: Mobile Environments, Call Centers and Clinics* (2010), pp. 61–90.

[200] Walter J. Scheirer, Anderson de Rezende Rocha, Archana Sapkota, and Terrance E. Boult. "Toward Open Set Recognition." In: *IEEE Trans. Pattern Anal. Mach. Intell.* 35.7 (2013), pp. 1757–1772.

[201] Thomas Schlegl, Philipp Seeböck, Sebastian M. Waldstein, Ursula Schmidt-Erfurth, and Georg Langs. "Unsupervised Anomaly Detection with Generative Adversarial Networks to Guide Marker Discovery." In: *25th International Conference on Information Processing in Medical Imaging(IPMI).* Vol. 10265. Lecture Notes in Computer Science. Springer, 2017, pp. 146–157.

[202] Bernhard Schölkopf, John C. Platt, John Shawe-Taylor, Alexander J. Smola, and Robert C. Williamson. "Estimating the Support of a High-Dimensional Distribution." In: *Neural Comput.* 13.7 (2001), pp. 1443–1471.

[203] Kanta Shimonishi, Kota Dohi, and Yohei Kawaguchi. "Anomalous Sound Detection Based on Sound Separation." In: *24th Annual Conference of the International Speech Communication Association (Interspeech).* ISCA, 2023, pp. 2733–2737.

[204] Stepan Shishkin, Danilo Hollosi, Simon Doclo, and Stefan Goetze. "Active Learning for Sound Event Classification using Monte-Carlo Dropout and PANN Embeddings." In: *6th Workshop on Detection and Classification of Acoustic Scenes and Events (DCASE).* 2021, pp. 150–154.

[205] Suwon Shon, Najim Dehak, Douglas A. Reynolds, and James R. Glass. "MCE 2018: The 1st Multi-Target Speaker Detection and Identification Challenge Evaluation." In: *20th Annual Conference of the International Speech Communication Association (Interspeech).* ISCA, 2019, pp. 356–360.

[206] Robert H. Shumway and David S. Stoffer. *Time series analysis and its applications.* Vol. 3. Springer, 2000.

[207] Karen Simonyan and Andrew Zisserman. "Very Deep Convolutional Networks for Large-Scale Image Recognition." In: *3rd International Conference on Learning Representations (ICLR).* 2015.

[208] Aleksandr Sizov, Kong Aik Lee, and Tomi Kinnunen. "Unifying Probabilistic Linear Discriminant Analysis Variants in Biometric Authentication." In: *Proc. S+SSPR.* Software available at https://sites.google.com/site/fastplda/. Springer. 2014, pp. 464–475.

[209] Jake Snell, Kevin Swersky, and Richard S. Zemel. “Prototypical Networks for Few-shot Learning.” In: *Advances in Neural Information Processing Systems 30: Annual Conference on Neural Information Processing Systems (NIPS).* 2017, pp. 4077–4087.

[210] David Snyder, Daniel Garcia-Romero, Gregory Sell, Daniel Povey, and Sanjeev Khudanpur. “X-Vectors: Robust DNN Embeddings for Speaker Recognition.” In: *International Conference on Acoustics, Speech and Signal Processing (ICASSP).* IEEE, 2018, pp. 5329–5333.

[211] Stanley Smith Stevens, John Volkmann, and Edwin Broomell Newman. “A scale for the measurement of the psychological magnitude pitch.” In: *The Journal of the Acoustical Society of America* 8.3 (1937), pp. 185–190.

[212] Kaori Suefusa, Tomoya Nishida, Harsh Purohit, Ryo Tanabe, Takashi Endo, and Yohei Kawaguchi. “Anomalous Sound Detection Based on Interpolation Deep Neural Network.” In: *International Conference on Acoustics, Speech and Signal Processing (ICASSP).* IEEE, 2020, pp. 271–275.

[213] Cecilia Summers and Michael J. Dinneen. “Improved Mixed-Example Data Augmentation.” In: *Winter Conference on Applications of Computer Vision (WACV).* IEEE, 2019, pp. 1262–1270.

[214] Yanmin Sun, Andrew K. C. Wong, and Mohamed S. Kamel. “Classification of Imbalanced Data: a Review.” In: *Int. J. Pattern Recognit. Artif. Intell.* 23.4 (2009), pp. 687–719.

[215] Jiantong Tian, Hejing Zhang, Qiaoxi Zhu, Feiyang Xiao, Haohe Liu, Xinhao Mei, Youde Liu, Wenwu Wang, and Jian Guan. *First-shot Anomalous Sound Detection with GMM Clustering and Finetuned Attribute Classification using Audio Pretrained Model.* Tech. rep. DCASE2023 Challenge, 2023.

[216] Giuseppe Valenzise, Luigi Gerosa, Marco Tagliasacchi, Fabio Antonacci, and Augusto Sarti. “Scream and gunshot detection and localization for audio-surveillance systems.” In: *Fourth International Conference on Advanced Video and Signal Based Surveillance (AVSS).* IEEE, 2007, pp. 21–26.

[217] Satvik Venkatesh, Gordon Wichern, Aswin Subramanian, and Jonathan Le Roux. *Disentangled surrogate task learning for improved domain generalization in unsupervised anomalous sound detection.* Tech. rep. DCASE Challenge, 2022.

[218] Satvik Venkatesh, Gordon Wichern, Aswin Shanmugam Subramanian, and Jonathan Le Roux. “Improved Domain Generalization via Disentangled Multi-Task Learning in Unsupervised Anomalous Sound Detection.” In: *7th Workshop on Detection and Classification of Acoustic Scenes and Events (DCASE).* Tampere University, 2022, pp. 196–200.

[219] Sergey Verbitskiy, Milana Shkhanukova, and Viacheslav Vyshegorodtsev. *Unsupervised Anomalous Sound Detection Using Multiple Time-Frequency Representations.* Tech. rep. DCASE Challenge, 2022.

[220] Vikas Verma, Alex Lamb, Christopher Beckham, Amir Najafi, Ioannis Mitliagkas, David Lopez-Paz, and Yoshua Bengio. "Manifold Mixup: Better Representations by Interpolating Hidden States." In: *36th International Conference on Machine Learning (ICML).* Vol. 97. Proceedings of Machine Learning Research. PMLR, 2019, pp. 6438–6447.

[221] Phongtharin Vinayavekhin, Tadanobu Inoue, Shu Morikuni, Shiqiang Wang, Tuan Hoang Trong, David Wood, Michiaki Tatsubori, and Ryuki Tachibana. *Detection of Anomalous Sounds for Machine Condition Monitoring using Classification Confidence.* Tech. rep. DCASE2020 Challenge, 2020.

[222] Dirk Von Zeddelmann, Frank Kurth, and Meinard Müller. "Perceptual audio features for unsupervised key-phrase detection." In: *International Conference on Acoustics, Speech and Signal Processing (ICASSP).* IEEE. 2010, pp. 257–260.

[223] Feng Wang, Jian Cheng, Weiyang Liu, and Haijun Liu. "Additive Margin Softmax for Face Verification." In: *IEEE Signal Processing Letters* 25.7 (2018), pp. 926–930.

[224] Hao Wang, Yitong Wang, Zheng Zhou, Xing Ji, Dihong Gong, Jingchao Zhou, Zhifeng Li, and Wei Liu. "CosFace: Large Margin Cosine Loss for Deep Face Recognition." In: *Conference on Computer Vision and Pattern Recognition (CVPR).* Computer Vision Foundation / IEEE Computer Society, 2018, pp. 5265–5274.

[225] Jindong Wang, Cuiling Lan, Chang Liu, Yidong Ouyang, and Tao Qin. "Generalizing to Unseen Domains: A Survey on Domain Generalization." In: *Thirtieth International Joint Conference on Artificial Intelligence (IJCAI).* ijcai.org, 2021, pp. 4627–4635.

[226] Lei Wang et al. *First-Shot Unsupervised Anomalous Sound Detection Using Attribute Classification and Conditional Autoencoder.* Tech. rep. DCASE2023 Challenge, 2023.

[227] Yaqing Wang, Quanming Yao, James T. Kwok, and Lionel M. Ni. "Generalizing from a Few Examples: A Survey on Few-shot Learning." In: *ACM Comput. Surv.* 53.3 (2021), 63:1–63:34.

[228] Yu Wang, Nicholas J. Bryan, Mark Cartwright, Juan Pablo Bello, and Justin Salamon. "Few-Shot Continual Learning for Audio Classification." In: *International Conference on Acoustics, Speech and Signal Processing (ICASSP).* IEEE, 2021, pp. 321–325.

[229] Yu Wang, Mark Cartwright, and Juan Pablo Bello. “Active Few-Shot Learning for Sound Event Detection.” In: *23rd Annual Conference of the International Speech Communication Association (Interspeech)*. ISCA, 2022, pp. 1551–1555.

[230] Yu Wang, Justin Salamon, Nicholas J. Bryan, and Juan Pablo Bello. “Few-Shot Sound Event Detection.” In: *International Conference on Acoustics, Speech and Signal Processing (ICASSP)*. IEEE, 2020, pp. 81–85.

[231] Pete Warden. “Speech Commands: A Dataset for Limited-Vocabulary Speech Recognition.” In: *CoRR* abs/1804.03209 (2018).

[232] Yuming Wei, Jian Guan, Haiyan Lan, and Wenwu Wang. *Anomalous Sound Detection System with Self-challenge and Metric Evaluation for DCASE2022 Challenge Task 2*. Tech. rep. DCASE Challenge, 2022.

[233] Kilian Q. Weinberger and Lawrence K. Saul. “Distance metric learning for large margin nearest neighbor classification.” In: *Journal of machine learning research* 10.2 (2009).

[234] Yandong Wen, Kaipeng Zhang, Zhifeng Li, and Yu Qiao. “A discriminative feature learning approach for deep face recognition.” In: *European Conference on Computer Vision (ECCV)*. Springer. 2016, pp. 499–515.

[235] Gordon Wichern, Ankush Chakrabarty, Zhong-Qiu Wang, and Jonathan Le Roux. “Anomalous Sound Detection Using Attentive Neural Processes.” In: *Workshop on Applications of Signal Processing to Audio and Acoustics (WASPAA)*. IEEE, 2021, pp. 186–190.

[236] Kevin Wilkinghoff. “General-Purpose Audio Tagging by Ensembling Convolutional Neural Networks based on Multiple Features.” In: *Detection and Classification of Acoustic Scenes and Events Workshop (DCASE)*. Tampere University of Technology, 2018, pp. 44–48.

[237] Kevin Wilkinghoff. “On Open-Set Classification with L3-Net Embeddings for Machine Listening Applications.” In: *28th European Signal Processing Conference (EUSIPCO)*. IEEE, 2020, pp. 800–804.

[238] Kevin Wilkinghoff. “On Open-Set Speaker Identification with I-Vectors.” In: *Odyssey - The Speaker and Language Recognition Workshop (Odyssey)*. ISCA, 2020, pp. 408–414.

[239] Kevin Wilkinghoff. “Using Look, Listen, and Learn Embeddings for Detecting Anomalous Sounds in Machine Condition Monitoring.” In: *Detection and Classification of Acoustic Scenes and Events Workshop (DCASE)*. 2020, pp. 215–219.

[240] Kevin Wilkinghoff. “Combining Multiple Distributions based on Sub-Cluster AdaCos for Anomalous Sound Detection under Domain Shifted Conditions.” In: *Detection and Classification of Acoustic Scenes and Events Workshop (DCASE)*. 2021.

[241] Kevin Wilkinghoff. "Sub-Cluster AdaCos: Learning Representations for Anomalous Sound Detection." In: *International Joint Conference on Neural Networks (IJCNN)*. IEEE, 2021.

[242] Kevin Wilkinghoff. *An outlier exposed anomalous sound detection system for domain generalization in machine condition monitoring.* Tech. rep. DCASE Challenge, 2022.

[243] Kevin Wilkinghoff. "Design Choices for Learning Embeddings from Auxiliary Tasks for Domain Generalization in Anomalous Sound Detection." In: *International Conference on Acoustics, Speech and Signal Processing (ICASSP)*. IEEE, 2023.

[244] Kevin Wilkinghoff. *Fraunhofer FKIE submission for Task 2: First-Shot Unsupervised Anomalous Sound Detection for Machine Condition Monitoring.* Tech. rep. DCASE2023 Challenge, 2023.

[245] Kevin Wilkinghoff. "AdaProj: Adaptively Scaled Angular Margin Subspace Projections for Anomalous Sound Detection with Auxiliary Classification Tasks." Submitted to 9th Workshop on Detection and Classification of Acoustic Scenes and Events (DCASE), arXiv:2403.14179. 2024.

[246] Kevin Wilkinghoff. "Self-Supervised Learning for Anomalous Sound Detection." In: *International Conference on Acoustics, Speech and Signal Processing (ICASSP)*. IEEE, 2024, pp. 276–280.

[247] Kevin Wilkinghoff and Alessia Cornaggia-Urrigshardt. "On choosing decision thresholds for anomalous sound detection in machine condition monitoring." In: *24th International Congress on Acoustics (ICA)*. The Acoustical Society of Korea, 2022.

[248] Kevin Wilkinghoff and Alessia Cornaggia-Urrigshardt. "TACos: Learning Temporally Structured Embeddings for Few-Shot Keyword Spotting with Dynamic Time Warping." In: *International Conference on Acoustics, Speech and Signal Processing (ICASSP)*. IEEE, 2024, pp. 9941–9945.

[249] Kevin Wilkinghoff, Alessia Cornaggia-Urrigshardt, and Fahrettin Gökgöz. "Two-Dimensional Embeddings for Low-Resource Keyword Spotting Based on Dynamic Time Warping." In: *14th ITG Conference on Speech Communication (ITG Speech)*. VDE-Verlag, 2021, pp. 9–13.

[250] Kevin Wilkinghoff and Fabian Fritz. "On Using Pre-Trained Embeddings for Detecting Anomalous Sounds with Limited Training Data." In: *31st European Signal Processing Conference (EUSIPCO)*. IEEE, 2023, pp. 186–190.

[251] Kevin Wilkinghoff and Keisuke Imoto. "F1-EV Score: Measuring the Likelihood of Estimating a Good Decision Threshold for Semi-Supervised Anomaly Detection." In: *International Conference on Acoustics, Speech and Signal Processing (ICASSP)*. IEEE, 2024, pp. 256–260.

[252] Kevin Wilkinghoff and Frank Kurth. “Why do Angular Margin Losses work well for Semi-Supervised Anomalous Sound Detection?” In: *IEEE/ACM Trans. Audio Speech Lang. Process.* 32 (2024), pp. 608–622.

[253] Huang Xie and Tuomas Virtanen. “Zero-Shot Audio Classification Via Semantic Embeddings.” In: *IEEE/ACM Trans. Audio Speech Lang. Process.* 29 (2021), pp. 1233–1242.

[254] Jia Yafei, Bai Jisheng, and Huang Siwei. *Unsupervised Abnormal Sound Detection Based on Machine Condition Mixup.* Tech. rep. DCASE2023 Challenge, 2023.

[255] Peng Yan, Ahmed Abdulkadir, Paul-Philipp Luley, Matthias Rosenthal, Gerrit A. Schatte, Benjamin F. Grewe, and Thilo Stadelmann. “A Comprehensive Survey of Deep Transfer Learning for Anomaly Detection in Industrial Time Series: Methods, Applications, and Directions.” In: *IEEE Access* 12 (2024), pp. 3768–3789.

[256] Hanfang Yang, Kun Lu, Xiang Lyu, and Feifang Hu. “Two-way partial AUC and its properties.” In: *Statistical methods in medical research* 28.1 (2019), pp. 184–195.

[257] Jiawei Yang, Susanto Rahardja, and Pasi Fränti. “Outlier detection: how to threshold outlier scores?” In: *International Conference on Artificial Intelligence, Information Processing and Cloud Computing (AIIPCC).* ACM, 2019, 37:1–37:6.

[258] Qien Yu, Muthu Subash Kavitha, and Takio Kurita. “Autoencoder framework based on orthogonal projection constraints improves anomalies detection.” In: *Neurocomputing* 450 (2021), pp. 372–388.

[259] Ying Zeng, Hongqing Liu, Lihua Xu, Yi Zhou, and Lu Gan. *Robust Anomaly Sound Detection Framework for Machine Condition Monitoring.* Tech. rep. DCASE Challenge, 2022.

[260] Chenxu Zhang, Yao Yao, Rui Qiu, Shengchen Li, and Xi Shao. *Unsupervised Anomalous Sound Detection Using Denoising-Detection System Under Domain Shifted Conditions.* Tech. rep. DCASE2021 Challenge, 2021.

[261] Hanlin Zhang, Yi-Fan Zhang, Weiyang Liu, Adrian Weller, Bernhard Schölkopf, and Eric P. Xing. “Towards Principled Disentanglement for Domain Generalization.” In: *IEEE/CVF Conference on Computer Vision and Pattern Recognition (CVPR).* IEEE, 2022, pp. 8014–8024.

[262] Hongyi Zhang, Moustapha Cisse, Yann N. Dauphin, and David Lopez-Paz. “Mixup: Beyond empirical risk minimization.” In: *6th International Conference on Learning Representations (ICLR).* Openreview.net, 2018.

[263] Minghu Zhang, Xin Li, and Lili Wang. “An Adaptive Outlier Detection and Processing Approach Towards Time Series Sensor Data.” In: *IEEE Access* 7 (2019), pp. 175192–175212.

[264] Xiao Zhang, Rui Zhao, Yu Qiao, Xiaogang Wang, and Hongsheng Li. “AdaCos: Adaptively Scaling Cosine Logits for Effectively Learning Deep Face Representations.” In: *Conference on Computer Vision and Pattern Recognition (CVPR).* IEEE, 2019, pp. 10823–10832.

[265] Shuyang Zhao, Toni Heittola, and Tuomas Virtanen. “Active Learning for Sound Event Detection.” In: *IEEE/ACM Trans. Audio Speech Lang. Process.* 28 (2020), pp. 2895–2905.

[266] Qiping Zhou. *ArcFace Based Sound Mobilenets for DCASE 2020 Task 2.* Tech. rep. DCASE2020 Challenge, 2020.

[267] Yifan Zhou and Yanhua Long. *Attribute Classifier with Imbalance Compensation for Anomalous Sound Detection.* Tech. rep. DCASE2023 Challenge, 2023.

[268] Manli Zhu and Aleix M. Martinez. “Subclass discriminant analysis.” In: *IEEE Trans. Pattern Anal. Mach. Intell.* 28.8 (2006), pp. 1274–1286.

[269] Christian Zieger, Alessio Brutti, and Piergiorgio Svaizer. “Acoustic Based Surveillance System for Intrusion Detection.” In: *6th International Conference on Advanced Video and Signal Based Surveillance (AVSS).* IEEE, 2009, pp. 314–319.